MANIPAL
ACADEMY *of* HIGHER EDUCATION
(Deemed to be University under Section 3 of the UGC Act, 1956)

Theoretical and Experimental Investigations into Causality, its Measures and Applications

A Thesis to be Submitted to
Manipal Academy of Higher Education

For fulfillment of the requirement for the
Award of the Degree
of
Doctor of Philosophy
By

Aditi Kathpalia

Under the Guidance of

Dr. Nithin Nagaraj
Associate Professor

Consciousness Studies Programme,
School of Humanities,
National Institute of Advanced Studies,
Indian Institute of Science Campus, Bengaluru-560012

MANIPAL
ACADEMY of HIGHER EDUCATION
(Deemed to be University under Section 3 of the UGC Act, 1956)

DECLARATION BY THE CANDIDATE

I declare that this thesis, submitted for the degree of **Doctor of Philosophy** to Manipal Academy of Higher Education, is my original work, conducted under the supervision of my guide, **Dr. Nithin Nagaraj**. I also wish to inform that no part of the research has been submitted for a degree or examination at any university. References, help and material obtained from other sources have been duly acknowledged.

Aditi Kathpalia
PhD Scholar
National Institute of Advanced Studies
Bengaluru

February, 2021

MANIPAL
ACADEMY *of* HIGHER EDUCATION
(Deemed to be University under Section 3 of the UGC Act, 1956)

CERTIFICATE

This is to certify that the work incorporated in this thesis "**Theoretical and Experimental Investigations into Causality, its Measures and Applications**", submitted by **Ms. Aditi Kathpalia** was carried out under my supervision. No part of this thesis has been submitted for a degree or examination at any university. References, help and material obtained from other sources have been duly acknowledged.

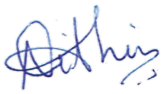

Dr. Nithin Nagaraj
Associate Professor
National Institute of Advanced Studies
Bengaluru

February, 2021

Contents

Acknowledgement

First and foremost, I would like to thank my thesis supervisor, Dr. Nithin Nagaraj, who is the prime reason behind the success of this thesis work. I can never forget our discussions over long walks in the IISc Campus where so many research ideas would enthrall us, the many hours we would spend together in fixing the intricacies of our research papers, the zeal with which he would deliver lectures on myriad topics and the words by which he would encourage and challenge me to focus on higher and higher goals. He has been a mentor not only on the academic aspects of my life, but also on the personal and spiritual fronts. I am grateful that I could meet and work with him during my tenure as an intern at General Electric, John F. Welch technology Center, Bengaluru in 2014. This short tenure of 3 months inspired me to pursue my PhD under his guidance that has come to fruition as this thesis.

I wish to extend my thanks to the members of my Student Advisory Committee – Prof. Sangeetha Menon from NIAS, Dr. Sridharan Devarajan from the Centre from Neuroscience, IISc and Dr. Karthi Balasubramainian from Amrita Vishwa Vidyapeetham, Coimbatore. They have provided regular feedback and support to me during the course of my PhD. Dr. Sridharan's guidance has been of immense help in the neuroscience-related applications of the causality developed measure. Dr. Karthi's expertise came of much help in dealing with the significance testing aspects of the proposed causality measure. I would like to express my gratitude to Prof. Aditya Murthy, Motor Control Lab, Centre for Neuroscience, IISc and his student Vaibhav Thakur who provided us with electroencephalography recordings of human subjects for brain connectivity analysis during motor task. They were also very kind to give their comments

on the analysis we performed on this data, which has been included in Chapter 4.

I am very thankful to Nikita Agarwal, who was a Junior Research Fellow at NIAS and helped with the analysis of electrocorticographic recordings from monkeys. This contributed to one section of work in Chapter 4. I would also like to thank Abhijith MA, Aishwarya Nambissan , Aswathi Gopinath and Krishnapriya M who were undergraduate interns in our Lab. The work I did together with them contributed to many of the results in Chapter 7.

I would like to extend my thanks to Harikrishnan NB and Pranay Yadav, Research Assistants in our Lab, who are not only fellow colleagues but also good friends. We had a number of interesting discussions ranging from causality to life, during my PhD.

I am grateful to Prof. P.G. Vaidya, my academic grandadvisor. I had the fortune to meet him once during my PhD while traveling to San Diego, USA for a conference. I have been deeply inspired not only by that meeting, but also by his research work and the stories that I have heard about him from Dr. Nithin. His work on *Asymptotic stability and chaotic synchronization* inspired my work on *causal stability* included in Chapter 6.

I am thankful to the PhD programme at National Institute of Advanced Studies for providing me with a platform and all the facilities for conducting my research . In this regard, I would like to thank the Directors at NIAS during my tenure – past Director Late Prof. Baldev Raj and current Director Prof. Shailesh Nayak. I would also like to acknowledge the PhD committee and the academic heads during my tenure – Dr. T.S. Gopi Rethinaraj , Prof. Sundar Sarukkai and Prof. BK Anitha were readily available for discussing any PhD matters with us. I was a part of the Consciousness Studies

Programme team at NIAS, that provided us very good opportunities to deliver talks and also listen to speakers from multiple disciplines, helping in my inter-disciplinary growth and learning. I extend my thanks to all the members of the team. I would also like to thank the entire administrative team at NIAS, especially Ms. Sandhya and Mr. Aithal for helping me with myriad matters relating to the PhD, hostel and conference travel. Finally, I would like to thank the library staff, Ms. Hamsa and Ms. Vijayalakshmi, for helping me use the library resources. I am also grateful to IISc for letting me avail their various courses and workshops.

I am grateful to Science and Engineering Research Board (SERB-DST) for awarding me a scholarship to travel for an international conference in San Diego, USA. I am also grateful to Tata Trusts for providing funding for international conference travel to Antwerp, Belgium. I would also like to acknowledge the partial financial support by Cognitive Science Research Initiative (CSRI-DST): Grant No. DST/CSRI/2017/54(G), Science and Technology for Yoga and Meditation (SATYAM-DST): Grant No. DST/SATYAM/2017/45(G) and Tata Trusts, pertaining to domestic conference travel and provision of computational resources.

I extend my thanks to my mentors in my previous research projects – Prof. Hans Torp, Dr. Kajoli Banerjee Krishnan and Mr. Promit Biswas. Their guidance helped me to grow as a researcher, providing a foundation on which this PhD research could be conducted.

I am thankful to my friends – Ekta, Ankita, Mohit and Smriti for their support during the course of my PhD. Special thanks also to my long-time friend and now fiánce, Anurag for all his support, help and encouragement. I am also grateful to

my Yoga teacher, Mr. K.C. Ananda, without whose refreshing and uplifting morning classes, I would not have been as invigorated to carry out my daily study and research activities.

Finally, I would like to express my gratitude towards my family – my parents, grandparents and sister. Without the unconditional love and support of my parents, it would have been impossible to complete this thesis. My father's own research pursuits and his guidance on matters related to research and PhD were a constant driving source for me.

OM TAT SAT

List of Figures

List of Tables

List of Abbreviations

A_{P_C}	Compressive Potential based Temporal Asymmetry
AR	Autoregressive
AS	Anticipating Synchronization
C	Complexity
CC	Dynamical Compression-Complexity
CCC	Compression-Complexity Causality
$CCC_{Eff.}$	Effective Compression-Complexity Causality
CCC_{Net}	Net Compression-Complexity Causality
CCM	Convergent Cross Mapping
CI_{net}	Net Causal Influence
CMI	Conditional Mutual Information
CR	Complexity Rate
DC	Dynamical Complexity
DCM	Dynamic Causal Modeling
ECoG	Electrocorticography
EEG	Electroencephalography
ETC	Effort to Compress
FT	Fourier Transform
GC	Granger Causality
GLM	Generalized Linear Model
IAAFT	Iterative Amplitude Adjusted Fourier Transform
ICC	Interventional Complexity Causality
IIT	Integrated Information Theory
JSD	Jensen-Shannon Divergence

KLD	Kullback-Leibler Divergence
LRP	Lateralized Readiness Potential
LZ	Lempel-Ziv
NCA	Network Causal Activity
NGC	Non-linear Granger Causality
NSRPS	Non-Sequential Recursive Pair Substitution
P_C	Compressive Potential
PCI	Perturbational Complexity Index
PI	Predictability Improvement
RIP	Restricted Isometry Property
SEM	Structural Equation Modeling
TE	Transfer Entropy

Abstract

A major part of human scientific endeavour aims at making causal inferences of observed phenomena. While some of the studies conducted are experimental, others are observational, the latter often making use of recorded data. Since temporal data can be easily acquired and stored in todays world, time-series causality estimation measures have come into wide use across a range of disciplines such as neuroscience, earth science and econometrics. In this context, model-free/data-driven methods for causality estimation are extremely useful, as the underlying model generating the data is often unknown. However, existing data-driven measures such as Granger Causality and Transfer Entropy impose strong statistical assumptions on the data and can only estimate causality by *associational* means. Associational causality, being the most rudimentary level of causality has several limitations. In this thesis, we propose a novel *Interventional Complexity Causality* scheme for time series measurements so as to capture a higher level of causality based on *intervention* which until now could be inferred only through model-based measures. Based on this interventional scheme, we formulate a *Compression-Complexity Causality (CCC)* measure that is rigorously tested on simulations of stochastic and deterministic systems and shown to overcome the limitations of existing measures. CCC is then applied to infer causal relations from real data

mainly in the domain of neuroscience. These include the study of brain connectivity in human subjects performing a motor task and a study to distinguish between awake and anaesthesia states in monkeys using electrophysiological brain recordings.

Through theoretical and empirical advances in causality testing, the thesis also makes contributions to a number of allied disciplines. A causal perspective is given for the ubiquitous phenomenon of *chaotic synchronization*. One of the major contributions in this regard is the introduction of the notion of *Causal Stability* and formulation (with proof) of a novel *Causal Stability Synchronization Theorem* which gives a condition for complete synchronization of coupled chaotic systems. Further, we propose and test for techniques to analyse causality between sparse signals using *compressed sensing*. A real application is demonstrated for the case of sparse neuronal spike trains recorded from rat prefrontal cortex. The area of temporal-reversibility detection of time-series is also closely linked to the domain of causality testing. We develop and test a new method to check for time-reversibility of processes and explore the behaviour of causality measures on coupled time-reversed processes.

Chapter 1

Introduction

This chapter provides a brief introduction to the field of causal inference in science. This is followed by a more detailed description of time-series based causality testing methods. Important research gaps identified in the domain of time-series causality estimation are then outlined building up to a discussion on the focus of this thesis. The thesis is divided into two parts: Part I and Part II. A brief synopsis of each of the Chapters in Part I and Part II of the thesis is given.

1.1 Introduction

Making causal inferences of observed phenomena is a major and important aspect of scientific studies. Methods for discovery of causal relationships lie on a broad spectrum from experimental to observational studies. While simpler and smaller systems can be experimented with by use of interventions which can be repeated, for larger and more complex systems observational studies are more practical. In the present day, with increased technology for data acquisition and storage, discovery of causal relations using available temporal data recorded from several variables of desired systems has become

immensely popular. Several time-series causality estimation methods are being used for this purpose. The research in this thesis is centred around the theme of time series causality estimation – placing the existing techniques in a mathematical framework, improving the methodology of estimation and overcoming the limitations of existing methods. Along with proposing a novel scheme and estimation technique towards this end, the thesis also makes significant theoretical and empirical contributions to other scientific domains that intersect the field of causality estimation.

1.2 Literature Review

1.2.1 Causality in Sciences

Most studies in natural as well as social sciences are centred around the theme of determining cause-effect relationships between processes or events. Such studies are being conducted from the early 20th century onwards. While some studies are observational, others involve experiments to understand the nature of dependencies. Examples of observational studies involve, studying the particle size and fertility of soil, availability of water, diseases or pests in a particular place in order to study their effect on crop yield; or observing the death rates of smoking vs non-smoking people to determine its influence on mortality. On the other hand, an example of experimental study would be studying a diseased group of people who are being administered medication to check its efficacy against a control group.

1.2.2 Three types of statistical causality

Cox and Wermuth have given three notions (levels) of statistical causality based on existing approaches for estimating causality [1]. The zero-level view of causality is basically a statistical association, i.e. non-independence with the cause happening before the effect. This association cannot be done away with by conditioning on other features or variables of the system that could be potential causes for the perceived effect. For example, when looking at the causal influence that greenhouse gases in the atmosphere have on increasing temperature of earth's surface, other features such as solar output which are also potential causes of the effect in question need to be conditioned. Only then can greenhouse gases be said to have an effect on earth's temperature. In mathematical terms, it is essentially a multiple-regression like analysis showing a dependence that is not explained away by other appropriate explanatory variables. This type was studied by Good (1961,1962) [2, 3] and by Suppes (1970) [4]. In a time-series context, it was formalized as Wiener-Granger causality by Granger (1969) [5] and later, formulated in a more general context by Schweder (1970) [6] and by Aalen (1987) [7].

In the first-level view of causality, the aim is to compare the outcomes arising under different interventions, given two or more (possible) interventions in a system. For example, consider the case of two medical interventions, D_1 and D_0 – a treatment drug and a control respectively, only one of which can be used on a particular patient. The outcome observed with D_1 use is compared with the outcome that would have

been observed on that patient had D_0 been used, other things being equal. If there is evidence that use of D_1 instead of D_0 causes a change in outcome, then it can be said that D_1 *causes* that *change*. The key principles of such kind of experimental design for *randomized control trials* were developed mainly at Rothamsted (Fisher, 1926, 1935; Yates, 1938, 1951) [8, 9]. This way of inferring causation may have a decision-making objective or may require the conduction of a controlled experiment, although that is not always the case. For example, when trying to check whether an anomalous gene causes a particular disease, the intervention as between the abnormal and normal version of the gene is hypothetical (since explicit intervention is not possible) and moreover no immediate decision-making process is generally involved. Rubin (1974) [10] adapted the notions of causality to observational studies using a representation similar to Fisher's. The definition of causality in the above discussed first-level view is explicitly comparative and has been the most widely used in scientific studies.

Suppose that preliminary analysis in a scientific context has established a pattern of dependencies or associations or have provided reasonable evidence of first- or zero-level causality. Second-level causality is used for explaining *how these dependencies arose* or *what underlying generating process were involved for the causal relationships observed*. On several occasions, this will require incorporating information from previous studies in the field or by doing laboratory experiments. Attempts in this regard started with graphical representations of causal path diagrams by Sewall Wright (Wright, 1921, 1934) [11, 12] and was later advocated by Cochran (1965) [13]. Currently, Non Parametric Structural Equations Models (NPSEMs) (Pearl, 2000) [14] which provide a very

general data-generating mechanism suitable for encoding causation, dominate the field.

Each of the above types for determining causality have their own pros and cons and their use depends on the motive and the nature of the study. While first-level causal estimation, that mostly involves randomization experiments, may make the conclusions of the study more secure, it fails to reveal the biological, or psychological, or physical processes working behind the effect observed. On the other hand, zero-level causality suffers from the criticism that there is no *intervention* involved to observe the causal effect of *doing* something on the system. The second-level of causality requires field knowledge and cannot be solely data driven.

1.2.3 Causation as against Correlation

We have often heard the saying 'Correlation does not imply Causation'. But even to this date, there are several scientific studies which make erroneous conclusions regarding a variable being a cause of another, merely on the basis of observed correlation value. Thus it becomes necessary to clarify the meaning and use of these two terms.

Correlation is a statistical concept which tells how strongly are a pair of variables linearly related and change together. It does not tell us the 'why' and 'how' behind the relationship but it just tells that a mathematical relationship potentially exists. For example, Pearson's correlation coefficient for a pair of random variables (X, Y) is given as:

$$\rho_{X,Y} = \frac{\mathbb{E}[(X - \mu_X)(Y - \mu_Y)]}{\sigma_X \sigma_Y}, \tag{1.1}$$

where, the numerator is the covariance of variables X, Y and σ_X, σ_Y are the standard

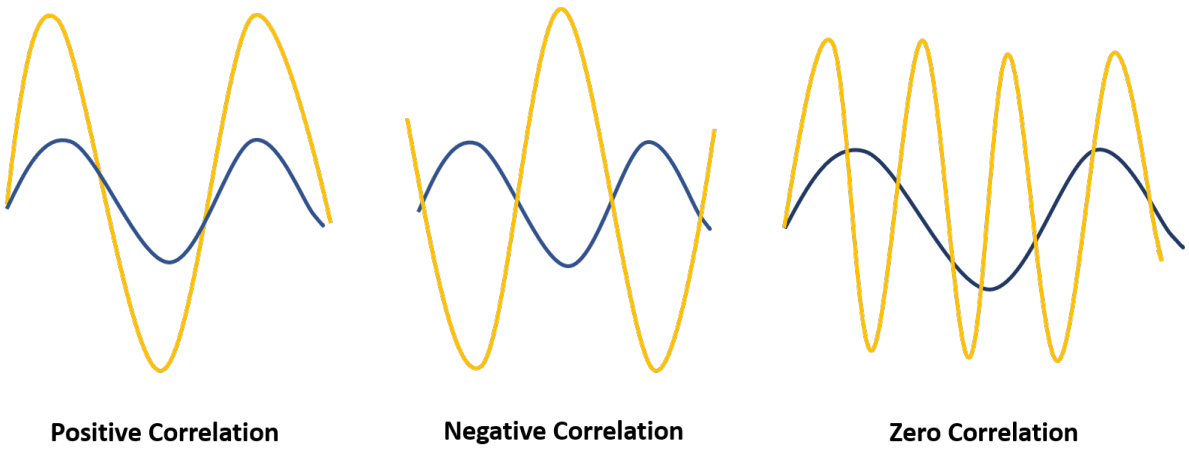

Figure 1.1: Positive, negative and zero correlation between two variables. The variation of one variable is shown in yellow (grey in print) while that of the other is shown in blue (black in print). In case of positive correlation, both the variables change in the same direction (i.e., increase or decrease together). In case of negative correlation, the two variables change in the opposite direction (when one increases the other decreases). In case of zero correlation, there is no relationship between the trend of variation observed in the two variables.

deviations of X and Y respectively. $\mathbb{E}$ is the expectation and μ_X, μ_Y are the means of X and Y respectively. Note that: $-1 \leq \rho_{X,Y} \leq +1$ and is always symmetric $\rho_{X,Y} = \rho_{Y,X}$. The closer the magnitude is to 1, the stronger is the relationship between the variables. Figure 1.1 illustrates two signals with positive, negative and zero correlation. An example of positive correlation would be between temperature in a region and sale of coolers – as temperature increases (decreases), sale of coolers also increases (decreases). However, as temperature increases (decreases), the sale of heaters decreases (increases), indicating negative correlation. An example of zero correlation would be between the amount of tea consumed by an individual and his/her level of intelligence.

In contrast, causation indicates that one event is a direct or indirect result of the occurrence of another event. A variable X can be said to be a *cause* of another variable

Y if it makes a difference to Y and the difference X makes must be a difference from what would have happened without it. This definition is adapted from the definition of a 'cause' given by philosopher David Lewis [15]. As discussed in the previous section, there are several means for estimating causality. Unlike correlation, causation is asymmetric.

Interestingly, for conventional statistics, causation was a non-scientific concept and as per the ideas prevalent in the late 19th and early 20th century, all analysis could be reduced to correlation. Since correlation got rigorously mathematically defined first (when scientist Galton was in search of a tool for causation) and causation seemed to be only a limited category of correlation, the latter became the central tool. Moreover, the pioneers of statistics such as Pearson felt that causation is only a matter of re-occurrence of certain sequences and science can in no way demonstrate any inherent necessity in a sequence of events nor prove with certainty that the sequence must be repeated [15].

However, later on, since most studies were in search of causal inferences and agents for their experimental/observational data and were at the same time using the famous statistical tool of correlation, they ended up incorrectly deducing the existence of causation based on results from correlation measures. Of the several infamous studies, an example is of the 2012 paper published in the *New England Journal of Medicine* claiming that chocolate consumption could enhance cognitive function. The basis for this conclusion was that the number of Nobel Prize laureates in each country was strongly correlated with the per capita consumption of chocolate in that country. One error that

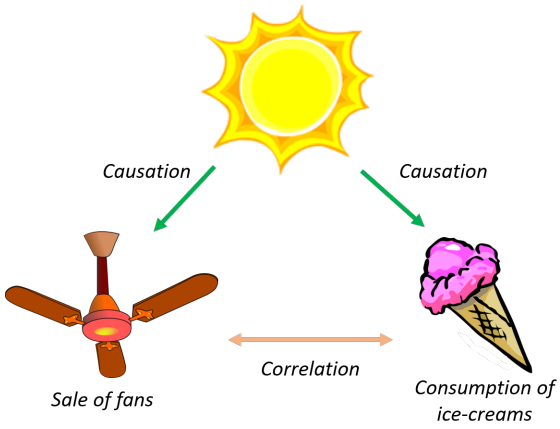

Figure 1.2: High correlation between 'sale of fans' and 'consumption of ice-creams' as a result of a *confounding variable*, 'temperature in a region'.

the authors of the paper made was deducing individual level conclusions (regarding enhancement of cognitive level) based on group level (country) data. There was no data on how much chocolate Nobel laureates consumed. It is possible that the correlation between the two variables arose because of a common factor – the prosperity of the country which affected both the access to chocolate as well as availability of higher education in the country.

There are several cases in everyday life where we can observe that correlation between two variables increases because of a common cause variable influencing the observed variables. This common cause variable is referred to as the *confounding variable* which results in a spurious association between the two variables. Figure 1.2 shows the example of the confounding variable 'temperature in a region' influencing the observed variables 'sale of fans' and 'consumption of ice-creams', resulting in a high correlation between the latter two variables.

1.2.4 The Ladder of Causation

Judea Pearl, in his latest book, 'The Book of Why', gives three levels for a causal learner [15]. His work on machine learning convinced him that for machines to learn to make decisions like humans, they cannot continue to make associations based on data alone but needed to have causal reasoning analogous to the human mind. In the 'Ladder of Causation' that he proposes, the three levels are – (1) Association, (2) Intervention and (3) Counterfactuals, when arranged from the lower rung to the higher rung.

Association involves observing regularities in the data to associate a past event with a future one. Animals learn in this way, for example, this is what a cat does when it observes a mouse and tries to predict where it will be a moment later. Pearl argues that machine learning algorithms even till today operate in this mode of 'association'. Correlation based measures such as those discussed in Section 1.2.2 under zero-level view of causality, work based on association. Intervention, at a higher level than association, involves actively changing what is there and then observing its effect. For example, when we take a paracetamol to cure our fever, it is an act of intervention on the drug level in our body to affect the fever. Randomized control trials as well as model-based causality measures (which aim to find the underlying generating mechanism) fall in this category. These have been discussed in Section 1.2.2 as the first and second levels of causality.

The highest rung on the Ladder of Causation is that of Counterfactuals. This involves imagination. No experiment can actually change history (since time travel

is not practical), but if I take paracetamol when I have fever and after a few hours I ask 'was it the paracetamol that cured my fever?', then I am exercising the power of my imagination to infer the cause of my fever being cured. To date, there is no computational method to establish causality by such counterfactual reasoning.

1.2.5 Causality estimation from time-series

After describing the broad field of causal inference and the means to classify the existing causality measures, let us move to the domain of time-series causality estimation which is the main focus of this thesis. Several mathematical methods have been developed that can be applied on temporal measurements that have been acquired and stored. These methods can be broadly divided into two categories: model-free or data-driven or non-parametric measures and model-based or parametric measures. Parametric/model-based methods assume a fixed set of parameters and their distributions. Models with these parameters are assumed for the given data and the best model is selected out of the assumed models. Non-parametric/model-free methods, on the other hand, do not make any assumptions on the data, its distribution and there are no fixed set of parameters. Model-based measures can also be thought of as data-driven since the model and its parameters are selected based on data. However, for the purpose of this thesis, we refer to model-free methods as data-driven because they are so in the true sense, they do not make any assumptions on the plausible underlying models. The measures falling under each of these two categories are briefly discussed below:

Data-driven causality measures

In the present day scenario, data is readily available and typically in large quantity. Also, to infer certain kinds of cause-effect relationships, it may be difficult or impossible to conduct intervention experiments. Thus, an increasing number of studies are now using data-driven measures of causality testing. While model-based causality measures would give more information about the underlying mechanism, when field knowledge is not adequately available, it may not be feasible to design such models. In such scenarios as well, model-free, data driven measures are useful. These are being employed in fields such as neuroscience [16, 17], climatology [18, 19], econometrics [20, 21], physics and engineering [22].

Several methods of causality which use time series data have been developed. One of the earliest and popular methods in this regard is Granger Causality (GC) [5]. Other methods that were proposed later include Transfer Entropy (TE) [23], Non-linear Granger Causality [24] and Information flow [25, 26]. All these methods are based on Wiener's idea [27], which defines a simple and elegant way to estimate causality from time series data. According to Wiener, if a time series X *causes* a time series Y, then past values of X should contain information that help predict Y above and beyond the information contained in past values of Y alone. Wiener's approach to causation and the idea behind GC and TE which are based on it is given in Box 1.

Box 1

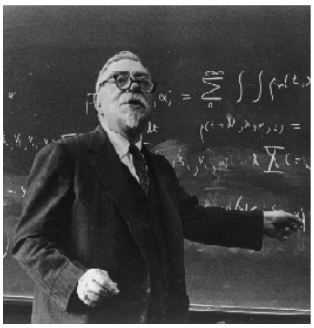

Norbert Wiener (1894-1964) (left) and Clive W.J. Granger (1934-2009) (right) – pioneers in the field of time series based causality estimation. Granger was awarded the Nobel Memorial Prize in Economic Sciences in 2003 for his work on methods for analyzing economic time series with common trends.

Wiener's idea:

According to Wiener, if a time series X *causes* a time series Y, then past values of X should contain information that help predict Y above and beyond the information contained in past values of Y alone [27].

Several methods are based on this approach and the idea behind each one of them is stated below. If, with the inclusion of past of X -

- prediction power of Y ↑, then there is a non-zero **Granger Causality** from X to Y.
- uncertainty of Y ↓, then there is a non-zero **Transfer Entropy** from X to Y.

Other model-free methods for causality testing from time series data include Convergent Cross Mapping [28], Topological Causality [29] etc. These measures capture causality based on the topological properties of dynamical systems. We discuss a few important methods below along with their applications and limitations.

Granger Causality (GC) is a statistical concept of causality that is based on prediction. This was the first method proposed directly based on Wiener's approach and hence is often referred to as Wiener-Granger Causality [27]. To check if a process X *Granger causes* another process Y, two separate autoregressive processes of Y are modeled for consideration –

$$Y(t) = \sum_{\tau=1}^{\infty}(a_\tau Y(t-\tau)) + \sum_{\tau=1}^{\infty}(c_\tau X(t-\tau)) + \varepsilon_c, \tag{1.2}$$

$$Y(t) = \sum_{\tau=1}^{\infty}(b_\tau Y(t-\tau)) + \varepsilon, \tag{1.3}$$

where t denotes any time instance, a_τ, b_τ, c_τ are coefficients at a time lag of τ and $\varepsilon_c, \varepsilon$ are error terms in the two models. Assuming that X and Y are covariance stationary[1], whether X causes Y or not can be predicted by the log ratio of the prediction error variances:

$$F_{X\to Y} = \ln \frac{var(\varepsilon)}{var(\varepsilon_c)}. \tag{1.4}$$

[1]A process is said to be covariance (or weak-sense) stationary if its mean does not change with time and the covariance between any two terms of its observed time-series depends only on the relative positions of the two terms, that is, on how far apart they are located from each other, and not on their absolute position [30].

This measure is called the F-statistic. If the model represented by equation (1.2) is a better model for $Y(t)$ than equation (1.3), then $\text{var}(\varepsilon_c) < \text{var}(\varepsilon)$ and $F_{X\to Y}$ will be greater than 0, suggesting that X *Granger causes* Y. Though this concept of causality uses an autoregressive model, in principle, the measure is applicable for a wide range of covariance stationary processes [31, 32]. This led the method to be abundantly applied for data-driven causality estimation in diverse disciplines [16,33,34]. In practice, however, it has been shown that the method often fails to identify the correct causal influences for nonlinear time series [35]. The method also suffers limitations when applied to sub-sampled [36] and noisy [37] time-series.

Transfer Entropy (TE) quantifies the influence of a time-series J on transition probabilities of a time-series I [23]. This method makes the assumption that the time-series I and J are stationary markov processes in which the probability of an event at any time point depends only on the state(s) attained by the processes in a limited number of past time points. TE measures the penalty to be paid in terms of excess amount of info-theoretic bits by assuming that the current state i_{n+1} of a variable I is independent of the past states $j_n^{(l)}$ of a variable J, i.e. assuming its distribution to be $p(i_{n+1}|i_n^{(k)})$ instead of $p(i_{n+1}|i_n^{(k)}, j_n^{(l)})$. Here k and l denote the number of past states of I and J respectively, on which the probability distribution of any state i_{n+1} of process I is dependent. Mathematically,

$$TE_{J\to I} = \sum_{i,j} p(i_{n+1}, i_n^{(k)}, j_n^{(l)}) \log_2 \frac{p(i_{n+1}|i_n^{(k)}, j_n^{(l)})}{p(i_{n+1}|i_n^{(k)})} bits. \tag{1.5}$$

If I and J are independent processes, then $p(i_{n+1}|i_n^{(k)}, j_n^{(l)}) = p(i_{n+1}|i_n^{(k)})$ for all n, k, l and hence the above quantity will be zero. Intuitively, $TE_{J\to I}$ captures the flow of information (in bits) from a process J to a process I. In general, $TE_{J\to I} \neq TE_{I\to J}$. Interestingly, TE and GC have been shown to be equivalent for Gaussian variables [38].

Just like GC, TE too is a very widely used measure of causality estimation across disciplines [17, 22, 39]. In addition to the assumption on markovianity and stationarity made by TE which reduce the scope of its application, the method suffers from a number of limitations. Some of these include spurious performance of the measure in the case of datasets with low temporal resolution and the presence of observational noise [40].

Non-linear Granger Causality – A number of extensions of Granger Causality have come up in order to make its estimation non-parametric [41] or to improve it in terms of applicability to non-linear data [24, 42, 43]. We allude here to the implementation in [24], which has come into wide use and also shown to have better performance than some of the other GC extensions [35]. This method is a kernel version of GC. Kernel algorithms basically embed data into a Hilbert space, and search for linear relations in that space. Hilbert spaces here are spaces of kernel functions, where these functions can be thought of as correlation or covariance functions. The nonlinearity of the regression model can be controlled by choosing different kernel functions such as a polynomial of appropriate order or a Gaussian kernel. Another advantage of the method is that it avoids the problem of overfitting which arises as the complexity of the model increases by use of a strategy based on the geometry of reproducing kernel Hilbert spaces [44].

Kernel based GC has been used for a number of applications with a majority of them being in the domain of neuroscience [24, 45, 46]. While the method has been demonstrated to perform well on autoregressive and simple deterministic chaotic coupled systems, it shows false-positive couplings in case of complex systems comprising of chaotic processes [35].

Convergent Cross Mapping (CCM) – While GC has been developed for stochastic processes where the influences of different causal variables can be well separated, Convergent Cross Mapping is developed for deterministic processes that are not completely random. Inspired from dynamical systems' theory, it can be applied even when causal variables have synergistic effects [28]. This method uses Takens' embedding theorem [47], in a fundamental way. According to this theorem, observations from a single variable of the system can be used to reconstruct the attractor manifold of the entire dynamical system. CCM exploits the fact that two variables will be causally related if they are from the same dynamical system. If a variable X causes Y, then the lagged (past) values of Y can help to estimate states of X. This is true because of Taken's theorem – manifold M_Y (or M_X) of any one observed variable Y, will have a diffeomorphism (one to one mapping that preserves differentiable structure) to the true manifold, M and hence the manifolds of two variables M_Y and M_X will be diffeomorphic. However, this cross mapping is not symmetric. If X is unidirectionally causing Y, past values of Y will have information about X, but not the other way round. Thus, the state of X will be predictable from M_Y, but Y not from M_X.

Though CCM doesn't perform a detailed model based analysis, it is based on the assumption that the data is from dynamical systems where Taken's embedding theorem holds. Hence, the method is invalid for time series such as those obtained from autoregressive processes. Also, the method has a number of weaknesses which have been demonstrated by its inability to detect correct causality strength and direction in several instances of intermediate to strong coupling between dynamical systems and also in the presence of noise [48, 49]. CCM has been applied to ecology studies [28, 50] as well as climate science [51].

There are several other causality methods based on the GC principle such as Partial Directed Coherence [52], Direct Transfer Function [53] and Modified Direct Transfer Function [54]. There are also a number of other methods based on non-linear state space analysis such as Predictability Improvement [55] and Topological Causality [29]. These methods are not as widely used as the above discussed methods. These have not been used anywhere in the thesis. We leave it at the mention of these methods and do not describe their working.

Model-based Causality Measures

In cases where domain-knowledge is available and it is easy to perform lab-experiments to develop causal models underlying the generation of provided time series data, model-based causality estimation methods can be used. These kind of methods are both hypothesis (model) and data led and rest on performing a comparison between a set of assumed models, selecting the best model and optimizing its parameters. Structural

Equation Modeling (SEM) [14] and Dynamic Causal Modeling (DCM) [56] are examples of these kinds of methods.

SEM includes a diverse set of computer algorithms, mathematical models and statistical methods that fit networks of constructs to data. The links between constructs of an SEM model may be estimated with independent regression equations or sometimes through more complicated techniques. In addition to being used in medicine, environmental science and engineering, SEM has also found applications in social science disciplines such as accounting and marketing [14]. On the other hand, DCM was developed in the context of neuroscience. Its objective is to estimate coupling between different brain regions and to identify how the coupling is affected by environmental changes (i.e. say, temporal or contextual). Models of interaction between different cortical areas (nodes) are formulated in terms of ordinary or stochastic differential equations. The activity of the hidden states of these nodes maps to the measured activity based on another model. Bayesian model inversion is done to determine the best model and its parameters for the system using the acquired data.

1.3 Important Research Gaps Identified

The three levels of statistical causality are useful as a broad framework for classifying existing methods of causality analysis in the sciences – this includes experimental, observational as well as those studying underlying causal mechanisms. On the other hand, the ladder of causation was recently introduced in the context of machine learning algorithms and to discuss their potential capabilities to make useful causal inferences.

It provides a classification for all possible levels of understanding that a causal learner is capable of. These levels of course are from a very human-centric understanding of causation. However, as humans, this is the best standard for classification that we have at our disposal. The ladder, hence, is a very useful tool to understand the futuristic properties that we should expect and try to develop in machines and algorithms if we want them to at least come to a level of causal understanding possible in humans.

In the context of time series causality estimation also, the ladder can be adapted to categorize existing methods. This would be useful in knowing where we stand and where we need to go. In fact, we can expect to develop the requisite causal capabilities in automated machines only if we can decipher causal relations using simple mathematical formulations and implement them as algorithms for given temporal data. We use the ladder here to demonstrate where the existing time series causality methods stand and to highlight the research gaps in literature. Figure 1.3 depicts the ladder, asking relevant 'Questions' for causation from a time series perspective, giving 'Examples' from everyday life and showing the time series analysis 'Methods' that fall in each category.

Data-driven measures such as GC and TE assume the inherent separability of 'cause' and 'effect' samples in time series data and are thus able to estimate only Associational Causality (Figure 1.3), which is at the first rung on the ladder of causation. While GC looks at the linear relationship between the cause-effect samples, TE uses the Markovian property of dependence between the samples. Non-linear Granger Causality is on the same boat as GC, instead of looking at linear relationship, it looks at non-linear relationship between samples. CCM can be thought of as being partly model-based and

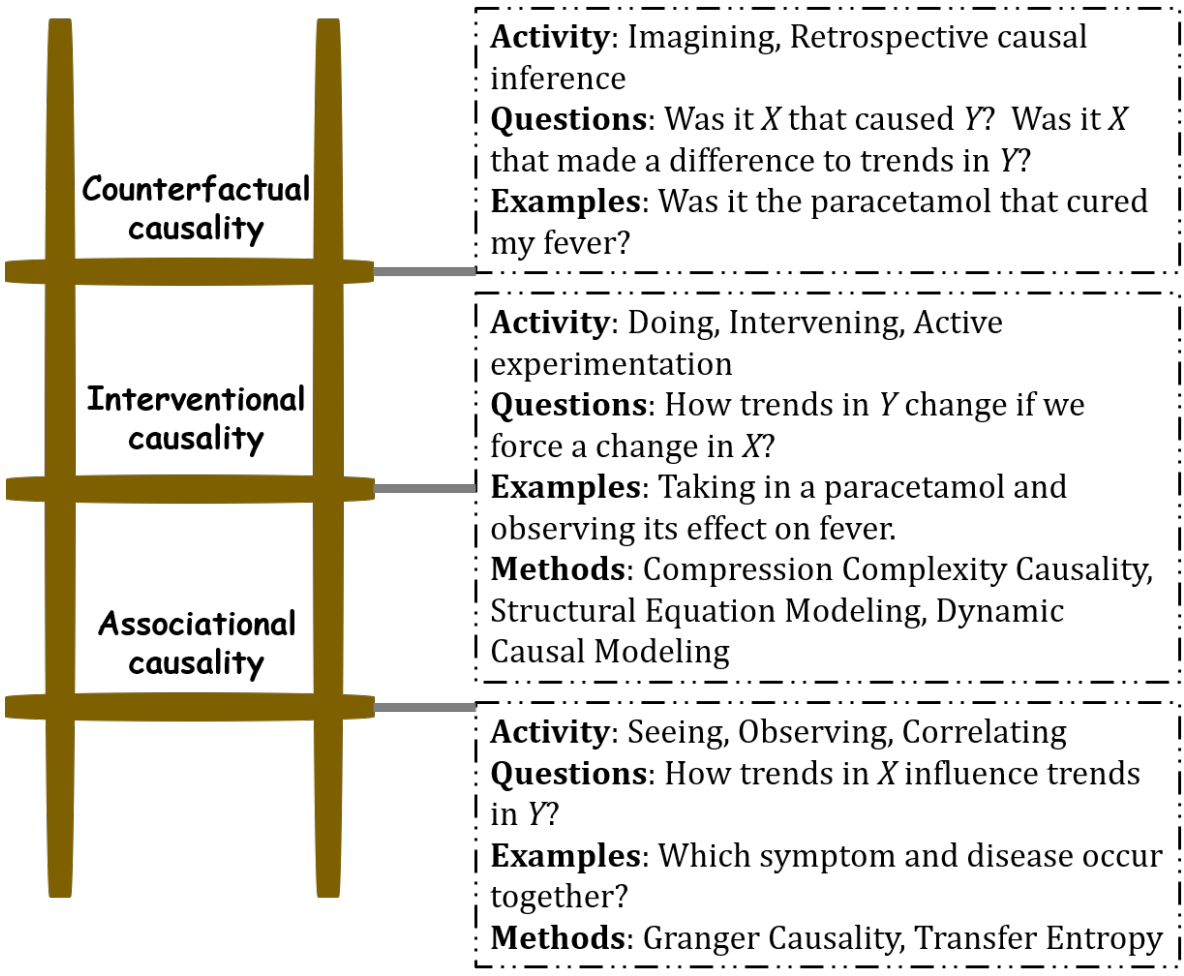

Figure 1.3: The Ladder of Causation, adapted from [15], for time series analysis.

partly associational. After assuming a generic model of dynamical system, it looks at the ability of the shadow attractor manifold of one time series to estimate the other time series. The latter is accomplished by estimating the correlation between the original and estimated time series.

Association being the most rudimentary form of estimating causation, associational causality methods suffer from some very evident limitations. Many a times, cause and effect may co-exist in blocks of measurements or a single measurement. This may be the inherent nature of the dynamics of the process or a result of sampling being

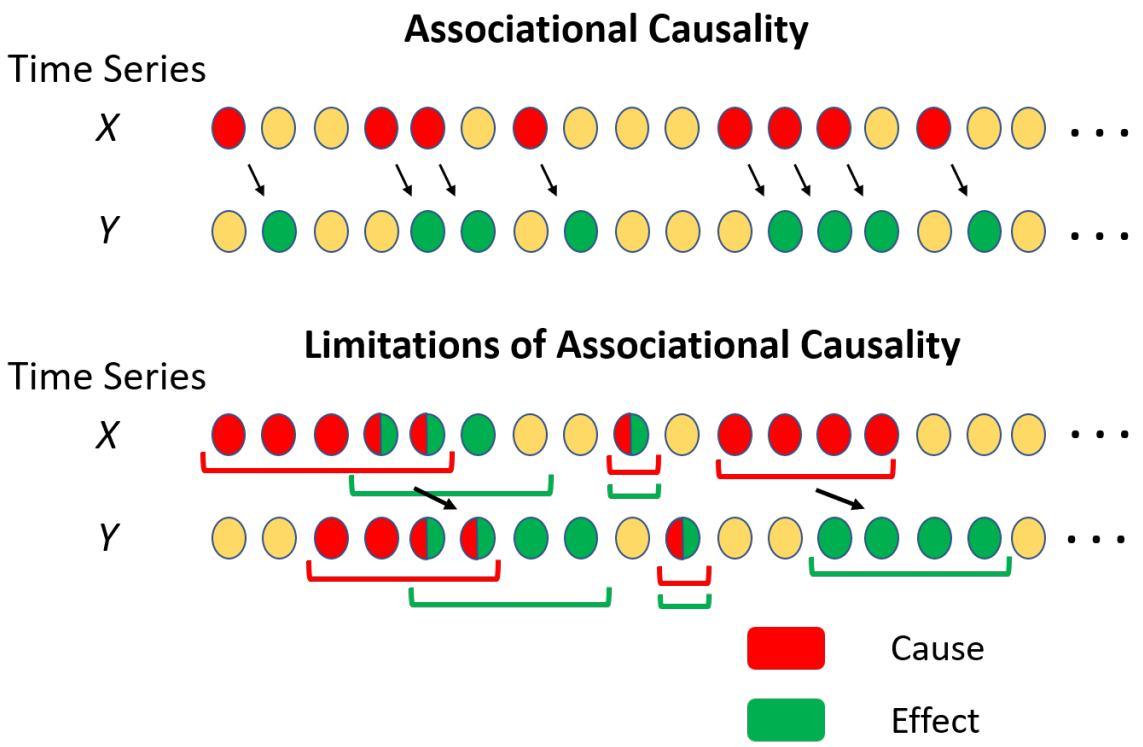

Figure 1.4: Associational Causality is based on cause-effect separability of samples. It has limitations when cause-effect samples are overlapping. It may happen for continuous time processes which when sampled may result in cause-effect information being simultaneously present in blocks of data or even in a single sample.

done at a scale different from the spatio-temporal scale of cause-effect dynamics (for example, during acquisition of measurements). Associational Causality measures are not appropriate in such scenarios. For a pair of time series X and Y, with X causing Y, an illustration of associatonal causality and its limitations are shown in Figure 1.4.

Model based causality methods can be said to be on the second level of Intervention on the ladder of causation. While these methods do not directly intervene, they invert the assumed model to obtain its various parameters based on the available data. The complete model can then be helpful to intervene, such as to make predictions about situations for which data is unavailable. However, the limitations of these methods is

that they are restricted to a few applications where domain-knowledge is available and reliable models can be constructed.

One of the major methodological gaps in the existing literature of time series causality estimation methods is the absence of data-driven measures that can inform of interventional causality. Further, each of the methods for data-driven causality estimation have their own specific limitations. While some methods are suitable for stochastic processes, others are contained only to deterministic processes [35]. In addition, as discussed in the description provided in their specific sections, the methods show poor performance in the presence of noise, short length of signals and subsampling [35–37, 48, 57]. With respect to applications to real-world datasets, each of these methods can be improved in myriad ways [58].

The field of causal inference is still a developing field. The initial resistance to causality as a science slowed down the progress and acceptance of the field (see Section 1.2.3). In the recent years, though the developed techniques have seen numerous applications, there are only a handful examples of the science being used to make theoretical and fundamental empirical advances in other disciplines. Of the existing few, one of the well known active areas of research in this regard is towards improving and innovating machine learning algorithms [15,59]. Others include applications in the field of communication systems [60] and thermodynamics [61, 62]. There are however many fields in which causality can make potential contributions. For instance, the field of *chaotic synchronization* which deals with coupled chaotic systems has seen a number of applications of causality measures [63, 64], but has still not seen any fundamental con-

tribution with respect to the mathematical aspects of synchronizing systems. Another example is the field of coupled *sparse* signals. Many natural signals such as human speech and natural images are sparse in some domain [65]. Model-based causality estimation methods are used regularly to estimate coupling between sparse signals [66, 67]. However, there is no literature investigating as to when and how data-driven methods can be used to infer causal relationships between these signals.

1.4 Structure and Focus of this Thesis

This thesis is divided into two parts and aims to fill the research gaps outlined above. In the first part of the thesis, we deal with the issues related to the methodology of existing data-driven time-series causality estimation methods. All existing methods test for causality by associational means and there is no measure to check for causality based on the higher levels on the ladder of causation. In addition, the existing methods have their specific limitations as discussed in Section 1.2.5. In order to infer higher levels of causation, we propose a novel data-based interventional causality estimation scheme and a practical implementation of a causality measure based on this scheme. This measure called *Compression-Complexity Causality (CCC)* is tested on simulated datasets and its performance is compared with existing methods. It is shown to overcome the limitations of existing methods in a number of realistic scenarios of low temporal resolution, filtering and missing samples. Post this, CCC is applied for some useful applications on real-world datasets. Also, an extension of CCC is proposed for estimating causal influences in networks.

In the second part of the thesis, the science of causality helps us to make some important contributions to other related disciplines especially those which deal with coupled systems. For example, we provide a *spatial* interpretation to the phenomenon of synchronization in coupled chaotic systems using the lens of causality testing. Synchronization has all along been thought of as a temporal phenomenon with research focusing on understanding the temporal conditions which lead systems to synchronization [68, 69]. For the first time, in our work, we provide (spatial) causal conditions to determine synchronizability of coupled chaotic systems. In this regard, we formulate and prove a *causal stability synchronization theorem* as a necessary and sufficient condition for synchronization and also provide empirical conditions to determine which variables of the given systems on coupling will lead the systems to synchronization.

Another domain which the thesis contributes to includes causality analysis of *sparse* signals, where, to the best of our knowledge, only model-based methods have been prevalent till date. We develop means that allow application of GC, a data-driven measure, to determine causal relations between sparse signals. The method proposed has the additional benefit of estimating causal relations in the *compressive* domain when *compressed sensing* [65] techniques are used to acquire or store signals.

We also look at analysis of processes which have been time-reversed, as in are made to exhibit reverse dynamics of the original process by flipping it along the temporal direction. For these processes, the assumption of 'cause preceding the effect' no longer holds. It thus becomes interesting to analyse and compare the behavior of time-series causality estimation methods on these processes. We also develop a means to check

whether the processes are *time-reversible* or *time-irreversible* (that is, whether or not the statistical properties of time-series change on reversing them).

In the following subsections, we elaborate on the contents of all the chapters in the two parts of the thesis.

1.4.1 Contents of Part I of the thesis

Part I of the thesis comprises of the following chapters. A synopsis of each of the chapters is provided.

- **Chapter 2** – Causality testing methods are being widely used in various disciplines of science. Model-free methods for causality estimation are very useful, as the underlying model generating the data is often unknown. However, existing model-free/data-driven measures assume separability of cause and effect at the level of individual samples of measurements and unlike model-based methods do not perform any intervention to learn causal relationships. These measures can thus only capture causality which is by the associational occurrence of 'cause' and 'effect' between well separated samples. In real-world processes, often 'cause' and 'effect' are inherently inseparable or become inseparable in the acquired measurements. In this chapter, a novel measure called Compression-Complexity Causality (CCC) is proposed that uses an adaptive interventional scheme to capture causality which is not merely associational. The scheme is based on characterizing complexities associated with the dynamical evolution of processes on short windows of measurements. The proposed measure, CCC, captures not only the

quantity (strength) of causality, but also its quality. The latter information is provided by the sign of the CCC value. How positive and negative CCC values result and the information they provide is also discussed in this chapter.

- **Chapter 3** – In this chapter, CCC is rigorously tested on simulations and its performance is compared with that of existing measures, Granger Causality and Transfer Entropy. Comparison with measures Convergent Cross Mapping and Non-linear Granger Causality is also done for some datasets. The proposed measure is shown to be robust to the presence of noise, long-term memory, filtering and decimation, low temporal resolution (including aliasing), non-uniform sampling, finite length signals and presence of common driving variables. Also, CCC is compared with model-dependent measure Dynamic Causal Modelling for a case of simulated fMRI signals. This chapter also discusses parameter selection criteria and rationale for CCC to be applied on different datasets. Analysis of computational time complexity as well as significance testing analysis for estimated CCC values are also discussed in this chapter.

- **Chapter 4** – Causality testing of time series data has numerous applications in fields such as earth sciences, neuroscience, econometrics, epidemiology and engineering. The strengths of CCC measure inherent in its formulation (discussed in Chapter 2) and as revealed from simulation studies (in Chapter 3) are expected to be useful in overcoming the limitations of existing measures for successfully determining causal relations from real-world datasets. In this chapter, CCC is applied

for testing causal interactions between populations of organisms in a predator-prey ecosystem as well as voltage-current recordings obtained from a squid giant axon. Further, causality analysis was done for analysing brain connectivity during fixation, instruction, planning and movement phases of a motor task presented to 5 human subjects. Motor tasks involve a complex process wherein signals are communicated between different brain regions. We use causality testing techniques CCC and Nonlinear Granger Causality and apply it on electroencephalographic time series data acquired from the subjects in order to understand connectivity at different stages of motor planning and movement process.

Causality testing techniques also find applications in some approaches to measure consciousness based on computing the strength of complex causal neural interactions in the brain. In this chapter, we propose a novel quantitative measure of consciousness - Network Causal Activity, which is based on CCC. This measure is used to distinguish different states of consciousness (awake and anaesthesia) based on analyzing electrocorticographic signals from the lateral cortex of four monkeys.

- **Chapter 5** – Most real-world systems are multivariate with complex network relationships. Discovering correct causal relationships is very important for such networks found in the study of fields such as climatology, epidemiology, neuroscience, economics etc. In order to capture causality from one variable to another in a network, in the presence of other variables which may or may not be having

causal influences to the considered target variable, use of conditional CCC, discussed in Chapter 2 has limitations and may not give accurate results. This is primarily because:

1. The formulation of conditional CCC does not allow us to capture the direct causal influence between variables, removing the indirect effects by intermediate variables in the causal pathway.
2. It is difficult to compute joint ETC for large number of variables. The large dictionaries constructed from the variables become difficult to handle, making complexity estimation inadequate over short lengths of data taken.

To address the above two problems, the concepts of Effective CCC and Equivalent ETC are introduced and defined in this chapter. Effective CCC is then used to estimate causal connections in simulated networks of autoregressive processes corrupted with measurement noise and having long term memory (simulated for short length time-series) and its performance is compared with that of multivariate Granger Causality.

1.4.2 Contents of Part II of the thesis

Part II of the thesis comprises of the following chapters. A synopsis of each of the chapters is provided.

- **Chapter 6** – Synchronization of chaotic systems is a ubiquitous phenomenon that arises when these systems are coupled. Chaotic synchronization has found

applications in living systems, human cognition and neuroscience as well as in physics, chemistry and engineering. In many natural and physiological instances, synchronization may occur desirably or undesirably. Causality testing has the potential to offer useful analysis tools to identify and deal with these occurrences in an appropriate manner. In this chapter, we deal with two-fold important aspects of synchronization using causality as described below:

1. Synchronization has been understood as a temporal phenomenon. Here, we use the lens of causality testing to provide a complementary spatial perspective to the phenomenon by introducing the novel idea of causal stability. We also propose and prove a causal stability synchronization theorem and propose an empirical criterion to identify synchronizing variables in coupled identical chaotic dynamical systems. This is an important theoretical contribution to the field of chaotic synchronization and causality testing and has potential for real world applications, such as in the control of chaos.

2. Anticipating Synchronization (AS) is a counterintuitive form of synchronization, where the slave (driven system) dynamics evolve ahead in time of the master (driving system) dynamics. This phenomenon has been found to be stable in several real systems. It is shown for the difficult case of an AS simulated system that Granger Causality fails in causality estimation. However, CCC, when used with high resolution (large bin size) of the data can inform correct causal relations.

- **Chapter 7** – Many naturally occurring signals such as human speech and natural images are sparse in some domain. Compressed sensing enables sparse signals to be acquired, stored and transmitted in a linearly compressed fashion and finds applications in magnetic resonance imaging, photography, transmission electron microscopy etc. Linear compression is achieved by matrix multiplication of the input sparse signals with a random sensing matrix (for e.g., independent Gaussian entries) and recovery is enabled by nonlinear optimization techniques. Causality testing on such data is required to make useful inferences without reconstructing them to the sparse domain. Also, for some cases, it may be impossible to determine causal structure for data in sparse domain without the assumption of a model for given data. In this chapter, we design structured sensing matrices having Toeplitz and Circulant structure that preserve causality (as measured by Granger Causality) between sparse autoregressive coupled input signals in the compressed domain. An application is also shown for real sparse neural signals, where Granger Causality is unable to detect the correct causality in the sparse domain, but the causality becomes discoverable in the compressed domain by application of these structured sensing matrices.

- **Chapter 8** – Detection of temporal reversibility of a given process is an interesting time series analysis scheme. Apart from itself serving as a feature to characterize time series processes (such as non-linear processes), it also gives insights on the underlying processes generating the data. Moreover, time reversal

of given data provides a promising tool for analysis of causality measures as well as studying causal properties of processes. Reversibility detection measures have been widely employed for the study of ecological, epidemiological and physiological time series. Effort-to-Compress (ETC) is a well-established robust method to characterize complexity of time series for analysis and classification. CCC, a causality measure based on ETC, proposed in Chapter 2, captures data-driven interventional causality. It is shown to give reliable performance for measurements from stochastic, chaotic and real-world systems in Chapters 3 and 4. In this chapter, we apply CCC on time-reversed coupled processes and show that the measure is free of the assumption that 'the cause precedes the effect', making it a great tool for causal analysis of reversible processes. Further, we propose a novel measure for detection of temporal reversibility of processes, called the Compressive potential based asymmetry measure. Compressive potential is computed based on the ETC algorithm. The asymmetry measure compares the probability of occurrence of patterns at different scales between the forward time and time-reversed process. We test the performance of Compressive potential asymmetry measure on a number of simulated processes.

Suggested reading order – It is suggested that Chapters 2 and 3 be read first in that order. Chapters 2 and 3 are prerequisites for Chapters 4, 5, 6 and 8. Also, Chapter 5 is a prerequisite for Chapter 8. Chapter 7 is stand alone. Chapter 9 is to be read last.

Part I

Contributions to Causal Inference

Chapter 2

A Novel Measure: Compression-Complexity Causality

Causality testing methods are being widely used in various disciplines of science. Model-free methods for causality estimation are very useful, as the underlying model generating the data is often unknown. However, existing model-free/data-driven measures assume separability of cause and effect at the level of individual samples of measurements and unlike model-based methods do not perform any intervention to learn causal relationships. These measures can thus only capture causality which is by the associational occurrence of 'cause' and 'effect' between well separated samples. In real-world processes, often 'cause' and 'effect' are inherently inseparable or found to be inseparable in the acquired measurements. In this chapter, a novel measure called Compression-Complexity Causality (CCC) is proposed that uses an adaptive interventional scheme to capture causality which is not merely associational. The scheme is based on characterizing complexities associated with the dynamical evolution of processes on short windows of measurements. The proposed measure, CCC, captures not only the quantity

(strength) of causality, but also its quality. The latter information is provided by the sign of the CCC value. How positive and negative CCC values result and the information they provide is also discussed in this chapter.

2.1 Introduction

The 'Ladder of Causation' very rightly arranges hierarchically the abilities of a causal learner [15]. The three levels proposed are − 1. Association, 2. Intervention and 3. Counterfactuals, when arranged from the lower rung to the higher rung. Currently, causality learning and inferring algorithms using only data are still stuck at the lowermost rung of 'Association'.

Measures such as Granger Causality (GC) [5] and its various modifications [24, 41], as well as, Transfer Entropy (TE) [23] that are widely being used across various disciplines of science — neuroscience [16,17], climatology [18,19], econometrics [20,21], engineering [22] etc., are largely 'model-free'/ 'data-driven' measures of causality. The working of these measures is briefly discussed in Chapter 1. These measures make minimal assumptions about the underlying physical mechanisms and depend more on time series characteristics [16]. Hence, they have a wider scope compared to specific model assumptions made by methods such as Dynamic Causal Modelling [56] and Structural Equation Modeling [14]. However, the assumptions made by these methods are often ignored in practice, resulting in erroneous causality estimates on real world datasets. These measures can accurately quantify the degree of coupling between given time series only if assumptions (such as linearity, stationarity and presence of Gaussian

noise in case of GC and stationarity, markovian in case of TE) are satisfied. Thus, these methods, when correctly applied, can infer the presence of causality when it is by 'association' alone and not due to higher levels on the Ladder of Causation. To explain this better, consider a case where the 'cause' and 'effect' are inseparable. This can happen even when the time series satisfies stationarity but is non-markovian or in several instances when it is non-stationary. In fact, the stated assumptions are quite unlikely to be met in practice considering that acquired data are typically samples of continuous/discrete evolution of real world processes. These processes might be evolving at spatio-temporal scales very different from the scales of measurements. As a result, cause and effect may co-exist in a single measurement or overlap over blocks of measurements, making them inseparable. In such a scenario, it would be incorrect to estimate causality by means of correlations and/or joint probabilities which implicitly assumes the separability of 'cause' and 'effect'. Both GC and TE make this assumption of separability. Circularly, to characterize a time series sample as purely a 'cause' or an 'effect' is possible only if there is a clear linear/markovian separable relationship. When cause and effect are inseparable, 'associational' measures of causality such as GC and TE are insufficient and we need a method to climb up the ladder of causation.

Intervention based approaches to causality rank higher than association. It involves not just observing regularities in the data but actively changing what is there and then observing its effect. In other words, we are asking the question — *what will happen if we 'do' something?* Given only data and not the power to intervene on the experimental set up, intervention can only be done by building strong, accurate models. Model-

based causality testing measures, alluded to before and discussed in Section 1.2.5, will fall in this category. They invert the model to obtain its various parameters, and then intervene to make predictions about situations for which data is unavailable. However, these methods are very domain specific and the models require specific knowledge about the data. With insufficient knowledge about the underlying model which generated the data, such methods are inapplicable.

Given only data that has already been acquired without any knowledge of its generating model or the power to intervene on the experimental/real-world setting, we can ask the question — what kind of intervention is possible (if at all) to infer causality? The proposed 'interventional causality' approach will not merely measure 'associational causality' because it does not make the assumption that the cause and its effect are present sample by sample (separable) as is done by existing model-free, data based methods of causality estimation.

Even in cases where cause and its effect are inseparable, which is probably true for most real-world processes, the change in the dynamics of processes would contain information about causal influences between them. With this understanding, we propose the novel idea of data-based, model-free **Interventional Complexity Causality (ICC)**. The notion of ICC is formalized using Compression-Complexity to define **Compression-Complexity Causality (CCC)**.

Other methods for causality estimation based on compression have been proposed in literature [70, 71], but the very philosophy behind our method and its implementation are very different from these existing methods.

In this chapter, we first introduce the idea of Dynamical Complexity and its specific realization Dynamical Compression-Complexity. These are discussed in Section 2.2. ICC and its specific case CCC are discussed in Section 2.3. CCC shows some interesting properties. The sign of CCC value helps to give information on the 'qualitative' nature of causality. How positive and negative CCC are a possibility and what are its implication on the kind of causal influence is detailed in Section 2.4.

2.2 Dynamical Complexity (DC) and Dynamical Compression-Complexity (CC)

There can be scenarios where cause and effect co-exist in a single temporal measurement or blocks of measurements. For example, this can happen (a) inherently in the dynamics of the generated process, (b) when cause and effect occur at different spatio-temporal scales, (c) when measurements are acquired at a scale different from the spatio-temporal scale of the cause-effect dynamics (continuous or discrete). In such a case, probabilities of joint occurrence is too simplistic an assumption to capture causal influences. On the other hand, the very existence of causality here is actually resulting in a change of joint probabilities/correlations which cannot be captured by an assumption of static probabilities. To overcome this problem, we capture causality using the idea of *dynamical complexity*. Inseparable causal influences within a time series (or between two time series) would be reflected in their dynamical evolution. Dynamical Complexity (DC) of a single time series X is defined as below -

$$DC(\Delta X|X_{past}) = C(X_{past} + \Delta X) - C(X_{past}), \tag{2.1}$$

where ΔX is a moving window of length w samples and X_{past} is a window consisting of immediate past L samples of ΔX. '+' refers to appending, for e.g., for time series $A = [1, 2, 3]$ and $B = [p, q]$, then $A + B = [1, 2, 3, p, q]$. $C(X)$ refers to complexity of time series X. DC, thus varies with the temporal index of ΔX and can be averaged over the entire time series to estimate its average DC.

It is important to note that dynamical complexity is very different from *complexity rate* (CR), which can be estimated as follows -

$$CR(\Delta X|X_{past}) = C(X_{past}, \Delta X) - C(X_{past}), \tag{2.2}$$

where $C(X_{past}, \Delta X)$ is the *joint* complexity of X_{past} and ΔX. Complexity rate can be seen as a generalization of Shannon entropy rate [72], the difference being that the former can be computed using any notion of complexity, not just entropy. As is evident from the equation, CR is estimated based on the joint occurrences of ΔX and X_{past}, while DC captures temporal change in complexities on the evolution of the process. In case of inseparability of cause and effect, it would be inappropriate to use CR to infer causal relationships.

Now for this notion of "complexity", that has been referred to in this section several times, there is no single unique definition. As noted in [73], Shannon entropy [72] is a very popular and intuitive measure of complexity. A low value of Shannon entropy indicates high redundancy and structure (low complexity) in the data and a high value indicates low redundancy and high randomness (high complexity). For ergodic sources, owing to Shannon's noiseless source coding theorem [72], (lossless) compressibility of

the data is directly related to Shannon entropy. However, robustly estimating compressibility using Shannon entropy for short and noisy time series is a challenge [74]. Recently, the notion of compression-complexity has been introduced [74] to circumvent this problem. Compression-complexity defines the complexity of a time series by using optimal lossless data compression algorithms. It is well acknowledged that data compression algorithms are not only useful for compression of data for efficient transmission and storage, but also act as models for learning and statistical inference [75]. Lempel-Ziv (LZ) Complexity [76] and Effort-To-Compress (ETC) [77] are two measures which fall in this category.

As per the minimum description length principle [78], that formalizes the Occam's razor, the best hypothesis (model and its parameters) for a given set of data is the one that leads to its best compression. Extending this principle for causality, an estimation based on dynamical complexity (compressibility) of time series would be the best possible means to capture causally influenced dynamics.

Out of the complexity measures discussed before, ETC seemed to be most suitable for estimation of dynamical complexity. It has been demonstrated that both LZ and ETC outperform Shannon entropy in accurately characterizing the dynamical complexity of both stochastic (Markov) and deterministic chaotic systems in the presence of noise [73, 74]. Further, ETC is shown to reliably capture complexity of very short time series where even LZ fails [74], and for analyzing short RR tachograms from healthy young and old subjects [79]. Recently, ETC has been used to propose a compression-complexity measure for networks [80].

Though we intend to use ETC as a compression-complexity measure for estimating dynamical complexity, we briefly discuss the origin of ETC and its relation to data compression. ETC is defined as the effort to compress the input sequence using the lossless compression algorithm known as Non-sequential Recursive Pair Substitution (NSRPS) [81]. An offline grammar based data compression algorithm, very similar to the NSRPS scheme, called 'Re-Pair', has also been developed and used independently. Re-Pair has been shown to achieve high lossless compression ratios and to offer good performance for decompression but has the drawback of high memory consumption [82].

In order to faithfully capture the process dynamics, DC is required to be estimated on overlapping short-length windows of time series data. Infotheoretic quantities (like shannon entropy), which are based on computation of probability densities, are not the ideal choice here (owing to finite-length effects). Compression-complexity measures are more appropriate choices. Because of the advantages of ETC over LZ mentioned above, we use ETC to formulate our measure of causality discussed in the next section. Before that, we describe how individual and joint compression complexities are computed using ETC [77] in the subsections below.

2.2.1 ETC measure for a time series: $ETC(X)$

Since ETC expects a symbolic sequence as its input (of length > 1), the given time series should be binned appropriately to generate such a sequence. Once such a symbolic sequence is available, ETC proceeds by parsing the entire sequence (from left to right) to find that pair of symbols in the sequence which has the highest frequency of occurrence.

This pair is replaced with a new symbol to create a new symbolic sequence (of shorter length). This procedure is repeated iteratively and terminates only when we end up with a constant sequence (whose entropy is zero since it consists of only one symbol). Since the length of the output sequence at every iteration decreases, the algorithm will surely halt. The number of iterations needed to convert the input sequence to a constant sequence is defined as the value of ETC complexity. For example, the input sequence '12121112' gets transformed as follows: $12121112 \mapsto 33113 \mapsto 4113 \mapsto 513 \mapsto 63 \mapsto 7$. Thus, $ETC(12121112) = 5$. ETC achieves its minimum value (0) for a constant sequence and maximum value $(m-1)$ for a m length sequence with distinct symbols. Thus, we normalize the ETC complexity value by dividing by $m-1$. Thus normalized $ETC(12121112) = \frac{5}{7}$. Note that normalized ETC values are always between 0 and 1 with low values indicating low complexity and high values indicating high complexity.

2.2.2 Joint ETC measure for a pair of time series: $ETC(X, Y)$

We perform a straightforward extension of the above mentioned procedure ($ETC(X)$) for computing the joint ETC measure $ETC(X, Y)$ for a pair of input time series X and Y of the same length. At every iteration, the algorithm scans (from left to right) simultaneously X and Y sequences and replaces the most frequent jointly occurring pair with a new symbol for both the pairs. To illustrate it by an example, consider, $X = 121212$ and $Y = abacac$. The pair (X, Y) gets transformed as follows: $(121212, abacac) \mapsto (1233, abdd) \mapsto (433, edd) \mapsto (53, fd) \mapsto (6, g)$. Thus, $ETC(X, Y) = 4$ and normalized value is $\frac{4}{5}$. It can be noted that $ETC(X, Y) \leq ETC(X) + ETC(Y)$.

2.3 Interventional Complexity Causality (ICC) and Compression-Complexity Causality (CCC)

To measure how the dynamics of a process Y influence the dynamics of a process X, we intervene to create new hypothetical blocks of time series data, $Y_{past} + \Delta X$, where Y_{past} is a window of length L samples, taken from the immediate past of the window ΔX. These blocks are created by 'surgery' and do not exist in reality in the data that is already collected. Interventional Complexity Causality (ICC) is defined as the change in the dynamical complexity of time series X when ΔX is seen to be generated jointly by the dynamical evolution of both Y_{past} and X_{past} as opposed to by the reality of the dynamical evolution of X_{past} alone.

This formulation is actually in line with Wiener's idea, according to which, time series Y causes X, if incorporating the past of Y helps to improve the prediction of X [27]. While GC is based on the notion of improved predictability and TE on reduction of uncertainty, ICC is based on the notion of change in 'dynamical complexity' when information from the past of Y is brought in, in order to check its causal influence on X. The difference between existing approaches and the proposed measure is that the effect of Y on X is analyzed based on 'associational' means in case of the former and by 'interventional' means in case of the latter. With this formulation, ICC is designed to measure *effect*, like GC and TE and not the *mechanism*, as in Dynamic Causal Modelling [16, 83]. To elaborate on this aspect, ICC cannot explicitly quantify the interaction coefficients of the underlying generative model (physical mechanism), but

will only estimate causal influence based on change in dynamical complexities. It is, however, expected that ICC will be closer to the underlying mechanism than existing methods, because, by its very formulation, it taps on causes and their effects based on dynamical evolution of processes.

Mathematically,

$$ICC_{Y_{past}\rightarrow\Delta X} = DC(\Delta X|X_{past}) - DC(\Delta X|X_{past}, Y_{past}), \tag{2.3}$$

where $DC(\Delta X|X_{past})$ is as defined in Eq. 2.1 and $DC(\Delta X|X_{past}, Y_{past})$ is as elaborated below:

$$DC(\Delta X|X_{past}, Y_{past}) = C(X_{past} + \Delta X, Y_{past} + \Delta X) - C(X_{past}, Y_{past}), \tag{2.4}$$

where $C(\cdot, \cdot)$ refers to joint complexity. ICC varies with the moving temporal window ΔX and its corresponding Y_{past}, X_{past}. To estimate average causality from time series Y to X, $ICC_{Y_{past}\rightarrow\Delta X}$ obtained for all ΔXs are averaged.

The above is the generic description of ICC that can be estimated using any complexity measure. For the reasons discussed in Section 2.2, we would like to estimate ICC using the notion of Dynamical Compression-Complexity estimated by the measure ETC. The measure would then become Interventional Compression-Complexity Causality. For succinctness, we refer to it as Compression-Complexity Causality or CCC. To estimate CCC, time series blocks X_{past}, Y_{past}, $X_{past} + \Delta X$, and surgically created $Y_{past} + \Delta X$ are separately encoded (binned) — converted to a sequence of symbols using 'B' uniformly sized bins for the application of ETC[1]. For the binned time series

[1]Henceforth, the same variables are used to denote the binned/encoded versions of the blocks.

blocks, X_{past}, Y_{past}, $X_{past} + \Delta X$, $Y_{past} + \Delta X$, to determine whether Y_{past} caused ΔX or not, we first compute dynamical compression-complexities, denoted by CC,

$$CC(\Delta X|X_{past}) = ETC(X_{past} + \Delta X) - ETC(X_{past}), \tag{2.5}$$

$$CC(\Delta X|X_{past}, Y_{past}) = ETC(X_{past} + \Delta X, Y_{past} + \Delta X) - ETC(X_{past}, Y_{past}), \tag{2.6}$$

Eq. 2.5 gives the dynamical compression-complexity of ΔX as a dynamical evolution of X_{past} alone. Eq. 2.6 gives the dynamical compression-complexity for ΔX as a dynamical evolution of both X_{past} and Y_{past}. $ETC(\cdot)$ and $ETC(\cdot, \cdot)$ refer to individual and joint *effort-to-compress* complexities. For estimating ETC from these small blocks of data, short-term stationarity of X and Y is assumed.

We now define Compression-Complexity Causality $CCC_{Y_{past} \to \Delta X}$ as:

$$CCC_{Y_{past} \to \Delta X} = CC(\Delta X|X_{past}) - CC(\Delta X|X_{past}, Y_{past}). \tag{2.7}$$

Averaged CCC from Y to X over the entire length of time series with the window ΔX being slided by a step-size of δ is estimated as —

$$CCC_{Y \to X} = \overline{CCC}_{Y_{past} \to \Delta X} = \overline{CC}(\Delta X|X_{past}) - \overline{CC}(\Delta X|X_{past}, Y_{past}), \tag{2.8}$$

If $\overline{CC}(\Delta X|X_{past}, Y_{past}) \approx \overline{CC}(\Delta X|X_{past})$, then $CCC_{Y \to X}$ is statistically not different from zero, implying no causal influence from Y to X. At times, if obtained $CCC_{Y \to X}$ is non-zero and high, that may also mean no causation. But, at this time $CCC_{Y \to X}$ should be statistically significantly not different from the population of CCC values obtained from surrogate data generated by random shuffling[2] of observations of Y (X

[2]The aim here is to destroy the temporal structure in the driver or 'cause' time series (i.e., the time series from which causal influence is to be checked to the other time series).

can be kept intact in this case). The destruction of temporal structure in Y results in an increase in $CCC_{Y\to X}$ compared to when the causal structure was intact. However, if $CCC_{Y\to X}$ is statistically significantly different from zero and is also less than the highest possible $CCC_{Y\to X}$, obtained by surrogate analysis as described above, then we infer that Y causes X. Random shuffling of Y provides an upper bound for CCC at which there exists no causation. For details and demonstration of surrogate significance testing analysis, please see Section 3.4.2. The reason for existence of data-dependent upper bound for CCC is also discussed in the same section.

In general, for values of CCC between zero and the upper bound, a higher magnitude of $CCC_{Y\to X}$ implies a higher degree of causation from Y to X. The length of X_{past}, Y_{past}, L is chosen by determining the correct intervention point. This is the temporal scale at which Y has a dynamical influence on X. Detailed criteria and rationale for estimating L and other parameters used in CCC estimation: w (length of ΔX), δ and B for any given pair of time series are discussed in Chapter 3 (Section 3.3).

CCC is invariant to local/global scaling and addition of constant value to the time series. As CCC is based on binning of small blocks of time series data, it is noise resistant. Furthermore, it is applicable to non-linear and short term stationary time series. Being based on dynamical evolution of patterns in the data, it is expected to be robust to sub-sampling and filtering.

For multivariate data, CCC can be estimated in a similar way by building dictionaries that encode information from all variables. Thus, to check conditional causality from Y to X amidst the presence of other variables (say Z and W), two time varying

dictionaries are built — D that encodes information from all variables (X, Y, Z, W) and D' that encodes information from all variables except Y (X, Z, W only). Once synchronous time series blocks from each variable are binned, the dictionary at that time point is constructed by obtaining a new sequence of symbols, with each possible combination of symbols from all variables being replaced by a particular symbol. The mechanism for construction of these dictionaries is discussed in the next subsection. Subsequently, dynamical compression-complexities are computed as:

$$CC(\Delta X|D'_{past}) = ETC(D'_{past} + \Delta X) - ETC(D'_{past}), \tag{2.9}$$

$$CC(\Delta X|D_{past}) = ETC(D_{past} + \Delta X) - ETC(D_{past}), \tag{2.10}$$

where $D'_{past} + \Delta X$ represents the lossless encoding of joint occurrences of binned time series blocks X_{past}+ΔX, Z_{past}+ΔX, W_{past}+ΔX and D'_{past} refers to the lossless encoding of joint occurrences of binned time series blocks X_{past}, Z_{past} and W_{past}. Similarly, $D_{past} + \Delta X$ represents the lossless encoding of joint occurrences of binned time series blocks $X_{past} + \Delta X$, $Y_{past} + \Delta X$,$Z_{past} + \Delta X$, $W_{past} + \Delta X$ and D_{past} refers to the the lossless encoding of joint occurrences of binned time series blocks X_{past}, Y_{past}, Z_{past} and W_{past}.

Conditional Compression-Complexity Causality, $CCC_{Y_{past}\rightarrow\Delta X|Z_{past},W_{past}}$, is then estimated as the difference of Eq. 2.9 and Eq. 2.10. Averaged Conditional Compression Complexity-Causality over the entire time series with the window ΔX being slided by a step-size of δ is given as below:

$$CCC_{Y\rightarrow X|Z,W} = \overline{CC}(\Delta X|D'_{past}) - \overline{CC}(\Delta X|D_{past}). \tag{2.11}$$

2.3.1 Dictionary building for conditional CCC

To estimate causality from time series Y to X, amidst the presence of other variables (say Z and W), two time varying dictionaries are built — D that encodes information from all variables (X, Y, Z, W) and D' that encodes information from all variables except Y (X, Z, W only). Suppose the time series blocks being considered at a time t are X_{past}, Y_{past}, Z_{past} and W_{past}, then the dictionary at that time D_{past} is built as follows. Suppose (for example)

$$\begin{pmatrix} X_{past} \\ Y_{past} \\ Z_{past} \\ W_{past} \end{pmatrix}$$

blocks of length 4 time points take values

$$\begin{pmatrix} 0 & 0 & 1 & 0 \\ 1 & 0 & 1 & 0 \\ 1 & 1 & 1 & 1 \\ 0 & 1 & 1 & 1 \end{pmatrix},$$

after each time series block (such as X_{past}) is binned using 2 bins. Then encoding in D_{past} is done based on assigning a particular value to each column. As each row in the first column can take 2 values, there exists a total of 16 possible combinations that the 4 rows can take together in a column. We encode information in 4 rows to a single row by assigning combinations of different values in the 4 rows an encoding from '0' to '15'. In the dictionary D_{past}, the above sequences are encoded as a single sequence —

$$\begin{pmatrix} 6 & 3 & 15 & 3 \end{pmatrix}.$$

The second dictionary D'_{past} at the same time constructed using all variables except Y similarly encodes blocks

$$\begin{pmatrix} X_{past} \\ Z_{past} \\ W_{past} \end{pmatrix}$$

taking values

$$\begin{pmatrix} 0 & 0 & 1 & 0 \\ 1 & 1 & 1 & 1 \\ 0 & 1 & 1 & 1 \end{pmatrix}$$

as

$$\begin{pmatrix} 2 & 3 & 7 & 3 \end{pmatrix}$$

assigning each column one particular state out of 8 possible states. Thus, for the above example, $D = (6, 3, 15, 3)$ and $D' = (2, 3, 7, 3)$. ETC can now be applied on the two dictionaries D and D' as these sequences are now just 1-dimensional symbolic sequences.

2.4 Positive and Negative CCC

The dynamical compression-complexities estimated for the purpose of CCC estimation, $CC(\Delta X|X_{past})$ and $CC(\Delta X|X_{past}, Y_{past})$, can be either positive or negative. For instance, consider the case when $CC(\Delta X|X_{past})$ becomes negative. This happens when $ETC(X_{past} + \Delta X)$ is less than $ETC(X_{past})$, which means that with the appending of ΔX, the sequence X_{past} has become more structured resulting in reduction of its complexity. The value of $CC(\Delta X|X_{past})$ is positive when appending of ΔX makes X_{past} less structured (hence more complex). Similarly, $CC(\Delta X|X_{past}, Y_{past})$ can also become negative when ETC realizes $X_{past} + \Delta X$, $Y_{past} + \Delta X$ to be more structured than X_{past}, Y_{past}. When the opposite is true, $CC(\Delta X|X_{past}, Y_{past})$ is positive.

Because of the values that $CC(\Delta X|X_{past})$ and $CC(\Delta X|X_{past}, Y_{past})$ can take, $CCC_{Y_{past}\rightarrow\Delta X}$ can be both positive or negative. How different cases result with different signs of the two quantities along with their implication on CCC is shown in Table 2.1. We see that the sign of $CCC_{Y_{past}\rightarrow\Delta X}$ signifies the 'kind of dynamical influence' that Y_{past} has on ΔX, whether this dynamical influence is similar to or different from that of X_{past} on ΔX. When $CCC_{Y_{past}\rightarrow\Delta X}$ is $-ve$, it signifies that Y_{past} has a different dynamical influence on ΔX than X_{past}. On the contrary, when $CCC_{Y_{past}\rightarrow\Delta X}$ is $+ve$, it signifies that Y_{past} has a dynamical influence on ΔX that is similar to that of X_{past}. On estimating the averaged CCC from time series Y to X, expecting that $CCC_{Y_{past}\rightarrow\Delta X}$ values do not vary much with time, we can talk about the kind of dynamical influence that time series Y has on X. For weak sense stationary processes, it is intuitive that the influence of Y on X would be very different from that on X due to its own past when the distributions of coupled time series Y and X are very different.

We verify this intuition by measuring probability distribution distances[3] between coupled processes Y and X using symmetric Kullback-Leibler Divergence (KL) and Jensen-Shannon Divergence (JSD). The trend of values obtained by these divergence measures is compared with the trend of CCC for different cases such as when CCC is positive or negative.

Unidirectionally coupled autoregressive (AR) processes were generated as per Eq. 3.1. Linearly (unidirectionally) coupled tent maps were generated as per Eqs. 3.3, 3.4 and

[3]It should be mentioned that strictly speaking KL and JSD are not distance measures since they don't satisfy the triangle inequality.

Table 2.1: Sign of Dynamical Compression-Complexities, $CC(\Delta X|X_{past})$ and $CC(\Delta X|X_{past}, Y_{past})$, and their resulting implication on the sign of estimated Compression Complexity-Causality, $CCC_{Y_{past}\to\Delta X}$.

$CC(\Delta X\|X_{past}, Y_{past})$ / $CC(\Delta X\|X_{past})$	$-ve$	$+ve$
$-ve$	$X_{past}+\Delta X$ was more structured than X_{past}. Further, two cases arise. 1. When $\|CC(\Delta X\|X_{past})\| > \|CC(\Delta X\|X_{past}, Y_{past})\|$, $CCC_{Y_{past}\to\Delta X} < 0$. Here, intervention by Y_{past} in the joint case **degraded the structure** by bringing patterns different from X_{past}. Dynamical influence of Y_{past} on ΔX is very different from the dynamical influence of X_{past} on ΔX. e.g.: CCC from independent tent map to dependent tent map. 2. When $\|CC(\Delta X\|X_{past})\| < \|CC(\Delta X\|X_{past}, Y_{past})\|$, $CCC_{Y_{past}\to\Delta X} > 0$. Intervention by Y_{past} in the joint case **enhanced the structure** by bringing patterns similar to X_{past}. Dynamical influence of Y_{past} on ΔX is very similar to the dynamical influence of X_{past} on ΔX .e.g.: CCC from independent autoregressive (AR) process to dependent AR process.	$CCC_{Y_{past}\to\Delta X}$ is $-ve$ always. $X_{past}+\Delta X$ was more structured than X_{past}. Intervention by Y_{past} in the joint case **degraded the structure**. Dynamical influence of Y_{past} on ΔX is very different from the dynamical influence of X_{past} on ΔX. e.g.: CCC from independent tent map to dependent tent map.
$+ve$	$CCC_{Y_{past}\to\Delta X}$ is $+ve$ always. $X_{past}+\Delta X$ was less structured than X_{past}. Intervention by Y_{past} in the joint case **enhanced the structure** by bringing patterns similar to X_{past}. Dynamical influence of Y_{past} on ΔX is very similar to the dynamical influence of X_{past} on ΔX.	$X_{past}+\Delta X$ was less structured than X_{past}. Further, two cases arise. 1. When $\|CC(\Delta X\|X_{past})\| > \|CC(\Delta X\|X_{past}, Y_{past})\|$, $CCC_{Y_{past}\to\Delta X} > 0$. Here, intervention by Y_{past} in the joint case **enhanced the structure** by bringing patterns similar to X_{past}. Dynamical influence of Y_{past} on ΔX is very similar to the dynamical influence of X_{past} on ΔX. 2. When $\|CC(\Delta X\|X_{past})\| < \|CC(\Delta X\|X_{past}, Y_{past})\|$, $CCC_{Y_{past}\to\Delta X} < 0$. Intervention by Y_{past} in the joint case **degraded the structure** by bringing patterns different from X_{past}. Dynamical influence of Y_{past} on ΔX is very different from the dynamical influence of X_{past} on ΔX .

non-linearly (unidirectionally) coupled tent maps were generated as per Eqs. 3.3, 3.5. Symmetric KL and JSD between distribution P and Q of coupled processes are estimated as per Eq. 2.12 and 2.14 respectively.

$$D_{\text{Symm KL}}(P, Q) = D_{\text{KL}}(P\|Q) + D_{\text{KL}}(Q\|P), \tag{2.12}$$

where,

$$\begin{aligned} D_{\text{KL}}(P\|Q) &= \sum_i P(i)\, \log\left(\frac{P(i)}{Q(i)}\right), \\ D_{\text{KL}}(Q\|P) &= \sum_i Q(i)\, \log\left(\frac{Q(i)}{P(i)}\right). \end{aligned} \tag{2.13}$$

$$\text{JSD}(P \parallel Q) = \frac{1}{2}D(P \parallel M) + \frac{1}{2}D(Q \parallel M), \tag{2.14}$$

where, $M = \frac{1}{2}(P + Q)$. Here, KL and JSD values are in units of nats.

Curves for KL, JSD and CCC estimated for increasing coupling between AR processes of order 1 and linearly as well as non-linearly coupled tent maps are shown in Figures 2.1, 2.2 and 2.3 respectively. The values displayed represent the mean over 50 trials. As the degree of coupling is varied for AR processes, there is no clear pattern in KL and JSD values. CCC values increase in the positive direction for increasing coupling, signifying that the dynamical influence from Y to X is similar to the influence on X from its own past. Also, when we took larger number of trials for AR, the values obtained by KL and JSD become confined to a smaller range and seem to converge towards a constant value indicating that the distributions of X and Y are quite similar. However, in case of coupled tent maps (both linear and non-linear coupling), as coupling is increased, the divergence between the distributions of the two coupled processes

increases, indicating that their distributions are becoming very different. The values of CCC grow in the negative direction showing that with increasing coupling the independent process Y has a very different dynamical influence on X compared to X's own past. Subsequently, due to the synchronization of Y and X, KL, JSD as well as CCC become zero. With these graphs, it may not be possible to find an universal threshold for the absolute values of KL/JSD above which CCC will show negative sign. However, if the distributions of the two coupled processes exhibit an increasing divergence (when the unidirectional coupling parameter is varied) then it does indicate that the independent process would have a very different dynamical influence on the dependent one when compared with that of the dependent process' own past, suggesting that the value of CCC will grow in the negative direction. The fact that KL/JSD and CCC do not have a one-to-one correspondence is because the former (KL and JSD) operate on first order distributions while the latter (CCC) is able to capture higher-order dynamical influences between the coupled processes. For non-stationary processes, our measure would still be able to capture the kind of dynamical influence, though distributions are not static.

Both positive and negative significant[4] CCC values imply existence of causal influence, but the nature of the dynamical influence of the *cause* on the *effect* is very different in these two cases. Causality turning 'negative' does not seem very intuitive at first, but all that it signifies is that the past of the *cause* variable makes the dynamics

[4]Significance analysis should first be performed using surrogate analysis techniques, as discussed in Section 3.4.2.

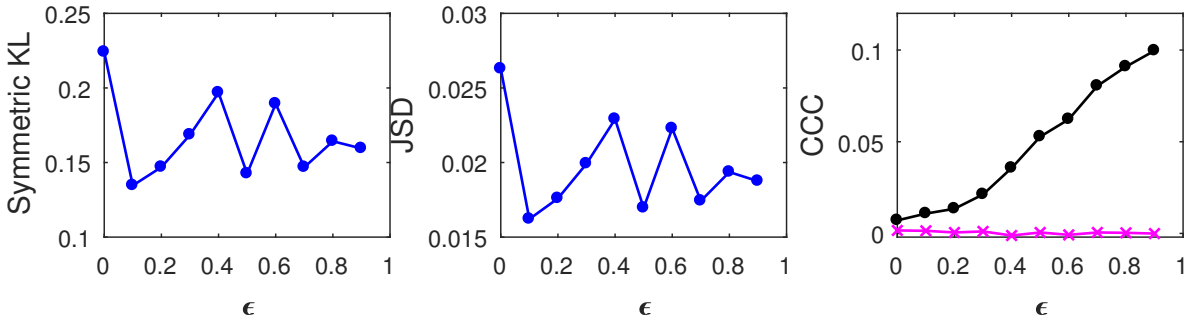

Figure 2.1: Mean values of divergence between distributions of coupled AR(1) processes using Symmetric Kullback-Leibler (KL) (subfigure (a)) and Jensen Shannon (JSD) divergences (in nats) (subfigure (b)), and the mean causality values estimated using CCC from Y to X (solid line-circles, black) and X to Y (solid line-crosses, magenta/grey in print) (subfigure (c)), as the degree of coupling, ϵ is varied. CCC values increase with increasing ϵ. There is no similarity in the trend of KL/JSD to CCC.

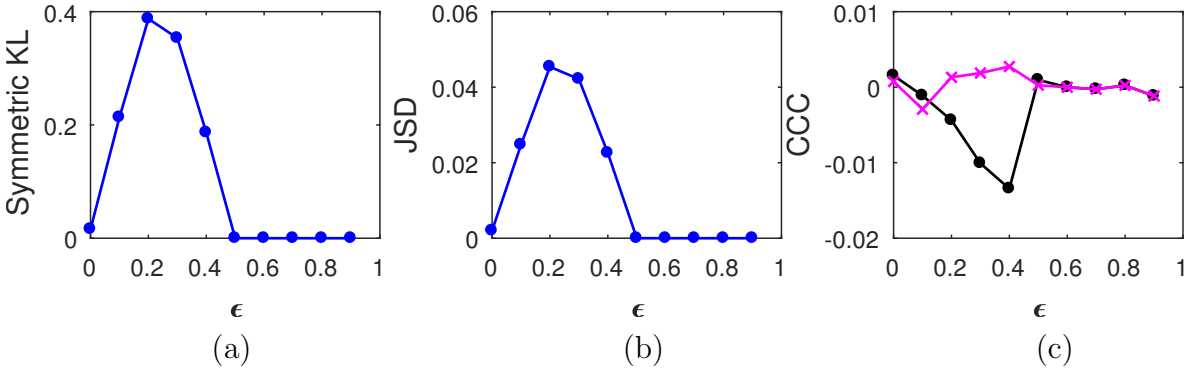

Figure 2.2: Mean values of divergence between distributions of linearly coupled tent maps using Symmetric Kullback Leibler (KL) (subfigure (a)) and Jensen Shannon (JSD) divergences (in nats) (subfigure (b)), and the mean causality values estimated using CCC from Y to X (solid line-circles, black) and X to Y (solid line-crosses, magenta/grey in print) (subfigure (c)), as the degree of coupling, ϵ is varied. For $\epsilon < 0.5$, CCC and KL/JSD are highly negatively correlated.

of the *effect* variable less predictable than its (*effect's*) own past. Such a unique feature could be very useful for real world applications in terms of 'controlling' the dynamics of a variable being effected by several variables. If a particular *cause*, out of several causes that makes the caused 'less predictable' and has 'intrinsically different' dynamics from

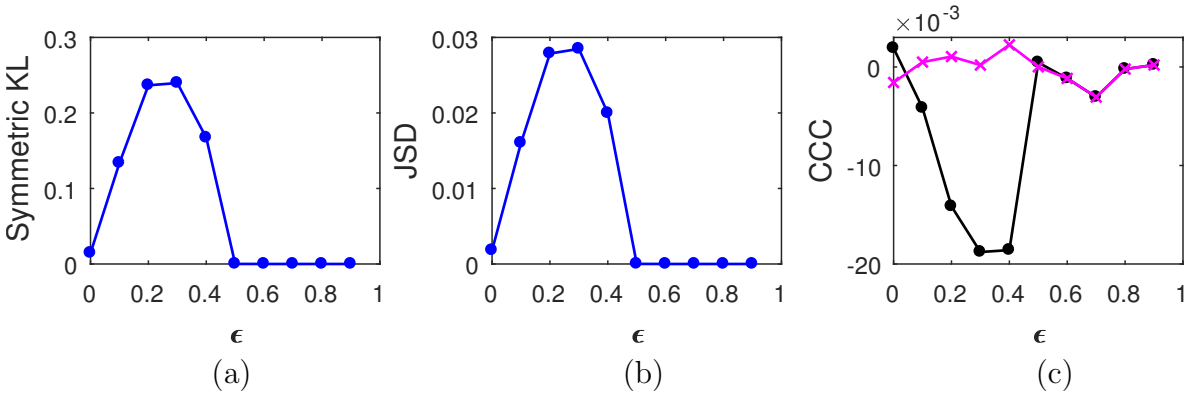

Figure 2.3: Mean values of divergence between distributions of non-linearly coupled tent maps using Symmetric Kullback Leibler (KL) (subfigure (a)) and Jensen Shannon (JSD) (subfigure (b)) divergences (in nats), and the mean of causality values estimated using CCC from Y to X (solid line-circles, black) and X to Y (solid line-crosses, magenta/ grey in print) (subfigure (c)), as the degree of coupling, ϵ is varied. For $\epsilon < 0.5$, CCC and KL/JSD are highly negatively correlated.

that of the *effect*, needs to be determined and eliminated, it can be readily identified by observing the sign of CCC. Informed attempts to inhibit and enforce certain variables of the system can then be made.

As the existing model-free methods of causality can extract only 'associational causality' and ignore the influence that the cause has on dynamics of the caused, it is impossible for them to comment on the nature of this dynamical influence, something that CCC is uniquely able to accomplish. Obviously, model based methods give full-fledged information about 'the kind of dynamical influence' owing to the model equations assumed. However, if there are no equations assumed (or known), then the sign and magnitude of CCC seems to be the best choice to capture the cause-effect relationship with additional information on the similarity (or its lack of) between the two dynamics.

2.5 Conclusions

In this chapter, we propose a novel data-based, model-free intervention approach to estimate causality for given time series. The *Interventional Complexity Causality* measure or ICC based on capturing causal influences from the dynamical complexities of data is formalized as *Compression-Complexity Causality* or CCC with the following properties —

- CCC operates on *windows* of the input time series (or measurements) instead of individual samples. It does not make any assumption of the separability of *cause* and *effect* samples.

- CCC doesn't make any assumptions of stochasticity, determinism, gaussianity, stationarity, linearity or markovian property. Thus, CCC can be applied to non-stationary/ non-linear/ non-gaussian/ non-markovian, short-term and long-term memory processes, as well as chaotic processes. CCC characterizes causal relationship based on dynamical complexity computed from windows of the input data.

- CCC is uniquely and distinctly novel in its approach since it does not estimate '*associational*' causality (first rung on Ladder of Causation) but performs '*intervention*' (second rung on the Ladder of Causation) to capture causal influences from the dynamics of the data.

- The point of 'intervention' (length L for creating the hypothetical data: Y_{past} +

ΔX) is dependent on the temporal scale at which causality exists within and between processes. It is determined adaptively based on the given data. This makes CCC a highly data-driven/data-adaptive method and thus suitable for a wide range of applications.

- Infotheoretic-based causality measures such as TE and others need to estimate joint probability densities which are very difficult to reliably estimate with short and noisy time series. On the other hand, CCC uses Effort-To-Compress or ETC complexity measure over short windows to capture time-varying causality and it is well established in literature that ETC outperforms infotheoretic measures for short and noisy data [74, 79].

- CCC can be either positive or negative (unlike TE and GC). By this unique property, CCC gives information about the *kind* of causal influence that is brought by one time series on another, whether this influence is *similar* ($CCC > 0$) to or *different* ($CCC < 0$) from the influence that the series brings to its own present.

Chapter 3

CCC: Testing on Simulations, Parameter Selection and Significance Testing

In this chapter, CCC is rigorously tested on simulations and its performance is compared with that of existing measures – Granger Causality and Transfer Entropy. Comparison with measures Convergent Cross Mapping and Non-linear Granger Causality is also done for some datasets. The proposed measure is shown to be robust to the presence of noise, long-term memory, filtering and decimation, low temporal resolution (including aliasing), non-uniform sampling, finite length signals and presence of common driving variables. Also, CCC is compared with model-dependent measure Dynamic Causal Modelling for a case of simulated fMRI signals. This chapter also discusses parameter selection criteria and rationale for CCC to be applied on different datasets. Analysis of computational time complexity as well as significance testing analysis for estimated CCC values are also discussed in this chapter.

3.1 Introduction

A measure of causality, to be robust for real data, needs to perform well in the presence of noise, filtering, low temporal and amplitude resolution, non-uniformly sampled signals, short length time series as well as presence of other causal variables in the system. Low temporal resolution data is common in the case of functional magnetic resonance imaging [84, 85] and other neurophysiological signals [86] as well as climate data [87]. Sometimes, the data may not be evenly (or uniformly) sampled as is observed in the case of financial time-series [88]. Also, many a times, low pass filtering is done to smooth out the acquired signals [89].

In this chapter, we rigorously simulate these cases and evaluate the performance of CCC measure by comparing with existing measures — Granger Causality (GC) and Transfer Entropy (TE). Also, CCC is compared with model-dependent Dynamic Causal Modeling (DCM) for a case of simulated fMRI signals. All these results are given in Section 3.2. In all cases, we take the averaged value of CCC over entire time series as computed by Eq. 2.8 (or Eq. 2.11 in the conditional case) and the parameters for CCC estimation are chosen as per the selection criteria and rationale discussed in the Section 3.3. GC estimation is done using the MVGC toolbox [31] in its default settings and TE estimation is done using MuTE toolbox [90]. Akaike Information Criteria is used for model order estimation with the maximum model order set to 20 in the MVGC toolbox, except where specified. Maximum number of lags to take for autocorrelation computation is done automatically by the toolbox. In the MuTE toolbox, the approach

of non-uniform embedding for representation of the history of the observed processes and of nearest neighbor estimator for estimating the probability density functions is used for all results in this paper. The number of lags to consider for observed processes was set to 5 and the maximum number of nearest neighbors to consider was set to 10, except where specified.

Significance testing of results obtained using CCC is demonstrated in Section 3.4. Since our implementation of CCC algorithm is not yet optimized, we give only an indicative analysis of computational time complexity for bivariate CCC in Section 3.5.

3.2 Simulation Testing Results and Discussion

3.2.1 Varying unidirectional coupling

AR(1)

Autoregressive processes of order one (AR(1)) were simulated as follows. X and Y are the dependent and independent processes respectively.

$$\begin{aligned} X(t) &= aX(t-1) + \epsilon Y(t-1) + \varepsilon_{X,t} \\ Y(t) &= bY(t-1) + \varepsilon_{Y,t}, \end{aligned} \tag{3.1}$$

where $a = 0.9$, $b = 0.8$, $t = 1$ to 1000s, sampling period = 1s. ϵ is varied from $0 - 0.9$ in steps of 0.1. Noise terms, $\varepsilon_Y, \varepsilon_X = \nu\eta$, where ν = noise intensity = 0.03 and η follows standard normal distribution. Figure 3.1 shows the performance of CCC along with that of TE and GC as mean values over 50 trials, (CCC settings: $L = 150$, $w = 15$, $\delta = 80$, $B = 2$). Standard deviation of CCC, TE and GC values are shown in Figure 3.2.

With increasing coupling, the causality estimated by CCC, TE as well as GC increases.

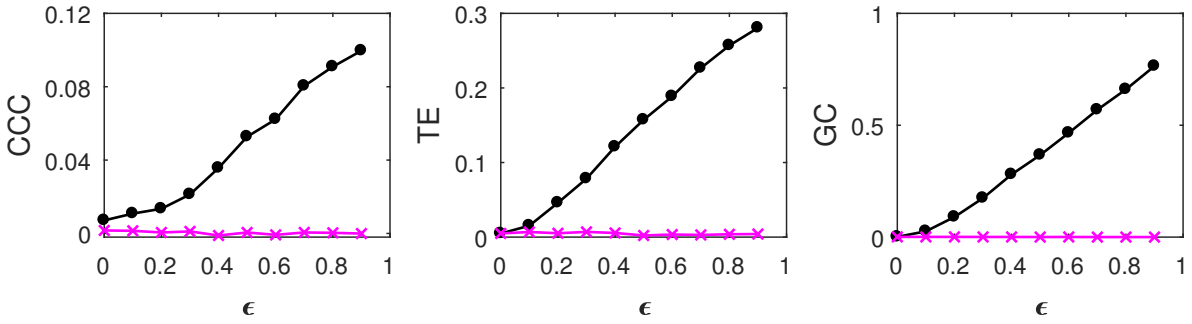

(a) (b) (c)

Figure 3.1: Mean causality values estimated using CCC (a), TE (b) and GC (c) for coupled AR(1) processes, from Y to X (solid line-circles, black) and X to Y (solid line-crosses, magenta/ grey in print) as the degree of coupling, ϵ is varied. CCC, TE as well as GC are able to correctly quantify causality.

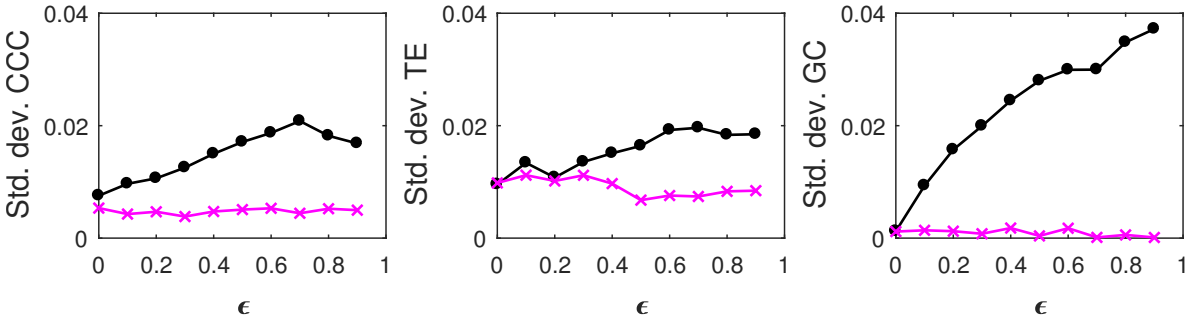

(a) (b) (c)

Figure 3.2: Standard deviation of causality values estimated using CCC (a), TE (b) and GC (c) for coupled AR(1) processes, from Y to X (solid line-circles, black) and X to Y (solid line-crosses, magenta/grey in print) as the degree of coupling, ϵ is varied.

AR(100)

Autoregressive processes of order hundred (AR(100): X dependent, Y independent) were simulated as follows.

$$\begin{aligned} X(t) &= aX(t-1) + \epsilon Y(t-100) + \varepsilon_{X,t} \\ Y(t) &= bY(t-1) + \varepsilon_{Y,t}, \end{aligned} \tag{3.2}$$

where $a = 0.9$, $b = 0.8$, $t = 1$ to 1000s (first 100 transients were removed from the simulated process), sampling period = 1s. ϵ is varied from $0 - 0.9$ in steps of 0.1. Noise

terms, $\varepsilon_Y, \varepsilon_X = \nu\eta$, where ν = noise intensity = 0.03 and η follows standard normal distribution. Figure 3.3 shows the performance of CCC along with that of TE and GC, as mean values over 50 trials. CCC settings were set as: $L = 150$, $w = 15$, $\delta = 80$, $B = 2$. Maximum model order was set to 110 in the MVGC toolbox while the number of lags to consider for observed processes was kept as 5 for TE estimation. For AR(100) processes, it is ideal to take lags greater than 100, in order to get correct causality estimates. However, for any given real data with unknown order, there is no obvious criterion to set these maximum lags. Further, TE computation for the settings used by us in the MuTE toolbox, when coupled with higher lags requires a much higher computational time compared to that taken by CCC and GC for the respective settings used. Hence, TE values for higher lags (=110) at each value of coupling were only computed using 20 trials and are included in Appendix A.

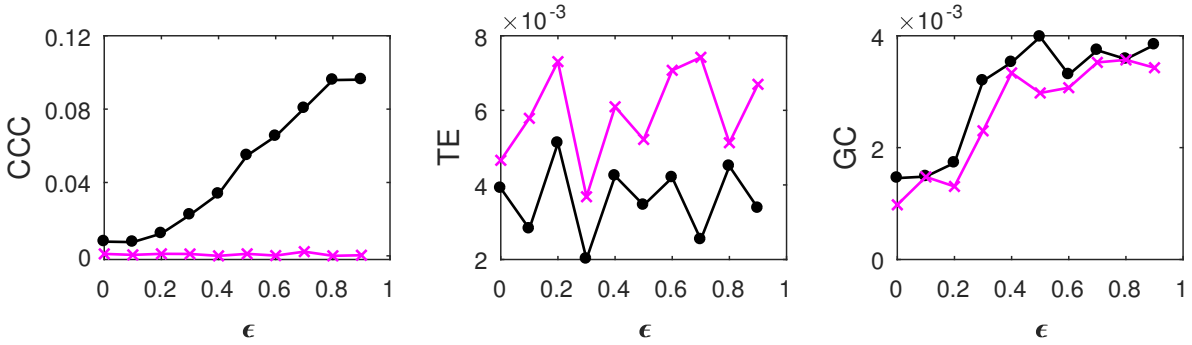

Figure 3.3: Mean causality values estimated using CCC (a), TE (b) and GC (c) for coupled AR(100) processes, from Y to X (solid line-circles, black) and X to Y (solid line-crosses, magenta/ grey in print) as the degree of coupling, ϵ is varied. Only CCC is able to reliably estimate the correct causal relationship for all values of ϵ while TE and GC fail.

CCC values increase steadily with increasing coupling for the correct direction of

causation. TE fails as it shows higher causality from X to Y for all ϵ. GC also shows confounding of causality values in two directions. Thus, causality in coupled AR processes with long-range memory can be reliably estimated using CCC and not using TE or GC. However, TE performance becomes better when it is computed with higher lags as shown in Figure A.1 in the Appendix. Range of standard deviation of CCC values from Y to X is 0.0076 to 0.0221 for varying parameter ϵ and that from X to Y is 0.0039 to 0.0053. These values are much smaller than the mean CCC estimates and thus, causality estimated in the direction of causation and opposite to it remain well separable. For TE, Y to X, standard deviation range is 0.0061 to 0.0090 and X to Y, standard deviation range is 0.0082 to 0.0118. For GC, Y to X, standard deviation range is 0.0012 to 0.0033 and X to Y, standard deviation range is 0.0015 to 0.0034.

Tent Map

Linearly and non-linearly coupled tent maps were simulated as per the following equations. Independent process, Y, is generated as:

$$\begin{aligned} Y(t) &= 2Y(t-1), \qquad 0 \leq Y(t-1) < 1/2, \\ Y(t) &= 2 - 2Y(t-1), \qquad 1/2 \leq Y(t-1) \leq 1. \end{aligned} \tag{3.3}$$

The linearly coupled dependent process, X, is as below:

$$\begin{aligned} X(t) &= \epsilon Y(t) + (1-\epsilon)h(t), \\ h(t) &= 2X(t-1), \qquad 0 \leq X(t-1) < 1/2, \\ h(t) &= 2 - 2X(t-1), \qquad 1/2 \leq X(t-1) \leq 1, \end{aligned} \tag{3.4}$$

where ϵ is the degree of linear coupling.

The non-linearly coupled dependent process, X, is as below:

$$\begin{aligned} X(t) &= 2f(t), \qquad 0 \leq f(t) < 1/2, \\ X(t) &= 2 - 2f(t), \qquad 1/2 \leq f(t) \leq 1, \\ f(t) &= \epsilon Y(t-1) + (1-\epsilon)X(t-1), \end{aligned} \tag{3.5}$$

where ϵ is the degree of non-linear coupling.

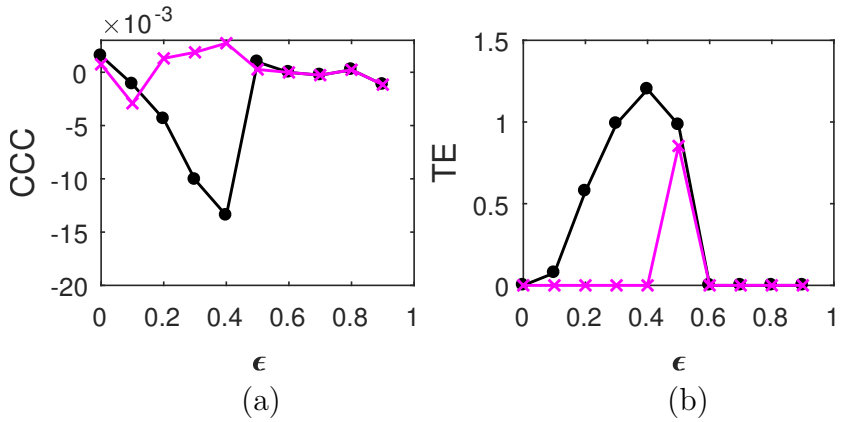

Figure 3.4: Mean of causality values estimated using CCC (a) and TE (b) for linearly coupled tent maps, from Y to X (solid line-circles, black) and X to Y (solid line-crosses, magenta/ grey in print) as the degree of coupling is increased. With increasing coupling (until synchronization), magnitude of CCC and TE values increases. CCC values are negative while TE are positive.

The length of the signals simulated in this case was 3000, i.e. $t = 1$ to 3000s, sampling period = 1s and the first 2000 transients were removed to yield 1000 points for causality estimation. Figures 3.4 and 3.5 show the performance of CCC and TE for linearly and non-linearly coupled tent maps respectively as ϵ is varied (CCC settings: $L = 100$, $w = 15$, $\delta = 80$, $B = 8$). The assumption of a linear model for estimation of GC was proved to be erroneous for most trials and hence GC values are not displayed. As ϵ is increased for both linear and non-linear coupling, $TE_{Y \to X}$ increases in the positive direction and then falls to zero when the two series become completely

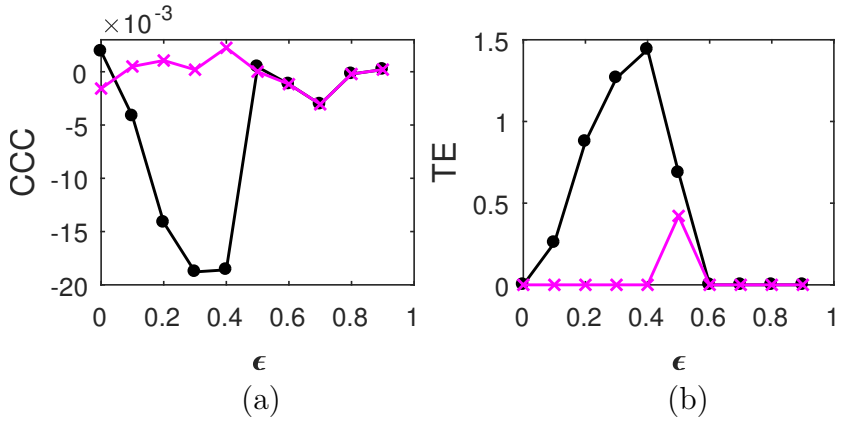

Figure 3.5: Mean of causality values estimated using CCC (a) and TE (b) for non-linearly coupled tent maps, from Y to X (solid line-circles, black) and X to Y (solid line-crosses, magenta/ grey in print) as the degree of coupling is increased. With increasing coupling (until synchronization), magnitude of CCC and TE values increases. CCC values are negative while TE are positive.

synchronized at $\epsilon = 0.5$. The trend of the magnitude of CCC values is similar to TE, however, $CCC_{Y \to X}$ increment is in negative direction. This is because of the fact that with increasing coupling the kind of dynamical influence from Y to X becomes increasingly different than the dynamical influence from the past values of X to itself.

In case of linear coupling, range of standard deviation of CCC values from Y to X is 0.0050 to 0.0087 for different values of ϵ and that from X to Y is 0.0051 to 0.0100. For TE, Y to X, standard deviation range is 0 to 1.4851 and X to Y, standard deviation range is 0 to 1.4225. For non-linear coupling, the range of standard deviation of CCC values from Y to X is 0.0057 to 0.0087 for different values of ϵ and that from X to Y is 0.0057 to 0.0102. For TE, Y to X, standard deviation range is 0 to 1.2854 and X to Y, standard deviation range is 0 to 1.0479.

For both CCC and TE, standard deviation values obtained indicate that there might

be confounding in the causality values in the direction of causation and the direction opposite to causation for low values of ϵ.

3.2.2 Varying process noise

The performance of causality measures as process noise is varied is shown in Figure 3.6 for coupled AR processes simulated as in Eq. 3.1, where $a = 0.9$, $b = 0.8$, $\epsilon = 0.8$, $t = 1$ to 1000s, sampling period = 1s, number of trials = 50. Noise terms, $\varepsilon_Y, \varepsilon_X = \nu\eta$, where ν = noise intensity is varied from 0.01 to 0.1 and η follows standard normal distribution. CCC settings: $L = 150$, $w = 15$, $\delta = 80$, $B = 2$. The range of standard deviation of CCC values from Y to X is 0.0162 to 0.0223 for different values of ϵ and that from X to Y is 0.0038 to 0.0058. For TE, Y to X, standard deviation range is 0.0182 to 0.0267 and X to Y, standard deviation range is 0.0063 to 0.0104. For GC, Y to X, standard deviation range is 0.0314 to 0.0569 and X to Y, standard deviation range is 0.0001 to 0.0002.

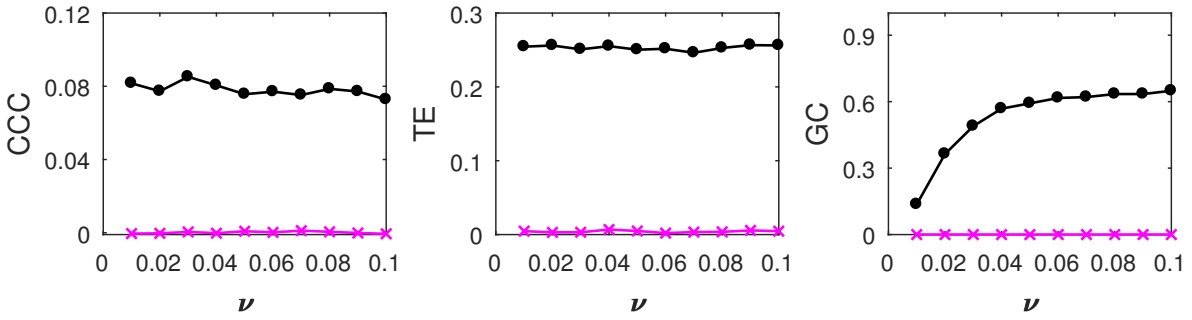

(a) (b) (c)

Figure 3.6: Mean causality values estimated using CCC (a), TE (b) and GC (c) for coupled AR processes, from Y to X (solid line-circles, black) and X to Y (solid line-crosses, magenta/grey in print) as the intensity of noise, ν is varied. All the three measures perform well in this case.

The performance of all three measures is fairly good in this case. Only GC values show a slightly increasing trend with increasing noise intensity.

3.2.3 Decimated coupled signals with uniform sampling

It is often the case that the rate of sampling of acquired measurements is not equal to the rate of generation of the process. Causal inferences are regularly made from such data [40], for e.g., fMRI signals [84, 85] as well as other neurophysiological recordings [86], climate data [87]. Two sets of coupled AR processes were first simulated and subsequently decimated.

Set 1 of AR processes, of order 1, were simulated as below:

$$\begin{aligned} Y(t) &= 0.7Y(t-1) + \varepsilon_{Y,t}, \\ X(t) &= 0.9X(t-1) + 0.8Y(t-1) + \varepsilon_{X,t}. \end{aligned} \tag{3.6}$$

Set 2 of AR processes, of order 5, were simulated as below:

$$\begin{aligned} Y(t) &= 0.7Y(t-5) + \varepsilon_{Y,t}, \\ X(t) &= 0.9X(t-5) + 0.8Y(t-1) + \varepsilon_{X,t}, \end{aligned} \tag{3.7}$$

where, noise terms, $\varepsilon_Y, \varepsilon_X = \nu\eta$, where ν = noise intensity = 0.03 and η follows standard normal distribution. The original length of X and Y simulated in both the sets is 2000. Upon decimation, the length of the time series reduces. β represents the decimation factor that scales the sampling frequency. As β is varied from 1 to 0.5, sampling frequency is scaled from its original value to half its value.

Set 1 of processes, being of order one, have low frequency components in the signal. As a result, even when β is reduced to 0.5, it does not lead to frequency folding in the spectrum of process Y and X. Frequency spectrum for a trial of X in this process is

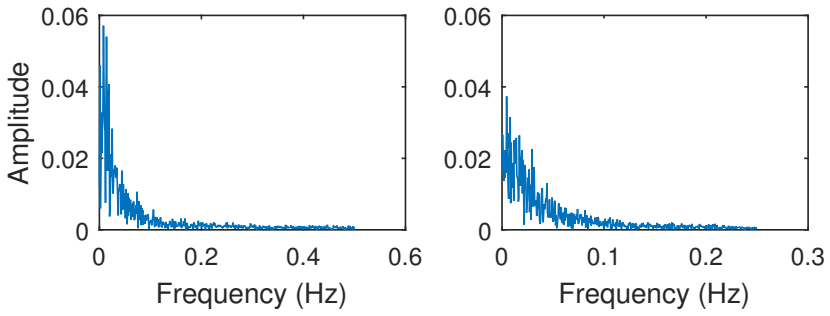

(a) (b)

Figure 3.7: Frequency Spectrum of dependent AR(1) process from *Set 1* without decimation (a) and when decimation factor equals 0.5 (b). The process does not undergo aliasing on decimation.

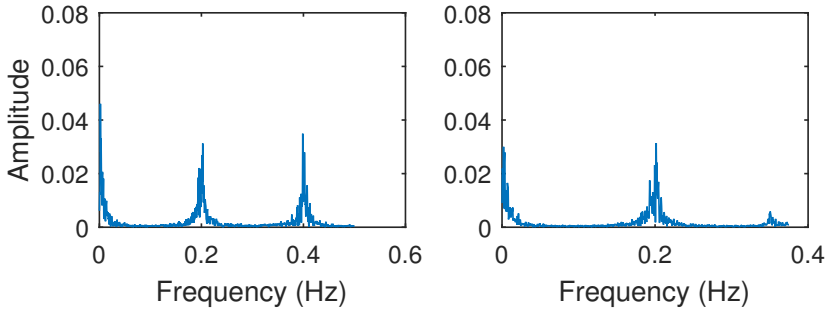

(a) (b)

Figure 3.8: Frequency Spectrum of of dependent AR(5) process from *Set 2* without decimation (a) and when decimation factor equals 0.75 (b). The process undergoes aliasing on decimation.

shown in Figure 3.7 for the original case and the case where β is reduced to 0.5. In case of *Set 2*, decimation of the signals Y and X leads to aliasing. This is because higher frequency components are present in the signals, leading to folding of these frequencies even as β is reduced to 0.8. The frequency spectrum for a trial of X for its non-decimated version and for decimation with β equal to 0.75 is shown in Figure 3.8.

Equal decimation of independent and dependent signal

When both signals Y and X from the two sets are decimated by scaling their sampling rate by an equal decimation factor, β, ranging from 1 to 0.5 at intervals of 0.05, the results obtained using the three methods, CCC, TE and GC are as shown in Figures 3.9 and 3.10. Figure 3.9 shows the results for *Set 1* while Figure 3.10 shows results for *Set 2* as mean causality values estimated over 10 trials. CCC settings for both sets: $L = 150$, $w = 15$, $\delta = 80$, $B = 2$.

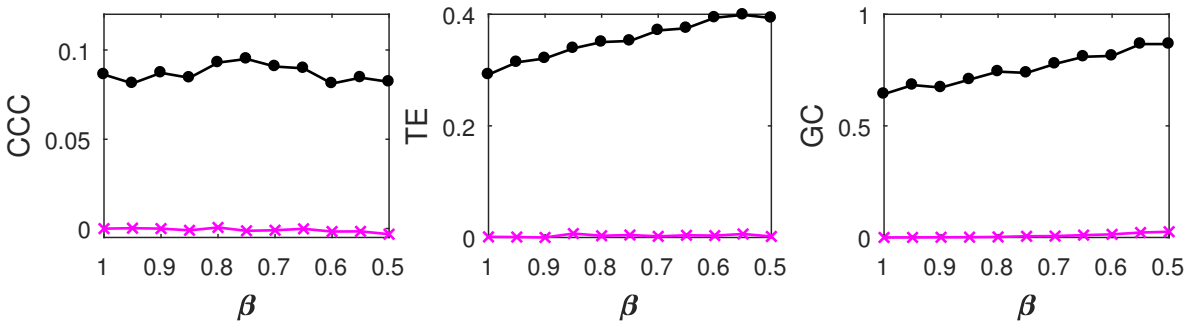

Figure 3.9: Mean causality estimated using CCC (a), TE (b) and GC (c) for coupled AR processes from Y to X (solid line-circles, black) and X to Y (solid line-crosses, magenta/ grey in print) as the decimation factor β is varied for both independent and dependent signal. The coupled AR processes simulated do not undergo frequency aliasing. All three measures perform fairly well in this case.

While the values of CCC are relatively consistent even upon decimation (with or without aliasing), those of TE and GC are stable only in case of non-aliased decimation. For GC and TE in the aliased case, even though there is no confounding of the causality direction, the magnitude of causality estimated is not consistent and reliable.

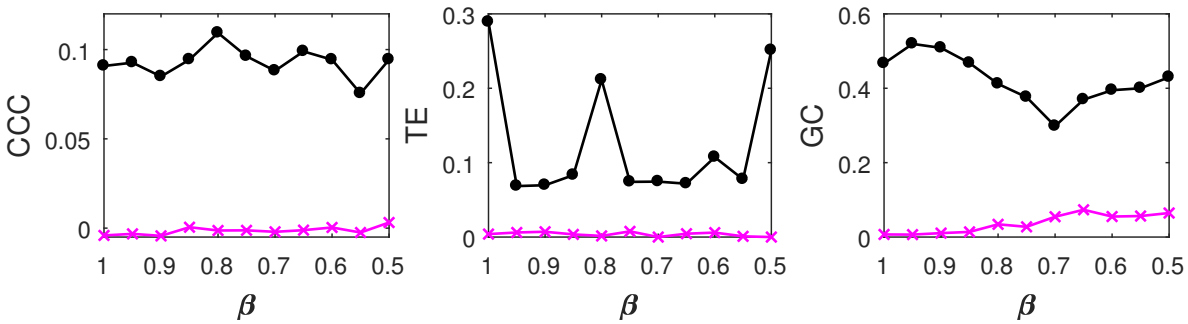

(a) (b) (c)

Figure 3.10: Mean causality estimated using CCC (a), TE (b) and GC (c) for coupled AR processes from Y to X (solid line-circles, black) and X to Y (solid line-crosses, magenta/ grey in print) as the decimation factor β is varied for both independent and dependent signal. The coupled AR processes simulated become frequency aliased. CCC values are stable compared to TE and GC.

Decimation of dependent signal

When only signal X is decimated by scaling its sampling rate by a decimation factor β, ranging from 1 to 0.5 at intervals of 0.05, the results obtained using the three methods CCC, TE and GC are as shown in Figures 3.11 and 3.12. Figure 3.11 shows the results for *Set 1* while Figure 3.12 shows results for *Set 2* as mean causality values estimated over 10 trials. For the length of the two signals to match, the independent signal considered is truncated at the length of the dependent signal. CCC settings for both sets: $L = 150$, $w = 15$, $\delta = 80$, $B = 2$.

In this scenario, for both non-aliased and aliased decimation, CCC estimates are much more stable and consistent (across β) when compared to those of TE and GC, where confounding in the direction of causality results even upon slightest decimation. It is clear from these results that CCC is the most robust, reliable and consistent among the three causality measures.

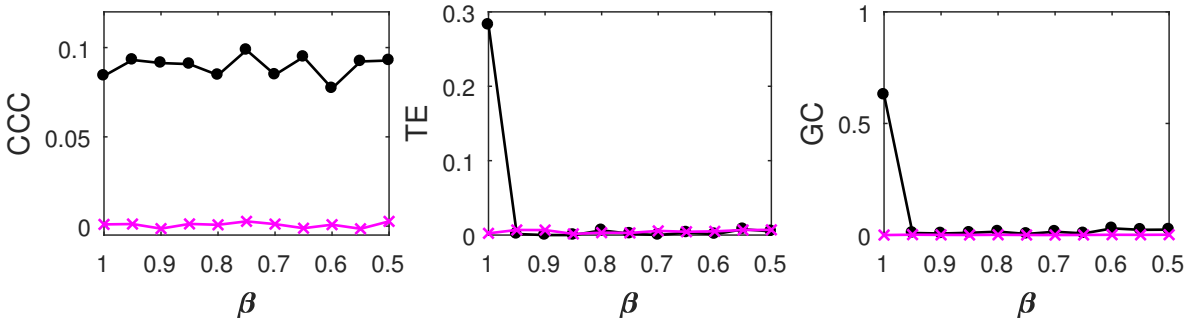

(a) (b) (c)

Figure 3.11: Mean causality estimated using CCC (a), TE (b) and GC (c) for coupled AR processes from Y to X (solid line-circles, black) and X to Y (solid line-crosses, magenta/ grey in print) as the decimation factor β is varied for the dependent signal. The dependent AR process simulated does not undergo frequency-aliasing. Only CCC can capture the correct direction and strength of coupling when β is decreased.

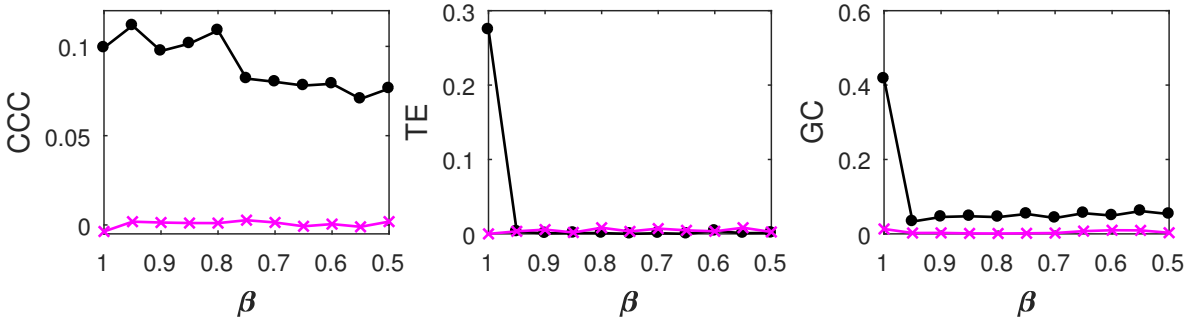

(a) (b) (c)

Figure 3.12: Mean causality estimated using CCC (a), TE (b) and GC (c) for coupled AR processes from Y to X (solid line-circles, black) and X to Y (solid line-crosses, magenta/ grey in print) as the decimation factor is varied for the dependent signal. The dependent AR process simulated becomes frequency aliased. Only CCC can capture the correct direction and strength of coupling when β is decreased.

3.2.4 Non-uniform sampling

Non-uniformly sampled/non-synchronous measurements are common in real-world physiological data acquisition due to jitters/motion-artifacts as well as due to the inherent nature of signals such as heart rate signals [91]. Also, in economics, the case of missing data is common [88]. To realistically simulate such a scenario, non-uniform sampling

was introduced by eliminating data from random locations of the dependent time series and then presenting the resulting series as a set with no knowledge of the time-stamps of the missing data. The percentage of non-uniform sampling/non-synchronous measurements (α) is the percentage of these missing data points.

AR processes with non-uniformly sampled signals were simulated as per Eq. 3.1 with $b = 0.7$, $a = 0.9$, $\epsilon = 0.8$. Noise terms, $\varepsilon_Y, \varepsilon_X = \nu\eta$, where ν = noise intensity = 0.03 and η follows standard normal distribution. Length of original time series, $N = 2000$, and is reduced upon increasing the percentage non-uniform sampling α. In order to match the lengths of the two time series, Y, the independent time series, is appropriately truncated to match the length of the dependent signal, X (this results in non-synchronous pair of measurements). CCC settings used: $L = 150$, $w = 15$, $\delta = 80$, $B = 2$. Mean causality estimated for 10 trials using the three measures with increasing increasing α, while $\nu = 0.03$, are shown in Figure 3.13.

Linearly coupled tent maps with non-uniformly sampled signals were simulated as per Eq. 3.3 and 3.4 with $\epsilon = 0.3$. Length of original time series, $N = 2000$, and is reduced upon increasing the percentage non-uniform sampling α. In order to match the lengths of the two time series, Y, the independent time series, is appropriately truncated to match the length of the dependent signal, X (this results in non-synchronous pair of measurements). CCC settings used: $L = 100$, $w = 15$, $\delta = 80$, $B = 8$. Mean causality estimated for 10 trials using the three measures with increasing increasing α, while $\nu = 0.03$, are shown in Figure 3.14.

As the results clearly indicate, both TE and GC fail when applied to non-uniformly

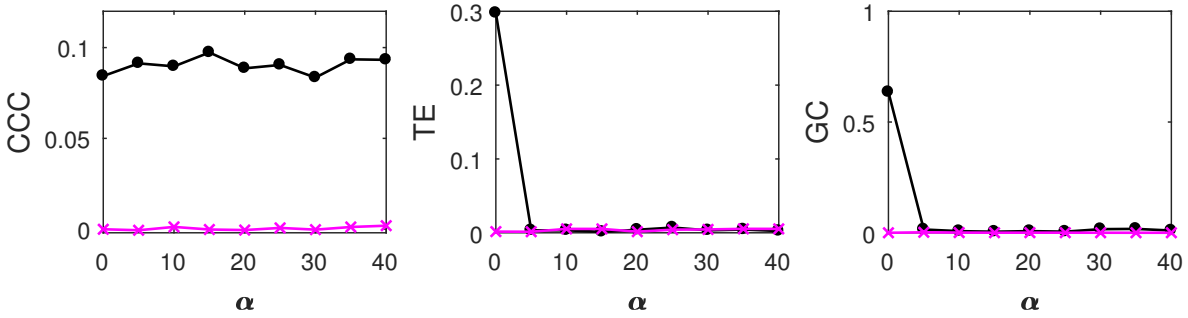

(a) (b) (c)

Figure 3.13: Mean causality values estimated using CCC (a), TE (b) and GC (c) for coupled AR processes from Y to X (solid line-circles, black) and X to Y (solid line-crosses, magenta/ grey in print) as the percentage of non-uniform sampling α is varied. CCC is the only measure that shows reliable, consistent and correct estimates of causality.

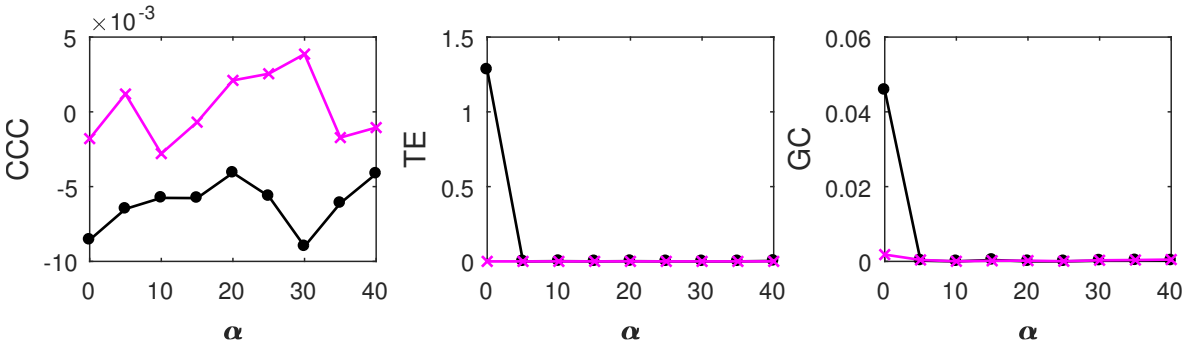

(a) (b) (c)

Figure 3.14: Mean causality values estimated using CCC (a), TE (b) and GC (c) for coupled tent maps from Y to X (solid line-circles, black) and X to Y (solid line-crosses, magenta) as the percentage of non-uniform sampling is varied. CCC is able to distinguish the causality direction but the separation between values is small. TE and GC fail completely.

sampled coupled AR and tent map processes. CCC values are relatively invariant to non-uniform sampling and thus could be employed in such scenarios.

3.2.5 Filtering of Coupled Signals

Acquired data preprocessing often involves low pass filtering to smooth out the signal [89]. At other times, high pass filtering is required to remove low frequency glitches from a high frequency signal. Also when the signals acquired are sampled at low frequencies, the effects due to decimation and filtering may add up and result in poorer estimates of causality. This is often the case in fMRI signals [84, 85].

To test these scenarios, AR processes were simulated as below:

$$\begin{aligned} Y(t) &= 0.7Y(t-5) + \varepsilon_{Y,t}, \\ X(t) &= 0.9X(t-5) + 0.8Y(t-1) + \varepsilon_{X,t}, \end{aligned} \tag{3.8}$$

where, noise terms, $\varepsilon_Y, \varepsilon_X = \nu\eta$, where $\nu =$ noise intensity $= 0.03$ and η follows standard normal distribution.

Causality values were estimated using CCC, TE and GC when simulated signals are low pass filtered using a moving average window of length 3 with step size 1. The results are shown in Table 3.1 as mean values over 10 trials. CCC settings used: $L = 150$, $w = 15$, $\delta = 80$, $B = 2$. The performance of the measures when coupled signals are decimated to half the sampling rate and then low pass filtered are also included in the table. The length of the original signal simulated is 2000 and is reduced to 1998 upon filtering and to 998 upon filtering and decimation.

From the table, we see that CCC can distinguish the direction of causality in the original case as well as in the filtering and decimation plus filtering case. Erroneously, TE shows significant causality in the direction opposite to causation upon filtering as well as upon decimation and filtering and GC shows significant causality in the direction

Table 3.1: Mean CCC, TE and GC estimates for coupled AR processes Y (independent) and X (dependent) as it is, upon filtering and upon decimation and filtering

System	**CCC**		**TE**		**GC**	
	$Y \rightarrow X$	$X \rightarrow Y$	$Y \rightarrow X$	$X \rightarrow Y$	$Y \rightarrow X$	$X \rightarrow Y$
Original	0.0908	-0.0041	0.2890	0.0040	0.3776	0.0104
Filtered	0.0988	0.0018	0.2398	0.0170	0.4787	0.0056
Decimated and Filtered	0.0753	0.0059	0.1270	0.0114	0.4321	0.0596

opposite to causation upon decimation and filtering. By this we can infer that CCC is highly suitable for practical applications which involve pre-processing such as filtering and decimation of measurements.

3.2.6 Conditional CCC on short length MVAR system

A system of three variables was simulated as per the following equations —

$$\begin{aligned} Z(t) &= 0.8Z(t-1) + \epsilon_{Z,t}, \\ X(t) &= 0.9X(t-1) + 0.4Z(t-100) + \epsilon_{X,t}, \\ Y(t) &= 0.9Y(t-1) + 0.8Z(t-100) + \epsilon_{Y,t}, \end{aligned} \tag{3.9}$$

where the noise terms, $\varepsilon_Z, \varepsilon_X, \varepsilon_Y = \nu\eta$, ν = noise intensity = 0.03 and η follows standard normal distribution. Length of time series simulated was 300 and first 50 transients were removed to yield short length signals of 250 time points.

The coupling direction and strength between variables X, Y, Z are shown in Figure 3.15(a). The mean values of causality estimated over 10 trials using CCC, TE and GC are shown in Figure 3.15 tables, (b), (c) and (d) respectively. CCC settings used: $L = 150$, $w = 15$, $\delta = 20$, $B = 2$. Maximum model order was set to 110 in the MVGC

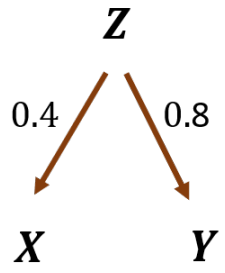

(a) Connectivity

To \ From	X	Y	Z
X	0	0.0029	0.0420
Y	-0.0026	0	0.0885
Z	0.0022	0.0046	0

(b) CCC

To \ From	X	Y	Z
X	0	0.0452	0.0121
Y	0.0176	0	0.0445
Z	0.0096	0.0247	0

(c) TE

To \ From	X	Y	Z
X	NaN	0.1566	0.0985
Y	0.0966	NaN	0.1052
Z	0.0045	0.0065	NaN

(d) GC

Figure 3.15: Mean causality values estimated using CCC (b), TE (c) and GC (d) for a system of three AR variables coupled as in (a). True positives are in green, true negatives in black and false positives in red. No false negatives were detected in any case.

toolbox for GC estimation. The number of lags to consider for observed processes was set to 110 and the maximum number of nearest neighbors to consider was set to 10 for TE estimation using the MuTE toolbox. In the tables, true positives are in green, true negatives in black and false positives are in red. No No false negatives were detected in any case. CCC detects correctly the true positives and negatives. GC and TE, on the other hand, detect the true positives but also shows some false positive couplings.

3.2.7 Comparison with Nonlinear Granger Causality (NGC) and Convergent Cross Mapping

For some of the systems considered above, the performance of methods – Non-linear Granger Causality (NGC) [24] and Convergent Cross Mapping [28] (CCM) was evaluated in order to compare their performance with results obtained using CCC. The working of these methods has been discussed in Chapter 1. CCM detects causality using the geometry of attractors of dynamical systems and is not applicable to AR systems. NGC can be applied to both coupled AR processes as well as chaotic systems. NGC toolbox described in [24, 92] and made available by the authors on GitHub [93], was used for analysis in all the experiments done. The parameter settings used in NGC are as follows: polynomial type of kernel with order 2 and order of the model set to 6 was used. CCM toolbox made available on Mathworks MATLAB File Exchange as a part of [94] was used for all analysis related to CCM. Time step for reconstruction was set to one and embedding dimension for reconstruction was set for automatic estimation.

Varying unidirectional coupling

For the system of unidirectionally coupled tent maps with linear coupling, simulated as per Eqs. 3.3 and 3.4 (with coupling from variable Y to variable X), NGC and CCM correlation cross map estimates are shown in Figure 3.16 as mean values over 50 trials. Same set of trials were used in the experiment as used in Section 3.2.1. All the settings, including the length of time series, transients eliminated and the number of trials taken, remain the same as in Section 3.2.1.

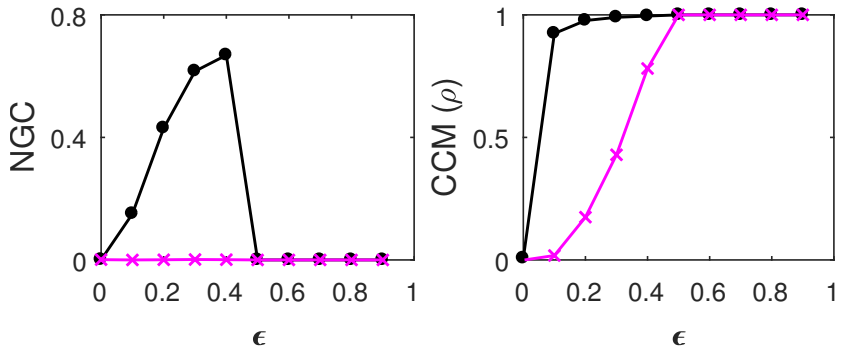

(a) (b)

Figure 3.16: Mean of causality values estimated using NGC (a) and CCM (b) for linearly coupled tent maps, from Y to X (solid line-circles, black) and X to Y (solid line-crosses, magenta/ grey in print) as the degree of coupling is increased. With increasing coupling (until synchronization), magnitude of NGC and CCM values increases in the direction of causality between the processes. CCM, however, shows spurious increment in the direction of no causation.

CCM cross map estimate (ρ) in the direction of coupling should be close to one (being higher for higher values of coupling). This is seen to be the case here as soon as coupling coefficient is made greater than zero. However, in the direction opposite to causation also, we get significant values of ρ, suggesting bidirectional coupling, which is incorrect. NGC values, increase only in the direction of causation as coupling is

increased and remain zero in the other direction. As ϵ is made > 0.5, the coupled time series synchronize and $CCM(\rho)$ values in both directions approach 1 while NGC values in the two directions become close to zero. NGC results are in line with that of CCC and TE shown in Figure 3.4.

Varying process noise

The performance of NGC on coupled AR processes as process noise is increased was also checked. Processes were simulated as per Eq. 3.1 and the same set of trials were used as in Section 3.2.2 with all settings remaining the same as earlier. The results (as mean values over 50 trials) are displayed in Figure 3.17. Like the measures, CCC, TE and GC, the performance of NGC is good in this case.

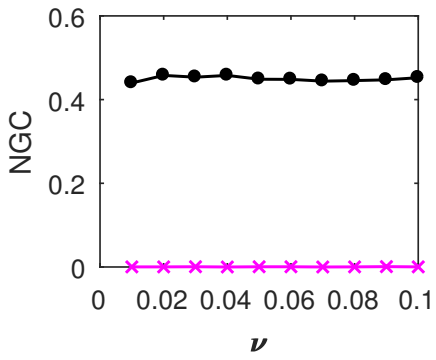

Figure 3.17: Mean of causality values estimated using NGC for AR processes, from Y to X (solid line-circles, black) and X to Y (solid line-crosses, magenta/ grey in print) as the intensity of noise, ν is varied. NGC performs well in this case.

Non-uniform sampling

NGC and CCM were also tested on non-uniformly sampled signals. NGC was applied to coupled AR(1) processes with non-uniform sampling while both NGC and CCM were applied to coupled tent map processes with non-uniform sampling. Trials generated as

in Section 3.2.4 were used here with all settings used for simulations being kept the same. Mean values of NGC over 10 trials for coupled AR processes as the percentage of non-uniform sampling is increased is shown in Figure 3.17. Mean values of NGC and CCM over 10 trials for coupled tent maps with increasing percentage of non-uniform sampling are shown in Figure 3.16.

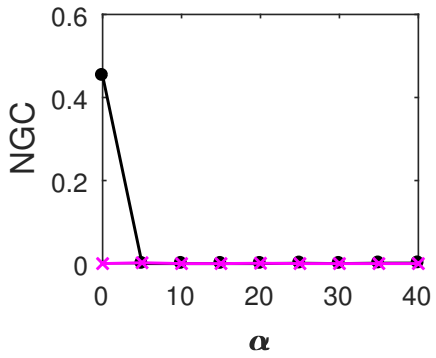

Figure 3.18: Mean of causality values estimated using NGC for coupled AR processes, from Y to X (solid line-circles, black) and X to Y (solid line-crosses, magenta/ grey in print) as the percentage of non-uniform sampling α is varied. With introduction of non-uniform sampling in the system, NGC is not able to distinguish the correct direction of causality. Compare this with Figure 3.13, where CCC shows consistently correct estimates of causality, even as α is increased to 40%.

NGC, in the correct causality direction, falls to zero as soon as non-uniform sampling is introduced in both coupled AR system as well as a coupled tent map system. In the case of CCM for tent maps, as well, with the introduction of non-uniform sampling, cross map estimates in both directions fall to zero and remain zero for all levels of percentage of non-uniform sampling. Based on these results as well as those in Section 3.2.4, amongst all the measures tested here, CCC, is the only measure that can correctly distinguish the coupling direction up to a high percentage of non-uniform sampling (40%).

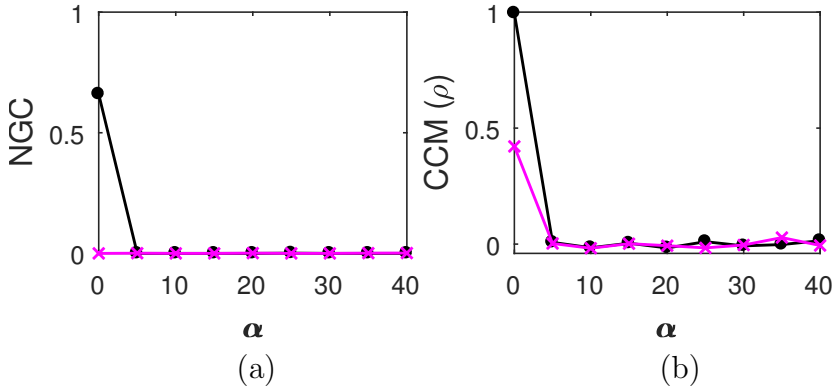

(a) (b)

Figure 3.19: Mean of causality values estimated using NGC (a) and CCM (b) for linearly coupled tent maps, from Y to X (solid line-circles, black) and X to Y (solid line-crosses, magenta/ grey in print) as the percentage of non-uniform sampling, α, is increased. With introduction of non-uniform sampling in the system, both NGC and CCM fail to distinguish the correct direction of causality. Compare this with Figure 3.14, where CCC shows relatively consistent estimates of causality, even as α is increased to 40%.

3.2.8 Comparison with Dynamic Causal Modelling (DCM)

DCM, unlike CCC, is a model-dependent effective connectivity estimation method. It can recover interaction coefficients of the underlying causal mechanism when an appropriate model and priors on parameters are known. We attempt to check if CCC can detect non-linear causal interactions in time series generated from fMRI simulations, where DCM is widely applied.

For comparison with DCM, synthetic data was generated as in [95], where a uni-directional and bidirectional coupling scheme is implemented between two simulated regions which generate observed BOLD (fMRI) responses. The MATLAB routine generating the data is available as a part of SPM8 toolbox, DEM_demo_DCM_LAP.m in DEM folder (Wellcome Trust Centre for Neuroimaging, London; www.fil.ion.ucl.ac .uk/spm/software/spm8/). The (neuronal) equations of motion simulated are as fol-

lows:

$$\frac{dx}{dt} = Ax(t) + v(t), \tag{3.10}$$

where $x(t) = [x_1(t), x_2(t), \ldots, x_n(t)]^T$ is a column vector of hidden neuronal states for n regions.

For unidirectional connectivity simulation, the connectivity matrix (A) was as follows:

$$A = \begin{bmatrix} -0.5 & 0.01 \\ 0.7 & -0.5 \end{bmatrix}. \tag{3.11}$$

For bidirectional connectivity simulation, A was:

$$A = \begin{bmatrix} -0.5 & 0.3 \\ 0.3 & -0.5 \end{bmatrix}. \tag{3.12}$$

For each scheme, 3000 time points of data was simulated for each region. DCM model inversion was done using the default settings, with the inversion approach and biophysical priors on parameters remaining as per the SPM8 routine settings. CCC estimation was done after removal of first 1000 transient time points of data, with the effective signal length being 2000. Parameters used for CCC estimation in both cases were set as: $L = 80$, $w = 30$, $\delta = 40$, $B = 16$. DCM estimates of posterior expectation on effective connectivity parameters and corresponding CCC estimates are shown in Tables 3.2 and 3.3.

As seen from the tables, CCC is able to correctly identify the direction and relative strengths of non-linear causal interactions. CCC is high in the direction of higher coupling in case of unidirectional coupling scheme. For bidirectional coupling, CCC values in the two directions are comparable.

To \ From	1	2
1	-0.3833	0.1716
2	0.2938	-0.3671

(a) Posterior Expectation (DCM)

To \ From	1	2
1	0	-0.0168
2	-0.0238	0

(b) CCC

Table 3.2: Connectivity between simulated unidirectionally coupled BOLD (fMRI) signal generating nodes. (a) Posterior estimates of effective connectivity using DCM. (b) Causality estimated using CCC.

To \ From	1	2
1	-0.3770	0.2630
2	0.2611	-0.3781

(a) Posterior Expectation (DCM)

To \ From	1	2
1	0	-0.0236
2	-0.0210	0

(b) CCC

Table 3.3: Connectivity between simulated bidirectionally coupled BOLD (fMRI) signal generating nodes. (a) Posterior estimates of effective connectivity using DCM. (b) Causality estimated using CCC.

3.3 Parameter selection for CCC: Criteria and Rationale

In Table 3.4, we summarize the criteria and rationale for choosing the four parameters (w, δ, B, L) of the proposed measure CCC and also give the values chosen for a number of systems. We have described the measure in the last chapter with the idea of intervention. Appropriate parameter selection criteria is done with the view to find out the correct intervention point for a time series to check its causal influence on another given time series . Put more specifically, the main task is choosing the correct value for the length of the time series block Y_{past} and accordingly for X_{past}.

The parameter w, which is the length of the moving window ΔX is fixed to 15 for

Table 3.4: Criteria and rationale for choosing the parameters (w, δ, B, L) for CCC. Values of each parameter chosen for Autoregressive (AR), Tent Map (TM), Squid Giant Axon System (SA) and Predator Prey Ecosystem (PP) are enlisted in the rightmost column. SA and PP are open access real-datasets. Details of their source as well as CCC results obtained for these systems are discussed in Chapter 4.

Parameter	**Description**	**Criteria**	**Rationale**	**Values Chosen**
w	Window length ΔX	Minimal data length over which CC rate can be reliably estimated.	Earlier studies have revealed that ETC is able to reliably capture complexity of even very short time series [79].	AR: 15 TM: 15 SA: 15 PP: 15
δ	Step-size	An overlap of $20-50\%$ between successive time series windows (X_{past} of length L) over which CC is estimated.	To capture the continuity of time series dynamics.	AR: 80 TM: 80 SA: 50 PP: 4*
B	Number of bins	Smallest number of symbols that capture the time series dynamics.	CCC requires symbolic sequences that represent the underlying dynamics.	AR: 2 TM: 8 SA: 2 PP: 8
L	Window length of immediate past to ΔX (X_{past}) and (Y_{past})	After choosing w, δ, B as above, to check causal influence from Y_{past} to ΔX, we plot $ETC(X_{past}+\Delta X)$ and $ETC(Y_{past}+\Delta X)$ vs. L. ***First criteria***: Choose a value of L at which the two curves are well separated. If the above criteria fails (there is an overlap in the ETC curves for all L), we plot $ETC(X_{past}, Y_{past})$ and $ETC(X_{past}+\Delta X, Y_{past}+\Delta X)$ vs. L. ***Second criteria***: Choose a value of L such that the two curves are well separated.	Well separation of the complexity values of time series blocks $(X_{past}+\Delta X)$ and $(Y_{past}+\Delta X)$ is taken to give maximum possible opportunity to Y_{past} to influence ΔX as against X_{past}. This L is hence the best intervention point. If no such value of L can be found, the maximum separation of curves (X_{past}, Y_{past}) and $(X_{past}+\Delta X, Y_{past}+\Delta X)$, gives the maximum opportunity to (X_{past}, Y_{past}) jointly to affect ΔX.	AR: 150 TM: 100 SA: 75 PP: 40

*This was an exception with 90% overlap as very short data length was available.

all the datasets used in this chapter other than the dataset simulated in Section 3.2.8. This is because for this dataset, no value of 'L' could be chosen for $w = 15$ (based on the criteria discussed in the subsection below). Hence, w was set to a higher value. It is chosen such that it contains sufficient number of data points over which CC rate can be reliably estimated. Earlier studies have revealed that ETC is able to reliably capture complexity of even very short time series (as small as length of 10 samples) [79]. δ, the step size by which the ΔX as well as X_{past} window is moved, is chosen based on the criteria of sufficient overlap $(20 - 50\%)$ between successive X_{past} windows of length L. B, the number of bins used to generate the symbolic sequence of the input time series is chosen such that it is sufficient to capture the underlying dynamics. It was found that for the AR processes, $B \geq 2$ is sufficient whereas the time series from the chaotic tent map requires at least $B = 8$.

Once w, δ, B are chosen, we choose L, the window length of X_{past}. For this, we analyze the curves of ETC measure as they vary with L, for different time series blocks as appropriate for a given dataset. A detailed description of selection criteria for L is discussed below.

3.3.1 Selection Criteria for L

We demonstrate the procedure for selection of L for the case of coupled AR processes and tent maps for which CCC performance is detailed in the previous section. Two open access real datasets of Squid Giant Axon system [96,97] and Predator Prey Ecosystem [98, 99] for which causal analysis using CCC is discussed in Chapter 4 were also

taken up to demonstrate criteria for selection of L. At the end, it is shown for a pair of independent processes that no L can be chosen for the system as there is no intervention point at which one has an influence on the other.

As discussed in Table 3.4, for given time series X and Y, we first plot $ETC(X_{past} + \Delta X)$ and $ETC(Y_{past} + \Delta X)$ vs. L when causality is to be checked from Y_{past} to ΔX. We choose a value of L at which the two curves are well separated. We start with an $L = 20(> w)$ and go up to $L = 300$ (in case of the predator prey ecosystem data, only 62 data points were available and thus we go up to $L = 40$). In Figures 3.20, 3.21, 3.22 and 3.23 which show these curves plotted for linearly and non-linearly coupled tent maps, predator prey and squid giant axon systems respectively, there exists some range of values of L for which the two curves are well separated. A value of L can thus be chosen from within this range. The choice of L for these curves is based on averaged ETC values for referred blocks over the entire time series. However, the choice of L may vary with time if we expect to have causality at different temporal scales with varying time. Moreover, for all the cases taken we have chosen the same values of L for checking causality from Y_{past} to ΔX and for checking causality from X_{past} to ΔY. These values can however be different depending on the curves of $ETC(X_{past} + \Delta X)$, $ETC(Y_{past} + \Delta X)$ and $ETC(Y_{past} + \Delta Y)$, $ETC(X_{past} + \Delta Y)$ respectively.

The separation between the curves $ETC(X_{past} + \Delta X)$ and $ETC(Y_{past} + \Delta X)$ is taken to give Y_{past} the maximum opportunity to cause ΔX. The complexities of these time series blocks will be very different at the scale at which there is an influence from past block of Y to the present block of X. Thus the choice of L is about adaptive

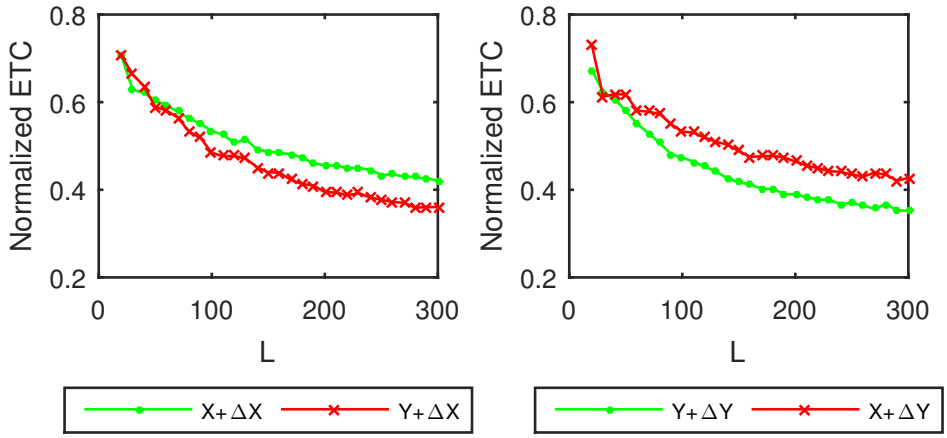

(a) (b)

Figure 3.20: Averaged $ETC(X_{past}+\Delta X)$, $ETC(Y_{past}+\Delta X)$ curves in subfigure (a) and $ETC(Y_{past}+\Delta Y)$, $ETC(X_{past}+\Delta Y)$ curves in subfigure (b) for linearly coupled tent maps ($\epsilon = 0.2$) with Y causing X (simulated as per Eq. 3.3, 3.4). $w = 15, \delta = 100, B = 8$ and L is incremented by a value of 5 data points each time. Using the first criteria for selection of L, $L = 100$ to 300.

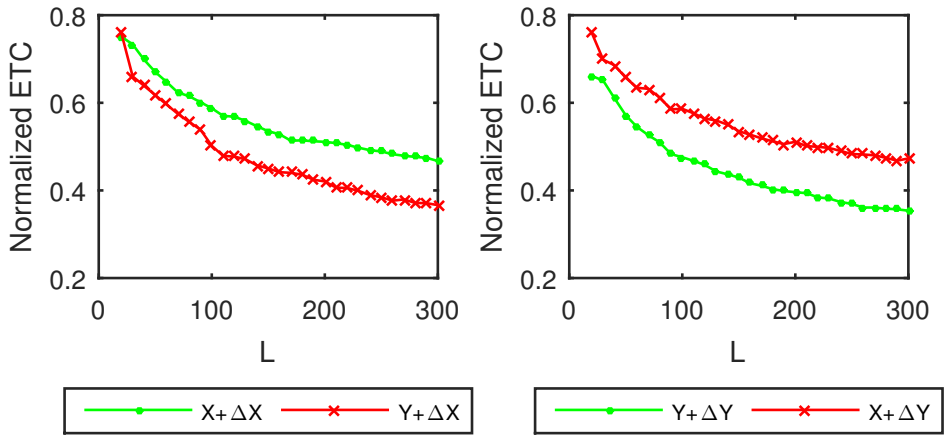

(a) (b)

Figure 3.21: Averaged $ETC(X_{past}+\Delta X)$, $ETC(Y_{past}+\Delta X)$ curves in subfigure (a) and $ETC(Y_{past}+\Delta Y)$, $ETC(X_{past}+\Delta Y)$ curves in subfigure (b) for non linearly coupled tent maps ($\epsilon = 0.2$) with Y causing X (simulated as per Eq. 3.3, 3.5). $w = 15, \delta = 100, B = 8$ and L is incremented by a value of 5 data points each time. Using the first criteria for selection of L, $L = 75$ to 300.

determination of the temporal scale at which causality exists from Y to X.

If the above criteria fails (there is an overlap in the curves), it means that at no

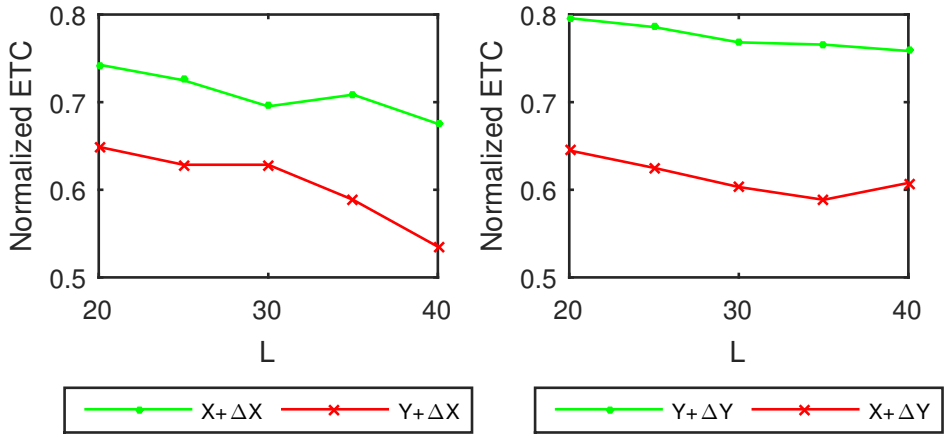

(a) (b)

Figure 3.22: Averaged $ETC(X_{past} + \Delta X)$, $ETC(Y_{past} + \Delta X)$ curves in subfigure (a) and $ETC(Y_{past} + \Delta Y)$, $ETC(X_{past} + \Delta Y)$ curves in subfigure (b) for predator prey ecosystem with Y representing Didinium (predator) population and X representing Paramecium (prey) population. $w = 15, \delta = 1, B = 8$ and L is incremented by a value of 5 data points each time. Using the first criteria for selection of L, $L = 20$ to 40. The results for this case are in the next chapter.

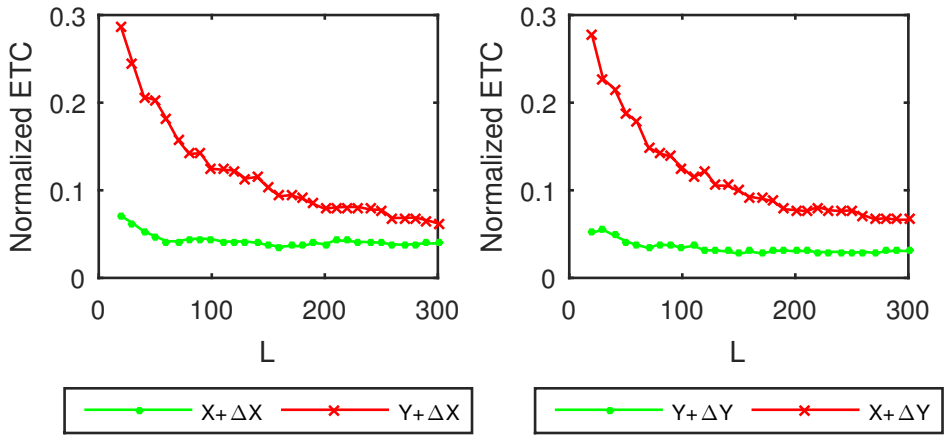

(a) (b)

Figure 3.23: Averaged $ETC(X_{past} + \Delta X)$, $ETC(Y_{past} + \Delta X)$ curves in subfigure (a) and $ETC(Y_{past} + \Delta Y)$, $ETC(X_{past} + \Delta Y)$ curves in subfigure (b) for squid giant axon system ('a5t01') with Y representing the applied stimulus current and X representing observed voltage. $w = 15, \delta = 100, B = 2$ and L is incremented by a value of 5 data points each time. Using the first criteria for selection of L, $L = 75$ to 300. Lower values of L are not used despite sufficient separation so as to avoid making computation based on the transient stage values. The results for this case are in the next chapter.

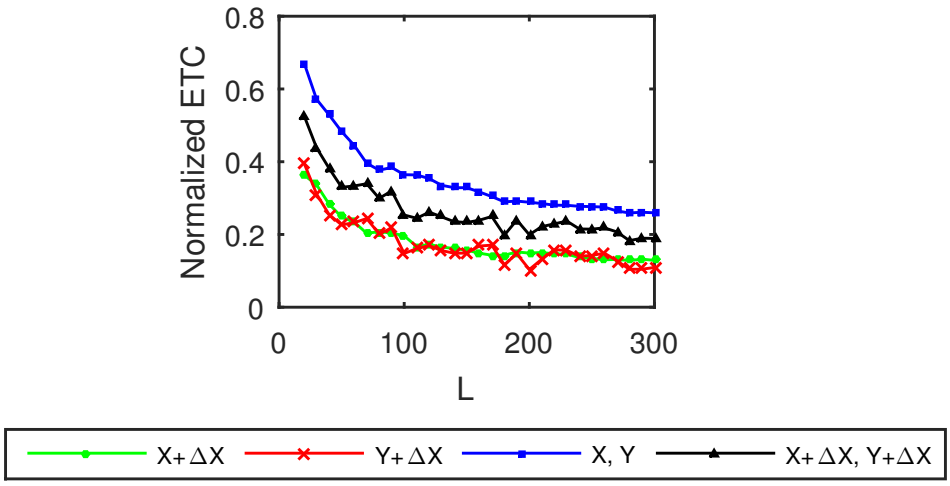

Figure 3.24: Averaged $ETC(X_{past} + \Delta X)$, $ETC(Y_{past} + \Delta X)$, $ETC(X_{past}, Y_{past})$, $ETC(X_{past} + \Delta X, Y_{past} + \Delta X)$ curves for coupled AR processes with Y causing X (simulated as per Eq. 3.1 with $\epsilon = 0.8$). $w = 15, \delta = 100, B = 2$ and L is incremented by a value of 5 data points each time.Using the second criteria for selection of L, $L = 100$ to 300.

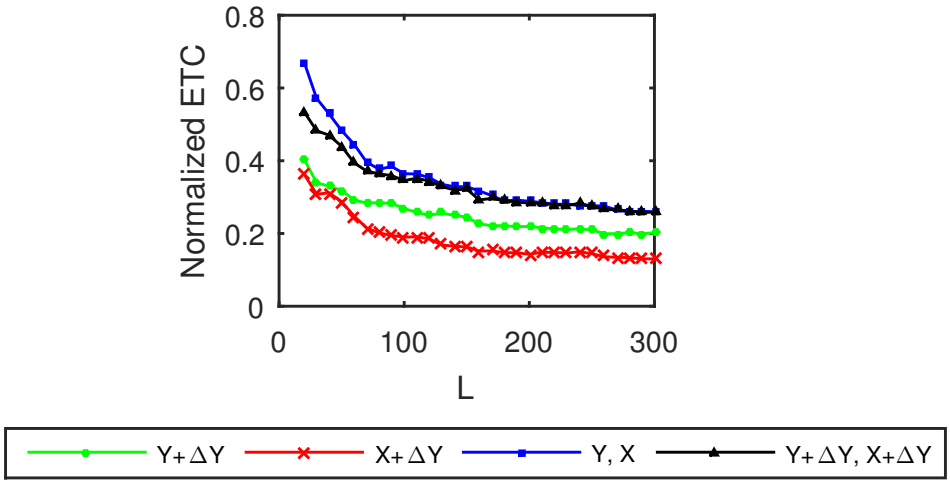

Figure 3.25: Averaged $ETC(Y_{past} + \Delta Y)$, $ETC(X_{past} + \Delta Y)$, $ETC(Y_{past}, X_{past})$, $ETC(Y_{past} + \Delta Y, X_{past} + \Delta Y)$ curves for coupled AR processes with Y causing X (simulated as per Eq 3.1 with $\epsilon = 0.8$). $w = 15, \delta = 100, B = 2$ and L is incremented by a value of 5 data points each time. Using the first criteria for selection of L, $L = 100$ to 300.

temporal scale can Y intervene to make visible its dynamical influence on ΔX (by change of complexity) as against the dynamical influence due to past of X. We then

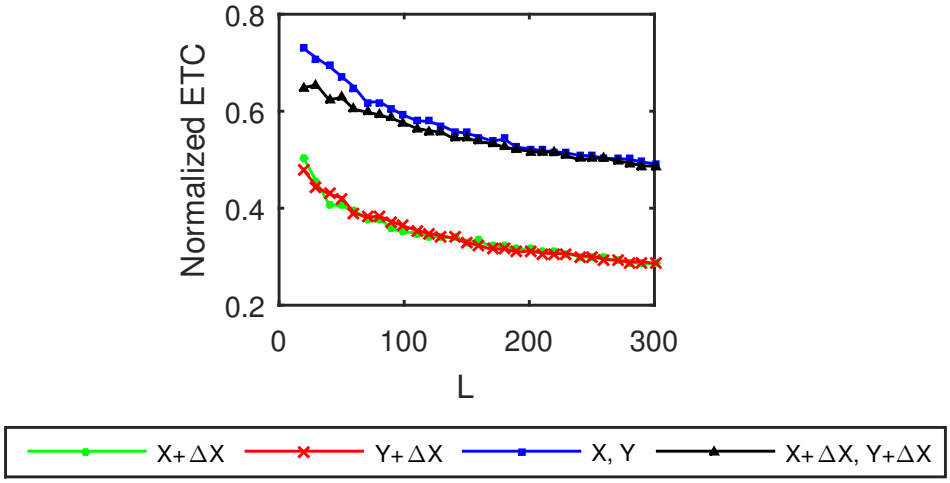

Figure 3.26: Averaged $ETC(X_{past} + \Delta X)$, $ETC(Y_{past} + \Delta X)$, $ETC(X_{past}, Y_{past})$, $ETC(X_{past} + \Delta X, Y_{past} + \Delta X)$ curves for independent processes Y and X. $w = 15, \delta = 100, B = 2$ and L is incremented by a value of 5 data points each time.

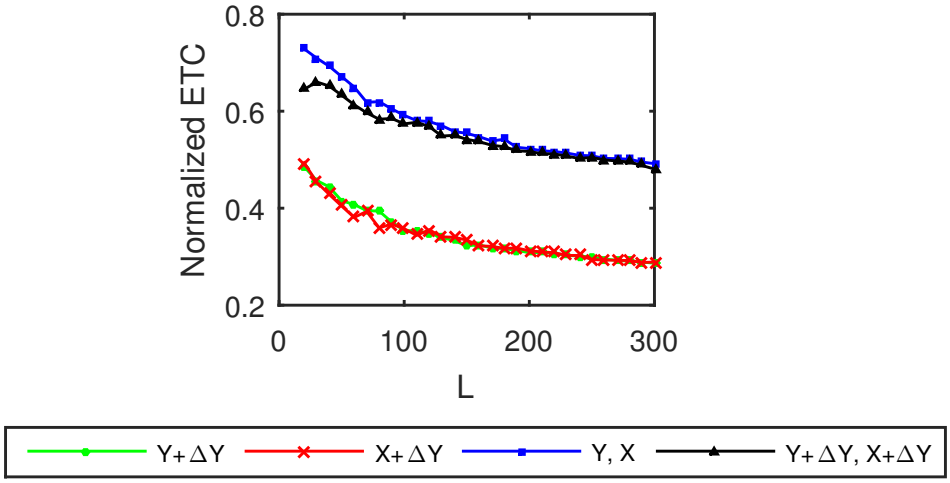

Figure 3.27: Averaged $ETC(Y_{past} + \Delta Y)$, $ETC(X_{past} + \Delta Y)$, $ETC(Y_{past}, X_{past})$, $ETC(Y_{past} + \Delta Y, X_{past} + \Delta Y)$ curves for independent processes Y and X. $w = 15, \delta = 100, B = 2$ and L is incremented by a value of 5 data points each time.

plot $ETC(X_{past}, Y_{past})$ and $ETC(X_{past} + \Delta X, Y_{past} + \Delta X)$ vs. L. We choose a value of L such that the two curves are well separated. In case of AR processes where the first criteria is not met due to the overlap between $ETC(X_{past} + \Delta X)$ and $ETC(Y_{past} + \Delta X)$, the second pair of curves is plotted as shown in Figure 3.24. The rationale behind this

criteria is to see at which intervention point L do X_{past}, Y_{past} jointly begin to have an influence on the dynamical evolution of ΔX.

If the two time series are independent or are constant in time and identical, both the above criteria are bound to fail (this is expected to happen at even higher values of w). This implies that there exists no temporal scale at which there is an influence from one of these time series to the other. For the case of two independent and uniformly randomly distributed real time series the curves for both criteria are shown in Figures 3.26 and 3.27. There exists no value of L at which there is a causality from Y to X or vice versa.

3.4 Significance testing of CCC

Significance testing for results obtained using CCC was done using two ways discussed below.

3.4.1 Distinguishing between presence and absence of couplings

For the case of coupled AR(1) processes and linearly coupled tent maps as simulated in Section 3.2.1, statistical significance testing was done to check if the causality estimated using CCC from $Y \to X$ (in the direction of coupling) was significantly different from the causality estimated from $X \to Y$ (in the direction of no coupling). CCC values as estimated in Section 3.2.1 for data from 50 trials were compared using a paired t-test at different levels of coupling to determine, whether, on average, $CCC_{Y \to X}$ was different from $CCC_{X \to Y}$. Table 3.5 displays the results of this significance analysis for AR(1) processes and Table 3.6 displays the results of the analysis for linearly coupled

tent maps. Each of the tables list the mean and standard deviation of CCC values in the two directions ($CCC_{Y\to X}$ and $CCC_{X\to Y}$), the value of the test statistic (t-value), degrees of freedom of the test (DF) and the p-value obtained. Null hypothesis that the mean of distributions $CCC_{Y\to X}$ and $CCC_{X\to Y}$ is the same, is rejected at a significance level, $\alpha = 0.05$. In other words, the two populations are indicated to be significantly different if the obtained p-value < 0.05.

From Table 3.5, it can be seen that the means of the two populations of CCC values, $CCC_{Y\to X}$ and $CCC_{X\to Y}$ are found to be significantly different for all values of coupling including zero coupling. For the case of zero coupling, mean $CCC_{Y\to X}$ is found to be of much lower value compared to when coupling is increased to a value of 0.1 and beyond. In this case, although the p-value is the highest (of all coupling values considered), it is still found to be much lower than the significance level. Thus, in the case of AR processes, while presence of coupling is distinguished clearly from its absence (in the opposite direction) for all values of coupling considered, the mean of the populations $CCC_{Y\to X}$ and $CCC_{X\to Y}$ was spuriously found to be different even in the absence of coupling in both directions using this method. A difference in the ETC complexity values in the cause-effect pair of coupled AR processes may be the reason for the observed difference in CCC values in the two directions when no coupling is present. Using an adaptive significance threshold that accounts for the difference in the complexity values of the coupled AR processes may help to distinguish between the existence and non-existence of coupling in this case.

For the case of coupled tent maps, it can be seen from Table 3.6, that there is found

Table 3.5: Student's paired samples t-test results to distinguish between causality values obtained using CCC, $CCC_{Y\to X}$ (in the direction of coupling) and $CCC_{X\to Y}$ (in the direction of no coupling), estimated from 50 trials of coupled AR(1) processes. DF refers to degrees of freedom of the test.

Coupling (ϵ)	**Mean ± Std. Dev.** $CCC_{Y\to X}$	**Mean ± Std. Dev.** $CCC_{X\to Y}$	***t*-value**	**DF**	***p*-value**	**Significant difference**
0	0.0071 ± 0.0075	0.0016 ± 0.0053	4.6	49	3.5×10^{-5}	yes
0.1	0.0108 ± 0.0097	0.0014 ± 0.0043	6.3	49	7.8×10^{-8}	yes
0.2	0.0133 ± 0.0106	0.0005 ± 0.0047	8.0	49	1.6×10^{-10}	yes
0.3	0.0213 ± 0.0125	0.0011 ± 0.0038	11.1	49	5.1×10^{-15}	yes
0.4	0.0357 ± 0.0150	-0.0011 ± 0.0047	16.5	49	1.2×10^{-21}	yes
0.5	0.0527 ± 0.0171	0.0005 ± 0.0051	21.7	49	8.3×10^{-27}	yes
0.6	0.0622 ± 0.0187	-0.0007 ± 0.0053	24.0	49	9.1×10^{-29}	yes
0.7	0.0804 ± 0.0208	0.0005 ± 0.0044	27.5	49	1.9×10^{-31}	yes
0.8	0.0909 ± 0.0182	0.0003 ± 0.0052	33.7	49	1.6×10^{-35}	yes
0.9	0.0996 ± 0.0168	-0.0007 ± 0.0050	42.2	49	3.3×10^{-40}	yes

to be no difference in the means of CCC values in the two directions in the case of zero coupling as well as in the case of low coupling (=0.1). The difference then becomes significant for higher values of coupling up to $\epsilon = 0.5$ at which the maps begin to synchronize. Once they are completely synchronized, the values of CCC obtained in

Table 3.6: Student's paired samples t-test results to distinguish between causality values obtained using CCC, $CCC_{Y\to X}$ (in the direction of coupling) and $CCC_{X\to Y}$ (in the direction of no coupling), estimated from 50 trials of linearly coupled tent-map processes. DF refers to degrees of freedom of the test. Coupled maps completely synchronize at $\epsilon > 0.5$ and the two populations become identical.

Coupling (ϵ)	**Mean ± Std. Dev.** $CCC_{Y\to X}$	**Mean ± Std. Dev.** $CCC_{X\to Y}$	**t-value**	**DF**	**p-value**	**Significant difference**
0	0.0015 ± 0.0070	0.0007 ± 0.0082	0.60	49	0.55	no
0.1	-0.0011 ± 0.0087	-0.0029 ± 0.0089	1.12	49	0.27	no
0.2	-0.0044 ± 0.0083	0.0013 ± 0.0096	-3.89	49	2.9×10^{-4}	yes
0.3	-0.0101 ± 0.0076	0.0019 ± 0.0100	-8.05	49	1.6×10^{-10}	yes
0.4	-0.0134 ± 0.0072	0.0027 ± 0.0061	-10.35	49	6.3×10^{-14}	yes
0.5	0.0009 ± 0.0050	0.0002 ± 0.0061	0.99	49	0.33	no
0.6	-0.0000 ± 0.0051	-0.0000 ± 0.0051	-	-	-	-
0.7	-0.0002 ± 0.0058	-0.0002 ± 0.0058	-	-	-	-
0.8	0.0002 ± 0.0062	0.0002 ± 0.0062	-	-	-	-
0.9	-0.0012 ± 0.0059	-0.0012 ± 0.0059	-	-	-	-

the two directions become exactly equal. Hence, significance testing analysis becomes meaningless after synchronization. Except at the lowest value of coupling ($\epsilon = 0.1$) considered here, significance analysis works well to distinguish between the CCC values indicating presence of coupling and those indicating its absence for all levels of coupling.

3.4.2 Analysis using surrogate data

In order to determine the significance of estimated CCC value obtained from a single realization of given coupled processes, surrogate analysis technique was implemented. This will also be useful to determine the presence of coupling(s) where bidirectional coupling could be present between a pair of time series and the aim is not just to distinguish between the direction in which the given time series are coupled and the direction in which they are not (as done in the previous subsection).

A single realization of linearly coupled tent maps, simulated as per Eqs. 3.3 and 3.4 with unidirectional coupling and the degree of coupling, ϵ set to 0.3 was taken. All settings used in simulation, including the length of the signal and transients removed as well as parameter settings for CCC estimation, remained the same as in Section 3.2.1.

The aim of generating surrogate data is to destroy causal relationship, if any, between the given pair of processes. Significance analysis for the case of coupled processes described above was done by generating surrogate data in the following two ways:

1. Using **stationary bootstrap** method. This method was implemented as proposed in [100]. It involves a procedure based on resampling blocks of observations of random length obtained from the original time series. The length of each block has a geometric distribution. This method has been used for generating surrogate data for significance testing of results obtained using other causality testing methods such as TE [101]. To generate surrogate data in our case, we generate resampled time series using the above procedure only for the driver time series

(from which causality to the other time series is computed) and leave the target time series same as the original. The probability parameter that determines the geometric probability distribution for length of each block is set to 0.1.

2. Using **Iterative Amplitude Adjusted Fourier Transform (IAAFT)** method. This method is described in [102]. It generates fourier transform (FT) based surrogates such that the power spectrum density and amplitude distribution of the original time series is maintained but the Fourier phases are randomized. FT based surrogate techniques have been implemented before in significance analysis of causality testing methods such as Conditional Mutual Information [103]. While using this technique for our analysis, IAAFT surrogate time series were generated for both the driver and target original time series.

The generated surrogate data is for the null hypothesis, H_0, that there is no causal dependence between the given pair of processes in the direction considered. To assess the statistical significance of CCC value between given pair of time series in any direction, say, $CCC_{Y\to X}$, surrogate data is generated as described using the two methods above with Y as the driver and X as the target. For estimating significance of $CCC_{X\to Y}$, separate ensemble of surrogate data is generated with X as the driver and Y as the target. z-test is then used to quantify the statistical deviation of CCC between original pair of processes from the CCC values obtained from the corresponding constructed ensemble of surrogate data. H_0 is rejected in favour of the alternate hypothesis of significant causality (using CCC) when the obtained p-value is less than or equal to

the significance level, $\alpha = 0.05$.

Using each of the two surrogate analysis methods discussed above, 50 surrogates for the considered case of coupled tent map processes were generated to test the significance of CCC obtained in each direction. Figure 3.28(a) depicts the position of true CCC value, $CCC_{Y\to X}$ with respect to the distribution of $CCC_{Y\to X}$ values obtained from the generated surrogate data using stationary bootstrap method. The null hypothesis of no coupling is correctly rejected in this case with the obtained p-value being 0.0009. Figure 3.28(b) depicts the same for $CCC_{X\to Y}$. In accordance with the ground reality of no coupling from X to Y, null hypothesis is not rejected in this case with the obtained p-value being 0.2863. Position of true CCC value, $CCC_{Y\to X}$, with respect to the distribution of $CCC_{Y\to X}$ values obtained from surrogate data generated using IAAFT method is shown in Figure 3.29(a). Null-hypothesis is correctly rejected using this method as well, with p-value of 0.0058. Figure 3.29(b) depicts the same for $CCC_{X\to Y}$. Null hypothesis is found to be not rejected here with a p-value of 0.2165.

Above described surrogate analysis techniques to determine the significance of obtained CCC between a given pair of coupled processes is found to work well in the case of deterministic chaotic tent map processes considered. These methods were, however, not found to be able to determine the significance of CCC values for coupled AR processes. When coupling is present between the processes, corresponding surrogate CCC values remain comparable to the true CCC value. So, we implemented the procedure of randomly shuffling the time series data of the driver variable to obtain surrogate data for coupled AR processes. The driven time series variable is kept the same as the origi-

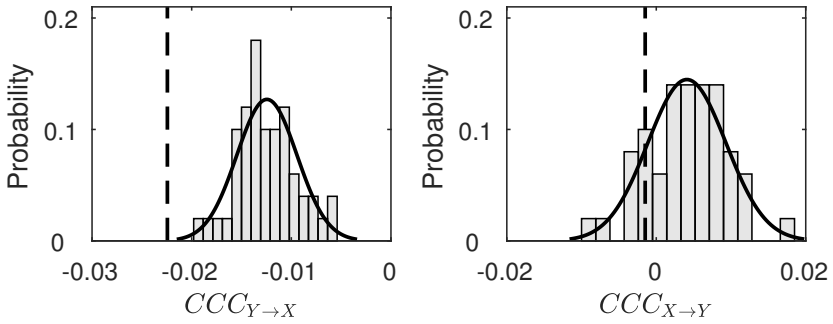

Figure 3.28: Significance testing analysis of CCC between linearly coupled tent map processes with coupling from Y to X using stationary bootstrap surrogate data generation method. Analysis for $CCC_{Y\to X}$ is shown in (a) and for $CCC_{X\to Y}$ is shown in (b). Dashed line indicates CCC value obtained for original series. Its position is indicated with respect to Gaussian curve fitted normalized histogram of surrogate CCC values that form the null hypothesis of no coupling between the processes. Null hypothesis is rejected in case of (a) and not rejected in case of (b).

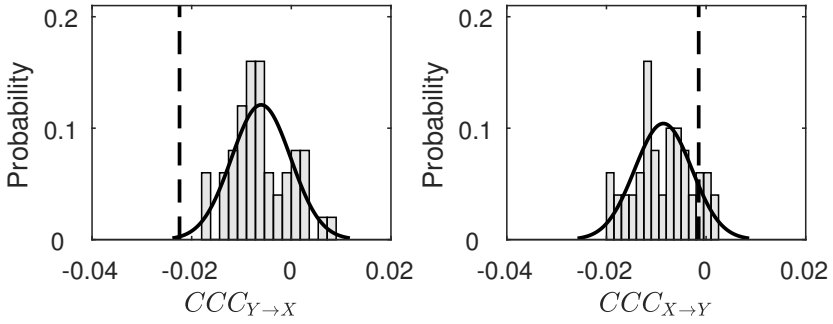

Figure 3.29: Significance testing analysis of CCC between linearly coupled tent map processes with coupling from Y to X using IAAFT surrogate data generation method. Analysis for $CCC_{Y\to X}$ is shown in (a) and for $CCC_{X\to Y}$ is shown in (b). Dashed line indicates CCC value obtained for original series. Its position is indicated with respect to Gaussian curve fitted normalized histogram of surrogate CCC values that form the null hypothesis of no coupling between the processes. Null hypothesis is rejected in case of (a) and not rejected in case of (b).

nal. This procedure seems to destroy the structure in AR time series much better than the surrogate data generation methods implemented before. The procedure of random shuffling has previously been used in other studies such as [53, 104] to determine the

significance of results obtained using causality testing methods.

Coupled AR(1) processes were simulated as in Section 3.2.1 using Eq. 3.1 with Y being the independent and X the dependent process. All settings including the coefficients chosen, length of time series taken and the parameters used for CCC were kept the same as before and ϵ was fixed to 0.6. Interestingly, in this case, $CCC_{Y\to X}$ for original time series was found to be towards the lower end of the tail of $CCC_{Y\to X}$ distribution obtained from surrogate data. Figure 3.30(a) depicts the position of true CCC value, $CCC_{Y\to X}$ with respect to the distribution of $CCC_{Y\to X}$ values obtained from the generated surrogate data using random shuffling method. Figure 3.30(b) depicts the same for $CCC_{X\to Y}$. It can be seen that CCC values for surrogate data became higher than CCC between original pair of time series in the direction in which coupling is present. The surrogate distribution for $CCC_{X\to Y}$ is centred closer to zero and the original $CCC_{X\to Y}$ falls safely in the range of surrogate distribution.

The above observed results seem counterintuitive but could be understood in the light of formulation of CCC and the fact that it gives qualitative information by being positive or negative. The details of positive and negative CCC as well as their relation to the 'kind' of information have already been discussed in Section 2.4. When CCC values are positive, it is known that the driver time series, Y_{past}, brings 'similar' kind of information to ΔX, as that brought by its own past, X_{past}. Let us consider the specific case of AR processes (as discussed in Table 2.1), with coupling from $Y \to X$ for which $CCC_{Y\to X} > 0$. In this case, the values obtained for compression-complexities, $CC(\Delta X|X_{past})$ and $CC(\Delta X|X_{past}, Y_{past})$, are both negative with $|CC(\Delta X|X_{past})| <$

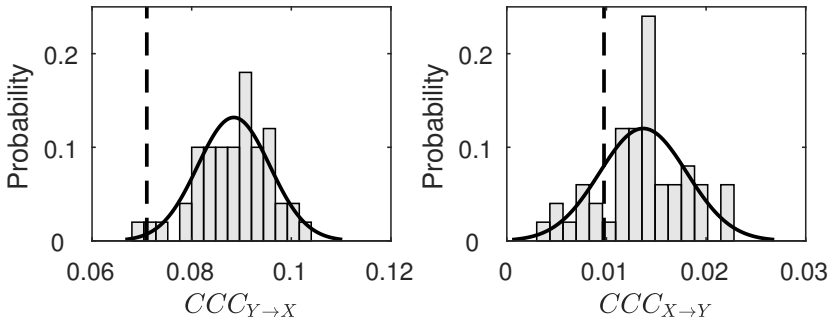

Figure 3.30: Significance testing analysis of CCC between AR processes with coupling from Y to X using random shuffling surrogate data generation method. Analysis for $CCC_{Y\to X}$ is shown in (a) and for $CCC_{X\to Y}$ is shown in (b). Dashed line indicates CCC value obtained for original series. Its position is indicated with respect to Gaussian curve fitted normalized histogram of surrogate CCC values that form the null hypothesis of no coupling between the processes. Null hypothesis is rejected in case of (a) and not rejected in case of (b).

$|CC(\Delta X|X_{past}, Y_{past})|$. This is because intervention by Y_{past} in the joint case enhances the structure by bringing patterns similar to X_{past}. When coupling $Y \to X$ is low, X is predominantly determined by its own past and very less by Y. In that sense, X is close to the independent AR process Y and hence $CCC_{Y\to X}$ is low. Here, X_{past} brings most information to ΔX and little is determined by Y_{past}. On the other hand, when coupling is high, Y_{past}, though determining ΔX with the same patterns as those brought by X_{past} to determine ΔX, is no longer close to X_{past}. This is because X_{past} now contains very little information for ΔX and the latter is mostly determined by Y_{past}. For this reason, $CC(\Delta X|X_{past}, Y_{past}) << CC(\Delta X|X_{past})$ in this case and $CCC_{Y\to X}$ attains a high positive value. Now, if Y_{past} is randomized and made even more different from X_{past} than it currently is, $CCC_{Y\to X}$ values end up increasing more. Thus, randomization of Y helps determine a bound for a given Y for the extent by which Y_{past} and X_{past} can

become most different in their attempt to determine ΔX. While Y_{past} being exactly the same as X_{past} was one extreme at which $CCC_{Y\to X} = 0$ because Y brings no new information; the other extreme for a given Y can be obtained by randomly shuffling it. In the latter case Y is most different from X (in the sense of influencing ΔX), and is no longer exhibiting control over ΔX. For a given Y which is not coupled to X, it is expected that the 'no control' scenario of Y over X cannot further be aggravated if Y is randomized. Here, $CCC_{Y\to X} \approx CCC_{Y_{rand}\to X}$, where Y_{rand} represents time series obtained by random shuffling of Y. Thus, for any Y, if $CCC_{Y\to X} \approx 0$ or $CCC_{Y\to X} \approx CCC_{Y_{rand}\to X}$, we can infer that there is no causality from $Y \to X$ based on CCC. Ideally, a number of surrogate time series Y_{rand} should be taken to check if $CCC_{Y\to X}$ is significantly different from the population $CCC_{Y_{rand}\to X}$.

With this understanding, we consider the $CCC_{Y_{rand}\to X}$ distribution as the distribution of our null hypothesis of no causation between the coupled AR processes taken for analysis. 50 surrogate datasets were generated. Gaussian curve fitted normalized histogram for $CCC_{Y_{rand}\to X}$ and $CCC_{X_{rand}\to Y}$ are shown in Figure 3.30(a) and Figure 3.30(b) respectively. As in the case of significance analysis of CCC for tent maps, z-test was used to quantify the statistical deviation of CCC between original pair of processes from the CCC values obtained from the corresponding constructed ensemble of surrogate data. The significance level, α, of the test was set to 0.05. The null hypothesis of no coupling was correctly rejected in the case of $CCC_{Y\to X}$ with the obtained p-value being 0.0162. Null hypothesis of no coupling was not rejected in the case of $CCC_{X\to Y}$ with the obtained p-value being 0.3698.

If the results are analyzed more closely, it seems that a non-zero upper bound (in the case of true $CCC > 0$ that we have considered) will be present only if a given Y when reorganized (from a shuffled extreme to an unshuffled extreme state) has the *potential* to cause the taken target time series. For instance, if we take the case of $CCC_{X \to Y}$ for the coupled AR processes (for any value of coupling coefficient, ϵ, from Y to X), the distribution of surrogate CCC values as well as original CCC value both remain close to zero. The upper bound value, being very much data dependent, here converges to the lower bound. Since the CCC of shuffled time series does not increase here, this indicates that even a reorganized version of X may not be possessing the potential to cause Y. This is interesting because in this way CCC may be able to detect processes which are containing causal information to other processes but not in the traditional cause followed by effect manner.

The procedure of randomly shuffling the driver time series to generate surrogate data for coupled tent map system was also implemented and found to yield results similar to Figure 3.28 and 3.29. Distribution of surrogate CCC values was found to take negative values of lower magnitude (close to zero) while original CCC value took a negative value of high magnitude in the presence of coupling. Results for significance analysis of CCC values obtained for tent maps and AR processes are consistent in the aspect that random shuffling of driver time series led the CCC values to attain the maximum possible value between given pair of time series. However, for AR processes the lower bound of CCC (zero) and the upper bound of maximum CCC value are different and for tent maps, the two are converging. In the case of tent maps, the

nature of their coupling results in both $CC(\Delta X|X_{past}, Y_{past})$ and $CC(\Delta X|X_{past})$ being negative with $|CC(\Delta X|X_{past}, Y_{past})| < |CC(\Delta X|X_{past})|$. When Y is made identical or close to identical with X, in that case $CC(\Delta X|X_{past}, Y_{past}) \approx CC(\Delta X|X_{past})$ and when Y is randomized, in that case too $CC(\Delta X|X_{past}, Y_{past})$ attains the highest negative value possible for it, which is $CC(\Delta X|X_{past}, Y_{past}) \approx CC(\Delta X|X_{past})$. It would be interesting to explore if a high negative value bound (that is, the other extreme bound) exists for $CCC_{Y\to X}$. If yes, we would like to see what transformations of given time series would help estimate that bound, and also what would be the meaning of that bound.

It should be noted that, when we took lower values of coupling ($\epsilon \leq 0.4$) between the pair of AR processes coupled from $Y \to X$, the true $CCC_{Y\to X}$ was not found to be significantly lower than the surrogate distribution $CCC_{Y_{rand}\to X}$. This was probably because randomly shuffling the driver time series was not sufficient to destroy further the weak causal structure from Y_{past} to ΔX (relative to X_{past}). The procedure seems to be not powerful enough to yield an appropriate surrogate distribution of CCC values representing no causal influence. CCC estimates causality using ETC which is based on capturing compressibility of patterns at different scales of the sequence. Hence, to get appropriate null distribution of CCC values using surrogate data, patterns in AR may be required to be perturbed at different scales.

3.5 Computational Time Complexity Analysis for CCC

To give an idea of the computational complexity of CCC, we do a simple timing analysis of running CCC on a coupled AR (100) system (Y causing X). The system is simulated as per Section 3.2.1 using Eq. 3.2 with the degree of coupling, ϵ, set to 0.7. The length of the signal taken was 1000.

For 100 runs of the same realization of the above process, the mean and standard deviation of timings (in seconds) required for running of CCC, TE and GC were estimated. This is the total timing required for computation of causality from Y to X as well as from X to Y. Results of this timing analysis are displayed in Table 3.7. Here as well, GC estimation was done using the MVGC toolbox in its default settings and TE estimation was done using MuTE toolbox. Akaike Information Criteria was used for model order estimation with the maximum model order set to 110 in the MVGC toolbox. In the MuTE toolbox, the approach of non-uniform Embedding for representation of the history of the observed processes and of nearest neighbor estimator for estimating the probability density functions with default settings as discussed in Section 3.1. Parameters for CCC used are: $L = 150, w = 15, \delta = 80, B = 2$.

Table 3.7: Mean and standard deviation of running times (in seconds) of CCC, TE and GC for simulated coupled AR(100) processes, taking 100 runs of a single realization of the process. Machine specifications: ubuntu 16.04 LTS, with Memory 31GiB, Processor: Intel Xeon(R) Silver 4108 CPU @ 1.80GHz*1 x 16, 64 bit, MATLAB 2017b

CCC (in s)	**TE** (in s)	**GC** (in s)
0.4145 ± 0.0125	16.4836 ± 0.9610	0.1826 ± 0.0124

From the above timing analysis, it is seen that mean running time of CCC is 0.4145s, which is slightly higher than that of GC but much less than TE. Therefore, from a computational point of view, it can be said that bivariate CCC can be easily scaled for hundreds of signals.

It should be noted that our MATLAB implementation is far from being optimized. Hence, these timing results are only indicative. Faster implementations of CCC will be developed in the future.

3.6 Conclusions and Future Work

In this chapter, we rigorously test for the performance of CCC on simulations. Using various instances of short-term and long-term memory autoregressive processes as well as chaotic processes, it is shown that CCC is highly robust and reliable. CCC overcomes the limitations of existing measures (GC, TE, NGC and CCM) in case of signals with long-term memory, low temporal resolution, noise, filtering, non-uniform sampling (non-synchronous measurements), as well as finite length signals. As future work, it will be worthwhile to explore the performance of other complexity measures such as Lempel-Ziv complexity for the proposed *Interventional Complexity Causality* approach.

Parameter selection criteria and rationale for the CCC measure are also proposed in this chapter. This criteria can be improved, and made even more data-adaptive by exploring ways of selecting appropriate values of w; using better binning strategies (instead of using uniformly sized bins) and consequently making appropriate choices for the parameter B. Methods such as TE have evolved to use better methods, such

as embedding for determining the past states to be chosen from time series (that help predict its present state) and have also chosen better means such as k-nearest neighbors estimators for computing required probability density functions [90]. As a better binning strategy, we employed a method by which the symbolic sequence computed from a given time series, contained approximately the same number of points in each bin. This was implemented by using the method of k-means clustering. This approach was similar to the method of equiquantization binning as has been implemented for the conditional mutual information causality method [103]. Preliminary results obtained using this method for CCC were not very different from those obtained by using uniformly sized bins. It will be interesting to check the performance of this method on different types of datasets. Other means of binning such as the Bandt and Pompe scheme [105] and others based on obtaining 'generating partition' of dynamical systems (thereby, helping in preserving their dynamical information) [106] will also be explored as part of future work. Though methods to choose selected values for the past (X_{past}) and present (ΔX) windows (as happens in embedding) may not make much sense for CCC (as it looks at the continuous dynamics of the processes and chooses a data adaptive intervention point), it will still be interesting to see the change in the performance of the measure when these schemes are implemented.

Significance testing of obtained CCC estimates has been done using two approaches. Student's t-test approach is used for distinguishing between the presence and absence of coupling using CCC value distributions from 'the direction of coupling' and 'opposite to the direction of coupling'. Here, it would be good to develop data based significance

level (threshold) settings for the t-test to get better results. The second method for significance analysis based on surrogate data has been illustrated for coupled tent maps and AR processes. In the case of tent maps with negative CCC, the surrogate distribution is centred close to zero and a highly negative value being significantly different from the surrogate population is classified as having a significant causal influence. On the other hand, for AR processes, surrogate data in which the temporal structure of causal influence is destroyed yields higher positive values of CCC as compared to the true CCC value in the direction of coupling. For tent maps, it would be interesting to explore if a 'high negative value' CCC bound exists analogous to the 'high positive bound' for AR and what would be the meaning of such a bound. For AR significance testing analysis, future work is to find appropriate surrogate data generation strategies when coupling strength between the considered processes is low in magnitude. These strategies would be aimed at better destroying the structure (at multiple scales, if possible) of coupled processes.

Computational time complexity results presented for CCC based on code running time comparison with existing methods is only indicative. As future work, we would like to develop faster implementations of the method.

Chapter 4

CCC Applications on Real-World Datasets

Causality testing of time series data has numerous applications in fields such as earth sciences, neuroscience, econometrics, epidemiology and engineering. The strengths of CCC measure inherent in its formulation (discussed in Chapter 2) and as revealed from simulation studies (in Chapter 3) are expected to be useful in overcoming the limitations of existing measures for successfully determining causal relations from real-world datasets. In this chapter, CCC is applied for testing causal interactions between populations of organisms in a predator-prey ecosystem as well as voltage-current recordings obtained from a squid giant axon. Further, causality analysis was done for analysing brain connectivity during fixation, instruction, planning and movement phases of a motor task presented to 5 human subjects. Motor tasks involve a complex process wherein signals are communicated between different brain regions. We use causality testing techniques – CCC and Nonlinear Granger Causality and apply it on electroencephalographic time series data acquired from the subjects in order to understand connectivity at differ-

ent stages of motor planning and movement process. Causality testing techniques also find applications in some approaches to measure consciousness based on computing the strength of complex causal neural interactions in the brain. In this chapter, we propose a novel quantitative measure of consciousness - Network Causal Activity, which is based on CCC. This measure is used to distinguish different states of consciousness (awake and anaesthesia) based on analyzing electrocorticographic signals from the lateral cortex of four monkeys.

4.1 Introduction

The application of causality measures across different disciplines of science has seen a tremendous increase in the recent years. This is not surprising as the very effort of science is to try to rationally understand the causes behind observed phenomena. Applications of existing causality measures on real world systems to infer causal relationships between variables of interest has proved enormously useful not only from the point of view of increasing scientific knowledge and understanding [16, 17, 22, 107] but also for making informed decisions for the society [18,58,108]. However, existing causality measures are restricted to specific kinds of data (or applications) by the nature of their formulation and/or exhibit limitations when the data made available is corrupted with noise or other artefacts [35, 36, 40, 48, 49, 58]. Limitations of some of the existing measures such as Granger Causality (GC) [5], Transfer Entropy (TE) [23], Non-linear Granger Causality (NGC) [24] and Convergent Cross Mapping [28] have been demonstrated in Chapter 3 using simulated data. CCC measure, proposed in Chapter 2, has

immense potential to be applied successfully for real world systems. Using simulations, its performance has been tested against existing measures in Chapter 3. This rigorous testing brought to light some of the unique strengths of CCC such as its robustness to noise, low temporal resolution, non-uniform sampling, filtering, long term memory as well as short length of signals. In this chapter, we use CCC to discover causal relationships of interest in some real world systems.

Simple bivariate real systems have been used to test the performance of causality measures. For example, causal relationship between recordings of heart rate and breathing rate in humans has been analyzed using TE [23] and NGC [24]. A simple predator-prey ecosystem was analyzed in [28]. In the first section of this chapter, we demonstrate the performance of CCC on the bivariate system comprised of the predator-prey ecosystem that has been used in [28]. The second bivariate system considered in this section is that of stimulus current and voltage recordings obtained by an experiment on the squid giant axon. Results using TE are also reported for these systems.

In the second section, we move on to analyzing a more complex system of brain interactions during different phases of a hand motor task. Use of techniques to analyze interactions between different brain regions is known as *brain connectivity* analysis [109, 110]. If the interactions are analyzed based on recorded neurophysiological signals from different regions of the brain by using techniques such as correlation, the analysis is known as *functional connectivity* analysis. Even asymmetric connections found using data based causality estimation measures (such as GC and TE) fall in

this category. On the other hand, if model based causal inference techniques (such as Dynamic Causal Modeling) are used to estimate the parameters of the model based on the recorded data, the analysis is known as *effective connectivity* analysis as it reflects the underlying mechanism of interactions [111]. In the last few decades, the use of functional connectivity analysis has increased tremendously in order to understand brain's functional architecture and operational principles [16, 111, 112]. As discussed in Section 2.3, CCC measures *effect* akin to measures GC and TE and not *mechanism*. However, we expect CCC estimates to have a close relation to the mechanism as it determines causes and effects based on dynamical evolution of the processes. In this work, we use CCC as well as NGC to analyze interactions using electroencephalographic signals recorded from five healthy human subjects engaged in a motor task. This analysis helps to reveal some interesting changes in causal connectivity of regions in the brain involved in motor planning and execution.

Finally, we use CCC for developing a novel method of measuring the level of consciousness. Characterizing consciousness, the inner subjective feeling that is present in every experience, is a hard problem in neuroscience [113], but has important clinical implications [114]. A leading neuro-scientific approach to understanding consciousness is to measure the complex causal neural interactions in the brain [115]. Elucidating the complex causal interplay between cortical neural interactions is a challenging task. A novel quantitative measure of consciousness - *Network Causal Activity* which is based on CCC is proposed in this work. This measure is used to analyze electrocorticographic signals from the lateral cortex of four monkeys during two states of consciousness (awake

and anaesthesia). Our results suggest that Network Causal Activity is consistently (and statistically) higher in the awake state as compared with anaesthesia state for all the monkeys.

4.2 Predator-Prey Ecosystem and Squid Giant Axon Recordings

CCC was applied to estimate causality on measurements from two real-world systems with bivariate recordings and compared with TE. System (a) comprised of short time series for dynamics of a complex ecosystem, with 71 point recording of predator (Didinium) and prey (Paramecium) populations, reported in [98] and originally acquired for [99], with first 9 points from each series removed to eliminate transients (Figure 4.1(a)). Length of signal on which causality is computed, $N = 62$, CCC settings used: $L = 40$, $w = 15$, $\delta = 4$, $B = 8$. These parameters were selected based on the parameter selection criteria discussed in Section 3.3; the curves for selection of L are shown in Figure 3.22. CCC is seen to aptly capture the higher (and direct) causal influence from predator to prey population and lower influence in the opposite direction (see Figure 4.1). The latter is expected, owing to the indirect effect of the change in prey population on predator. CCC results are in line with that obtained using Convergent Cross Mapping [28]. TE, on the other hand, fails to capture the correct dominant causality direction.

System (b) comprised of raw single-unit neuronal membrane potential recordings (V, in 10V) of squid giant axon in response to stimulus current (I, in V, 1V=5 $\mu A/cm^2$),

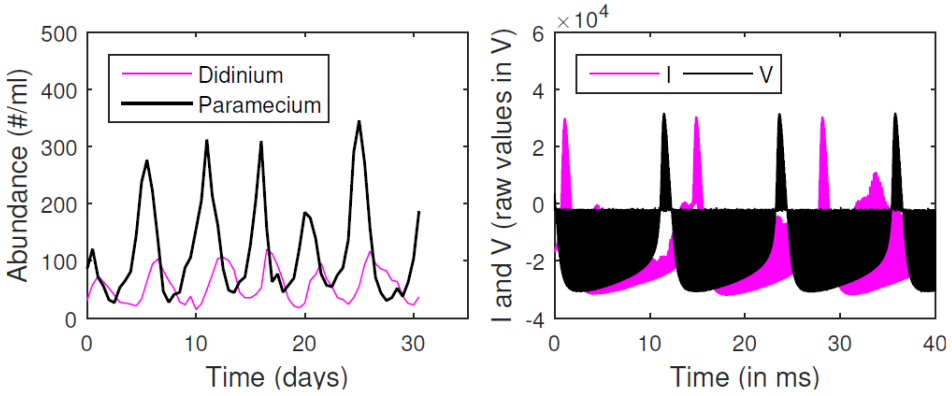

(a) Predator-Prey system. (b) Squid Axon system.

System	Details	CCC		TE	
		$Y \to X$	$X \to Y$	$Y \to X$	$X \to Y$
Predator-Prey	$Y = D_n$ $X = P_n$	0.116	-0.021	0.249	0.252
Squid Axon	$Y = I_{a3t01}$ $X = V_{a3t01}$	-0.142	-0.129	0	0.049
	$Y = I_{a5t01}$ $X = V_{a5t01}$	-0.142	-0.135	0.055	0.108
	$Y = I_{a7t01}$ $X = V_{a7t01}$	-0.153	-0.154	0.196	0.127

(c)

Figure 4.1: CCC, TE on real-world time series. (a) Time series showing population of *Didinium nasutum* (D_n) and *Paramecium aurelia* (P_n) as reported in [98], (b) Stimulus current (I) and voltage measurements (V) as recorded from a Squid Giant Axon ('a3t01') in [96]. (c): Table showing CCC and TE values as estimated for systems (a) and (b).

recorded in [96] and made available by [97]. Stochastically varying current was applied across the axon in order to study bistable switching behavior in neurons. We test for causation between I and V for three axons (1 trial each) labeled 'a3t01', 'a5t01' and 'a7t01', extracting 5000 points from each recording. Length of signal on which causality is computed, $N = 5000$, CCC settings used: $L = 75$, $w = 15$, $\delta = 50$, $B = 2$. These parameters were selected based on the parameter selection criteria discussed in

Section 3.3; the curves for selection of L are shown in Figure 3.23. We find that $CCC_{I\to V}$ is less than or approximately equal to $CCC_{V\to I}$ and both values are less than zero for the three axons (Figure. 4.1), indicating negative causality in both directions. This implies bidirectional dependence between I and V. Each brings a different dynamical influence on the other when compared to its own past. TE fails to give consistent results for the three axons.

4.3 Brain Connectivity during Motor Task

Connectivity analysis of signals arising from different parts of the brain during motor tasks has recently gained a lot of interest. Such studies are extremely useful to study the motor pathway, interactions between different brain regions involved in a motor task as well as brain regions involved in motor deficits. Motor experiments have been conducted on normal and pathological humans as well as primates. Researchers have utilized a range of electrophysiological techniques (such as electroencephalography, local field potentials, magnetoencephalography) [116–118] and neuroimaging techniques (such as functional magnetic resonance imaging, functional near infrared spectroscopy) [119–122] as well as a combination of both [123] for the analysis of functional connectivity during motor tasks. The above studies make use of different causality estimation techniques to analyze brain networks involved in motor task with a majority of them applying GC.

In this section, we use the proposed measure CCC for the brain connectivity analysis during motor task. NGC is also used in the analysis to ascertain if there is consistency or difference in the performance of the two measures. The analysis is done for elec-

troencephalographic (EEG) data acquired from subjects performing a novel reaching task (discussed in the following subsection). We consider four different phases of the task including resting phase, instruction phase, planning phase and movement phase. The connectivity between different brain regions chosen for analysis is compared in the different phases. Thus, the novelty in our work lies in the causality measures used, the motor task performed by subjects as well as the connectivity comparison done across the different phases considered.

4.3.1 Dataset Description

Data for analysis was obtained from Prof. Aditya Murthy's Lab on Motor Control, Indian Institute of Science, Bengaluru, India (V. Thakur and A. Murthy, personal communication, May 21, 2020). A brief description of the experimental setup and acquisition protocol is provided below. The data was from a behavioral task in which the subjects performed a novel reaching task where they had to move their hand from the central fixation spot to the target spot according to the the instructions provided. Electroencephalography and electromyography recordings were made during the task. For each subject, each trial was 7000 ms long. With the initiation of the trial, subjects were presented with a gray colored fixation spot where they had to fixate their eyes and index finger of the right hand (all subjects were right handed males). After 530 ms, fixation box changed its color. This was followed by an instruction time of 780 ms. After this, a target appeared on the screen, at a distance of 12 cm from the fixation point. The target was randomized to be at the top left or bottom right positions of

the screen with equal probability. The go cue was indicated by changing of the filled fixation box to unfilled. Subjects were told to make a reaching movement towards the target as soon as the go cue was presented. Hand and eye movements of the subjects were tracked throughout the study. Based on certain criteria on the timings of hand movement (if it starts too long after the go cue, or total duration of movement is too short or too long), some trials were discarded. Other trials, in which there was eye blinking, head movement or eye movement were also discarded.

EEG activity was recorded passively from 22 Ag/AgCl electrodes mounted on an elastic cap (by EasyCap company, Germany) which was worn by the subjects on their heads. The positions of the electrodes were marked on the cap as per the international 10/20 system. EEG signals were sampled at 1kHz. The electrodes from which activity was recorded include FP1, FP2, F3, F4, FC1, FC2, C3, C4, CP1, CP2, P3, P4, O1, O2, FC5, FC6, Fz, FCz, Cz, Pz, and Iz. The AFz electrode was used as the ground for all recordings and averaged activity of linked left mastoid, and right mastoid was used as reference.

For our analysis, we consider trials in which the subjects were instructed to make slow hand movements from the fixation spot to the target spot and there was no time lag between the appearance of the target on the screen and the go cue. Before using the EEG recordings for brain connectivity analysis, each trial was individually detrended and notch filtered. Out of 10 subjects for which data was made available, we took 5 randomly chosen subjects for our analysis. For each subject, first 50 correct trials were taken.

To analyse connectivity during different phases of the task, the recorded activity for each trial and from each electrode was divided into the following different phases:

1. Fixation Time or FT is the time beginning from the initiation of the trial and lasts up to 500 ms. During this time the subject fixates on the gray colored box displayed on the screen.

2. Instruction Time or IT is the time from fixation offset to target onset. This period is taken to last for 750 ms during which instruction is provided to the subject regarding how to make the movement.

3. Reaction Time or RT is the time from when the Go signal appears till hand movement onset. The beginning of hand movement was found as follows: first, the time when velocity reached 10% of maximum velocity of the trial was extracted and used as an initial onset marker. Moving back from this marker, the onset was considered when the velocity was not significantly different from the baseline hand movement fluctuation. RT can be thought of as the planning phase of the movement at which the subjects have all the instructions, as to the 'where, when and how' of the movement. All trials are aligned at the time at which Go cue appears to extract the data for this phase. RT will be different for each trial. By observing the time it takes from Go cue to movement onset across trials from different subjects, we fix the RT period to last for 300 ms. This value lies towards the lower end of the distribution of RT values and was taken to consider a safe time duration for the subjects where the considered time samples do not extend beyond

the RT range. This choice of RT period was decided over email conversation (V. Thakur and A. Murthy, personal communication, October 8, 2019).

4. Movement Time or MT is the time from movement onset and lasts until the finger reaches the target. Hand movement onset is computed as discussed in the last point. To extract the data for this phase, all trials were aligned at their movement onset. MT will be different for different trials. We fix MT to last for 500 ms, in order to keep it close to the average time taken for slow movement, as observed from different trials taken from all the the subjects. This value was also decided over email communication (V. Thakur and A. Murthy, personal communication, October 8, 2019).

The data with preprocessing as discussed above and after alignment along the four phases described above was made available by Prof. Aditya Murthy's Lab group (V. Thakur and A. Murthy, personal communication, May 21, 2020).

The lateralized readiness potential (LRP) is an event-related potential that is observed when the person gets ready to move one hand, arm, leg or foot. It is a negative potential that can be observed over the motor cortex and other surrounding brain regions governing movement, contralateral to the responding hand [124, 125]. To ensure that the LRP signature was visible in the acquired data, we obtained the LRP plot by averaging raw signals from all the 10 subjects, using all the correct trials obtained from each subject. EEG activity from MT aligned phase was taken from the following 4 electrodes: FC1, FC2 (left and right fronto-central/ premotor cortex), C3, C4 (left

and right central/ motor cortex). The data from these electrodes was lateralized by subtracting the right electrode activity from the corresponding left electrode activity for each trial. The resulting signals were then averaged across all the considered electrodes for all the subjects taken together. The resulting LRP plot is shown in Figure 4.2. The dip in the potential before movement onset is visible in the figure.

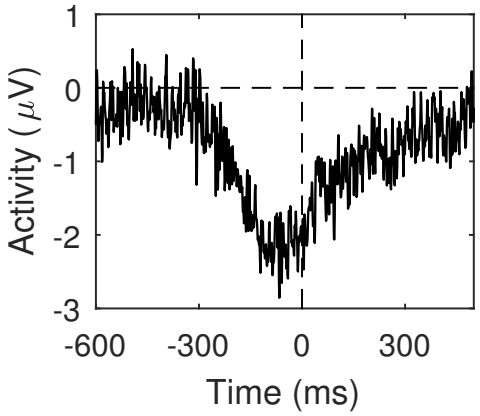

Figure 4.2: Lateralized readiness potential using averaged raw EEG signals (from electrodes – FC1, FC2, C3, C4) from 10 subjects, using all the correct trials per subject. The trials are aligned along movement onset which is represented by a vertical dotted line in the figure.

Since, we took the data from 5 subjects, 50 trials per subject for connectivity analysis, we also plot the LRP for this data alone. These trials were detrended and notch-filtered before further analysis. LRP obtained from the same electrodes as before (FC1, FC2, C3, C4), for this pre-processed data is shown in Figure 4.3.

4.3.2 Results and Discussion

Connectivity analysis was done in two ways. In the first case, connectivity was analyzed taking the signals without lateralization. The results for this analysis are discussed under the section 'Contralateral Ipsilateral Analysis'. Contralateral here basically refers to

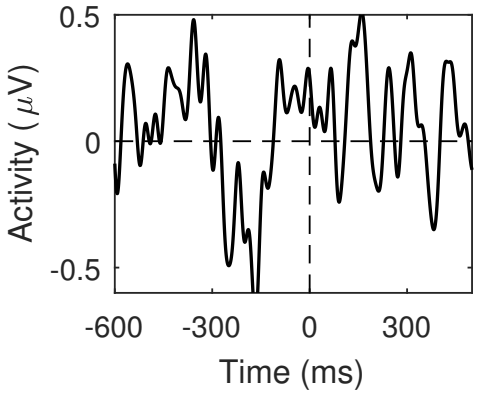

Figure 4.3: Lateralized readiness potential using averaged pre-processed EEG signals (from electrodes – FC1, FC2, C3, C4) from 5 subjects with 50 trials per subject. The trials are aligned along movement onset which is represented by a vertical dotted line in the figure.

the side of the brain contralateral (opposite) to the moving (right) hand and ipsilateral refers to the side of the brain ipsilateral to (or on the same side as) the moving hand. In the second case, the recordings were lateralized by subtracting the right electrode activity from the corresponding left electrode activity. The results for this analysis are discussed in 'Lateralized Analysis'. All connections were analyzed using both bivariate CCC and bivariate NGC.

Contralateral Ipsilateral Analysis

For this analysis, we consider only the premotor and motor regions, that is, the recordings from electrodes FC1, FC2 and C3, C4 respectively. CCC as well as NGC were used to analyze the causality between premotor and motor regions (both directions) contralateral to the movement (FC1 and C3), ipsilateral to the movement (FC2 and C4) as well as cross connections between the contralateral premotor region and ipsilateral motor region as well as between ipsilateral premotor region and contralateral motor

region. These four connections in both directions were analyzed for all the 5 subjects for the four phases considered.

The parameters used for estimation of CCC from the considered signals were set to $L = 120, w = 30, B = 4$. δ, the step size for moving window, was set to be different for different phases as the length of the available recordings was different for each of the phases. These parameters were selected according to the parameter selection criteria discussed in 3.3. For FT and MT signals which were taken for 500 ms (with 500 time points), δ was set as 50. For RT data which was shorter, lasting for 300 ms, δ was taken to be 30 and for IT data, lasting for 750 ms, δ was set as 70. For NGC estimation, the parameters were set as follows: polynomial type of kernel of order 2 and model order also set to 2 was used. Values of the two measures were computed for 50 trials taken per subject. As per significance analysis embedded in the NGC toolbox, if a non-zero value of the measure is obtained, then it can be said to be significant [24, 45, 92]. Using this criterion only, we classified a connection as being significant or insignificant for NGC. For performing significance analysis for CCC, the observations in each trial of the considered driver[1] variable were randomly shuffled once to obtain a surrogate time series for the connection being considered. The set of 50 surrogate time series generated from 50 trials of the driver can be considered as the surrogate data ensemble for the driver. The time series for the target[2] variable were kept the same as the original. z-test was done to check if the CCC values from original time series (for the driver-target pair

[1]The variable 'from' which causality is being checked.
[2]The variable 'to' which causality is being checked.

chosen) were a part of the distribution of surrogate CCC values. The null hypothesis of insignificant CCC values was rejected if the original CCC values were found to be different from the distribution of surrogate CCC values at a significance level of 0.05. This test was the same as done for significance testing of CCC values obtained from coupled autoregressive (AR) processes as discussed in Section 3.4.2. The CCC values for the connections between different brain regions were found to be positive for all the analyses performed in this work. In that sense, these processes can be considered to be AR-like. As is observed for AR processes, the CCC values for surrogate data are found to be increased compared to CCC values obtained from original coupled time series.

In Figures 4.4, 4.5, 4.6 and 4.7, mean of CCC and NGC values over 50 trials for the five subjects are displayed for the considered connections during four different phases: FT, IT, RT and MT respectively. Each figure displays the mean strength of causation as the height of the bar. All premotor to motor connections whether from contralateral premotor to contralateral motor, ipsilateral premotor to ipsilateral motor, contralateral premotor to ipsilateral motor or ipsilateral premotor to contralateral motor are displayed together as adjacent bars for each subject, in order to compare their strengths for the subject. Similar is the case for motor to premotor connections. These results are also displayed in a different manner in Appendix B. In the Appendix, the variation in the strength of each of the four connections (in both directions) is shown with varying phase helping in a comparison of the strength of any given connection across different phases. As per the significance analysis criteria discussed in the last paragraph, all connections computed based on NGC and CCC between the four different regions con-

sidered were found to be significant causal connections. This happened to be the case for all the four phases.

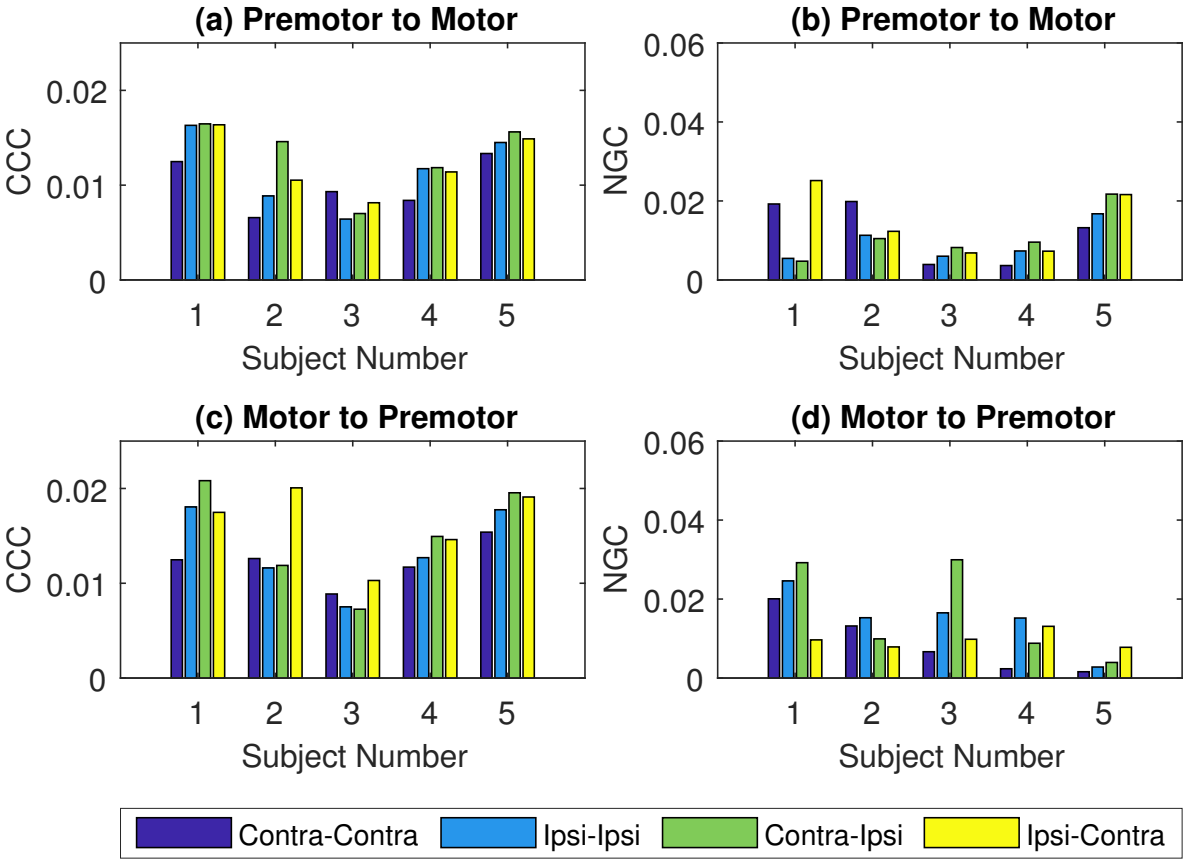

Figure 4.4: Mean causality values for the fixation time or FT phase displayed as height of bars for 5 subjects with each bar corresponding to the following regions: violet - contralateral premotor and contralateral motor, blue - ipsilateral premotor and ipsilateral motor, green - contralateral premotor and ipsilateral motor, yellow - ipsilateral premotor and contralateral motor. CCC estimates are shown in (a) for the direction premotor to motor and in (c) for the direction motor to premotor. NGC estimates are shown in (b) for the direction premotor to motor and in (d) for the direction motor to premotor.

High connectivties were observed for all premotor to motor connections obtained using the CCC measure in all the 4 phases. Similar was the case for motor to premotor connections. For the FT phase, for 4 subjects out of 5, premotor to motor connectivity

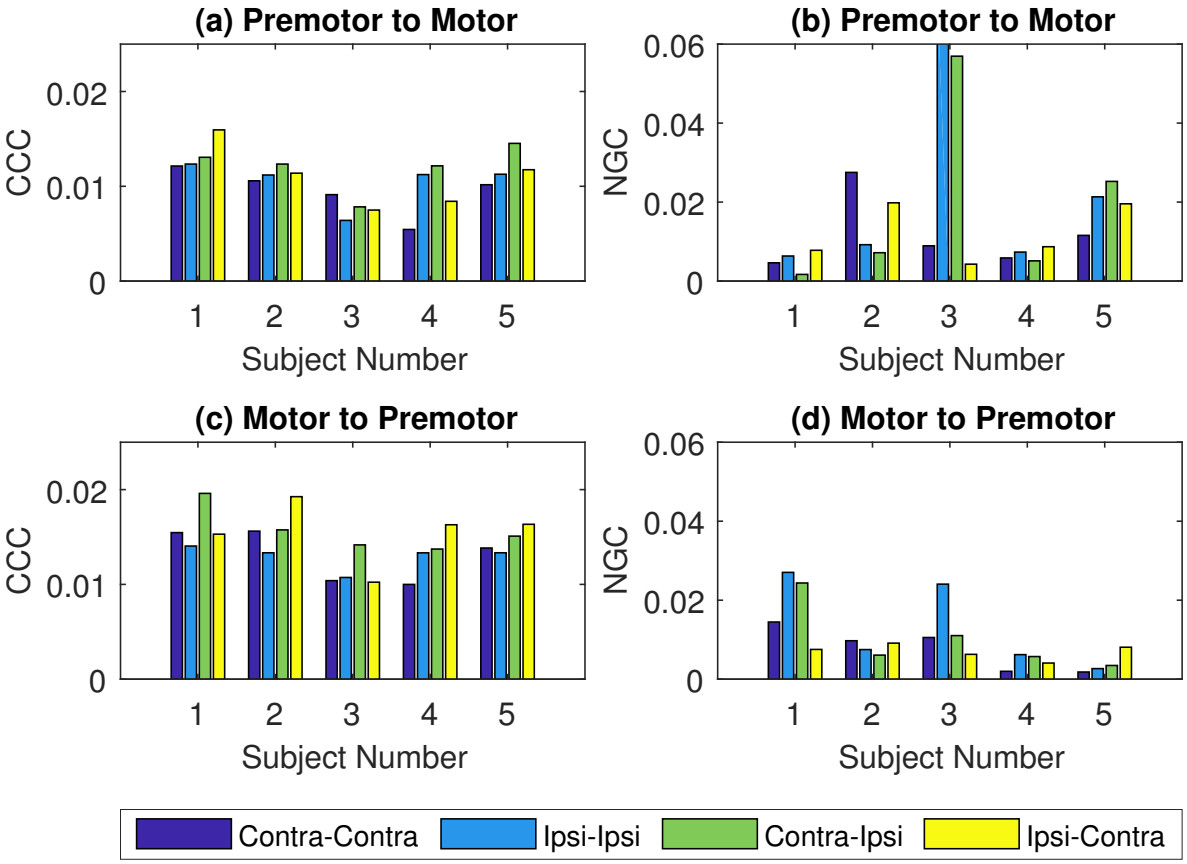

Figure 4.5: Mean causality values for the instruction time or IT phase displayed as height of bars for 5 subjects with each bar corresponding to the following regions: violet - contralateral premotor and contralateral motor, blue - ipsilateral premotor and ipsilateral motor, green - contralateral premotor and ipsilateral motor, yellow - ipsilateral premotor and contralateral motor. CCC estimates are shown in (a) for the direction premotor to motor and in (c) for the direction motor to premotor. NGC estimates are shown in (b) for the direction premotor to motor and in (d) for the direction motor to premotor.

on the ipsilateral side was slightly higher than on the contralateral side. Interestingly, during the RT phase, premotor to motor connectivity on the contralateral side became higher than the connectivity on the ipsilateral side. In case of motor to premotor connectivity also, during the FT phase, for 3 out of 5 subjects ipsilateral side connectivity was higher than the contralateral side. During the RT phase, however, 4 out of 5

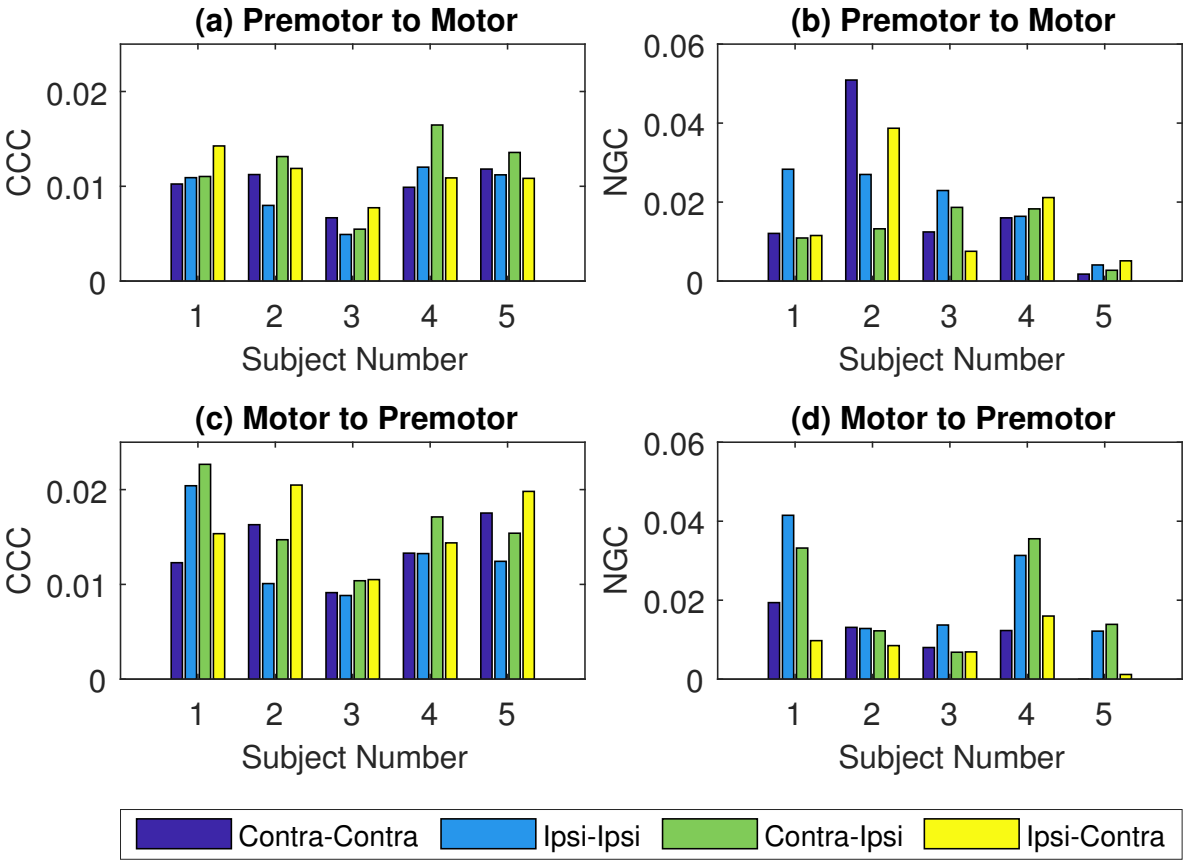

Figure 4.6: Mean causality values for the reaction time or RT phase displayed as height of bars for 5 subjects with each bar corresponding to the following regions: violet - contralateral premotor and contralateral motor, blue - ipsilateral premotor and ipsilateral motor, green - contralateral premotor and ipsilateral motor, yellow - ipsilateral premotor and contralateral motor. CCC estimates are shown in (a) for the direction premotor to motor and in (c) for the direction motor to premotor. NGC estimates are shown in (b) for the direction premotor to motor and in (d) for the direction motor to premotor.

subjects showed higher connectivity on the contralateral side. These changes seem to indicate motor preparation. If we compare contralateral to ipsilateral connectivity and vice versa for premotor to motor and motor to premotor connections, they remain high and comparable in each phase. However, if we compare across phases, there does seem to be a drop in the strength of these connections (especially for the premotor to motor

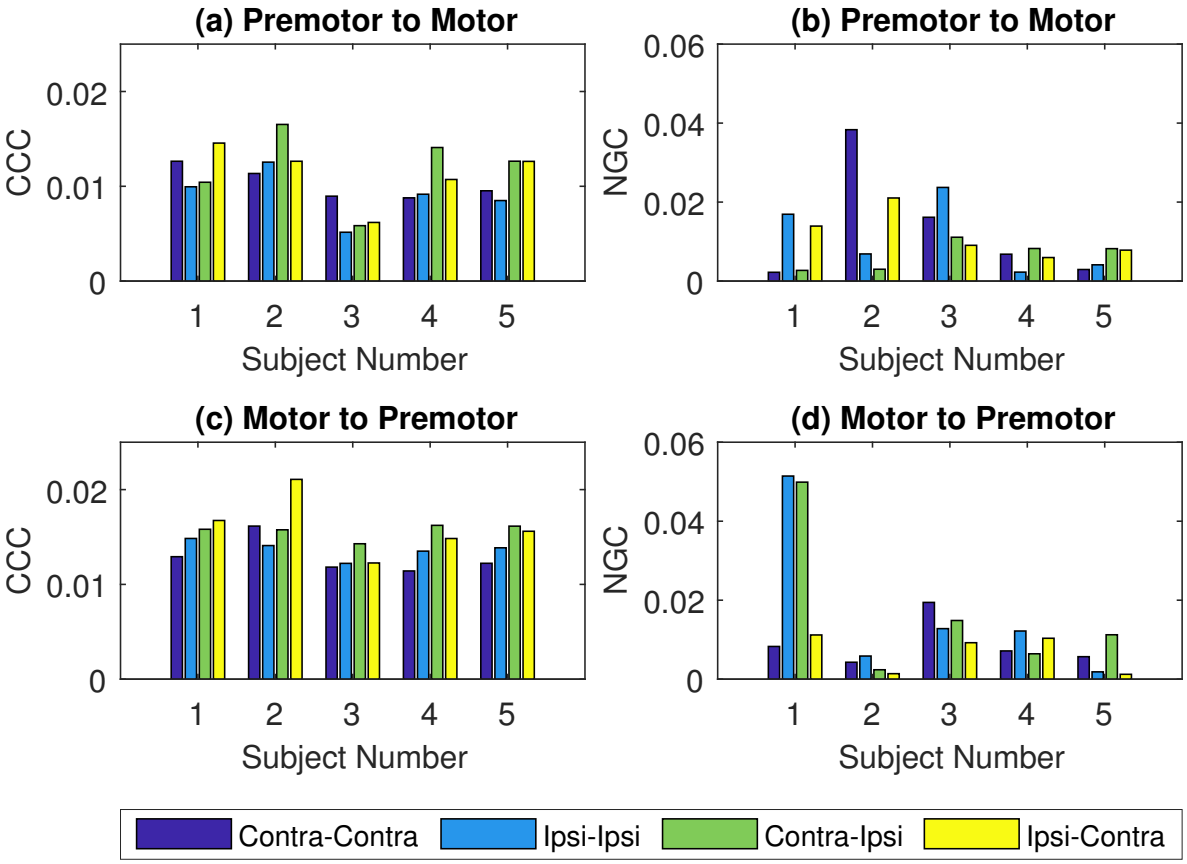

Figure 4.7: Mean causality values for the movement time or MT phase displayed as height of bars for 5 subjects with each bar corresponding to the following regions: violet - contralateral premotor and contralateral motor, blue - ipsilateral premotor and ipsilateral motor, green - contralateral premotor and ipsilateral motor, yellow - ipsilateral premotor and contralateral motor. CCC estimates are shown in (a) for the direction premotor to motor and in (c) for the direction motor to premotor. NGC estimates are shown in (b) for the direction premotor to motor and in (d) for the direction motor to premotor.

direction) during the IT, RT and MT phases when compared with the FT phase. This could probably be due to the fact that these cross connections are not useful in the focused planning and movement of the right hand. This can be seen more clearly from Figures B.3 and B.4 given in Appendix B.

Significant connections are also found using NGC for all premotor to motor and

motor to premotor connections considered. The patterns observed in NGC values across different phases were not the same as those observed for CCC. One observation is that, during the RT phase, in general all connections seemed to increase in strength when compared with other phases. This is better visible in Figures B.1-B.4 and could be an indicator of motor preparation. Also, for all the phases, for a majority of the subjects, the ipsilateral connections (both premotor to motor and vice versa) were of greater strength when compared to the corresponding contralateral connections.

Lateralized Analysis

For this analysis, using lateralized data, we check for connectivity (both directions) between the following pair of electrodes: premotor (FC) - motor (C), motor (C) - parietal (P), motor (C) - centroparietal (CP) and premotor (FC) - prefrontal (FP). The parameters used for CCC and NGC estimation and procedure for the significance analysis of their estimates remain the same as in the previous section. Mean of CCC and NGC values are presented in a graphical representation for the four phases in Figures 4.8 – 4.17. Each figure represents connectivity for a single subject using CCC or NGC for all the 4 phases. For each pair considered in the graph, the dominant direction of causality is indicated using a black edge while the opposite direction is indicated using a gray edge. However, if the causality for the dominant direction falls within a range of 0.0020 of the causality for the opposite edge, then the former is also displayed in gray color. In this case, because of very little difference between the causality values, no edge can be considered to be dominant over the other and we can take it as a case of

bidirectional causation with equal influence on both sides. The value of 0.0020, which is taken as the threshold, was set arbitrarily by observing the maximum and the minimum mean CCC and NGC values obtained from amongst all subjects for all the connections taken. Maximum and minimum CCC values were 0.0246 and 0.0009 respectively and maximum and minimum NGC values were 0.0730 and 0.0006 respectively. Figures 4.18-4.21 represent the same results, showing the variation in the strength of each of the four connections separately (in both the directions) with the variation of the phase for all the five subjects together.

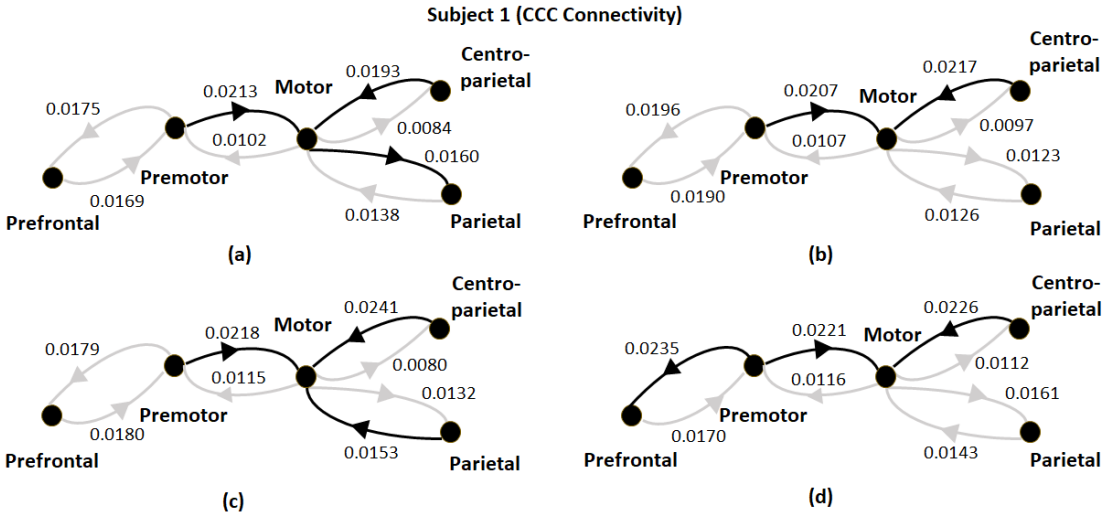

Figure 4.8: Connectivity analysis for subject 1 using CCC between lateralized signals obtained from the following pair of electrodes: premotor (FC) - motor (C), motor (C) - parietal (P), motor (C) - centroparietal (CP) and premotor (FC) - prefrontal (FP). Results are displayed for the four different phases considered: (a) Fixation Time or FT, (b) Instruction Time or IT, (c) Reaction Time or RT and (d) Movement Time or MT. Black edge corresponds to the dominant direction of causality and the faded one to the non-dominant direction between the pair.

Significant bidirectional causalities were estimated for all the considered pairs, for all the subjects for all the phases taken. This was seen for both CCC and NGC. A number

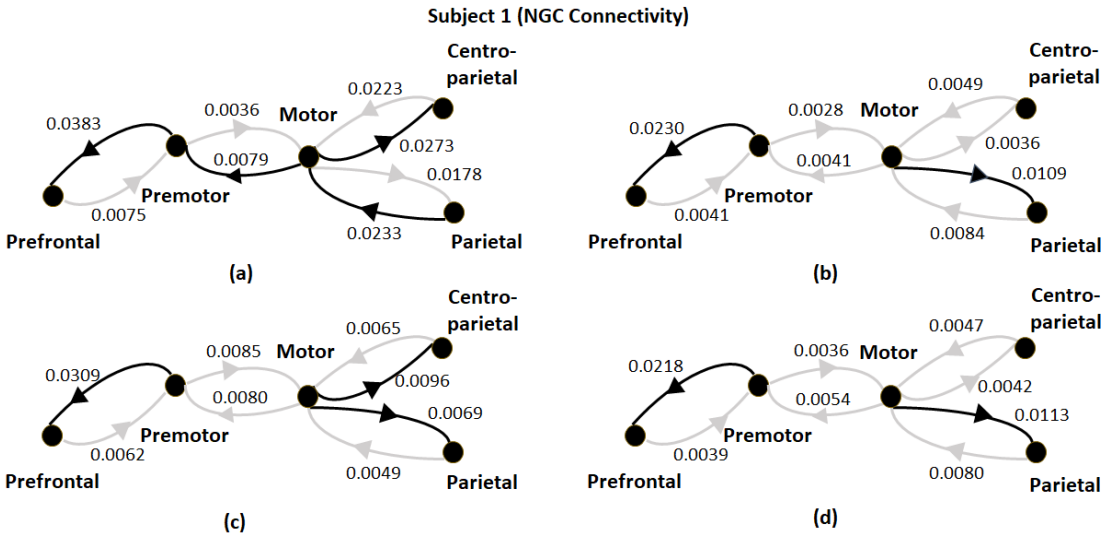

Figure 4.9: Connectivity analysis for subject 1 using NGC between lateralized signals obtained from the following pair of electrodes: premotor (FC) - motor (C), motor (C) - parietal (P), motor (C) - centroparietal (CP) and premotor (FC) - prefrontal (FP). Results are displayed for the four different phases considered: (a) Fixation Time or FT, (b) Instruction Time or IT, (c) Reaction Time or RT and (d) Movement Time or MT. Black edge corresponds to the dominant direction of causality and the faded one to the non-dominant direction between the pair.

of interesting observations could be made from the analysis. The causal influence using CCC from the premotor to the motor region for all the subjects for all the phases was the dominant causal connection in comparison to the motor to premotor connection. Further, premotor to motor CCC values were found to increase during the RT phase in comparison to its values obtained for FT, IT and MT phases for 3 out of 5 subjects (subject numbers 1, 2 and 4). This could be a signature for motor activity preparation.

In case of NGC, for 3 out of 5 subjects (subject nos. 3,4 and 5) the motor to premotor connection was dominant over the premotor to motor connection for almost all the phases. However, as observed for the CCC measure, the premotor to motor connection increased in strength during the RT phase as compared to its observed

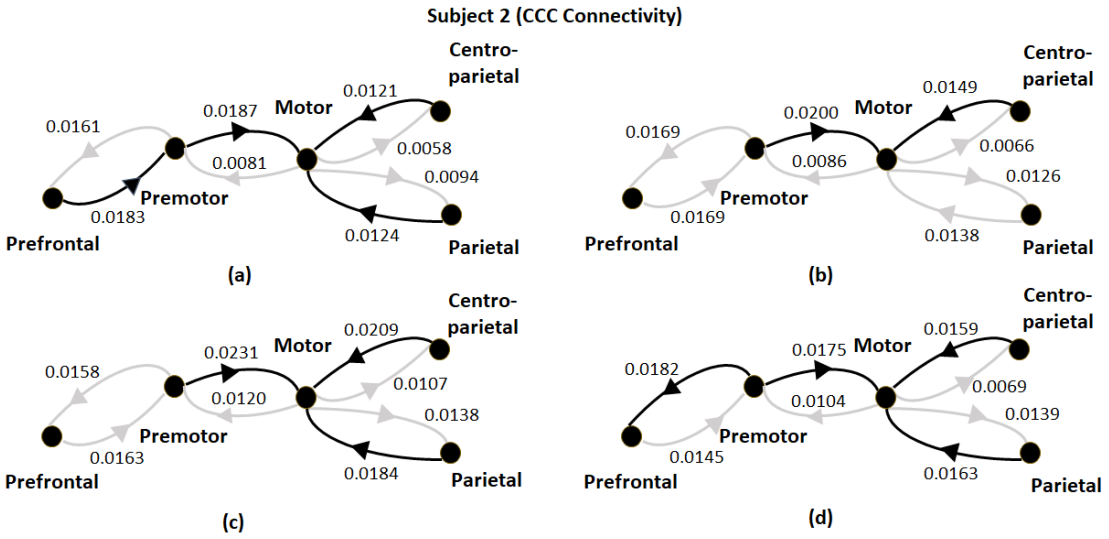

Figure 4.10: Connectivity analysis for subject 2 using CCC between lateralized signals obtained from the following pair of electrodes: premotor (FC) - motor (C), motor (C) - parietal (P), motor (C) - centroparietal (CP) and premotor (FC) - prefrontal (FP). Results are displayed for the four different phases considered: (a) Fixation Time or FT, (b) Instruction Time or IT, (c) Reaction Time or RT and (d) Movement Time or MT. Black edge corresponds to the dominant direction of causality and the faded one to the non-dominant direction between the pair.

strengths during FT, IT and MT phases. This was the case for 4 out of 5 subjects, with the only exception to this being subject no. 3 (which was also an exception for the CCC case). Interestingly, for a majority of the cases NGC strength also increased for motor to premotor connection during the RT phase in comparison to its strength during all the other phases. Since the premotor to motor connection increase during RT was consistent for both CCC and NGC, it seems to be a strong indicator for motor preparation activity.

For the motor and parietal regions, bidirectional connectivity was observed using both CCC and NGC with the dominant direction of causation being very subject and phase specific. For motor and centro-parietal regions, there was no clear pattern in the

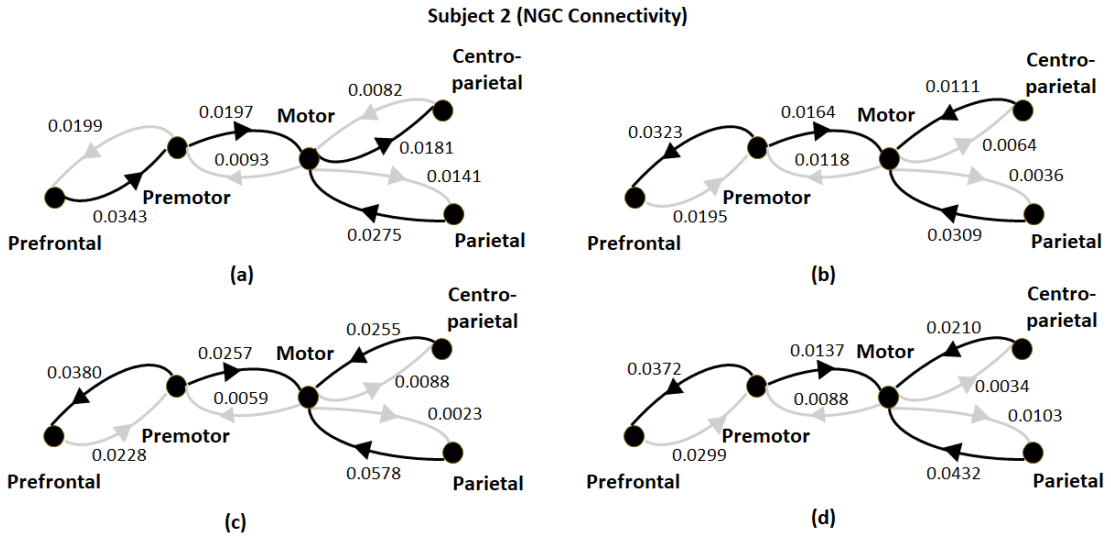

Figure 4.11: Connectivity analysis for subject 2 using NGC between lateralized signals obtained from the following pair of electrodes: premotor (FC) - motor (C), motor (C) - parietal (P), motor (C) - centroparietal (CP) and premotor (FC) - prefrontal (FP). Results are displayed for the four different phases considered: (a) Fixation Time or FT, (b) Instruction Time or IT, (c) Reaction Time or RT and (d) Movement Time or MT. Black edge corresponds to the dominant direction of causality and the faded one to the non-dominant direction between the pair.

causality estimated in the two directions using NGC. For many cases (different phases that were taken for different subjects), the estimated causality in both directions had very low values and remained close to zero. However, when CCC was used to study motor and centro-parietal connectivity, the centro-parietal to motor connection was found to be of much higher strength, dominating over the opposite connection for which CCC values remained small, closer to zero. Also, for a majority of cases, that is 3 out of 5, the centroparietal to motor connection increased in strength during the RT phase as compared to the other phases. For the premotor and prefrontal regions, bidirectional connections were seen using the NGC measure. But other than that there seemed to be no clear pattern emerging for different phases across subjects. CCC too

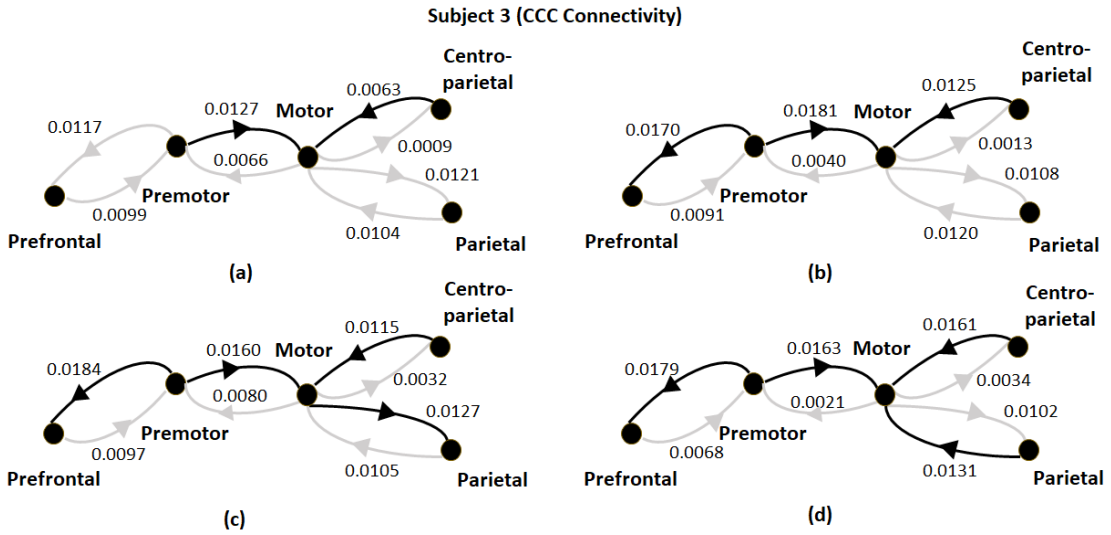

Figure 4.12: Connectivity analysis for subject 3 using CCC between lateralized signals obtained from the following pair of electrodes: premotor (FC) - motor (C), motor (C) - parietal (P), motor (C) - centroparietal (CP) and premotor (FC) - prefrontal (FP). Results are displayed for the four different phases considered: (a) Fixation Time or FT, (b) Instruction Time or IT, (c) Reaction Time or RT and (d) Movement Time or MT. Black edge corresponds to the dominant direction of causality and the faded one to the non-dominant direction between the pair.

showed bidirectional connectivity between the two regions for all the phases for all the subjects. In addition, for a majority of subjects (nos. 1, 2, 5), it was seen that bidirectional causality with almost equal influences in the two directions for the phases FT, IT and RT was changed for the MT phase in which the premotor to prefrontal influence became dominant in comparison to the influence in the opposite direction.

4.3.3 Conclusions and Future Work

In this section we have presented some preliminary results using bivariate CCC and NGC for the study of connectivity between different regions of the brain involved in performing motor task. Earlier work studying unilateral hand movements looked at

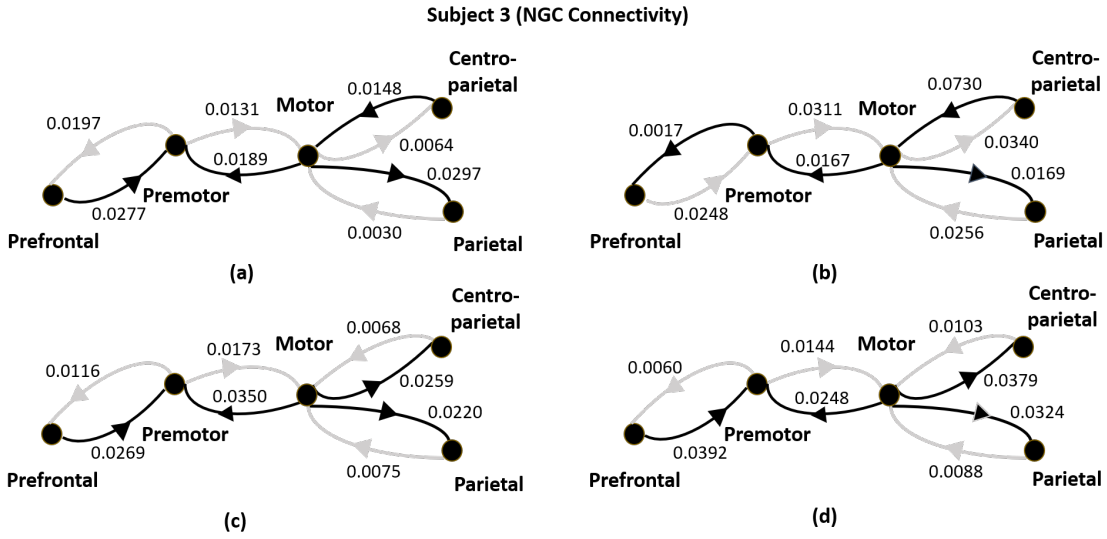

Figure 4.13: Connectivity analysis for subject 3 using NGC between lateralized signals obtained from the following pair of electrodes: premotor (FC) - motor (C), motor (C) - parietal (P), motor (C) - centroparietal (CP) and premotor (FC) - prefrontal (FP). Results are displayed for the four different phases considered: (a) Fixation Time or FT, (b) Instruction Time or IT, (c) Reaction Time or RT and (d) Movement Time or MT. Black edge corresponds to the dominant direction of causality and the faded one to the non-dominant direction between the pair.

connections between the contralateral motor cortex, contralateral premotor cortex and contralateral prefrontal cortex [116, 117, 123, 126]. These studies found either unidirectional or bidirectional connectivity between these three regions. In this study we analyze connections between the motor and premotor areas on the contralateral side, ipsilateral side as well as cross connections between one of the areas taken on the contralateral side and the other on the ipsilateral side. Bidirectional causalities were found between all the areas considered here. Using lateralized signals, connections were analyzed between the pairs: premotor-motor, motor-parietal, motor-centroparietal and premotor-prefrontal cortex. Here too bidirectional connections were determined between all the pairs considered. The comparison of connectivity during four phases, namely, fixa-

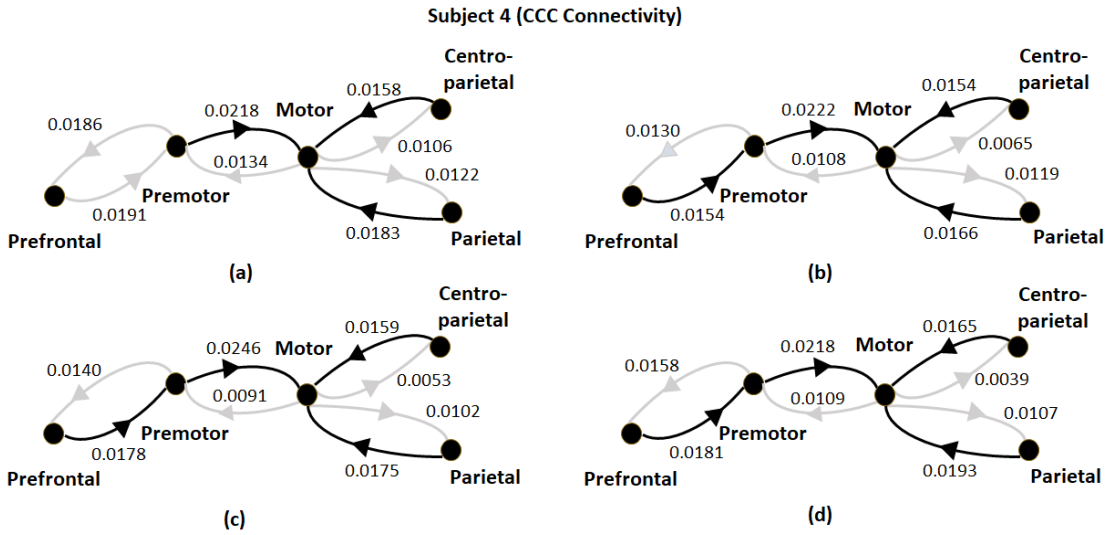

Figure 4.14: Connectivity analysis for subject 4 using CCC between lateralized signals obtained from the following pair of electrodes: premotor (FC) - motor (C), motor (C) - parietal (P), motor (C) - centroparietal (CP) and premotor (FC) - prefrontal (FP). Results are displayed for the four different phases considered: (a) Fixation Time or FT, (b) Instruction Time or IT, (c) Reaction Time or RT and (d) Movement Time or MT. Black edge corresponds to the dominant direction of causality and the faded one to the non-dominant direction between the pair.

tion, instruction, reaction and movement considered helped to identify some causal connections involved in the motor planning and execution phase. One of the important indicators identified was the increase in premotor to motor connectivity during the reaction or RT phase when causality estimation was done based on lateralized signals. Based on non-lateralized signal analysis using CCC, it was also found that premotor to motor connectivity became dominant in comparison to motor to premotor connectivity during the RT phase. Also, the centroparietal to motor connectivity (lateralized) as estimated by CCC seemed to increase during the RT phase and premotor to prefrontal connection became dominant with respect to the connection in the opposite direction during movement or MT phase. These too could be potential indicators of movement

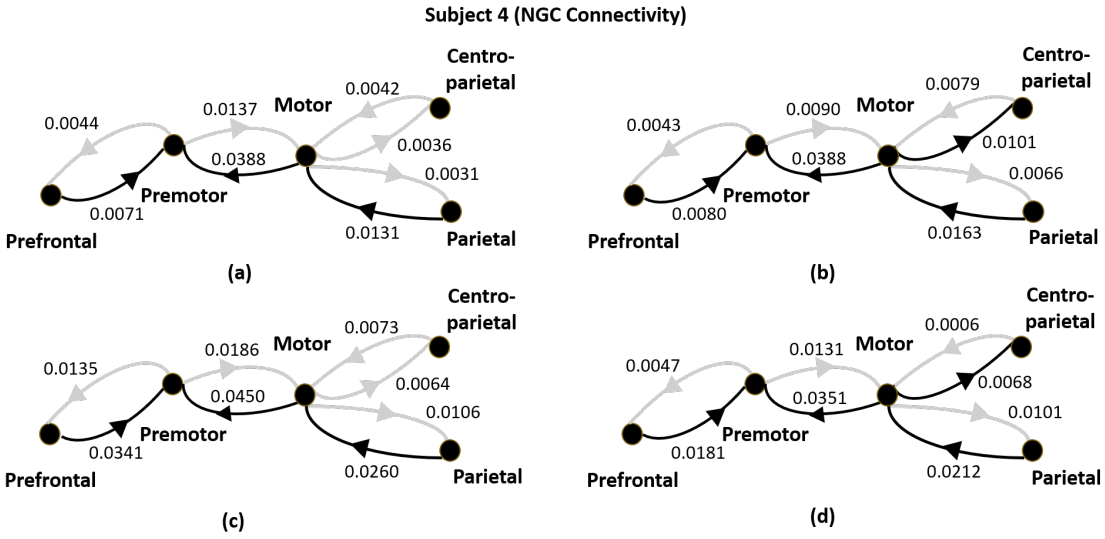

Figure 4.15: Connectivity analysis for subject 4 using NGC between lateralized signals obtained from the following pair of electrodes: premotor (FC) - motor (C), motor (C) - parietal (P), motor (C) - centroparietal (CP) and premotor (FC) - prefrontal (FP). Results are displayed for the four different phases considered: (a) Fixation Time or FT, (b) Instruction Time or IT, (c) Reaction Time or RT and (d) Movement Time or MT. Black edge corresponds to the dominant direction of causality and the faded one to the non-dominant direction between the pair.

planning and execution.

The analysis done here has a number of limitations and can be improved in several aspects. Source localization of EEG signals should be done in order to remove volume conduction effects. These effects can lead to presence of shared noise and signal between different electrode recordings. Further, conditional/ effective causality estimation measures need to be used in order to estimate only the direct causal influences and remove the indirect ones. The study also needs to be made more robust by considering a larger number of subjects and more trials per subject. More connections could be considered between the brain regions taken in the current study and other brain regions can be included to make the study more comprehensive. Also, for NGC analysis a second

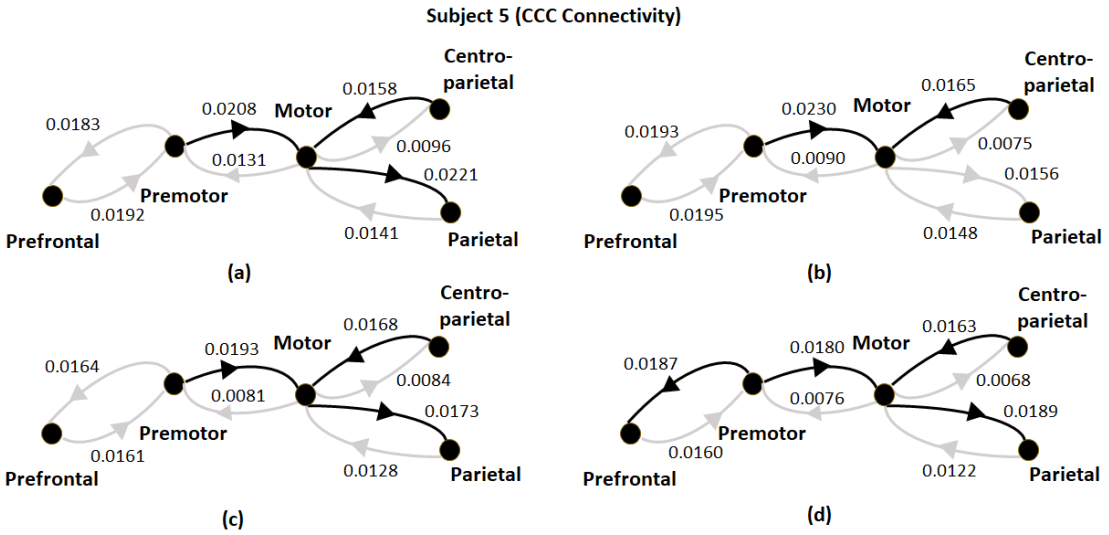

Figure 4.16: Connectivity analysis for subject 5 using CCC between lateralized signals obtained from the following pair of electrodes: premotor (FC) - motor (C), motor (C) - parietal (P), motor (C) - centroparietal (CP) and premotor (FC) - prefrontal (FP). Results are displayed for the four different phases considered: (a) Fixation Time or FT, (b) Instruction Time or IT, (c) Reaction Time or RT and (d) Movement Time or MT. Black edge corresponds to the dominant direction of causality and the faded one to the non-dominant direction between the pair.

kind of significance testing using surrogate data could be included to make the results more rigorous. All these aspects will be dealt as part of future work and are outside the scope of the current dissertation. It will also be interesting to do a comparison of connectivity during slow hand movement trials as taken in this study with fast hand movement trials and those involving some hold duration between appearance of target on the screen and the indication of Go cue. Data for these cases was made available by Prof. Aditya Murthy's Group (V. Thakur and A. Murthy, personal communication, May 21, 2020) . As future work, we would like to extend our analysis to these cases as well.

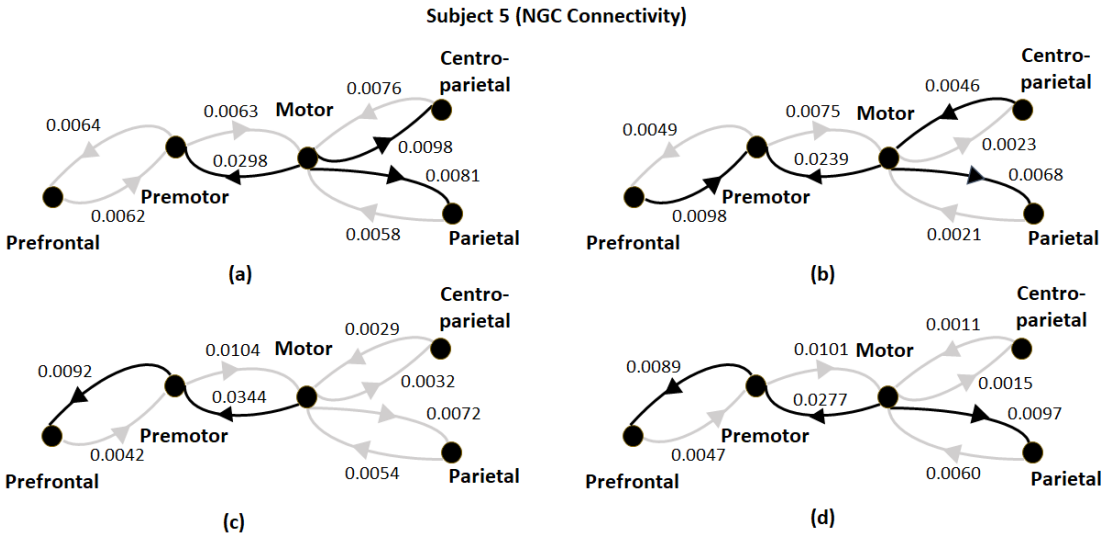

Figure 4.17: Connectivity analysis for subject 5 using NGC between lateralized signals obtained from the following pair of electrodes: premotor (FC) - motor (C), motor (C) - parietal (P), motor (C) - centroparietal (CP) and premotor (FC) - prefrontal (FP). Results are displayed for the four different phases considered: (a) Fixation Time or FT, (b) Instruction Time or IT, (c) Reaction Time or RT and (d) Movement Time or MT. Black edge corresponds to the dominant direction of causality and the faded one to the non-dominant direction between the pair.

4.4 Measuring Consciousness using CCC based Network Causal Activity Measure

Understanding *Consciousness* – the inner subjective feeling that is present in every experience (eg., in "seeing" a red rose, in the "feeling" of pain, in the "tasting" of tea etc.), is the final frontier of biomedical research. Defining, modeling and measuring consciousness is considered a *hard* problem [113]. Consciousness largely bounds two facets, namely, the "level" of consciousness and the "content" of consciousness. Experiences such as coma, different stages of anaesthesia and certain stages of sleep seem to indicate a loss of consciousness [127]. Quantitatively, consciousness can be featured

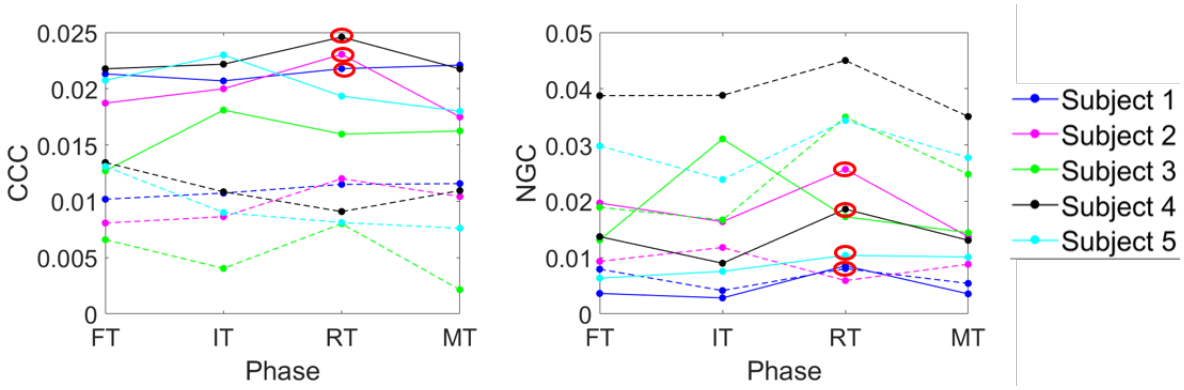

Figure 4.18: Connectivity analysis for all the subjects using CCC (left) and NGC (right) between lateralized signals obtained from the electrode pair: premotor (FC) - motor (C). Results are displayed as a variation in connectivity with a variation in the phases, which occur in the following successive order: (1) Fixation Time or FT, (2) Instruction Time or IT, (3) Reaction Time or RT, (4) Movement Time or MT. Premotor to motor connectivity variation is indicated using solid lines and motor to premotor connectivity variation is indicated using dashed lines. CCC as well as NGC connectivity from premotor to motor increases during the RT phase as compared to the rest of the phases, for a majority of the subjects. This is represented by points encircled in red.

as the distributed cortical activity in the sub-cortical regions of the brain relating to the conscious content at any instant. Qualitatively, consciousness is the most essential aspect of our daily experience as it plays a big role in decision making and adaptive planning [115].

Measuring consciousness is a great aid to clinical assessments as it helps in building computational and psychological models; and in providing philosophical aspects to understand the principles connecting brain activity to consciousness experience of wakeful individuals and individuals with physiological, pharmacological and pathological loss of consciousness. Recently, a number of scientific measures of consciousness have been proposed, each having their own theoretical and mathematical framework. We shall

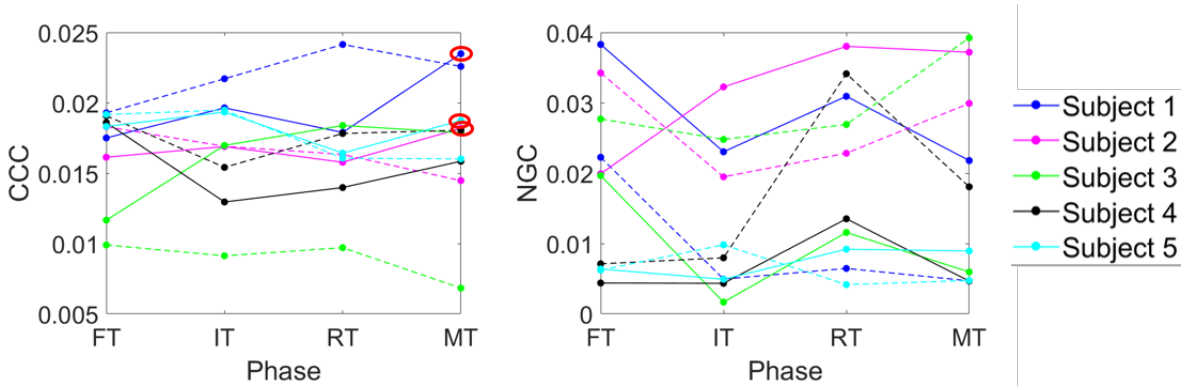

Figure 4.19: Connectivity analysis for all the subjects using CCC (left) and NGC (right) between lateralized signals obtained from the electrode pair: premotor (FC) - prefrontal (FP). Results are displayed as a variation in connectivity with a variation in the phases, which occur in the following successive order: (1) Fixation Time or FT, (2) Instruction Time or IT, (3) Reaction Time or RT, (4) Movement Time or MT. Premotor to prefrontal connectivity variation is indicated using solid lines and prefrontal to premotor connectivity variation is indicated using dashed lines. CCC connectivity from premotor to prefrontal increases during the MT phase as compared to the rest of the phases, for a majority of the subjects. This is represented by points encircled in red.

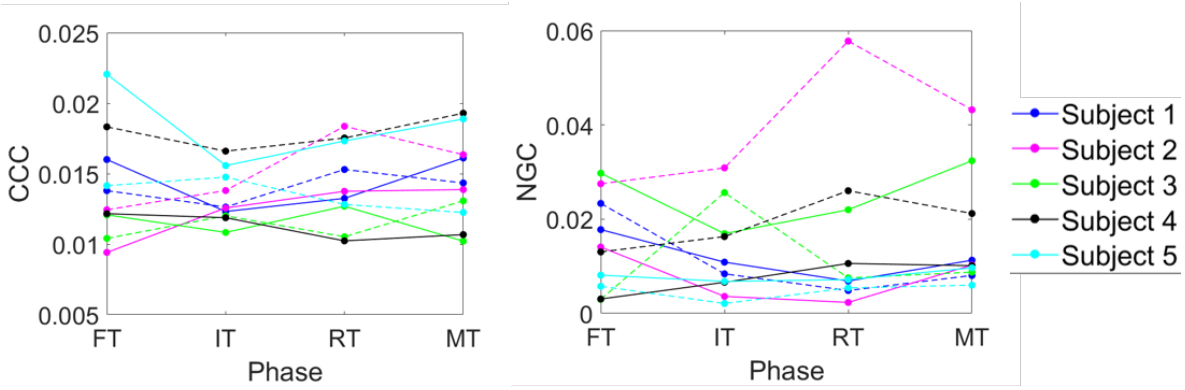

Figure 4.20: Connectivity analysis for all the subjects using CCC (left) and NGC (right) between lateralized signals obtained from the electrode pair: motor (C) - parietal (P). Results are displayed as a variation in connectivity with a variation in the phases, which occur in the following successive order: (1) Fixation Time or FT, (2) Instruction Time or IT, (3) Reaction Time or RT, (4) Movement Time or MT. Motor to parietal connectivity variation is indicated using solid lines and parietal to motor connectivity variation is indicated using dashed lines.

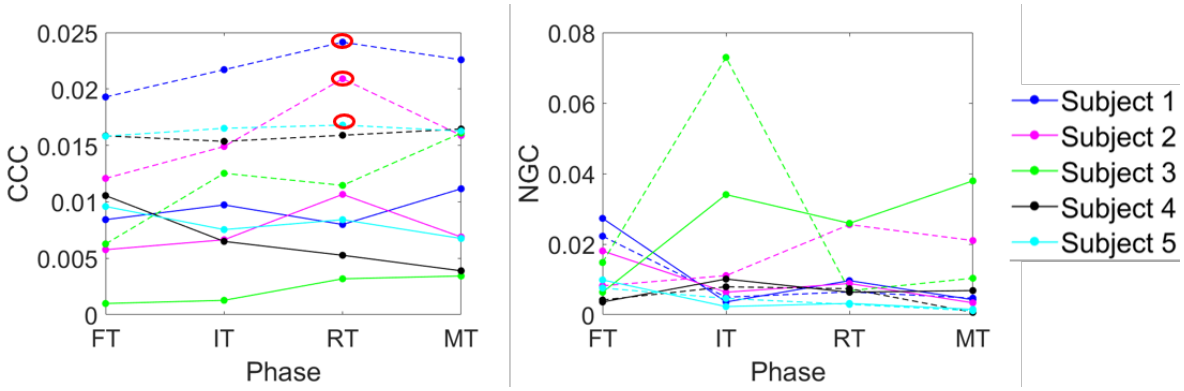

Figure 4.21: Connectivity analysis for all the subjects using CCC (left) and NGC (right) between lateralized signals obtained from the electrode pair: motor (C) - centroparietal (CP). Results are displayed as a variation in connectivity with a variation in the phases, which occur in the following successive order: (1) Fixation Time or FT, (2) Instruction Time or IT, (3) Reaction Time or RT, (4) Movement Time or MT. Motor to centroparietal connectivity variation is indicated using solid lines and centroparietal to motor connectivity variation is indicated using dashed lines. CCC connectivity from centroparietal to motor increases during the RT phase as compared to the rest of the phases, for a majority of the subjects. This is represented by points encircled in red.

briefly describe a few of them here.

Tononi's Integrated Information Theory of Consciousness (IIT) is a leading scientific theory [128, 129] that conceptualizes the criteria for assessing the consciousness level of any system, quantitatively, as well as, qualitatively. According to IIT, if a system *intrinsically* possesses both *integrated* and *differentiated* states of *information*, then it is bound to possess some level of consciousness (indicated by the symbol Φ in the theory). Non-zero values of Φ conforms the system is in a conscious state. Neurobiologically, the number of connections of neurons in brain networks as well as their complex dynamical interactions contributes to the quantification of Φ, not necessarily only the number of neurons. Perturbational Complexity Index (PCI) [130] is a theory-driven index formulated to evaluate the level of consciousness in a clinical scenario. In order to calculate

PCI, the cortex of brain is perturbed with trans-cranial magnetic stimulation to invoke distributed activity in the thalamocortical brain networks. These spatio-temporal responses are then compressed to measure their algorithmic complexity which is normalized and calibrated to yield an index of consciousness level known as PCI. A high value of PCI indicates a high and significant amount of complex interactions of neural activity in cortical areas. Another measure of consciousness, Neural Complexity [131], aims to quantify the interplay between statistically independent (functionally segregated) and statistically interdependent (functionally integrated) neuronal groups in the brain. For any dynamical system, it is an information theoretic measure that captures the mutual information present between the different active subsets of the whole system [132]. Yet another measure of consciousness, known as Causal Density [133, 134], defines consciousness as the fraction of significant causal interactions in brain networks using the GC measure [5]. In [80, 135], there is a review of other scientific measures of consciousness which are similar to the ones described here. The aforementioned measures are categorized under *Complexity Theories of Consciousness* (please see [114]).

In [136], a simple model of spectral Granger bivariate causality is applied to visualize the information flow between different parts of cortex for different states – conscious and unconsciousness induced by different means, in monkeys. This enabled the investigation of large-scale information flow and causal interactions specific to different frequency-modes in the brain. A switch in the frequency-mode of neural communication was found to characterize the difference between different levels of consciousness in monkeys.

In this study, we propose a novel, time domain, *Network Causal Activity (NCA)*

approach to discriminate different levels of consciousness. CCC measure, which is proposed in Chapter 2 of the thesis and rigorously tested on simulated data for realistic scenarios in Chapter 3 is used for the formulation of NCA. Instead of frequency domain analysis used in [136], we use NCA to differentiate between conscious and unconscious states in monkeys.

4.4.1 Materials and Methods

Subjects and Data Acquisition

For our work, we have used a subset of the dataset from the study conducted by Yanagawa *et al.* [136] which is made available in the public server neurotycho.org (http://neurotycho.org/) [137]. In their study, electrocorticographic (ECoG) signals sampled at 1 kHz were recorded by a Cerebus data acquisition system (Blackrock, UT, USA) from the lateral cortex of four monkeys (George, Chibi, Su, Kin2) using 128 channels electrodes during different stages of sleep, wakefulness and anaesthesia on different days. A complete description about the experiment can be found in [136]. In this thesis, we have focused on only the awake (eyes-opened) and ketamine-medetomidine induced anaesthetized conditions.

Dataset Description

From the recorded neural data collected from the experiments of the study in [136], 3 non-overlapping windows of 5s each (corresponding to 5000 time points) were extracted from 126 channels to construct a sustained network of neural interactions for all the four monkeys in two states – *awake* (eyes open, conscious state) and *anaesthetized* (drugged

using Ketamine and Medetomidine, loss of consciousness state) condition. We excluded data from two channels (nos. 73 and 123) since these were found to be corrupted and hence unsuitable for computation of causality values. The data was used in the acquired form without any re-referencing or pre-processing.

Network Causal Activity (NCA)

NCA is proposed as a quantitative measure of consciousness to capture average (significant) causal influence activity between all the elements or subsystems of a given system. Bivariate CCC as defined in Section 2.3 is used to estimate the causal influences for NCA.

NCA for multi-variate time series data $\mathbf{M}$ (with m variables[3]) is defined as the total average *significant* pairwise CCC values across all possible pairs. Mathematically,

$$NCA\big(\mathbf{M}\big) = \frac{1}{n} \sum_{j,k=1, j\neq k}^{j,k=m} CCC^{*}_{j\to k} \ , \tag{4.1}$$

where there are n number of *significant* CCC values among all possible pairwise combinations of the m variables. Here, the notion of significance is defined differently from that discussed in Section 3.4. In this case, CCC value from the j-th time series to the k-th time series is said to be significant ($CCC^{*}_{j\to k}$) if it is in the highest 10% (in magnitude) of all pairwise CCC values obtained for the given multi-variate time series [4]. The ideal thing to do would be to first check for the signficance of all pairwise CCC values obtained for multi-variate data taken based on surrogate significance testing analysis

[3]If each of these series has N time samples, then $\mathbf{M}$ is a $m \times N$ matrix. There would be $m^2 - m$ pairwise CCC values out of which the highest n are taken as *significant*.

[4]Alternatively, we could define a CCC value as being significant (for NCA) if it is greater than some set threshold T

introduced in Section 3.4.2. (we could use the procedure of random shuffling of the observations from driver time series to obtain the surrogate data in this case). Then out of these CCC values which are found to be significant, the top 10% of the values should be chosen. In this study, we skip the step of surrogate significance testing since with the use of bivariate CCC, we expect to find all the connections giving high CCC values as being significant, as any two regions will be directly or indirectly causally related.

We estimated the pairwise CCC values for three non-overlapping windows of ECoG signals of 4 monkeys in *Awake* (conscious) and *Anaesthesia* (loss of consciousness) states. The settings that were chosen for estimating CCC are: $L = 150$, $w = 30$, $\delta = 200$ (the step-size for the moving window), $B = 2$. These settings were chosen based on CCC parameter selection criteria as discussed in Section 3.3 These calculated CCC values are then used to estimate NCA using Eq.4.1 ($N = 5000$, $m = 126$, $n = 1575$).

4.4.2 Analysis and Discussion

Mean and standard deviation of pairwise CCC values across 126 ECoG signal channels of 4 different monkeys for 3 different windows, each of 5 seconds duration, are given in Table 4.1 and Table 4.2 for the *awake* and *anaesthesia* states respectively. In Figure 4.22, histograms of pairwise CCC values for each monkey for window w_1 (*awake*) and w_1' (*anaesthesia*) are shown. In Table 4.3, the NCA estimates are given for all the monkeys for 3 different windows for both the states. The top 10% significant CCC values were used in computation of NCA. From these tables, we can infer the following:

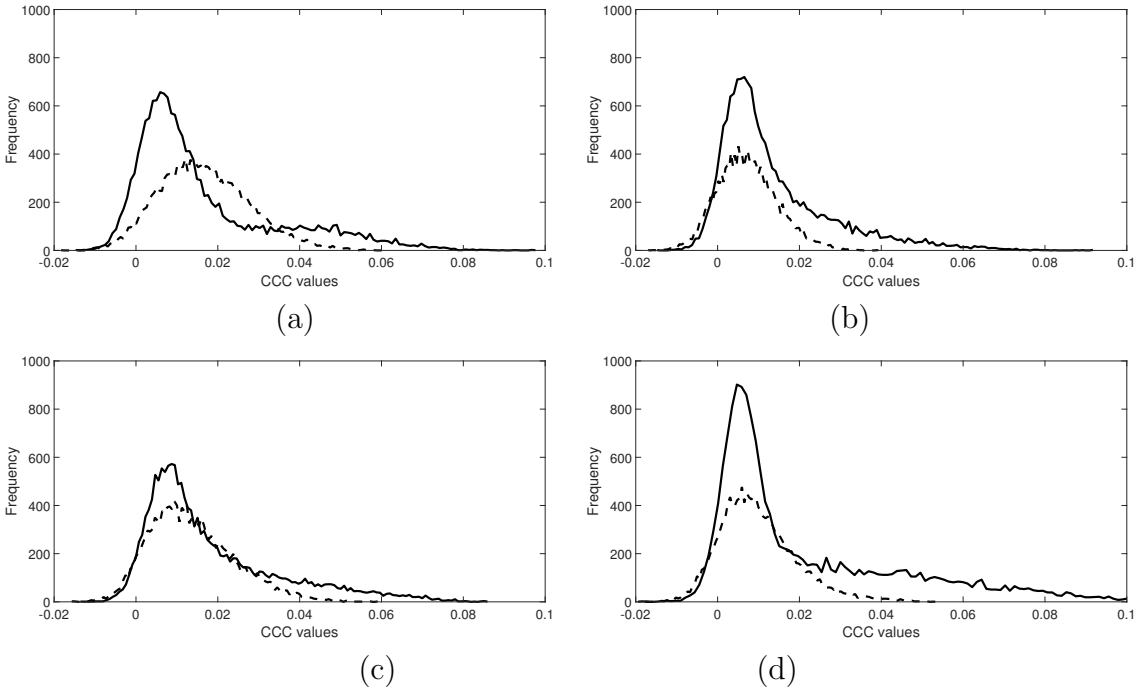

Figure 4.22: Histogram of pairwise CCC values across 126 ECoG signal channels for each monkey for window w_1 (*awake*) and w_1' (*anaesthesia*): (a) George, (b) Chibi, (c) Su, (d) Kin2. Solid line (-) is for the *Awake* state and dotted line (- -) is for the *Anaesthesia* state. ECoG dataset obtained from [136].

1. It is found that the standard deviations of CCC values in the awake state are *consistently higher* than that of the anaesthesia state in all the windows for all the monkeys (except for one window in case of monkey Su). This finding implies that there are a higher number of differentiated causal neural interactions in the awake state as compared to anaesthesia state.

2. Mean NCA is *consistently higher* in awake state as compared to anaesthesia state across all the windows for all the monkeys. This is intuitive, since in the awake state we expect the average significant causal neural interactions to be of a higher magnitude.

Table 4.1: Mean and standard deviation of pairwise CCC values across 126 ECoG signal channels of different monkeys during awake state for 3 different windows, each of 5 seconds duration. ECoG dataset obtained from [136].

Monkeys	Awake		
	CCC: Mean (μ) $\pm$ Standard Deviation (σ)		
	w_1	w_2	w_3
George	0.0165 ± 0.0176	0.0139 ± 0.0130	0.0158 ± 0.0153
Chibi	0.0138 ± 0.0139	0.0159 ± 0.0156	0.0162 ± 0.0142
Su	0.0183 ± 0.0164	0.0192 ± 0.0168	0.0107 ± 0.0110
Kin2	0.0220 ± 0.0241	0.0246 ± 0.0222	0.0186 ± 0.0196

3. The mean CCC values for awake state is significantly higher than the mean CCC value for the anaesthesia state. In order to substantiate this result statistically, a formal hypothesis '2 sample student's t-test' was performed for all the monkeys on data pooled over all the three windows of awake (w_1, w_2, and w_3) as well as anaesthesia (w_1', w_2', and w_3'). The t-test results are summarized as follows:

   - For George, the mean of awake state (0.0154 ± 0.0155) is significantly greater ($t_{94498} = -4.5272$, $p = 0$) than that of anaesthesia state (0.0150 ± 0.0109).
   - For Chibi, the mean of awake state (0.0153 ± 0.0146) is significantly greater ($t_{94498} = -93.7679$, $p = 0$) than that of anaesthesia state (0.0081 ± 0.0083).
   - For Su, the mean of awake state (0.0161 ± 0.0155) is significantly greater ($t_{94498} = -38.0216$, $p = 0$) than that of anaesthesia state (0.0128 ± 0.0107).

Table 4.2: Mean and standard deviation of pairwise CCC values across 126 ECoG signal channels of different monkeys during anaesthesia state for 3 different windows, each of 5 seconds duration. ECoG dataset obtained from [136].

Monkeys	Anaesthesia		
	CCC: Mean (μ) $\pm$ Standard Deviation (σ)		
	w_1'	w_2'	w_3'
George	0.0168 ± 0.0111	0.0143 ± 0.0107	0.0140 ± 0.0106
Chibi	0.0073 ± 0.0074	0.0080 ± 0.0084	0.0088 ± 0.0090
Su	0.0137 ± 0.0104	0.0106 ± 0.0098	0.0140 ± 0.0116
Kin2	0.0099 ± 0.0094	0.0114 ± 0.0099	0.0096 ± 0.0096

Table 4.3: Network Causal Activity (NCA) estimates for all the monkeys for 3 different windows for both awake and anaesthesia states. The top 10% significant CCC values were used in computation of NCA. Mean NCA for awake state is higher than that of anaesthesia.

Monkeys	Awake				Anaesthesia			
	Network Causal Activity				Network Causal Activity			
	w_1	w_2	w_3	Mean	w_1'	w_2'	w_3'	Mean
George	0.0564	0.0427	0.0482	0.0491	0.0378	0.0354	0.0355	0.0362
Chibi	0.0460	0.0512	0.0477	0.0483	0.0214	0.0248	0.0263	0.0242
Su	0.0555	0.0570	0.0356	0.0494	0.0344	0.0308	0.0391	0.0347
Kin2	0.0765	0.0727	0.0632	0.0708	0.0292	0.0307	0.0284	0.0294

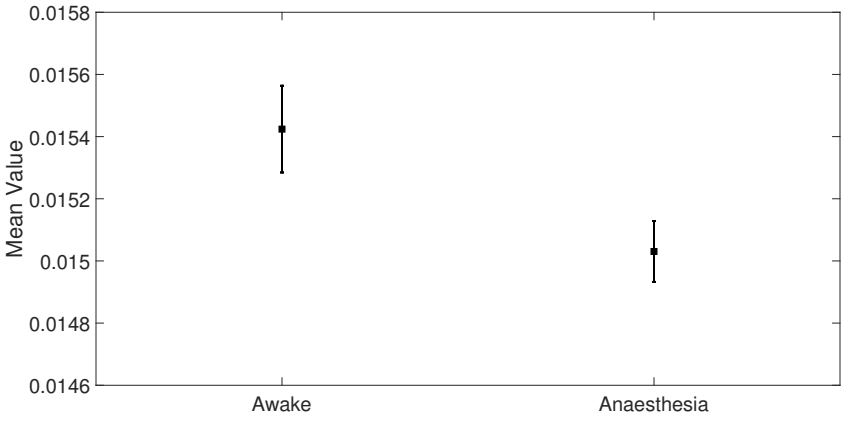

Figure 4.23: 95% confidence intervals for mean CCC values of pooled data of all windows (each of 5 second interval) of George accounting for $47,250$ samples, for *awake* as well as *anaesthesia* state showing a clear separation between the two.

- For Kin2, the mean of awake state (0.0217 ± 0.0222) is significantly greater ($t_{94498} = -103.0372$, $p = 0$) than that of anaesthesia state (0.0103 ± 0.0097).

A graphical depiction of this hypothesis test for 'George' is done in Figure 4.23.

4.4.3 Conclusions and Future Work

Measuring Network Causal Activity or NCA, i.e., the average significant causal interactions in the brain, is a promising approach towards understanding consciousness. Our work demonstrates that NCA, measured by estimating CCC values of ECoG signals in monkeys can differentiate states of consciousness (awake vs. anaesthesia). Both, mean CCC and mean NCA estimates are statistically significantly higher for awake state when compared with anaesthesia state. Going forward, it is worthwhile to estimate NCA for different stages of sleep and other states of consciousness (such as coma, vegetative state). Use of conditional/ effective CCC instead of bivariate CCC may help

to give more reliable results. Further, NCA could be computed by estimating pairwise CCC between fewer brain regions, for example, by using averaged activity obtained from neighboring electrodes and/or using only electrical activity from selected brain regions. This will help to reduce the computational complexity required for estimating NCA especially when recordings from a large number of electrodes are available. Potentially, NCA could be further developed to provide robust measure of consciousness in clinical applications.

Chapter 5

Effective CCC for Networks

Most real-world systems are multivariate with complex network relationships. Discovering correct causal relationships is very important for such networks found in the study of fields such as climatology, epidemiology, neuroscience, economics etc. In order to capture causality from one variable to another in a network, in the presence of other variables which may or may not be having causal influences to the considered target variable, use of conditional CCC, discussed in Chapter 2 has limitations and may not give accurate results. This is primarily because:

1. *The formulation of conditional CCC does not allow us to capture the direct causal influence between variables, removing the indirect effects by intermediate variables in the causal pathway.*

2. *It is difficult to compute joint ETC for large number of variables. The large dictionaries constructed from the variables become difficult to handle, making complexity estimation inadequate over short lengths of data taken.*

To address the above two problems, the concepts of Effective CCC and Equivalent ETC

are introduced and defined in this chapter. Effective CCC is then used to estimate causal connections in simulated networks of autoregressive processes corrupted with measurement noise and having long term memory (simulated for short length time-series) and its performance is compared with that of multivariate Granger Causality.

5.1 Problem in Existing Formulation and the Introduction of Effective CCC

Let us consider the example of a system of variables X, Y, Z, W, taken in Section 2.3 for which we estimate conditional CCC from Y to X. For computing $CCC_{Y\to X|Z,W}$, two time varying dictionaries are built: D that encodes information from all variables (X, Y, Z, W) and D' that encodes information from all variables except Y (X, Z, W only). Using these dictionaries, dynamical compression complexities are estimated as:

$$CC(\Delta X|D'_{past}) = ETC(D'_{past} + \Delta X) - ETC(D'_{past}), \tag{5.1}$$

$$CC(\Delta X|D_{past}) = ETC(D_{past} + \Delta X) - ETC(D_{past}), \tag{5.2}$$

For explicit details on D'_{past} and D_{past}, please refer to Section 2.3. Conditional CCC, $CCC_{Y_{past}\to\Delta X|Z_{past},W_{past}}$, is then estimated as the difference of Eq. 5.1 and Eq. 5.2. Averaged Conditional CCC over the entire time series with the window ΔX being slided by a step-size of δ is given as below:

$$CCC_{Y\to X|Z,W} = \overline{CC}(\Delta X|D'_{past}) - \overline{CC}(\Delta X|D_{past}). \tag{5.3}$$

What effectively this quantity is capturing is the causality from Y to ΔX given that ΔX is an outcome of evolution of the (X, Z, W) model. It is thus Y's contribution to all variables (including X) in the system that are supposedly contributing to evolution of ΔX. This, however, is not the direct contribution of Y to X alone, removing all the indirect means of transfer of information to X – and that is what we are interested in estimating with the network data presented to us. To make this more clear, let us consider the variables X, Y, Z, W having a particular network structure as depicted in Figure 5.1. Then to extract the direct causal influence from Y to X, the indirect effect from Y to X, which is transmitted via Z and W needs to be eliminated. The causal effect captured via CCC from variable Y to X using bivariate $CCC_{Y\to X}$ is the total cascaded effect in the network, inclusive of effects from Y to Z, Z to W and W to X. The cascaded effect from Y up to a higher *hierarchical* level (W), thus, needs to be eliminated from $CCC_{Y\to X}$ (we suppose X to be at the lowest level of *hierarchy* in this network as there is no other variable existing downstream to it and being caused by it; similarly Y is at the highest level of *hierarchy*). Also, the influence that is transmitted from W to X (and mediated by Z) which ultimately arises from Y needs to be removed from $CCC_{Y\to X}$ to capture the direct influence from Y to X that exists external to the cascaded network effects. This can be done by subtracting the total causal influence from Y to X (which is bivariate $CCC_{Y\to X}$) and the sum of causal influences from Y to W ($CCC_{Y\to W}$) and the effect arising from Y which is transmitted to X via (X, Z, W) model evolving to ΔX. A pictorial analog for this is subtracting the solid box and the sum of two dashed boxes in Figure 5.1. Effective CCC, $CCC_{Eff.(Y\to X)}$ in the network

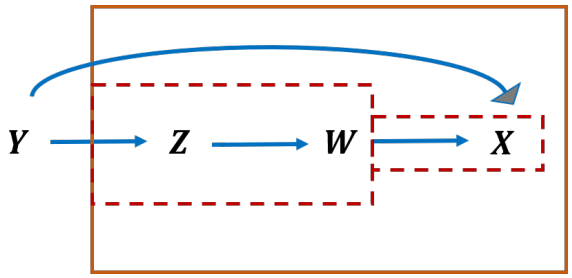

Figure 5.1: A four variable network where causality from Y to X is to be determined.

is thus given by:

$$CCC_{Eff.(Y\to X)} = CCC_{Y\to X} - CCC_{Y\to W} - CCC_{Y\to X|Z,W}. \tag{5.4}$$

Similarly, other effective CCC's in the network can be computed as follows:

$$CCC_{Eff.(Y\to W)} = CCC_{Y\to W} - CCC_{Y\to Z} - CCC_{Y\to W|Z}, \tag{5.5}$$

$$CCC_{Eff.(Z\to X)} = CCC_{Z\to X} - CCC_{Z\to W} - CCC_{Z\to X|W}. \tag{5.6}$$

CCC to a level of hierarchy from a level above itself is just the simple bivariate CCC. Thus, $CCC_{Eff.(Y\to Z)}$, $CCC_{Eff.(Z\to W)}$ and $CCC_{Eff.(W\to X)}$ remain the same as $CCC_{Y\to Z}$, $CCC_{Z\to W}$ and $CCC_{W\to X}$ respectively. Also, above defined effective CCCs are to be estimated only if there is a *significant* bivariate CCC for a pair of variables. Significance is decided based on a set threshold (this is discussed in the following paragraphs). Since bivariate CCC always captures the direct as well as indirect influences, it is the bivariate CCC based causal graph that needs to be pruned in order to compute the effective CCC value between a pair of variables in a network. Based on the number of significant input bivariate CCC values to each variable, the hierarchical levels for placement of the variables in a network are decided and consequently the effective CCC

values estimated. In the example in Figure 5.1, in an ideal situation, variable Y will have zero input significant CCCs (considered from all other variables) and is thus is at level 1. Variable Z will have significant input CCC from only one other variable, Y and is thus at level 2, W will have significant input CCC from 2 other variables (direct from Z and indirect from Y), and is thus at level 3. X will have 3 input significant CCCs from Y (direct+ indirect), Z (indirect) and W (direct), and is thus at level 4. It is possible to have more than one variable at a single level. This method works only for directed acyclic graphs or to capture the net causal information flow in a particular direction for a given network. The steps of the algorithm which computes effective CCC connectivities for given data from directed acyclic graph network of four variables are as follows:

1. Input multivariate data matrix containing observations from given network variables.

2. Compute bivariate CCC values between each pair of variables.

3. Based on the above values, decide the level of hierarchy for each network variable in the following way:

   (a) If bivariate CCC from all other variables to a variable is insignificant, then the latter variable is at the first or topmost level of hierarchy. Significance of bivariate CCC is decided based on comparison with a set threshold, th_1, with the obtained value being insignificant if it is less than th_1. Significance in points (b), (c), (d) below is also decided, based on this criteria.

(b) If a variable has significant bivariate CCC from one other variable in the network, and at least one variable at the first level (based on criteria (a)) exists having a causal influence to this particular variable, then this variable is a second level variable. However, if no 'first level' variable exists, then this variable is qualified as a first level variable. The sole existing significant bivariate CCC value to this variable is likely to be spurious.

(c) If a variable has significant bivariate CCC from two other variables in the network, and a variable at the second level (based on criteria (b)) exists having a causal influence to this particular variable, then this variable is a third level variable. However, if no 'second level' variable exists, then this variable is qualified as a second level variable. One of the two existing significant CCC values to the variable in this case, is likely to be spurious or there exist more than one first level variables contributing to the second level variable.

(d) If a variable has significant bivariate CCC from three other variables in the network, and a variable at the third level exists having a causal influence to this particular variable, then it is a fourth level variable. However, if no third level variable exists but at least one second level variable exists, then this variable is qualified as a third level variable. One of the three existing significant CCC values to it is likely to be spurious in this case or more than one first/second level variables are contributing to it. However, if, even a

second level variable doesn't exist, then the variable is qualified as a second level variable. Two of the three significant CCC values are likely to be spurious in this case or more than two (exactly three in the four variable case) first level variables are contributing to this second level variable.

4. For all the first level variables in the network, effective CCC value is computed to them from all other variables as being equal to the bivariate CCC value. All these computed CCCs are insignificant (based on comparison with a set threshold, th_1). In fact, that was the reason for these variables to have been qualified as first level. Hence, the signifcance of all these causalities is set to zero.

5. If one or more second level variables exist in the network, all causal influences to this variable are from a level above itself (first level). Hence, bivariate CCC is used to estimate the causality from all other variables to this variable. If these CCCs are significant based on comparison with threshold, th_1, significance of corresponding effective CCCs between pairs of variables are set to 1 and remains zero otherwise.

6. If one or more third level variables exist in the network, effective CCC from second level (one level above) to third level is determined to be the bivariate CCC between the pair. Its significance is determined based on th_1, as in the step above. If a first level variable exists in this network and there is a possible causal pathway from this first to third variable (determined based on whether bivariate CCC between first to third is significant based on comparison with th_1 and there

exists a second level variable from which effective CCC to this particular third has been already qualified as being significant), then effective CCC from first to third is determined as from $Y \rightarrow W$, as in Eq. 5.5 above, after estimating conditional CCC from first to third variable given second variable. The significance of this effective CCC is determined based on comparison with a threshold, th_2.

7. If a fourth level variable exists in the network, effective CCC from third to fourth level variable is the same as corresponding bivariate CCC, its significance being determined by th_1. Effective CCC from second to fourth level is estimated in the same way as from first to third level, determined as from Z to X, as in Eq. 5.6 above. The significance of this effective CCC is determined based on threshold, th_3. For computing effective CCC from first to fourth level, if bivariate CCC from first to fourth is significant based on th_1, then effective CCC from first to fourth is computed as from Y to X as in Eq. 5.4 after estimating conditional CCC from first to fourth given the second and third level variables. This effective CCC is qualified as significant based on comparison with threshold, th_4.

The thresholds th_1, th_2, th_3, th_4, which are used to determine the significance of CCC values are determined empirically based on the results obtained for the datasets considered.

5.2 Problem of Joint ETC Computation and Equivalent ETC based Computation

Once the problem of formulation is solved and we compute effective CCC to capture causality between a pair of variables given other variables in a network, another issue crops up at the level of computation. In order to compute conditional CCCs such as $CCC_{Y\to X|Z,W}$, $CCC_{Y\to W|Z}$ and $CCC_{Z\to X|W}$ in Eqs. 5.4,5.5 and 5.6 for the network in Figure 5.1 and similar such quantities relevant to other networks, joint ETC of several time sequences needs to be estimated. For this, time varying dictionary of several variables needs to be constructed as discussed in Section 2.3. As the number of variables in a network grow, for a particular chosen number of bins B for encoding each time series variable, the total possibilities of losslessly encoded symbol at each time point that represents all variables together grows exponentially with the number of variables in the given network, being equal to B^n possibilities for n variables in the network. Thus, it can be said that the resulting 'number of bins' (let's say b) has increased for computation of ETC of requisite temporal sequences. Because of this, not only does ETC estimation take more time, but also computation of dynamical complexities for short windows w of ΔX as in Eqs. 5.1 and 5.2 based on short pasts, D' and D of length L (used for conditional CCC estimation) becomes difficult. With higher number of variables and the total possible encodings at each time point increased, the patterns in D and D' influence limited number of patterns in ΔX. Thus, these dictionaries are unable to accurately capture the complexity of their immediate (potential) future evolution. On

the other hand, if parameters L and w are made large, the causal information from immediate past is lost. Thus, we propose an alternate means to capture dynamical complexity for high dimensional data. This is by defining *equivalent ETC*. Trends in changes of dynamical complexities (or bivariate CCC/conditional CCC) estimated by joint and equivalent ETCs are found to be similar for two and three variable systems. In the next subsection, we discuss the equivalent ETC formulation based on theoretical understanding of ETC.

5.2.1 Equivalent ETC

Details on the working of *ETC* algorithm are given in Chapter 2 in Section 2.2. Here, we discuss the theoretical underpinnings for the measure, that will later help us to propose equivalent ETC formulation.

Let Y be a given sequence of symbols of length N, $Y = a_1a_2a_3a_4 \dots a_N$, where $a_1, a_2, a_3, a_4, \dots a_N \in \{b_1, b_2, b_3 \dots b_m\}$. Thus, $a_1, a_2, a_3, a_4, \dots a_N$ can take one of m possible symbols.

We define the following for Y:

Y_1: the given sequence Y as it is.

Y_2: transformed Y, once the most frequently occurring pair in Y has been substituted with another symbol, i.e. the sequence after first iteration of the ETC algorithm.

Y_i: transformed sequence after $i-1$ iterations of the ETC algorithm, where at each

iteration the most frequently occurring pair in that sequence is being substituted by a new symbol.

Y_{n+1}: transformed sequence Y after n iterations, where no more iterations after this are possible and hence n is the ETC value.

X_1: most frequently occurring pair in Y_1. In other words, it is the first most dominant shortest *pattern* (of length 2).

X_2: most frequently occurring pair in Y_2. In other words, it is the second most dominant shortest pattern (of length 2 in Y_2, but may be of length 2 or 3 in the original sequence, Y).

X_i: most frequently occurring pair in Y_i.

X_n: most frequently occurring pair in Y_n. It is the n^{th} most dominant shortest pattern.

Let Z be the event of joint occurrence of paired patterns $(X_1, X_2, X_3, \ldots X_n)$ occurring at different levels of transformations of Y. The probability of joint occurrence of these events is given as –

$$\begin{aligned} p(Z) =& p(X_1, X_2, X_3, \ldots X_n), \\ =& p(X_n|X_1, X_2, \ldots X_{n-1}) \cdot p(X_1, X_2, \ldots X_{n-1}), \\ =& p(X_n|X_1, X_2, \ldots X_{n-1}) \cdot p(X_{n-1}|X_1, X_2, \ldots X_{n-2}) \cdot p(X_1, X_2, \ldots X_{n-2}), \quad (5.7) \\ & \vdots \\ =& p(X_n|X_1, X_2, \ldots X_{n-1}) \cdot p(X_{n-1}|X_1, X_2, \ldots X_{n-2}) \ldots p(X_2|X_1)p(X_1). \end{aligned}$$

Total self information, $G(Z)$ contained in the joint occurrence of patterns $(X_1, X_2, X_3, \ldots X_n)$ can therefore be written as:

$$\begin{aligned} G(Z) &= -\log(p(Z)), \\ &= -\log(p(X_1)) - \log(p(X_2|X_1)) - \log(p(X_3|X_1, X_2)) \ldots - \log(p(X_n|X_1, X_2, \ldots X_{n-1})). \end{aligned} \tag{5.8}$$

We approximate the conditional probability, say $p(X_i|X_1, X_2, \ldots X_{i-1})$ in the above formulation by observing the frequency of pattern, X_i, in the sequence Y_i in which all prior replacements $X_1, X_2, \ldots X_{i-1}$ have been done. Thus, if $q_1, q_2, \ldots q_n$ are the frequency of occurrence of patterns $X_1, X_2, \ldots X_n$ in $Y_1, Y_2, \ldots Y_n$ respectively, then Eq. 5.8 can be written as:

$$\begin{aligned} G(Z) &= -\log\left(\frac{q_1}{N}\right) - \log(\frac{q_2}{N - q_1}) - \log\left(\frac{q_3}{N - q_1 - q_2}\right) \ldots - \log\left(\frac{q_n}{N - q_1 - q_2 \ldots - q_{n-1}}\right), \\ &= -\log\left(\frac{q_1}{N}\right)\left(\frac{q_2}{N - q_1}\right)\left(\frac{q_3}{N - q_1 - q_2}\right) \ldots \left(\frac{q_n}{N - q_1 - q_2 \ldots - q_{n-1}}\right). \end{aligned} \tag{5.9}$$

As seen above, ETC algorithm reduces the length of sequence at each iteration by transforming the original sequence Y. Thus, the *compression* achieved by the ETC algorithm at any step of the algorithm can be seen as the fractional reduction in length of the sequence achieved at that step. Let us suppose the equivalent (or average) compression (or fractional reduction in length) being done by ETC at each iteration be denoted by x. Then, if ETC algorithm takes n steps to stop,

$$x^n = \left(\frac{q_1}{N}\right)\left(\frac{q_2}{N - q_1}\right)\left(\frac{q_3}{N - q_1 - q_2}\right) \ldots \left(\frac{q_n}{N - q_1 - q_2 \ldots - q_{n-1}}\right), \tag{5.10}$$

Taking natural logarithm on both sides,

$$n \cdot \log(x) = \log\left(\left(\frac{q_1}{N}\right)\left(\frac{q_2}{N-q_1}\right)\left(\frac{q_3}{N-q_1-q_2}\right)\ldots\left(\frac{q_n}{N-q_1-q_2\ldots-q_{n-1}}\right)\right),$$
$$n = \frac{\log\left(\left(\frac{q_1}{N}\right)\left(\frac{q_2}{N-q_1}\right)\left(\frac{q_3}{N-q_1-q_2}\right)\ldots\left(\frac{q_n}{N-q_1-q_2\ldots-q_{n-1}}\right)\right)}{\log(x)}. \tag{5.11}$$

Using Eq. 5.9 in Eq. 5.11

$$n = -\frac{1}{\log(x)} \cdot G(Z),$$
$$n = k \cdot G(Z), \tag{5.12}$$

where $k = -1/\log(x)$. Thus, ETC can be seen as a constant multiplied by total self-information contained in the joint occurrence of most dominant (shortest) patterns at all levels (scales) of the sequence. For estimating equivalent ETC of l given sequences based on the above formulation, let $x_1, x_2, x_3, \ldots x_l$ be the equivalent (or average) per step compression for each of the given sequences and their respective total compression (the quantity, $((\frac{q_1}{N})(\frac{q_2}{N-q_1})(\frac{q_3}{N-q_1-q_2})\ldots(\frac{q_n}{N-q_1-q_2-\ldots-q_{n-1}}))$ in case of the sequence considered above) be $A_1, A_2, A_3, \ldots A_l$. The above quantities are computed in the process of determining the number of ETC steps $n_1, n_2, n_3, \ldots n_l$, for each of the sequences separately. Then *equivalent ETC* for the l sequences is estimated by computing geometric mean of the total compression achieved for all given sequences. Equivalent number of ETC steps required for compression of l given sequences, n_{eq}, is then given as:

$$(x_1 \cdot x_2 \ldots x_l)^{(n_{eq}/l)} = (A_1 \cdot A_2 \ldots A_l)^{(1/l)},$$
$$n_{eq} = \frac{\log(A_1 \cdot A_2 \ldots A_l)}{\log(x_1 \cdot x_2 \ldots x_l)}. \tag{5.13}$$

Because of the problems discussed in joint ETC computation, equivalent ETC is used instead of joint ETC for effective CCC estimation in networks. Both bivariate

and conditional CCC terms used for estimation of effective CCC employ equivalent ETC formulation in the results discussed in next section.

5.3 Results

Four-variable networks of autoregressive (AR) processes were generated for two cases as follows:

Case 1: AR(1) processes with measurement noise.

$$\begin{aligned} X_1(t) &= a_1X_1(t-1) + b_1X_2(t-1) + c_1X_3(t-1) + d_1X_4(t-1) + \epsilon_{1,t}, \\ X_2(t) &= a_2X_1(t-1) + b_2X_2(t-1) + c_2X_3(t-1) + d_2X_4(t-1) + \epsilon_{2,t}, \\ X_3(t) &= a_3X_1(t-1) + b_3X_2(t-1) + c_3X_3(t-1) + d_3X_4(t-1) + \epsilon_{3,t}, \\ X_4(t) &= a_4X_1(t-1) + b_4X_2(t-1) + c_4X_3(t-1) + d_4X_4(t-1) + \epsilon_{4,t}, \end{aligned} \tag{5.14}$$

is a system of four variables with $\epsilon_1, \epsilon_2, \epsilon_3, \epsilon_4 = \nu\eta$, where ν=noise intensity=0.03 and η follows standard normal distribution. Measurement noise (additive white Gaussian noise) of the form of $\nu'\eta$ was added to each of the processes with $\nu' = 0.05$. Ten different types of this network were simulated with the adjacency matrix:

$$D = \begin{bmatrix} a_1 & b_1 & c_1 & d_1 \\ a_2 & b_2 & c_2 & d_2 \\ a_3 & b_3 & c_3 & d_3 \\ a_4 & b_4 & c_4 & d_4 \end{bmatrix}, \tag{5.15}$$

taking values as follows:

Type 1:

$$D_1 = \begin{bmatrix} 0.7 & 0 & 0 & 0.9 \\ 0 & 0.7 & 0 & 0.8 \\ 0 & 0 & 0.7 & 0.9 \\ 0 & 0 & 0 & 0.7 \end{bmatrix}, \tag{5.16}$$

Type 2:

$$D_2 = \begin{bmatrix} 0.7 & 0 & 0 & 0.9 \\ 0.9 & 0.7 & 0 & 0 \\ 0.9 & 0 & 0.7 & 0 \\ 0 & 0 & 0 & 0.7 \end{bmatrix}, \tag{5.17}$$

Type 3:

$$D_3 = \begin{bmatrix} 0.7 & 0 & 0 & 0.9 \\ 0 & 0.7 & 0.8 & 0 \\ 0.9 & 0 & 0.7 & 0 \\ 0 & 0 & 0 & 0.7 \end{bmatrix}, \tag{5.18}$$

Type 4:

$$D_4 = \begin{bmatrix} 0.7 & 0 & 0 & 0.9 \\ 0.9 & 0.7 & 0.8 & 0 \\ 0.9 & 0 & 0.7 & 0 \\ 0 & 0 & 0 & 0.7 \end{bmatrix}, \tag{5.19}$$

Type 5:

$$D_5 = \begin{bmatrix} 0.7 & 0 & 0 & 0.9 \\ 0 & 0.7 & 0.8 & 0.9 \\ 0.9 & 0 & 0.7 & 0 \\ 0 & 0 & 0 & 0.7 \end{bmatrix}, \tag{5.20}$$

Type 6:

$$D_6 = \begin{bmatrix} 0.7 & 0 & 0 & 0.9 \\ 0.9 & 0.7 & 0.8 & 0.9 \\ 0.9 & 0 & 0.7 & 0 \\ 0 & 0 & 0 & 0.7 \end{bmatrix}, \tag{5.21}$$

Type 7:

$$D_7 = \begin{bmatrix} 0.7 & 0 & 0 & 0.9 \\ 0 & 0.7 & 0.8 & 0 \\ 0.9 & 0 & 0.7 & 0.9 \\ 0 & 0 & 0 & 0.7 \end{bmatrix}, \tag{5.22}$$

Type 8:

$$D_8 = \begin{bmatrix} 0.7 & 0 & 0 & 0.9 \\ 0.8 & 0.7 & 0.8 & 0 \\ 0.9 & 0 & 0.7 & 0.9 \\ 0 & 0 & 0 & 0.7 \end{bmatrix}, \tag{5.23}$$

Type 9:

$$D_9 = \begin{bmatrix} 0.7 & 0 & 0 & 0.9 \\ 0 & 0.7 & 0.8 & 0.9 \\ 0.9 & 0 & 0.7 & 0.9 \\ 0 & 0 & 0 & 0.7 \end{bmatrix}, \tag{5.24}$$

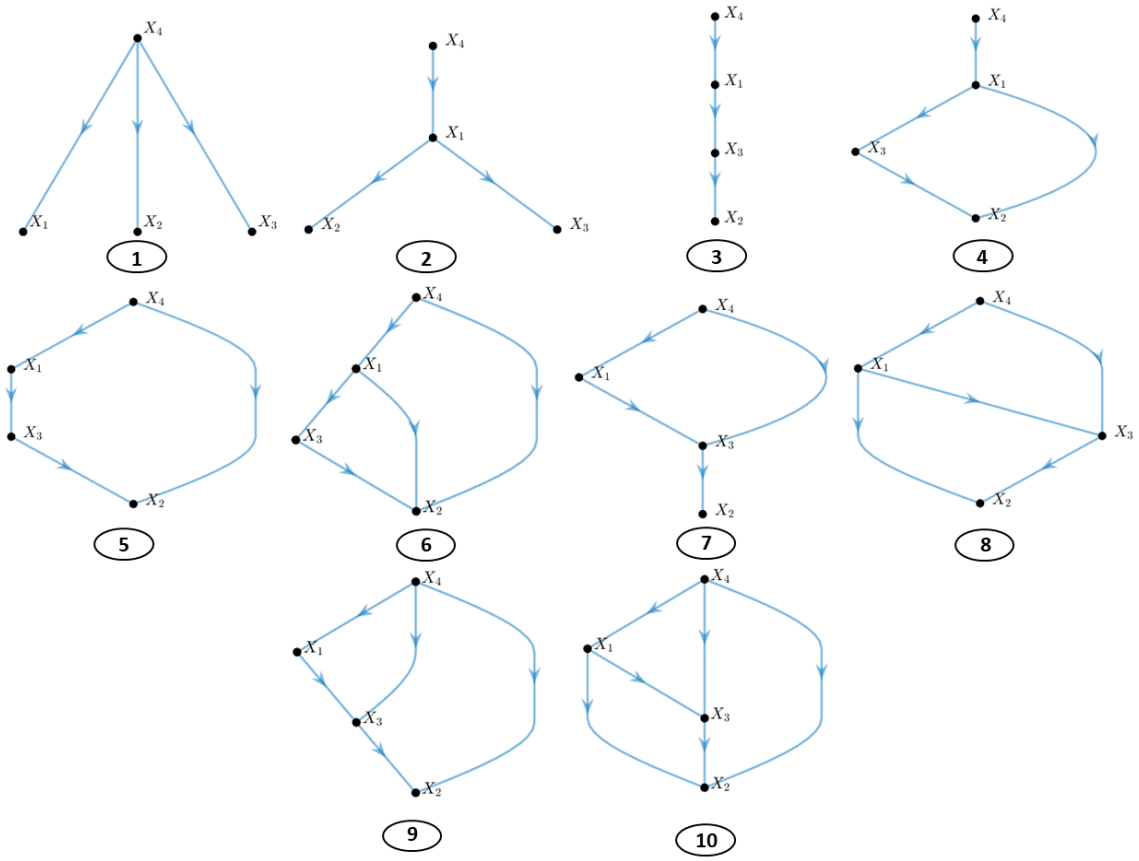

Figure 5.2: Ten types of simulated networks for two cases of autoregressive processes X_1, X_2, X_3, X_4. Self connections are not shown here.

Type 10:

$$D_{10} = \begin{bmatrix} 0.7 & 0 & 0 & 0.9 \\ 0.8 & 0.7 & 0.8 & 0.9 \\ 0.9 & 0 & 0.7 & 0.9 \\ 0 & 0 & 0 & 0.7 \end{bmatrix}, \tag{5.25}$$

Pictorial depiction of the directed graphs for these ten types of networks is shown in Figure 5.2.

Case 2: AR(50) processes. Equations determining the network are as below:

$$\begin{aligned}
X_1(t) &= a_1X_1(t-1) + b_1X_2(t-50) + c_1X_3(t-50) + d_1X_4(t-50) + \epsilon_{1,t},\\
X_2(t) &= a_2X_1(t-50) + b_2X_2(t-1) + c_2X_3(t-50) + d_2X_4(t-50) + \epsilon_{2,t},\\
X_3(t) &= a_3X_1(t-50) + b_3X_2(t-50) + c_3X_3(t-1) + d_3X_4(t-50) + \epsilon_{3,t},\\
X_4(t) &= a_4X_1(t-50) + b_4X_2(t-50) + c_4X_3(t-50) + d_4X_4(t-1) + \epsilon_{4,t},
\end{aligned} \tag{5.26}$$

is a system of four variables with $\epsilon_1, \epsilon_2, \epsilon_3, \epsilon_4 = \nu\eta$, where ν=noise intensity=0.03 and η follows standard normal distribution. Ten different types of this network were simulated with same adjacency matrices as for the ten types taken in Case 1.

For all the 20 cases (10 types of networks, for each of Case 1 and Case 2), 100 trials of the network with 400 observations from each variable (after removal of 200 transients) were taken. For each trial, the initial conditions were randomly chosen. Effective CCC values as well as conditional multivariate Granger Causality (GC) values were computed for all the cases taken in order to determine network connectivity. For the estimation of effective CCC, the parameters were set as: $w = 20, B = 4, \delta = 20, L = 140$[1] for both Cases 1 and 2 and the thresholds used were set as: $th_1 = 0.006, th_2 = 0.017, th_3 = 0.0001, th_4 = 0.0001$ for Case 1 and $th_1 = 0.007, th_2 = 0.017, th_3 = 0.002, th_4 = 0.002$ for Case 2. Akaike Information Criteria was used for model order estimation with the maximum model order set to 20 for Case 1 and 60 for Case 2 in the MVGC toolbox [31]. Computation of maximum number of lags to take for autocorrelation computation was done automatically by the toolbox. Significance testing of effective CCC, done

[1]These parameters were selected as they satisfied the parameter selection criteria (see Section 3.3) for a number of arbitrarily and independently selected pairs of variables chosen from the simulated network.

based on comparison with thresholds, and significance testing of GC F statistic as done automatically by the MVGC toolbox, yielded a binary matrix of connectivity between variables, with 1 indicating the presence and 0 the absence of directed causal connection between a pair of variables. It was checked whether connectivity between each pair of variables was correctly determined or not by each method for each trial. Based on that, true positive rate (TPR) or recall, true negative rate (TNR) or specificity, false positive rate (FPR), false negative rate (FNR), precision, F_1 score and accuracy were computed and compared for the two methods for each case. These quantities were estimated as follows:

$$\begin{aligned} TPR &= \frac{TP}{TP+FN}, \\ TNR &= \frac{TN}{TN+FP}, \\ Precision &= \frac{TP}{TP+FP}, \\ F_1Score &= \frac{2 \cdot Precision \cdot Recall}{Precision + Recall}, \\ Accuracy &= \frac{TP+TN}{TP+TN+FP+FN}, \end{aligned} \tag{5.27}$$

where TP denotes the number of true positives, TN, the number of true negatives, FP, the number of false positives and FN, the number of false negatives. The above quantities estimated for CCC and GC for all network types for Case 1 is listed in Table 5.1 and for Case 2 in Table 5.2. The averaged metrics (for CCC as well as GC) over all network types for each *Case* are shown as the last row in the corresponding tables and also depicted in bar graphs in Figure 5.3.

Table 5.1: Effective CCC and Conditional GC comparison for 10 types of networks simulated as per Case 1. For each network type, the statistics are computed over 100 trials.

Network Type	**Method**	**TPR**	**TNR**	**Precision**	**F_1Score**	**Accuracy**
1	**CCC**	0.58	0.97	0.87	0.69	0.87
	GC	1	0.66	0.50	0.66	0.75
2	**CCC**	0.90	0.90	0.75	0.82	0.90
	GC	1	0.60	0.46	0.63	0.70
3	**CCC**	0.85	0.78	0.57	0.68	0.80
	GC	1	0.77	0.59	0.74	0.83
4	**CCC**	0.90	0.84	0.74	0.81	0.86
	GC	1	0.66	0.60	0.75	0.78
5	**CCC**	0.81	0.84	0.71	0.76	0.83
	GC	1	0.66	0.59	0.75	0.77
6	**CCC**	0.87	0.92	0.88	0.87	0.90
	GC	1	0.66	0.68	0.81	0.80
7	**CCC**	0.87	0.83	0.72	0.79	0.84
	GC	1	0.76	0.67	0.80	0.84
8	**CCC**	0.83	0.90	0.85	0.84	0.87
	GC	1	0.73	0.72	0.84	0.84
9	**CCC**	0.83	0.90	0.86	0.85	0.87
	GC	1	0.63	0.66	0.79	0.79
10	**CCC**	0.84	0.99	0.98	0.91	0.91
	GC	1	0.67	0.75	0.86	0.84
Mean	**CCC**	**0.83**	**0.89**	**0.79**	**0.80**	**0.87**
	GC	**1**	**0.68**	**0.62**	**0.76**	**0.79**

Table 5.2: Effective CCC and Conditional GC comparison for 10 types of networks simulated as per Case 2. For each network type, the statistics are computed over 100 trials.

Network Type	Method	TPR	TNR	Precision	F_1Score	Accuracy
1	**CCC**	0.88	0.98	0.94	0.91	0.96
	GC	0.03	0.60	0.02	0.02	0.45
2	**CCC**	0.94	0.93	0.81	0.87	0.93
	GC	0.02	0.76	0.03	0.02	0.58
3	**CCC**	0.89	0.82	0.62	0.73	0.83
	GC	0.003	0.99	0.13	0.01	0.75
4	**CCC**	0.86	0.87	0.76	0.81	0.87
	GC	0.03	0.98	0.38	0.05	0.66
5	**CCC**	0.79	0.86	0.74	0.76	0.84
	GC	0.01	0.95	0.10	0.02	0.64
6	**CCC**	0.83	0.96	0.94	0.88	0.91
	GC	0.06	0.98	0.66	0.11	0.60
7	**CCC**	0.75	0.84	0.70	0.73	0.81
	GC	0.03	0.97	0.30	0.05	0.65
8	**CCC**	0.78	0.93	0.88	0.83	0.86
	GC	0.04	0.91	0.24	0.07	0.55
9	**CCC**	0.70	0.88	0.81	0.75	0.80
	GC	0.01	0.94	0.13	0.02	0.55
10	**CCC**	0.78	0.99	0.99	0.87	0.88
	GC	0.08	0.92	0.47	0.13	0.50
Mean	**CCC**	**0.82**	**0.91**	**0.82**	**0.81**	**0.87**
	GC	**0.03**	**0.90**	**0.25**	**0.05**	**0.59**

5.4 Discussion, Conclusions and Future Work

As seen from Section 5.1, what bivariate CCC captures is the total cascaded causal effect from one variable to another in a network, inclusive of the causal influence that has

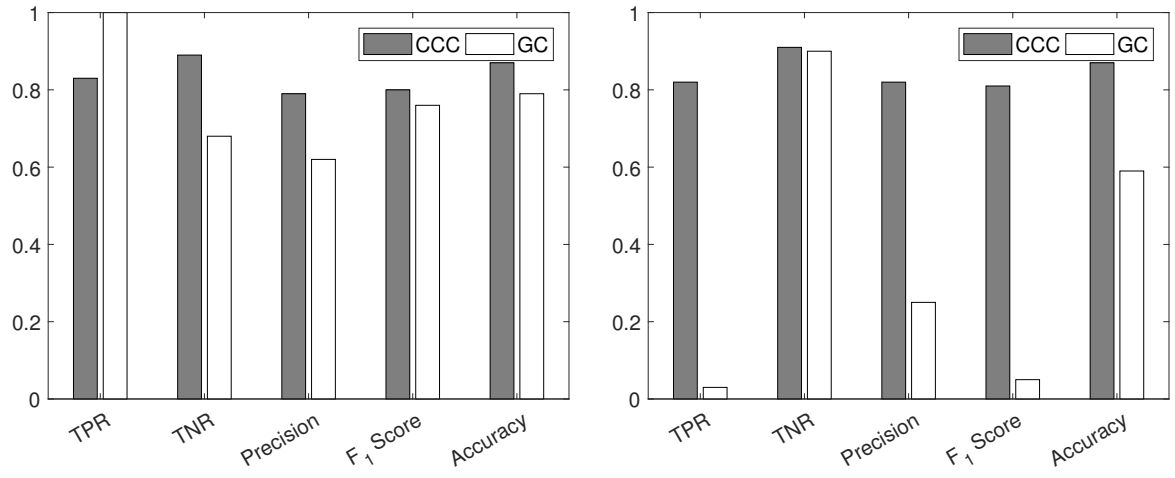

Figure 5.3: Averaged metrics for performance of CCC and GC over ten different types of networks taken for each of Case 1 (left) and Case 2 (right).

been passed on via the intermediate variables between the considered variables. This information can be of use and hence find applications for certain networks, however, many a times, we are interested in capturing only the direct causal influences. As a result, the method of effective CCC estimation has been developed. Some preliminary results for testing of effective CCC on simulated networks are shown in Section 5.3. The networks chosen are directed acyclic graphs, because the developed method uses the procedure of removing cascaded effects in a network so as to capture only the direct causal influences. Also, we have not taken networks in which there are two or more independent processes (say X and Y) that are generated using the same equations and only one of these processes is causing another process (say X causing Z) in the network. In this case, effective CCC estimates $X \to Z$ causality to be significant, but additional to that, it also estimates a significant effective CCC from $Y \to Z$. This is because the

nature of processes X and Y is same and since the nature of Z is derived from X, Z has also a potential to be caused from Y. Hence, it is not completely correct then to say that the causality estimated from $Y \rightarrow Z$ is erroneous. This issue also persists if there are two or more processes in the network which are not independent (or at the highest level of hierarchy) as in the previous example but at lower levels of hierarchy and are generated in the same manner. For example, let us consider the case in which a process X causes Y and Z with the same coupling coefficient and also the coupling coefficient to Y and Z from their own pasts is the same and further the process Y causes Q. For this case, effective CCC would estimate significant causation not only from Y to Q but also from Z to Q. This is again because of the nature of processes and Z having the potential to cause Q. Here again, it is not completely correct to say that the causality estimated from Z to Q is erroneous. Thus, for the network types simulated, we have eliminated the cases in which there are two or more processes generated in exactly the same manner and these processes are at a level of hierarchy other than the lowest level. Being at levels higher than the lowest, these processes would be either causing or having the potential to cause other processes in the network. Other than this, all topologies of 4 variable networks forming directed acyclic graphs have been considered – these are the 10 network types taken for the two cases. For these cases, effective CCC and conditional multivariate GC have been used to establish network causal connections.

The results demonstrate that CCC is promising for short, noisy and long range memory autoregressive processes. On comparison of $F_1 Score$ and $Accuracy$, effective CCC is found to perform better than GC for almost all network types taken in Case 1: AR(1)

processes with measurement noise. Only for Type 3 and Type 7, performance of GC is slightly better than CCC. In this case, TPR for GC is 1 for all network types, while TNR is lower, the average value being 0.68. For AR processes with measurement noise, GC is overestimating the number of causal connections than actually exist. Overall, CCC performs 10.13% better than GC in terms of average *Accuracy* and 5.26% better in terms of F_1Score. For all network types in Case 2, CCC performs much better than GC. Based on F_1Score, *Accuracy* and other parameters, GC is a very poor indicator of network connectivity for long range memory AR(50) processes simulated for short data length. In this case, TPR for GC is very poor, average value being 0.03, while TNR is high, the average value being 0.90. For AR processes with long term memory, GC is able to identify only a very few of the existing causal connections. Effective CCC, with accuracy remaining in the range of $0.80 - 0.96$, seems to be a promising measure to capture connectivity with short length datasets of long term memory. CCC performs 47.46% better than GC in terms of average *Accuracy* and 1520% better in terms of average F_1Score.

Future work would involve developing techniques to compute effective CCC for networks with bidirectional connections, that is networks having both feedforward and feedback connections, which is a challenging task. The developed method has been tested to work for five variables. In principle, the method could be extended to work for larger networks, but this is beyond the scope of this thesis. Furthermore, network connectivity for real world data from multivariate systems needs to be determined and its performance compared with existing measures. A prospective area of application

is that of transcriptional regulatory networks, where the measure would be tested. For the developed technique of effective CCC estimation, a method for data-adaptive estimation of optimal thresholds th_1, th_2, th_3, th_4, that determine the significance of $CCC_{Eff.}$ estimates, needs to be developed.

Part II

Advancements in Causality Analysis Contributing to Allied Disciplines

Chapter 6

Causality and Chaotic Synchronization

Synchronization of chaotic systems is a ubiquitous phenomenon that arises when these systems are coupled. Chaotic synchronization has found applications in living systems, human cognition and neuroscience as well as in physics, chemistry and engineering. In many natural and physiological instances, synchronization may occur desirably or undesirably. Causality testing has the potential to offer useful analysis tools to identify and deal with these occurrences in an appropriate manner. In this chapter, we deal with two-fold important aspects of synchronization using causality as described below:

1. *Synchronization has been understood as a temporal phenomenon. Here, we use the lens of causality testing to provide a complementary spatial perspective to the phenomenon by introducing the novel idea of causal stability. We also propose and prove a causal stability synchronization theorem and propose an empirical criterion to identify synchronizing variables in coupled identical chaotic dynamical systems. This is an important theoretical contribution to the field of chaotic*

synchronization and causality testing and has potential for real world applications, such as in the control of chaos.

2. *Anticipating Synchronization (AS) is a counterintuitive form of synchronization, where the slave (driven system) dynamics evolve ahead in time of the master (driving system) dynamics. This phenomenon has been found to be stable in several real systems. It is shown for the difficult case of an AS simulated system that Granger Causality fails in causality estimation. However, CCC, when used with high resolution (large bin size) of the data can inform correct causal relations.*

6.1 Introduction

Chaotic Synchronization is a phenomena that arises on coupling of chaotic systems. Pecora and Carroll's 1990 paper [68] followed by He and Vaidya's work in 1992 [69] were a revelation into chaotic synchronization and opened up an entire field of intense research. Later, synchronization began to be classified into its various types [138]. It was seen that for two or more chaotic systems, if a means of interaction is established by which they are able to exchange some information (via coupling), then they may synchronize in one of the following ways. The whole of the two systems may become completely identical with evolution over time (as in complete/identical synchronization), or they may become identical with a time delay (delayed/anticipating synchronization), or may become identical in phase (phase synchronization), or may become connected with a functional relationship (generalized synchronization).

Applications of synchronization of chaotic systems are ubiquitous - it is found to occur in specialized electronic circuits, optical arrays, physiological phenomena, social networks, superconductors and other biological and physical systems. Some examples include phase synchronization of two pendulum clocks hanging on a wall, synchronization of moon's rate of rotation with its orbital motion rate of revolution around the earth. With this, the moon always faces the same side towards the earth. The concept has also become important and found applications in engineering such as communication technologies, coupled laser systems and biochemical reactors. In the physiological realm, many examples of chaotic synchronization abound – activity of different heart muscle cells synchronize to produce its rhythmic beating, groups of neurons in the brain synchronize to perform certain functions, neighbouring functional units of kidney, called nephrons, attain phase synchronization of their pressure oscilations that regulate the flow of fluid [139].

Since synchronization is a result of coupling between systems, there has been some research, which has tried to analyze and understand the domain through causality testing methods. Given temporal data from coupled chaotic systems, these methods deal with estimation of inter-system strength and directionality of coupling. They have been helpful in identifying: (a) if the given systems are proceeding towards synchronization and, (b) which nodes in a given network are the strongest drivers and hence plausibly the focus for the origin of synchronization [140, 141]. Causality estimation measures employed in these studies include symbolic Transfer Entropy [63], conditional Mutual Information [64] and non-linear Granger Causality [42].

Unlike the above studies, in this chapter, we provide, for the first time, a mathematically rigorous treatment to the link between causality and synchronization by proving necessary and sufficient conditions for complete synchronization based on spatial causal influences. For this, we propose the concept of *causal stability* and prove the *causal stability synchronization theorem*. A novel empirical condition is also proposed to identify synchronizing variables in coupled identical chaotic dynamical systems based on intrasystem causal influences estimated using time series data of the driving system alone. While being an important theoretical contribution, this work also has potential real-world applications in the control of chaos. This work is discussed in Section 6.2.

In Section 6.3, we deal with causality detection in systems with Anticipating Synchronization (AS). Some chaotic systems though coupled in a unidirectional master-slave configuration, exhibit 'paradoxical' dynamics in which the time series of the slave begins to lead (anticipate) that of the master. Hence, causality detection for these systems based on time series data is a difficult task. Using a simulated coupled chaotic system with anticipation, we show Granger Causality (GC) is not a reliable measure for estimating causality in AS systems. Any existing studies making use of GC to infer the presence of AS in real world systems need to be revisited and revised while any future studies should proceed with caution. CCC when employed with high (binning) resolution of data is found to be successful for detecting causality in the simulated AS system. It is thus a potential measure that can be used in studies along this line.

6.2 Causal Stability and Synchronization

Synchronization is very well understood as a temporal phenomena which leads the coupled systems to converge or develop a dependence with time. Pecora and Carroll showed that negative conditional Lyapunov exponents of the non-driven slave subsystem are a necessary condition [68], while He and Vaidya proved that asymptotic stability of the non-driven subsystem is a necessary and sufficient condition for complete synchronization [69]. However, to the best of our knowledge, there exists no spatial perspective for understanding of synchronization. For ergodic dynamical processes, it is only natural to expect a spatial counterpart for temporal conditions of chaotic synchronization. In this work, we explore causal interactions within the master and slave systems to identify spatial influences that drive the slave to synchronize with its master. A master is an independent driving chaotic system while the slave is dependent, unidirectionally coupled to the driving master.

Sensitive dependence on initial conditions, the hallmark of chaos, implies that trajectories from nearby initial conditions diverge. However, when these chaotic systems are coupled, the *causal influence* of the master on the slave via information transmitted by the coupled variable may lead to synchronized behaviour. The causal influence of the coupled variable on the non-driven subsystem is of importance in this regard. If this influence is invariant to perturbation of the subsystems' initial conditions then we can expect chaotic synchronization.

Asymptotic stability [69] - the condition that the non-driven subsystem reaches the

same eventual state at a fixed time no matter what the initial conditions were, is both a necessary and sufficient condition for chaotic synchronization. We are interested in the question, *what is the cause of asymptotic stability of the subsystem?* Specifically, we explore what kind of causal influence does the forced variable have on this subsystem that leads it to be driven to the same eventual state each time. We formally derive and prove a necessary and sufficient condition for chaotic synchronization based on causal influence to the non-driven subsystem.

Furthermore, for identical master and slave systems, we provide an empirical criteria for determining which variables when coupled will result in synchronization. This is achieved by analyzing intra-system causal influences estimated entirely from time series data of the driving system alone. This is an important novel contribution with real world applications in the control of chaos, especially when we need to determine which nodes should be coupled for synchronization when the underlying equations are completely unknown. An important tool for this kind of causal analysis is the measure CCC, which was proposed in Chapter 2. The measure efficiently captures causal relationships between time series of coupled processes based on dynamical complexity. Since the measure provides not only the *quantity* (strength) of causality but also its *quality*, which is reflected in the sign of the estimated CCC value, it is able to identify variables which when coupled will lead to synchronization.

The proposed causality based conditions for synchronization are said to be *spatial* as they measure the causal influence between spatial (state) variables of the driver and slave systems. These conditions hold for chunks of time series data taken, starting at

any time point of the available data, post the removal of transients. On the other hand, the temporal condition of asymptotic stability holds true only after a fixed, sufficiently far enough time and is proved for time $t \to \infty$. Thus, the proposed spatial conditions are complementary to standard temporal conditions and will be useful in practical applications where limited data is available.

6.2.1 Synchronization via Causal Stability

Let a master system be governed by the following set of differential equations:

$$\dot{\mathbf{y}} = \mathbf{f}(t, \mathbf{y}), \tag{6.1}$$

where $\dot{\mathbf{y}}$ and $\mathbf{f}$ are vectors. As described in [69], the master system (Eq. 6.1) can be divided into two interdependent subsystems $\mathbf{p}$ and $\mathbf{q}$. The slave system also consists of two subsystems $\mathbf{p}'$ and $\mathbf{q}'$, whose functional form is identical to the corresponding master system. $\mathbf{p}'$ component of slave is completely overridden by the $\mathbf{p}$ component of master and will be referred to as the forced/driven variable. $\mathbf{q}'$ component is allowed to have initially different conditions and will be referred to as the non-driven subsystem. The equations for the master are as below:

$$\dot{\mathbf{p}} = \mathbf{h}(t, \mathbf{p}, \mathbf{q}), \quad \dot{\mathbf{q}} = \mathbf{g}(t, \mathbf{p}, \mathbf{q}), \tag{6.2}$$

and the slave system is given by:

$$\mathbf{p}' = \mathbf{p}, \quad \dot{\mathbf{q}}' = \mathbf{g}(t, \mathbf{p}, \mathbf{q}'). \tag{6.3}$$

As pointed before, the influence of the forced variable ($\mathbf{p}'$) on the non-driven subsystem ($\mathbf{q}'$) is important for our analysis of the behavior of slave dynamics. What is meant

by a *cause* or *causal influence*, has been discussed in Section 1.2.3. For evaluation of cause or causal influence based on time series analysis, the above definition of causality was formulated in a mathematical way by Wiener [27]. This has been discussed in Section 1.2.5. According to Wiener, "a time series Y is a cause for time series X if the past of Y contains information that helps predict X above and beyond the information contained in past values of X alone". This principle led to Wiener-Granger causality measure [5] or GC for coupled autoregressive processes. Subsequently, concepts related to information flow, such as Transfer Entropy [23] or Conditional Mutual Information [64] were developed for causality testing. These have been discussed in Section 1.2.5. The CCC measure, proposed in Chapter 2 is another measure. It captures causality based on dynamical evolution of processes.

Let us suppose the subsystem $\mathbf{p}$ comprises of the variable x and $\mathbf{p}'$ of variable x'. Also, the subsystem $\mathbf{q}$ comprises of the variables y and z and $\mathbf{q}'$ of variables y' and z'. We estimate the *net causal influence* input to the subsystem $\mathbf{q}'$ as below. The causal influence can be determined using any of the methods discussed above and is denoted by CI.

$$CI_{net(\mathbf{p}'\to\mathbf{q}')} = CI_{\mathbf{p}'\to\mathbf{q}'} - CI_{\mathbf{q}'\to\mathbf{p}'}, \tag{6.4}$$

which in this case reduces to:

$$\begin{aligned} CI_{net(x'\to y',z')} = {} & CI_{x'\to y'|z'} + CI_{x'\to z'|y'} \\ & -CI_{y'\to x'|z'} - CI_{z'\to x'|y'}. \end{aligned} \tag{6.5}$$

where $CI_{a\to b|c}$ is the conditional causal influence of a on b given time series c. In case of more than three variables, the conditioning is performed on all the remaining variables

(other than a and b).

We define *causal stability* for the subsystem $\mathbf{q}'$ as follows:

Definition 6.1 *Causal Stability:* The subsystem $\mathbf{q}'$ is said to be causally stable if:

$$|CI_{net(\mathbf{p}'(\mathbf{p}'_\mathbf{0})\rightarrow\mathbf{q}'(\mathbf{q}'_\mathbf{0}))} - CI_{net(\mathbf{p}'(\mathbf{p}'_\mathbf{0})\rightarrow\mathbf{q}'(\mathbf{q}'_\mathbf{1}))}| < \epsilon, \tag{6.6}$$

for arbitrarily small $\epsilon > 0$. $\mathbf{p}'(\mathbf{p}'_\mathbf{0})$ represents the solution trajectory of system $\mathbf{p}'$ started from initial vector $\mathbf{p}'_\mathbf{0}$, that is $\mathbf{p}'(t_1 : t_2; t_0, \mathbf{p}'_\mathbf{0})$, for all t_1 such that $t_{tr} < t_1 < +\infty$, $t_2 = t_1 + T$, $T > 0$ and transients for the trajectory last until t_{tr}. T is the length of the trajectory over which CI_{net} is estimated. $\mathbf{q}'(\mathbf{q}'_\mathbf{0})$ and $\mathbf{q}'(\mathbf{q}'_\mathbf{1})$ represent the solution trajectory of system $\mathbf{q}'$ started from initial vectors $\mathbf{q}'_\mathbf{0}$ and $\mathbf{q}'_\mathbf{1}$ respectively, that is $\mathbf{q}'(t_1 : t_2; t_0, \mathbf{q}'_\mathbf{0})$ and $\mathbf{q}'(t_1 : t_2; t_0, \mathbf{q}'_\mathbf{1})$, for the same t_1, t_2 defined above.

If the solution trajectory for $\mathbf{q}'$ in Eq. 6.3 is causally stable $\forall\ \mathbf{q}'_\mathbf{0} \in D(t_0)$, where $D(t_0) \subseteq R^n$, then $D(t_0)$ is called the region of causal stability. If $D(t_0) = R^n$, then the solutions are said to be *globally causally stable*. The requirement on $D(t_0)$ is that any two initial conditions for the slave subsystem $\mathbf{q}'$ taken from this region yield solution trajectories which at some finite point in time ($\geq t_{tr}$) come close to each other for some chunk of time. Intuitively, causal stability implies that the net causal influence input to the non-driven subsystem $\mathbf{q}'$ from the driven subsystem $\mathbf{p}'$ is *invariant* to the change in the initial conditions of $\mathbf{q}'$.

We define synchronization as:

Definition 6.2 *Synchronization*: Let us take two systems $\dot{\mathbf{y}} = \mathbf{f}(t, \mathbf{y})$ and $\dot{\mathbf{y}'} = \mathbf{f}'(t, \mathbf{y}')$, where $\mathbf{y}, \mathbf{y}' \in R^n$. Let their solutions be given by $\mathbf{y}(t; t_0, \mathbf{y_0})$ and $\mathbf{y}'(t; t_0, \mathbf{y}'_\mathbf{0})$, re-

spectively. $\mathbf{f}(t, \mathbf{y})$ synchronizes with $\mathbf{f}'(t, \mathbf{y}')$ if there exists $D(t_0) \subseteq R^n$, such that $\mathbf{y_0}, \mathbf{y'_0} \in D(t_0)$ implies

$$\|\mathbf{y}(t; t_0, \mathbf{y_0}) - \mathbf{y}'(t; t_0, \mathbf{y'_0})\| \to 0 \text{ as } t \to \infty. \tag{6.7}$$

We state and prove the following theorem:

Causal Stability Synchronization Theorem: The slave system $(\mathbf{p}', \mathbf{q}')$ synchronizes with the master system $(\mathbf{p}, \mathbf{q})$ *iff* there exists $D(t_0) \subseteq R^n$ such that when the initial conditions of the non-driven part of the slave system $\dot{\mathbf{q}'} = \mathbf{g}(t, \mathbf{p}, \mathbf{q}')$ fall in $D(t_0)$, the solution trajectory of $\mathbf{q}'$ is causally stable.

Proof:

Sufficient Condition: If there exists a $D(t_0) \subseteq R^n$ such that when the initial conditions of the non-driven part of the slave system $\dot{\mathbf{q}'} = \mathbf{g}(t, \mathbf{p}, \mathbf{q}')$ fall in $D(t_0)$, the solution trajectory of $\mathbf{q}'$ is causally stable, then, by the definition of causal stability,

$$|CI_{net(\mathbf{p}'(\mathbf{p'_0}) \to \mathbf{q}'(\mathbf{q'_0}))} - CI_{net(\mathbf{p}'(\mathbf{p'_0}) \to \mathbf{q}'(\mathbf{q'_1}))}| < \epsilon, \tag{6.8}$$

where $\mathbf{q'_0}$ and $\mathbf{q'_1}$ are two arbitrary initial conditions in $D(t_0)$. Let us suppose the net difference in causal influence that the presence of a variable $\mathbf{p}'$ makes on the future of $\mathbf{q}'$ above and beyond the past trajectory of $\mathbf{q}'$ is computed using a measure C [1]. Since $CI_{\mathbf{q}'(\mathbf{q'_0}) \to \mathbf{p}'(\mathbf{p'_0})} = 0$ and $CI_{\mathbf{q}'(\mathbf{q'_1}) \to \mathbf{p}'(\mathbf{p'_0})} = 0$ (as $\mathbf{p}'$ is fixed, taken from the master and the coupling is unidirectional), Eq. 6.8 reduces to:

$$\begin{aligned} &C(\Delta\mathbf{q}'(\mathbf{q'_0})|\mathbf{q}'(\mathbf{q'_0})_{past}, \mathbf{p}'(\mathbf{p'_0})_{past}) - C(\Delta\mathbf{q}'(\mathbf{q'_0})|\mathbf{q}'(\mathbf{q'_0})_{past}) \\ \approx\ &C(\Delta\mathbf{q}'(\mathbf{q'_1})|\mathbf{q}'(\mathbf{q'_1})_{past}, \mathbf{p}'(\mathbf{p'_0})_{past}) - C(\Delta\mathbf{q}'(\mathbf{q'_1})|\mathbf{q}'(\mathbf{q'_1})_{past}) \end{aligned} \tag{6.9}$$

[1] C could be an infotheoretic quantity such as conditional entropy or could be a complexity measure.

where $\Delta\mathbf{q}'(\mathbf{q}'_\mathbf{0})$ and $\Delta\mathbf{q}'(\mathbf{q}'_\mathbf{1})$ are the current window of time series data from the system $\mathbf{q}'$ started from initial conditions $\mathbf{q}'_\mathbf{0}$ and $\mathbf{q}'_\mathbf{1}$ respectively. $\mathbf{q}'(\mathbf{q}'_\mathbf{0})_{past}$ and $\mathbf{q}'(\mathbf{q}'_\mathbf{1})_{past}$ represent the immediate past values of the window from the system $\mathbf{q}'$ started from initial conditions $\mathbf{q}'_\mathbf{0}$ and $\mathbf{q}'_\mathbf{1}$ respectively. $\mathbf{p}'(\mathbf{p}'_\mathbf{0})_{past}$ represent synchronous past values from the system $\mathbf{p}'$ started from initial condition $\mathbf{p}'_\mathbf{0}$.

If the system $\mathbf{q}'$ is started from two nearby initial conditions, then their initial solution trajectories will be similar as the influence from the fixed master $\mathbf{p}(\mathbf{p_0})$ (= $\mathbf{p}'(\mathbf{p}'_\mathbf{0})$) time series has not yet come into play. Even if the initial conditions are far away, then the condition on $D(t_0)$ would require the trajectories to come close to each other for a chunk of time starting at some finite time t_s. Then, for this chunk of time, the trajectories are close to each other and hence:

$$C(\mathbf{q}'(\mathbf{q}'_\mathbf{0})_{past})_{t_s} = C(\mathbf{q}'(\mathbf{q}'_\mathbf{1})_{past})_{t_s}. \tag{6.10}$$

Also,

$$C(\Delta\mathbf{q}'(\mathbf{q}'_\mathbf{0})|\mathbf{q}'(\mathbf{q}'_\mathbf{0})_{past})_{t_s} = C(\Delta\mathbf{q}'(\mathbf{q}'_\mathbf{1})|\mathbf{q}'(\mathbf{q}'_\mathbf{1})_{past})_{t_s}. \tag{6.11}$$

The reason for the above two equalities for measure C is that it is computed using coarse grained time series (symbolic sequences) or k-nearest neighbor estimation techniques, rendering the measure to become equal for two close by trajectories. Eqs. 6.10 and 6.11 hold at time t_s and Eq. 6.9 (and 6.8) hold for all $t \geq t_s$. So, Eq. 6.9 is true at $t_1 = t_s + \Delta t$ where Δt is an arbitrary increment in time. For this to be true, conditions 6.10 and 6.11 need to also hold at t_1, because in order to maintain 6.8 for every small time step increment Δt starting at t_s, the measure C for the solution trajectories started at two

different initial conditions cannot drastically change, nor can the influence in each case from its own past to future. Also, the only drivers of system $\mathbf{q}'$, or specifically the contributors to the evolution of $\Delta\mathbf{q}'$ are the past of $\mathbf{q}'$ itself and the forced variable $\mathbf{p}'$ (which is fixed across different initial conditions of $\mathbf{q}'$). Since the measure C for the solution trajectories $\mathbf{q}'(\mathbf{q_0'})$ and $\mathbf{q}'(\mathbf{q_1'})$ is equal as well as the influence they bring to their future, these solution trajectories have been forced not to diverge but to converge as they were similar at t_s and need to maintain these conditions at t_1. Thus,

$$\|\mathbf{q}'(t, \mathbf{p}; t_0, \mathbf{p_0}, \mathbf{q_0'}) - \mathbf{q}'(t, \mathbf{p}; t_0, \mathbf{p_0}, \mathbf{q_1'})\| \to 0 \text{ as } t \to \infty. \tag{6.12}$$

Necessary Condition: If there exists a $D(t_0) \subseteq R^n$ such that when the initial conditions of the non-driven part of the slave system $\dot{\mathbf{q}}' = \mathbf{g}(t, \mathbf{p}, \mathbf{q}')$ fall in $D(t_0)$, the master and slave systems are synchronized. Suppose the master starts from initial condition $\mathbf{q_m}$ and $\mathbf{q_0'}$ and $\mathbf{q_1'}$ are two arbitrary initial conditions taken for the slave in the set $D(t_0)$. Then, by the definition of synchronization stated above,

$$\|\mathbf{q}'(t, \mathbf{p}; t_0, \mathbf{p_0}, \mathbf{q_0'}) - \mathbf{q}(t, \mathbf{p}; t_0, \mathbf{p_0}, \mathbf{q_m})\| \to 0, t \to \infty, \tag{6.13}$$

$$\|\mathbf{q}'(t, \mathbf{p}; t_0, \mathbf{p_0}, \mathbf{q_1'}) - \mathbf{q}(t, \mathbf{p}; t_0, \mathbf{p_0}, \mathbf{q_m})\| \to 0, t \to \infty. \tag{6.14}$$

Using Eqs. 6.13 and 6.14,

$$\|\mathbf{q}'(t, \mathbf{p}; t_0, \mathbf{p_0}, \mathbf{q_0'}) - \mathbf{q}'(t, \mathbf{p}; t_0, \mathbf{p_0}, \mathbf{q_1'})\| \to 0, t \to \infty. \tag{6.15}$$

Because of the uniqueness of solutions,

$$\mathbf{q}'(t, \mathbf{p}; t_0, \mathbf{p_0}, \mathbf{q_0'}) = \mathbf{q}'(t, \mathbf{p}; t_0, \mathbf{p_0}, \mathbf{q_1'}). \tag{6.16}$$

So, CI_{net} estimated from a fixed time series (for solution trajectory starting at any time t) to the two identical time series of system $\mathbf{q}'$ will be equal. Hence,

$$|CI_{net(\mathbf{p}'(\mathbf{p}'_0)\rightarrow\mathbf{q}'(\mathbf{q}'_0))} - CI_{net(\mathbf{p}'(\mathbf{p}'_0)\rightarrow\mathbf{q}'(\mathbf{q}'_1))}| = 0, \tag{6.17}$$

which implies causal stability of $\mathbf{q}'$. □

The above theorem is proved for the case of complete synchronization of identical master and slave systems with a subsystem of the slave being forced by the master. If the systems are non-identical but still a subsystem of the slave is forced and the systems undergo complete synchronization, we expect the theorem to be valid as all of its steps would still hold. Complete (identical) synchronization has been shown to hold for some configured networks of non-identical systems [142, 143]. A generalized version of this theorem may be applicable in such networks.

Empirical Study

The difference of CI_{net} to the non-driven subsystem of slave for two different initial conditions approaches zero when the system is led to synchronization and not otherwise, is demonstrated for the Lorenz system in Figure 6.1(b), whose simulation and CI_{net} estimation details are given below. CI_{net} is estimated using the CCC measure. CCC happened to be the most appropriate choice as it is a model-free measure of causality applicable for non-linear time series and has been tested on several real-world like scenario simulations as well as real world datasets (see Chapter 3 and Chapter 4). Moreover, for our purpose we need a measure, using which, causal influence can be

estimated over short lengths of windows taken from time series data. Info-theoretic measures based on probability density estimates do not perform very well in this regard. Furthermore, CCC is an interventional data-based causality measure based on dynamical evolution of processes and is not merely based on associational relations. In this regard, it is more faithful to the underlying mechanism generating the data. Lorenz system was simulated using Euler's method as per the following equations:

$$\dot{x} = \sigma(y - x), \dot{y} = x(\rho - z) - y, \dot{z} = xy - \beta z, \tag{6.18}$$

where, $\sigma = 10$, $\rho = 60$ and $\beta = 8/3$.

For any given system, CCC_{net} from one of its subsystems, say $\mathbf{p}$, to another subsystem, $\mathbf{q}$, can be estimated as:

$$CCC_{net(\mathbf{p}\to\mathbf{q})} = CCC_{\mathbf{p}\to\mathbf{q}} - CCC_{\mathbf{q}\to\mathbf{p}}. \tag{6.19}$$

For the Lorenz system, we take the example of simulated time series and describe the steps for computation of CCC_{net} from subsystem comprising of variable z to subsystem comprising of variables (x, y), that is,

$$CCC_{net(z\to x,y)} = CCC_{z\to x|y} + CCC_{z\to y|x} - CCC_{x\to z|y} - CCC_{y\to z|x}, \tag{6.20}$$

where $CCC_{a\to b|c}$ is the conditional CCC from a to b given time series c.

The steps are as below:

1. Simulate Lorenz system (x, y, z) as per equation 6.18 for 10,000 time points starting with random initial conditions (x_0, y_0, z_0). Remove the first 2000 transients to estimate CCC values from the next 8000 time points.

2. Set the parameters w, δ, B and L in accordance with parameter selection criteria as discussed in Section 3.3. The parameters selected for Lorenz are $L = 150$, $w = 15$, $\delta = 80$, $B = 8$.

3. Estimate conditional CCC values from the variable (z) to all other variables in the presence of the third variable ($CCC_{z\to x|y}$, $CCC_{z\to y|x}$) and also from all other variables to z ($CCC_{x\to z|y}$, $CCC_{y\to z|x}$). These values estimated are shown in the third column and third row respectively of Table 6.1(a). For computation of conditional CCC values, check details in Section 2.3. The code for conditional CCC estimation is available as a part of supplementary material of [144].

4. To estimate $CCC_{net(z\to x,y)}$, use equation 6.20. The value estimated for this is 0.0509 as shown in Table 6.1(a).

Master Lorenz (x, y, z) was simulated starting from initial conditions $(x_m, y_m, z_m) = (3, 4, 6)$. For the slaves' dynamics (x', y', z'), one of the variables was forced to be the same as the master – either $x = x'$ or $y = y'$ or $z = z'$. We fix one of the slaves S_0 to start with initial conditions: $(x'_0, y'_0, z'_0) = (7, 1, 6)$. The second slave $S_{k,\delta}$ was started within a sphere of radius $\delta\sqrt{3}$ from the first slave, its initial conditions are given by $(x'_{k,\delta}, y'_{k,\delta}, z'_{k,\delta}) = (x_0 + k_1\delta, y_0 + k_2\delta, z_0 + k_3\delta)$, where k_1, k_2, k_3 are independently chosen uniformly at random from the set $(-1, 1)$. As an example, for z-forcing in Lorenz system, the master and two slave attractors as well as their initial condition are depicted in Figure 6.1(a). 10,000 time points were simulated for both the master and the slave after removal of 2000 samples (transients). For three different settings of δ (

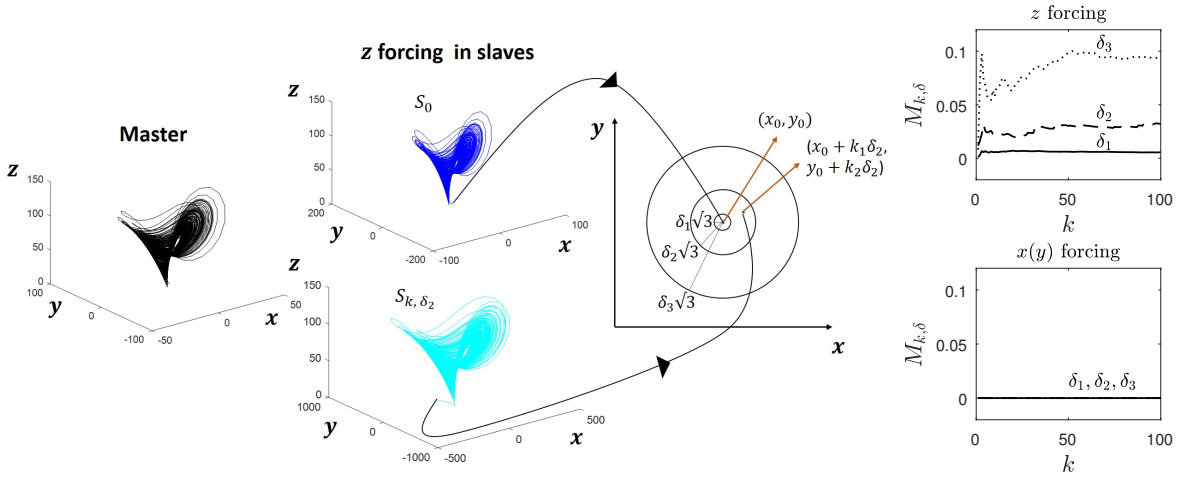

(a) (b)

Figure 6.1: (a) Master Lorenz attractor (leftmost). Slave Lorenz S_0 with forced z variable and fixed initial conditions (x_0, y_0) for x and y (middle, top). Slave Lorenz S_{k,δ_2} with forced z variable and initial conditions $(x_0 + k_1\delta_2, y_0 + k_2\delta_2)$ in a $\delta_2\sqrt{3}$ radius disc around (x_0, y_0) (middle, bottom). (b) Mean of absolute CCC_{net} differences, $M_{k,\delta}$, between a fixed slave Lorenz S_0 and secondary slave Lorenz $S_{k,\delta}$ for $k = 1, 2, \ldots, 100$ within a $\delta\sqrt{3}$ radius of S_0; $\delta_1 = 1$ (solid line), $\delta_2 = 10$ (dashed line) and $\delta_3 = 100$ (dotted line). Causal Stability satisfied for x and y forcing but not for z forcing.

$\delta_1 = 1, \delta_2 = 10, \delta_3 = 100$), we simulate several *secondary* slaves $S_{k,\delta}$ $(k = 1, 2, \ldots, 100)$. For increasing k, we estimate and plot the mean of the absolute differences in the CCC_{net} values between S_0 and secondary slaves in Figure 6.1(b). The mean is given by the following expression:

$$M_{k,\delta} = \frac{1}{k}\sum_{i=1}^{k} |CCC_{net}(S_0) - CCC_{net}(S_{i,\delta})|, \tag{6.21}$$

where

$$\begin{aligned} CCC_{net}(S_0) &= CCC_{net(z'(z_m)\to(x'(x'_0),y'(y'_0)))}, \\ CCC_{net}(S_{i,\delta}) &= CCC_{net(z'(z_m)\to(x'(x'_{k,\delta}),y'(y'_{k,\delta})))}, \end{aligned} \tag{6.22}$$

when z is forced $(z = z')$. The above analysis is done independently for x and y forcing

as well.

We see that since x and y forcing lead to synchronization of the slaves with the master, the difference in the CCC_{net} values turns out to be zero for any slave chosen from either of the discs. On the other hand, since z forcing does not lead to synchronization, mean CCC_{net} difference is non-zero and increases with increase in δ. From Figure 6.1(b), we infer that z forcing results in a *causally unstable* non-driven slave subsystem whereas x (or y) forcing leads to a *causally stable* non-driven slave subsystem. This successfully validates *causal stability synchronization theorem* for the Lorenz system.

While Eq. 6.8 is proven to be the necessary and sufficient condition for complete synchronization for identically coupled dynamical systems, we expect similar conditions to be derived for other forms of synchronization such as generalized synchronization.

6.2.2 Synchronizing Variables

As per the *causal stability synchronization theorem*, if the net input causal influence to the non-driven subsystem is invariant with change in initial conditions, those initial conditions are led to synchronize with the master. The net input causal influence to the non-driven subsystem happens to be the net output causal influence from the driven subsystem to the non-driven part. It can be said that, this particular influence is responsible for synchronization. For a slave which is synchronized with the master, the net causal influence from the driven to non-driven subsystem in the master and slave remains the same. It should be possible then to decide on the basis of the *nature*

of intra-system causal influences within the master, coupling of which variables may lead to synchronization. We term these as *synchronizing variables*. Given a network of several coupled dynamical systems, based on the time series of the driver system alone, the *causality* perspective that we have proposed in this paper, can resolve an important question – *what specific properties do synchronizing variables exhibit?* This kind of analysis can be very useful for networks where we wish to control chaos by adjusting magnitude and direction of coupling between systems as well as the selection of coupling variables.

To address this important question, we use the *sign of CCC* measure, since it gives information on the 'kind of dynamical causal influence' which the *cause* variable has on the *effect* variable. If the kind of dynamical influence from a variable x to another variable y is different from the past of y to itself, then $CCC_{x\to y} < 0$. On the other hand, if the kind of dynamical influence from a variable x to another variable y is similar to that from the past of y to itself, then $CCC_{x\to y} > 0$. This is true also for conditional causality estimation when more than two variables are there in the system. For further details on negative CCC please refer to Section 2.4.

While there can be various mechanisms for coupling dynamical systems to study chaotic synchronization, we consider the simplest case where forcing a particular variable in the slave system to become identical to that of the master system, may result in complete synchronization for all the variables. The slave and master are taken to be identical systems apart from their initial conditions for all the cases taken here. It is expected that the conditions (described below) will hold for subsystem forcing even in

a non-identical slave which is capable of being led to complete synchronization.

Lorenz system was simulated as per Eq. 6.18 with the same parameters as before. Other continuous-time dynamical systems simulated include – Rössler, Chen, Hindmarsh-Rose neuron model and a 5D system in the chaotic regime as well as the discrete time 2D Hénon map. Equations and parameters used for the simulation of these systems are as given below:

Rössler:

$$\begin{aligned} \frac{dx}{dt} &= -y - z \\ \frac{dy}{dt} &= x + ay \\ \frac{dz}{dt} &= b + z(x - c), \end{aligned} \tag{6.23}$$

where $a = 0.2$, $b = 0.2$ and $c = 9$.

Chen:

$$\begin{aligned} \frac{dx}{dt} &= a(y - x) \\ \frac{dy}{dt} &= (c - a)x - xz + cy \\ \frac{dz}{dt} &= xy - bz, \end{aligned} \tag{6.24}$$

where $a = 35$, $b = 3$, $c = 28$.

Hindmarsh-Rose:

$$\begin{aligned} \frac{dx}{dt} &= y - ax^3 + bx^2 - z + I \\ \frac{dy}{dt} &= c - dx^2 - y \\ \frac{dz}{dt} &= r(s(x - x_R) - z), \end{aligned} \tag{6.25}$$

where $a = 1$, $b = 3$, $c = 1$, $d = 5$, $s = 4$, $x_R = -8/5$, $r = 0.006$, $I = 3$.

5D system:

$$\begin{aligned}
\frac{\mathrm{d}x}{\mathrm{d}t} &= \sigma(y - x) + w, \\
\frac{\mathrm{d}y}{\mathrm{d}t} &= x(\rho - z) - y, \\
\frac{\mathrm{d}z}{\mathrm{d}t} &= xy - \beta z, \\
\frac{\mathrm{d}q}{\mathrm{d}t} &= -q^3 + w, \\
\frac{\mathrm{d}w}{\mathrm{d}t} &= -x - q - 8w.
\end{aligned} \tag{6.26}$$

where, $\sigma = 10$, $\rho = 60$ and $\beta = 8/3$.

Though the causal stability synchronization theorem is proved for continuous time systems, the sign of CCC values was analyzed to identify synchronizing variables even for discrete time systems. It has been shown earlier that when two one-dimensional Tent map systems are coupled, we get negative CCC from the independent map to the dependent map, showing that the kind of causal influence from the past of the independent map is different than influence from the dependent map's own past (Section 2.4). In order to identify synchronizing variables for discrete time systems using intra-system CCC values, we simulated the well-known 2D Hénon map in the chaotic regime,

Hénon:

$$\begin{aligned}
x_{n+1} &= 1 - ax_n^2 + y_n \\
y_{n+1} &= bx_n,
\end{aligned} \tag{6.27}$$

where, $a = 1.4$, $b = 0.3$ and n stands for discrete time.

For the above systems, intra-system conditional CCC values as well as CCC_{net} values from each variable are given in Table 6.1. For all the systems including Lorenz, 8000 time points of time series data were taken for CCC estimation after removal of

2000 transients [2]. The parameters used in the computation of CCC in case of Lorenz are $L = 150$, $w = 15$, $\delta = 80$, $B = 8$, in case of Rössler are $L = 300$, $w = 15$, $\delta = 200$, $B = 8$, in case of 5D system are $L = 450$, $w = 80$, $\delta = 300$, $B = 4$ and in case of Chen, Hindmarsh-Rose and Hénon are $L = 100$, $w = 15$, $\delta = 80$, $B = 8$. These parameters were selected on the basis of parameter selection criteria and rationale given in Section 3.3. Table 6.2 indicates which variables when forced lead to complete synchronization.

The CCC_{net} values from each variable to its subsystem for all the systems are summarized in Table 6.3. For the synchronizing variables, the CCC_{net} values are in bold font.

From Table 6.3 we formulate the following conditions:

- **Condition I**: A variable with $CCC_{net} > 0$ *never* leads to synchronizaton.
- **Condition II**: A synchronizing variable should always have its $CCC_{net} < 0$.
- **Condition III**: In most cases, a variable with the *least* CCC_{net} (and < 0) among all the variables in the system is a synchronizing variable.

We have an intuitive understanding for why Conditions I and II need to be true. The synchronizing variables influence their corresponding non-driven subsystems with $CCC_{net} < 0$ bringing a dynamical influence on the subsystem which is different from its own past. This kind of an influence constrains the subsystem of the slave to not

[2]While Lorenz was simulated using Euler's method, Rössler, Chen, Hindmarsh-Rose and the 5D system were simulated using the Runge Kutta fourth order method.

follow its own past dynamics and is thus driven by the forced variable towards complete synchronization. On the contrary, variable(s) with $CCC_{net} > 0$ are unable to constrain their subsystem(s) adequately to alter their dynamics towards complete synchronization

Table 6.1: Conditional CCC values estimated between variables of (a) Lorenz, (b) Rössler, (c) Chen, (d) Hindmarsh-Rose, (e) 5D continuous-time system, (f) Hénon and corresponding CCC_{net} values from each variable to its subsystem.

(a) Lorenz

To \ From	x	y	z
x	0	-0.0270	0.0390
y	-0.0250	0	0.0330
z	0.0251	-0.0040	0
CCC_{net}	**-0.0119**	**-0.0390**	**0.0509**

(b) Rössler

To \ From	x	y	z
x	0	0.0412	0.0730
y	0.0345	0	0.0724
z	0.0337	0.0288	0
CCC_{net}	**-0.0460**	**-0.0369**	**0.0829**

(c) Chen

To \ From	x	y	z
x	0	-0.0388	0.0769
y	-0.0271	0	0.0814
z	0.0299	0.0311	0
CCC_{net}	**-0.0353**	**-0.0620**	**0.0973**

Table 6.1: Contd.

(d) Hindmarsh-Rose

To \ From	x	y	z
x	0	0.0177	0.0716
y	0.0168	0	0.0763
z	0.0359	0.0720	0
CCC_{net}	**-0.0366**	**-0.0034**	**0.0400**

(e) 5D continuous-time system

To \ From	x	y	z	q	w
x	0	-0.0275	0.0163	0.0326	0.0287
y	-0.0160	0	0.0170	0.0356	0.0318
z	0.0090	-0.0021	0	0.0406	0.0413
q	0.0020	0.0009	0.0296	0	-0.0001
w	-0.0018	-0.0069	0.0291	0.0098	0
CCC_{net}	**-0.0570**	**-0.1039**	**0.0032**	**0.0861**	**0.0715**

(f) Hénon

To \ From	x	y
x	0	-0.0273
y	-0.0600	0
CCC_{net}	**-0.0600**	**-0.0273**

(Condition I). A variable with $CCC_{net} < 0$ (satisfies Condition II) but not the least (fails Condition III) *may* or *may not* lead to complete synchronization. For instance, in case of Lorenz and the 5D system, the x variable leads to synchronization while in Chen, x and in Hénon, y do not lead to synchronization. The exact reason(s)

Table 6.2: Indication of synchronizing variables for different dynamical systems. ✓implies the variable is synchronizing and ✗implies the variable is not synchronizing.

System \ Variable	x	y	z	q	w
Lorenz	✓	✓	✗	-	-
Rössler	✗	✓	✗	-	-
Chen	✗	✓	✗	-	-
Hindmarsh-Rose	✓	✓	✗	-	-
5D system	✓	✓	✗	✗	✗
Hénon	✓	✗	-	-	-

Table 6.3: CCC_{net} value from each variable to its subsystem for all the systems simulated (bold values correspond to synchronizing variables).

System \ CCC_{net}	x	y	z	q	w
Lorenz	**-0.0119**	**-0.0390**	0.0509	-	-
Rössler	-0.0460	**-0.0369**	0.0829	-	-
Chen	-0.0353	**-0.0620**	0.0973	-	-
Hindmarsh-Rose	**-0.0366**	**-0.0034**	0.0400	-	-
5D system	**-0.0570**	**-0.1039**	0.0032	0.0861	0.0715
Hénon	**-0.0600**	-0.0273	-	-	-

for this are still unclear and require further investigation. Condition I is a sufficient condition for non-synchronizing variable. Condition II is necessary but not sufficient for synchronizing variable whereas Condition III is a sufficient condition in most cases. One of the reasons why the variable with the least negative CCC_{net} value doesn't lead to synchronization for Rössler (Condition III is insufficient only for this system) could

be due to the nature of its equations. The variable x which has the least and negative CCC_{net} does not directly depend on itself but on the other two variables. This is not the case for synchronizing variables in any other system that we have considered. It is possible that the high negativity of CCC_{net} influence from x on the subsystem y, z is in fact due to y, the only other variable which has a negative CCC_{net}. Not surprisingly, it is found that y leads to synchronization and not x.

Visualizing Synchronizing Variables

Inspired by the notion of order parameters of the Kuramoto model [145,146], we propose a novel CCC_{net} order parameter as follows. For a D-dimensional non-linear dynamical system ($D > 1$), we define:

$$V_i = \{1, 2, \ldots, i-1, i+1, \ldots, D\}, \tag{6.28}$$

$$r = \sqrt{\sum_{i=1}^{D} CCC^2_{net(i \to V_i)}} \quad , \tag{6.29}$$

$$\theta_i = \sin^{-1}\left(\frac{CCC_{net(i \to V_i)}}{r}\right), \quad i = 1, \ldots, D. \tag{6.30}$$

The CCC_{net} order parameters $\eta_i = (r, \theta_i)$, $(i = 1, \ldots, D)$ are illustrated for a general system in Figure 6.2 (left). Corresponding to each variable, we plot a ball at (r, θ_i) (in polar co-ordinates). Based on this convention, balls will only be in the first or in the fourth quadrant. Balls in the first quadrant are non-synchronizing variables (marked in color Red) corresponding to $\theta > 0$ (or $CCC_{net} > 0$). Balls in the fourth quadrant corresponding to $\theta < 0$ (or $CCC_{net} < 0$) are of two types - Yellow and Green. The Green ball corresponds to that variable (if it exists) which has the *least* θ (CCC_{net}) and $\theta < 0$

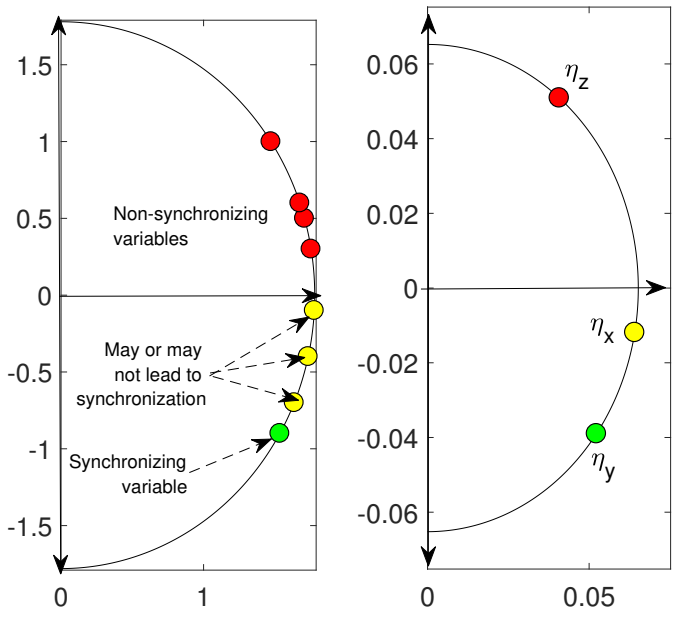

Figure 6.2: Plot of CCC_{net} order parameter $\eta_i = (r, \theta_i)$ for a general system (left). Red indicates non-synchronizing variable, Green indicates synchronizing variable and Yellow indicates a variable which may or may not synchronize. In case of Lorenz (right), $r = 0.0652$, $\theta_x = -0.1835$, $\theta_y = -0.6410$ and $\theta_z = 0.8954$. x and y are synchronizing variables. All angles in radians.

($CCC_{net} < 0$). This is always a synchronizing variable (except in the case of Rössler). The Yellow balls (if they exist) correspond to variables for which $\theta < 0$ ($CCC_{net} < 0$), but may or may not lead to synchronization. For the Lorenz system in Figure 6.2 (right), $\eta_1 = \eta_x = (r, \theta_x) = (0.0652, -0.1835)$, $\eta_2 = \eta_y = (r, \theta_y) = (0.0652, -0.6410)$ and $\eta_3 = \eta_z = (r, \theta_z) = (0.0652, 0.8954)$. In the case of Lorenz, we have one each ball of Red, Yellow and Green color. Both the Yellow and the Green balls correspond to synchronizing variables for Lorenz. The plots for other dynamical systems are depicted in Figure 6.3. The order parameter for *Rössler* is depicted separately in Figure 6.4. Red, Yellow and Green correspond to Conditions I, II and III respectively.

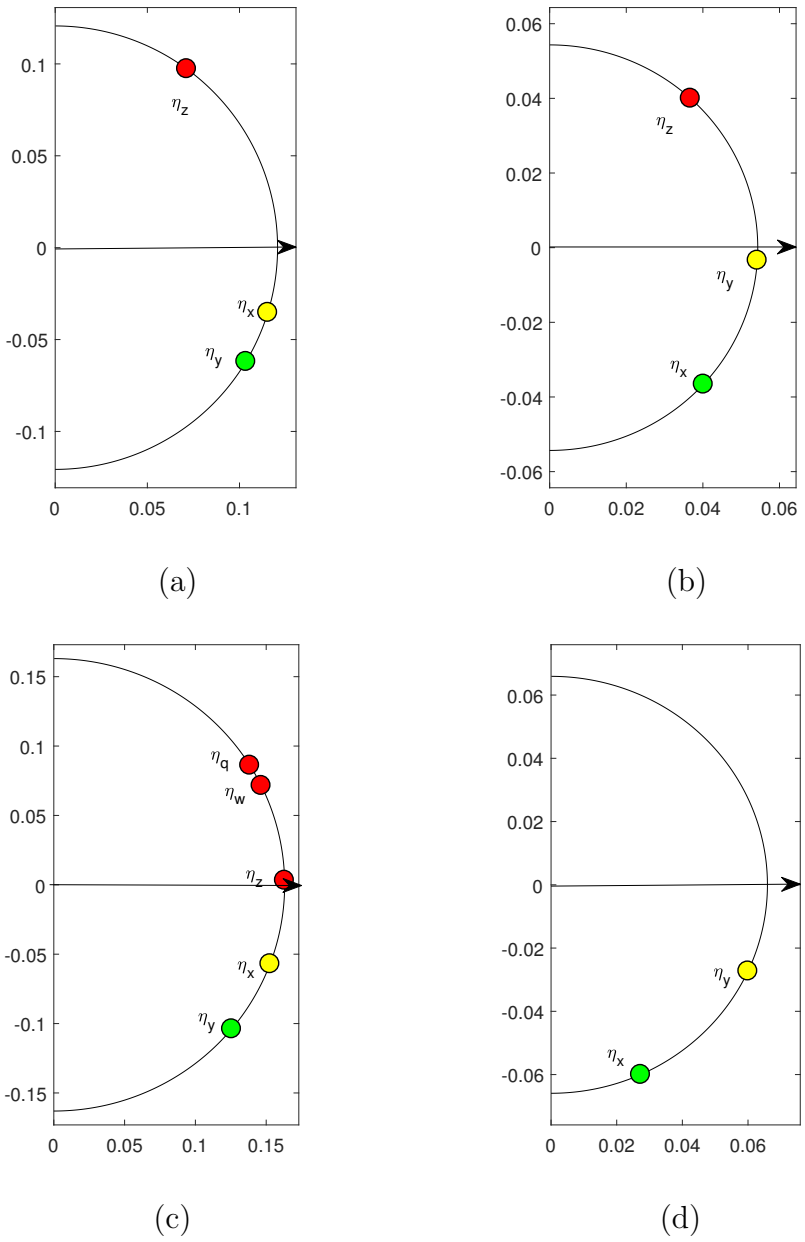

Figure 6.3: Plot of CCC_{net} order parameter $\eta_i = (r, \theta_i)$ for (a) *Chen*: $r = 0.1207$, $\theta_x = -0.2969$, $\theta_y = -0.5397$ and $\theta_z = 0.9381$, (b) *Hindmarsh-Rose*: $r = 0.0543$, $\theta_x = -0.7392$, $\theta_y = -0.0626$ and $\theta_z = 0.8276$, (c) *5D system*: $r = 0.1630$, $\theta_x = -0.3572$, $\theta_y = -0.6909$, $\theta_z = 0.0196$, $\theta_q = 0.5564$ and $\theta_w = 0.4539$, and (d)*Hénon*: $r = 0.0659$, $\theta_x = -1.1438$ and $\theta_y = -0.4270$. All angles in radians. Red indicates non-synchronizing variable, Green indicates synchronizing variable and Yellow indicates a variable which may or may not synchronize.

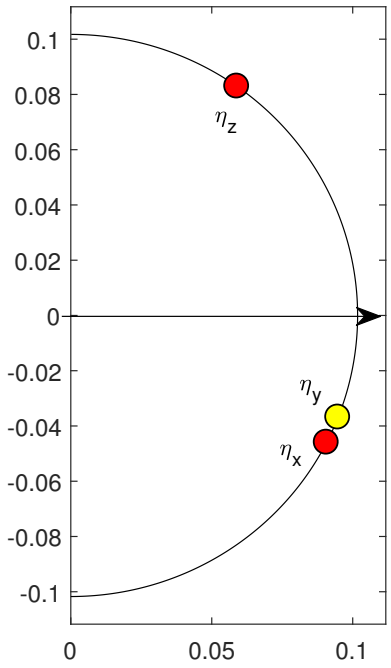

Figure 6.4: Plot of CCC_{net} order parameter $\eta_i = (r, \theta_i)$ for *Rössler*: $r = 0.1017$, $\theta_x = -0.4692$, $\theta_y = -0.3712$ and $\theta_z = 0.9525$. All angles in radians. Red indicates non-synchronizing variable, Green indicates synchronizing variable and Yellow indicates a variable which may or may not synchronize. *Rössler* being an exception, though θ_x is least and negative, x is non-synchronizing.

6.2.3 Conclusions and Future Work

In this section, we have introduced the novel concept of *causal stability* and proved the *causal stability synchronization theorem* as a necessary and sufficient condition for synchronization in chaotic continuous-time dynamical systems. The link between asymptotic stability and synchronization was proved in [69] with negative lyapunov exponents of the subsystem being its empirical condition [68]. In contrast, ergodicity of dynamical processes has allowed us to formulate an equivalent spatial condition, and along with it provide an empirical condition based on the sign of CCC_{net} for identification

of synchronizing variables. Along with other systems, the empirical condition has been verified for the Hindmarsh-Rose neuronal model. This is an important contribution for the control of chaos in networks where we do not know the underlying mechanism and wish to inhibit/facilitate synchronization between systems. Regulation of synchronization is of importance with regard to the brain as abnormal synchrony between regions can indicate various disorders. The proposed conditions have the potential to be useful here.

Future research would involve studying several other homogeneous and heterogeneous dynamical systems (both continuous and discrete-time systems) coupled in different ways to analyze the sign of their CCC_{net} values and to generalize the proposed theorem for other forms of synchronization, such as phase and generalized synchronization. Properties of the CCC_{net} order parameters $\{\eta_i\}_{i=1}^{D}$ as well as its relation to conditional lyapunov exponents needs to be further explored.

6.3 Causality Detection for Anticipating Synchronization

Anticipating Synchronization (AS) is a counterintuitive case of synchronization in which the temporal trajectory of the slave system becomes ahead of the master system in phase and 'anticipates' the dynamics of the latter. This phenomena was discovered by Voss [147]. AS has been shown to be stable in a variety of systems, theoretical as well as experimental including semiconductor lasers, electronic circuits etc. [148–154]. AS in neuronal models was first found by Ciszak et al. [151]. Now, there are several studies

which talk about AS in neuronal models [155–157] and evidences of its presence in the brain [158].

As for other forms of synchronization, causal measures are being employed to detect the correct direction of coupling in AS systems. This is obviously a much more difficult task, because causality measures work on time series data and the temporal nature of events in slave and master dynamics seem deceiving in case of AS. Some existing cauality measures that have been employed for this problem include GC [158] and TE [159]. Other causality inspired approaches, such as the Complexity-Causality plane have been proposed to quantify the 'relative synchronization phase' between the master and slave systems [160]. Further, the use of these measures is also being translated to confirm the presence of AS in real world systems [158].

In this section, we draw attention towards some issues in implementing and relying on just any available causality measure for detection of coupling direction in the challenging case of anticipating synchronization. It is shown for the case of a simulated system with anticipation that GC fails in correct causality estimation. Further, we also test if the proposed measure CCC can be used to detect the correct coupling direction in this case.

6.3.1 Failure of Granger Causality for estimation of causality in AS

After the pioneering work of Ciszak et al. [151], that showed AS in unidirectionally coupled neuronal models (Fitzugh Nagumo and a modified version of Hodgekin-Huxley),

many neuronal models with AS have been proposed [155–157]. The model proposed by [155] is more realistic and biologically plausible.

However, research did not proceed in this direction only. Inferences were made regarding presence of AS in real brain data based on use of causality measures. Real neuronal data, more specifically, local field potentials, captured from sensorimotor cortex of macaque monkeys were analyzed using spctral GC for the understanding of functional connectivity [118]. During the acquisition, the monkeys maintained a steady motor output while pressing a hand lever in a visual discrimination task. By means of spectral GC, directed causality strengths for different frequencies present in the acquired signals, as well as the phase lag between the considered cortical regions were computed.

Based on the analysis, it was seen that there was a discrepancy between the direction of causality and the phase lag between some of the considered brain regions. For example, for areas B_1 and B_2, if higher causal strength was found in the direction from B_1 to B_2, it wasn't necessarily the case that B_2 lagged behind B_1, in terms of its phase (or time delay). Along with this study, similar discordant results were reported in the study by Salazar et al. [161], where phase difference and GC were estimated between Posterior Parietal Cortex and Prefrontal Cortex in monkeys performing a working memory task. Here, dominant GC from parietal to frontal area seemed to be against the time lead of the frontal area.

To explain the above evidence of dominant causality between cortical regions being in one direction while phase indicating that the caused cortical region leads in time the

causal region, Matias et al. [158] came up with the model of coupled brain regions that displays the same properties as observed for real cases above. This model has been inspired from the phenomenon of AS in dynamical systems. With this, they suggest that primate cortex could be operating in the regime of AS when involved in certain cognitive tasks.

It is interesting to see that based on a measure like GC, such extreme suggestions such as that of AS in the brain are being made. GC has actually been developed for causality estimation for data when modelled as linear autoregressive processes. This does not mean that any other nonlinear processes cannot be modelled this way – for the class of covariance-stationary processes, we should be able to find vector autoregressive models that generically model the processes [31, 32]. However, the chosen model and hence causality value may not be reliable due to multiple reasons such as finite data length, several sources of noise in the acquired data, or the fact that the data does not fit into the domain of covariance stationary processes. We have shown the limitations of GC for some simulated systems in Chapter 3.

To demonstrate the performance of GC for a system with AS, a system of tent maps were generated as per the following equations. The master system $Y : [0, 1] \to [0, 1]$ is given as:

$$\begin{aligned} Y(t) &= f(Y(t-1)), \quad \text{where} \\ f(y) &= 2y, \qquad 0 \leq y < 1/2, \\ f(y) &= 2 - 2y, \qquad 1/2 \leq y \leq 1. \end{aligned} \tag{6.31}$$

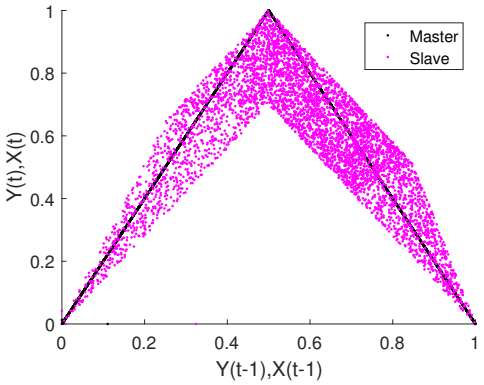

Figure 6.5: First return map of coupled master (Y) and slave (X) tent maps in anticipating synchronization configuration.

The slave system $X : [0, 1] \rightarrow [0, 1]$ is given as:

$$\begin{aligned} X(t) &= (1-\epsilon)f(X(t-1)) + \epsilon g(Y(t-1)), \quad \text{where} \\ g(y) &= (1-\alpha)f(y) + \alpha f^2(y), \end{aligned} \tag{6.32}$$

where, t represents discrete time, ϵ ($0 \leq \epsilon \leq 1$) is the degree of coupling and α ($0 \leq \alpha \leq 1$) is the anticipation parameter. The first return map of the master (Y) and the slave (X) is depicted in Figure 6.5. The figure has been plotted taking 5000 time points (after removal of 1000 transients) from the simulated system with ϵ set to 0.3 and α set to 1. The system was started with random initial conditions.

Spectral GC values from master to slave and vice versa at different frequencies as well as the amount of time lag (relative phase) of the slave from the master are plotted for three different levels of anticipation. MVGC toolbox with maximum order of the process set to 20 and all other settings in default mode was used for this computation. Figures 6.6, 6.7 and 6.8 correspond to α values 0 (no anticipation), 0.5 (moderate anticipation) and 1 (high anticipation) respectively. In these figures, process 1 denotes the simulated master (Y) and process 2 denotes the slave (X). Though the above

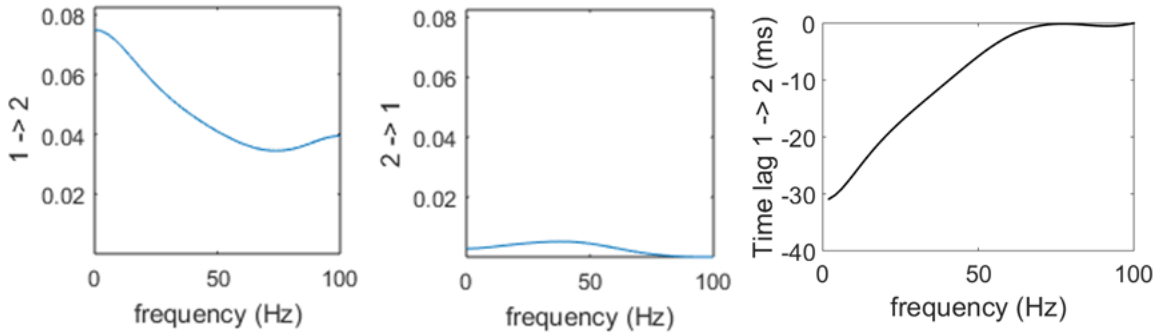

Figure 6.6: Spectral Granger Causality and phase lag between processes 1 (simulated master, Y) and 2 (simulated slave, X) with anticipation parameter, $\alpha = 0$. Causality is estimated correctly while lag is estimated incorrectly.

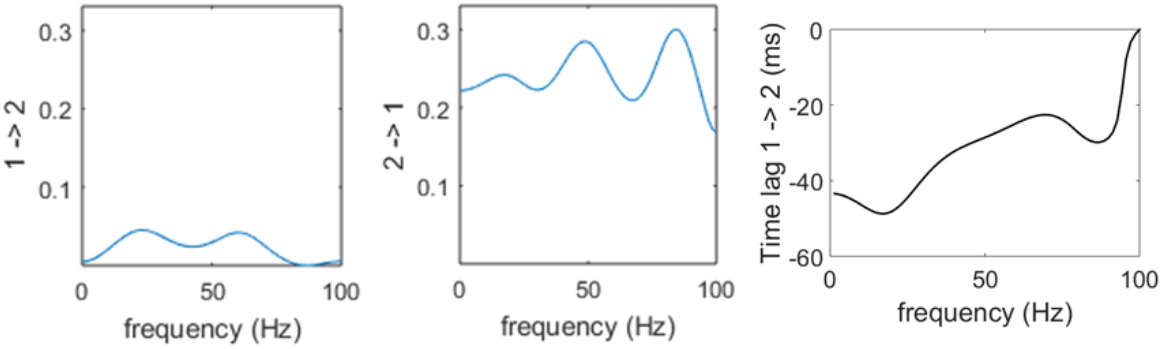

Figure 6.7: Spectral Granger Causality and phase lag between processes 1 (simulated master, Y) and 2 (simulated slave, X) with anticipation parameter, $\alpha = 0.5$. Causality is estimated incorrectly while lag is estimated correctly.

reported results are for a single trial each of 5000 time points, the results were found to be very similar even when 100 trials were taken.

It can be seen from Figure 6.6 that spectral GC identifies the correct direction of causality between Y (process 1) and X (process 2) when there is no anticipation in the coupled system. For this case, however, the time delay of 2 from 1 is negative, indicating that 2 is ahead of 1. This is incorrect as there is no anticipation in this case. When anticipation is increased and set at moderate level ($\alpha = 0.5$), Figure 6.7 indicates

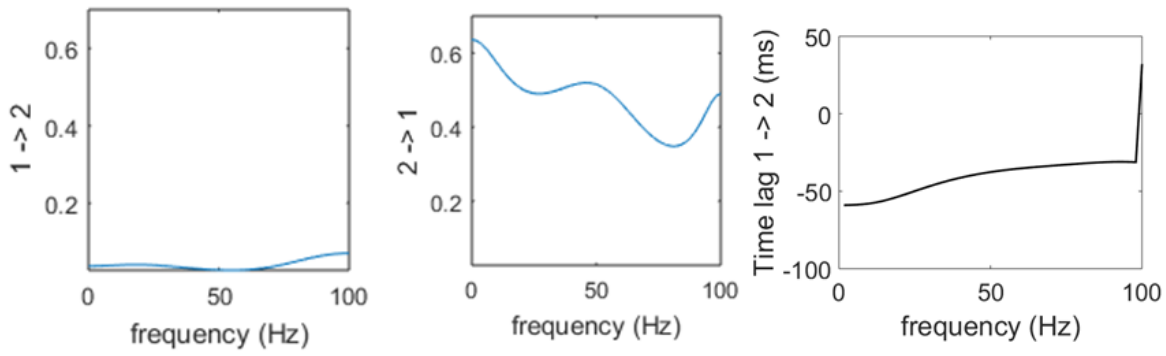

Figure 6.8: Spectral Granger Causality and phase lag between processes 1 (simulated master, Y) and 2 (simulated slave, X) with anticipation parameter, $\alpha = 1$. Causality is estimated incorrectly while lag is estimated correctly.

incorrect dominant causal direction from 2 to 1. Time lag of 2 from 1 is however negative, correctly indicating anticipation. Causality direction is identified incorrectly while the phase is identified correctly also for high anticipation in the system ($\alpha = 1$) (Figure 6.8).

We can see from the above results that it is not always reliable to use GC for non-linear systems with anticipation. GC fails here for anticipating tent map coupled system and hence to make conclusions about anticipation in the brain based on inter-cortical region GC is definitely problematic and one must proceed with great caution.

6.3.2 Compression Complexity Causality and Transfer Entropy for AS systems

Methods such as CCC and TE, are applicable to non-linear data and have been shown to be more robust than GC in estimating causality on certain types of datasets (see Chapter 3 and [35]). CCC and TE are not capable of determining the phase difference but only strength and direction of causality between time series. TE has been

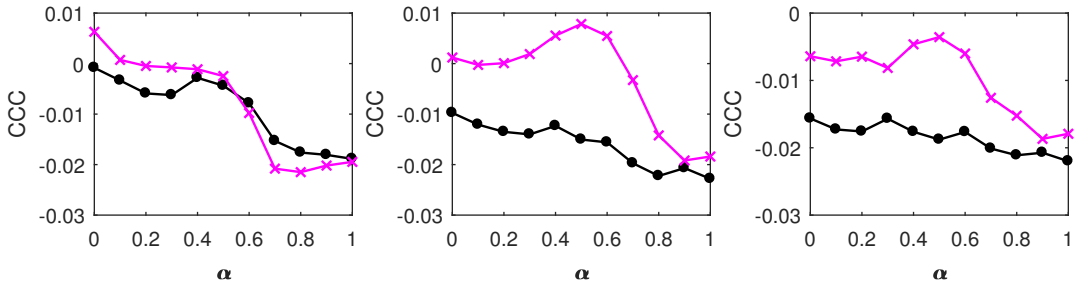

Figure 6.9: Mean CCC values over 50 trials of AS coupled tent maps, from process Y to X (solid line-circles, black) and X to Y (solid line-crosses, magenta/ grey in print) with varying anticipation parameter (α) when the number of bins used is set to (a) 4, (b) 8 and (c) 16. CCC is able to distinguish the correct direction of causality in cases (b) and (c), but not in case (a).

implemented on an anticipating logistic map coupled system and found to estimate the correct direction of causality when higher resolution is used for binning the sequences [159]. TE fails for 1 bit and 2 bit resolution (2 bins and 4 bins) of the data but is successful at 3 bit resolution (8 bins).

Here, we test for the performance of CCC on the coupled tent map system simulated using Eqs. 6.31 and 6.32 with ϵ set to 0.3. 50 trials of 1000 time points each (after removal of 2000 transients) were taken with values of the parameter α set ranging from 0 to 1 in steps of 0.1. Figures 6.9(a), (b) and (c) show the performance of CCC for bins, B (see Chapter 2 for more details on this parameter) set to 4, 8 and 16 respectively. Other parameters for the computation of CCC are fixed as: $L = 100, w = 15, \delta = 80$.

It can be seen from the figure that CCC is able to distinguish the correct dominant causal direction only when the number of bins are set to 8 or higher (16). For these cases, its performance is very good at lower levels of anticipation (upto $\alpha = 0.6$) and begins to decline post that. At higher levels of anticipation, CCC shows bidirectional

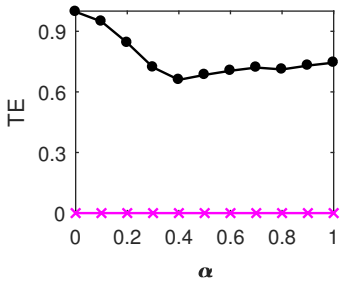

Figure 6.10: Mean TE values over 10 trials of AS coupled tent maps, from process Y to X (solid line-circles, black) and X to Y (solid line-crosses, magenta/ grey in print) with varying anticipation parameter (α). TE is able to determine the correct direction of causality when used with nearest neighbor estimator and using non-uniform embedding.

causation, with higher magnitude of causation remaining in the correct causal direction (Y to X). CCC is a total failure for number of bins set to 4. Please note that CCC is capable of negative causality estimation (which determines the qualitative nature of causal influence). Even in case of negative CCC, the magnitude gives the strength of causation (see Section 2.4).

We also used the measure TE to test for causation in this case with the MuTE toolbox [90]. Instead of binning the data, nearest neighbor estimator was used for estimating the probability density functions. For representation of the history of the observed processes, the approach of non uniform embedding was used. The number of lags to consider for observed processes was set to 5 and the maximum number of nearest neighbors to consider was set to 10. Figure 6.10 shows the mean values of TE estimated over ten trials as the value of α is varied. Fewer trials were taken in the case of TE as the MuTE code is computationally heavy and takes a long time to run. It is seen that TE as implemented here works well to distinguish the direction of causality for all values of α.

6.3.3 Discussion, Conclusions and Future Work

In the case of systems with AS, it is difficult to find the correct direction of coupling as the time series of the slave begins to anticipate the master. It is shown with the help of a simulated system of coupled tent maps that GC is not always a reliable measure for causality estimation in AS systems and also conversely, based on spectral GC strength and estimated phase, we cannot always reliably comment on whether a system is undergoing AS. When the simulated system was analyzed based on GC for the case of no anticipation, it showed causality to be in the correct direction from master to slave but incorrectly indicated the slave to be ahead of the master in phase – thereby, erroneously suggesting the presence of AS. When the system was simulated with anticipation greater than 0, dominant causality was indicated incorrectly from the slave to the master. Therefore, caution needs to be exhibited when making statements on the presence of AS in real world dynamical systems data based on GC analysis. For instance, the suggestion of AS in the primate brain during cognitive activity by Matias et. al [158] needs to be revisited with the use of adequate measures on the acquired data.

CCC when used with number of bins 8 or more is able to distinguish the dominant direction of coupling in AS. Also TE, when employed with nearest neighbor estimator to estimate the probability density functions and non uniform embedding for representation of the history of the observed processes identified the causal connections accurately.

Hahs and Pethel [159] have demonstrated the use of TE with binning on coupled AS

logistic maps and found that TE fails to detect correct causality direction for 2 and 4 bins but is successful when implemented with 8 bins. With an example of Markov Chain model of coupled shift maps, the authors analytically show that when low resolution data is used, there is no statistic that can correctly distinguish the causal process from the caused one under the AS scenario. This is because in the case of low resolution, new information (in the system) seems to become visible in the anticipatory slave first, instead of the master and thus the measures indicate that the slave predicts the master. To make it explicit, though the slave cannot perfectly predict the entire state of the master, it can predict the more significant bits. When higher resolution information becomes visible, it is clear that the new information was actually generated from the master, which in turn has an effect on the slave. The above explanation may also be applicable for CCC, as, when CCC is applied on data with less resolution (fewer bins), it is unable to find the true causal influences for an AS system.

For future work, we would like to analytically justify the failure of CCC for lesser number of bins for causality estimation in AS systems. Also, better binning strategies will be explored to improve the results obtained using CCC. CCC and TE are not capable of determining the phase difference between master and slave, which is essential to analyze AS systems. It would be interesting to study if modified versions of spectral GC phase or other existing approaches such as 'complexity-causality plane' [160] can be reliably used along with CCC and TE to comment on AS systems given only time series data. CCC and TE performance would also be tested on continuous time AS dynamical systems.

Chapter 7

Causality Analysis for Sparse Signals

Many naturally occurring signals such as human speech and natural images are known to be sparse in some domain. Compressed sensing enables sparse signals to be acquired, stored and transmitted in a linearly compressed fashion (with far fewer measurements than used by traditional methods) and finds applications in magnetic resonance imaging, photography, transmission electron microscopy etc. Linear compression is achieved by matrix multiplication of the input sparse signals with a random sensing matrix that satisfies some special properties (for e.g., independent Gaussian entries) and recovery is enabled by nonlinear optimization techniques. Causality testing on such data is required to make useful inferences without reconstructing them to the sparse domain. Also, for some cases, it may be impossible to determine causal structure for data in sparse domain without the assumption of a model for given data. In this chapter, we design structured sensing matrices having Toeplitz and Circulant structure that preserve causal relationships (as measured by Granger Causality) between sparse autoregressive coupled

input signals in the compressed domain. An application is also shown for real sparse neural signals, where Granger Causality is unable to detect the correct causality in the sparse domain, but the causality becomes discoverable in the compressed domain by application of these structured sensing matrices.

7.1 Introduction and Motivation

The use of compressed sensing technique for data compression, channel coding and signal acquisition is increasing widely in various domains, finding applications for designing cameras [162], magnetic resonance imaging techniques [163, 164], analog to digital conversion technologies [65]. It is thus becoming imperative to analyze the properties of signals and their interdependence in the compressed domain itself, avoiding the cumbersome task of reconstructing multiple signals, especially from large networks. In this chapter, we explore if the cause and effect relationships between variables in the raw domain can be deciphered in the compressed domain. An important application of this work would be in the domain of analyzing brain connectivity. To transmit, process and store high dimensional neural activity patterns, amidst a cacophony of interfering neural signals and neural noise, the brain employs efficient compression of information with low energy consumption and also robustly multiplexes neural signals. As a result, compressed-sensing based models for neural signals are being proposed [165, 166]. Apart from this, many acquired neural signals are sparse, precluding direct application of existing model-free techniques for functional connectivity analysis based on given neural data [66, 67]. To efficiently analyze brain/neural connectivity in such a scenario,

we propose a novel technique that would be useful.

7.1.1 Compressed Sensing

Compressed sensing is a signal processing technique that helps to capture, save, modify and send out large amounts of data efficiently. One application is in magnetic resonance imaging acquisition techniques [163, 164]. While sampling at the Nyquist rate ensures perfect recovery of the original bandlimited signal, compressed sensing makes signal recovery from under sampled data possible under certain conditions. It is crucial that the input signal be *sparse* when expressed in a proper basis and the basis in which it is acquired/sensed be *incoherent* with this sparsifying basis [65, 167]. *Sparsity* implies that a discrete-time signal depends on a number of degrees of freedom which is much smaller compared to its (finite) actual length. This means that these signals have concise representations when expressed in the proper basis ψ, called the sparsifying matrix. *Incoherence* is basically the idea that objects that have a sparse representation in ψ should spread out in the domain in which they are acquired (or sensed). This is analogous to the way a spike in the time domain is spread out in the frequency domain. In other words, incoherence means that the sampling/sensing waveforms have a very dense representation in ψ.

Sparse signal recovery can be represented as a Compressed sensing problem in the following way:

$$y = \phi x, \tag{7.1}$$

where y is the compressive measurement vector/ compressed signal (of dimension $M \times$

1), ϕ is the sensing matrix (of dimension $M \times N$), x is the input signal (of dimension $N \times 1$), which can be written in the form $\psi\alpha$, where ψ is the sparsifying matrix and α contains the coefficients. The input sparse vector x is in $\mathbb{R}^N$ and the output vector y is in $\mathbb{R}^M$. The sensing matrix ϕ which maps the space $\mathbb{R}^N$ to $\mathbb{R}^M$, has a rank $\leq M$ (and $M \ll N$).

ϕ must be such that $\phi x_1 \neq \phi x_2$ for all k-sparse $x_1 \neq x_2$, where k-sparse means that the maximum number of non-zero entries in x_1, x_2 are k. This property ensures that the mapping is invertible, so that no two output vectors are mapped to the same vector during recovery. For this to be the case, ϕ should have at least $2k$ rows, i.e. $M \geq 2k$.

Restricted Isometry Property (RIP) [168] is a standard tool for determining how efficiently the sensing matrix ϕ, captures information about sparse signals, so that it is possible to recover them. For integers $k = 1, 2, \ldots$, the isometry constant δ_k of a matrix ϕ is defined as the smallest number such that

$$(1 - \delta_k) \|x\|_{l_2}^2 \leq \|\phi x\|_{l_2}^2 \leq (1 + \delta_k) \|x\|_{l_2}^2 , \tag{7.2}$$

holds for all k-sparse vectors x[1]. A matrix ϕ fulfills an RIP of order k if δ_k is not too close to one. This means that the euclidean length of k-sparse signals is roughly preserved and so these k-sparse vectors cannot be in the null space of ϕ. This helps to ensure that their reconstruction is possible.

When the above conditions on ϕ are met, Eq. 7.1 still remains under-determined and will have infinitely many solutions. To recover the best solution to the signal x, back

[1] $\|v\|_{l_p}$ denotes the l_p norm of vector v computed as $\|v\|_{l_p} = (\sum_{i=1}^{n} |v_i|^p)^{1/p}$, with n being the length of the vector.

from the compressed measurements y, there are many well-known algorithms which either employ optimization techniques (such as l_1 minimization [169, 170]) or greedy approach (like Orthogonal Matching Pursuit [171]).

7.1.2 Causality Testing in the Compressed Domain

Today in many scientific and engineering problems, we are posed with underdetermined linear systems and sparse signals. Compressed sensing schemes are being employed widely for signal acquisition, storage and transmission. In such a scenario, it is essential to know whether we can check for causal relationships between compressed data without the need for reconstruction of signals. Also, we need to know, under what circumstances (such as, for what kind of sensing matrices) do causal relations present in the raw domain remain preserved in the compressed domain and hence causal analysis in the latter domain is meaningful. Sometimes, in case of sparse (and/or finite) data, available techniques for functional connectivity analysis may not perform adequately. In fact, point process generalized linear model (GLM) based techniques have been proposed for connectivity analysis of neural data in such a scenario [66,67]. As discussed in Chapter 1, model-based techniques have their limitations and cannot be applied universally. In this chapter, we discuss, if and how model-free techniques can help discover causal relations for sparse data by transforming them into compressed domain. To the best of our knowledge, both our problem statement and the proposed solution are novel and no work has been done before along this line.

When the connections in the network are sparse, there exist techniques such as

Lasso Granger [172], its several variations [173, 174], CaSPIAN [175] etc., that employ a combination of compressed sensing techniques (such as variable (model) selection e.g. - Lasso) and causality methods (such as Granger Causality). These are methods to infer network connectivity and are of use for study of systems such as Genetic Regulatory Networks. These methods are not to be confused with the work that we present in this chapter since none of these methods attempt to infer causal relationships in the compressed domain.

7.2 Structured Sensing Matrices for Causality Detection

A sensing matrix, A, on multiplication with the original $N \times 1$ sparse signal, x, yields a compressed signal, y, of dimension $M \times 1$, as per the equation, $y = Ax$. Here A has M rows and N columns. The signal x is said to be k-sparse if it contains up to k non-zero entries (and not more). Gaussian random values in A prove to be one of the most effective ways in helping recover x from y [176, 177]. However, compression using a random matrix results in hardly any properties of the original signal being preserved after compression (the drawback of randomization). In order to design sensing matrices that preserve causality, we explore matrices which possess some kind of structure while still satisfying necessary properties for sparse signal recovery.

7.2.1 Toeplitz and Circulant Sensing Matrices

Toeplitz and Circulant matrices have been shown to be effective sensing matrices for recovery of sparse signals [178, 179]. In fact, Toeplitz and partial random Circulant matrices have both been shown to satisfy the RIP property [180,181]. Toeplitz matrices are those matrices in which the rows get shifted to the right and the first element of a given row occupies the second position of the following row and the first element position in that row is occupied by a random element. In order to design an $M \times N$ Toeplitz matrix, we construct an N length row vector consisting of independent Gaussian entries $\mathcal{N}(0,1)$ (with zero mean and unit standard deviation). Entries of this row are shifted to the right for each new row with a random Gaussian value forming the first entry of that row. The structure of a Toeplitz matrix is as shown below:

$$T = \begin{bmatrix} p_1 & p_2 & p_3 & \cdots & p_N \\ r_1 & p_1 & p_2 & \cdots & p_{N-1} \\ r_2 & r_1 & p_1 & \cdots & p_{N-2} \\ \vdots & \vdots & \vdots & \ddots & \vdots \\ r_{M-1} & r_{M-2} & r_{M-3} & \cdots & p_{N-M+1} \end{bmatrix}_{M \times N} . \tag{7.3}$$

$p_i, r_i \sim \mathcal{N}(0,1)$, where i varies from 1 to N. Circulant matrices are similar to Toeplitz matrices with the variation that the rows are circularly shifted to the right with the last element of a given row forming the first element of the following row. A random Gaussian vector of length N is shifted circularly M times to form an $M \times N$ Circulant matrix as shown below:

$$C = \begin{bmatrix} q_1 & q_2 & q_3 & \cdots & q_N \\ q_N & q_1 & q_2 & \cdots & q_{N-1} \\ q_{N-1} & q_N & q_1 & \cdots & q_{N-2} \\ \vdots & \vdots & \vdots & \ddots & \vdots \\ q_{N-M+2} & q_{N-M+3} & q_{N-M+4} & \cdots & q_{N-M+1} \end{bmatrix}_{M \times N} . \tag{7.4}$$

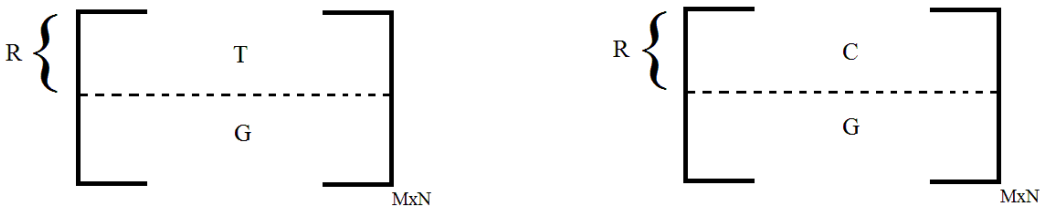

Figure 7.1: Structured sensing matrices. Left: Structured Toeplitz sensing matrix. Right: Structured Circulant sensing matrix. In both cases, $R \times N$ upper matrix has Toeplitz/Circulant structure while the $(M - R) \times N$ lower matrix is Gaussian, where $0 \leq R \leq M$.

$q_i \sim \mathcal{N}(0, 1)$, where i varies from 1 to N. In the sensing matrices used in this work, the degree by which a matrix has Toeplitz (T) or Circulant (C) structure is controlled by allowing only 'R' number of rows to have that structure. Rest of the entries of the matrix are Gaussian (G). This is illustrated in Figure 7.1.

7.3 Results

7.3.1 Simulations

A pair of sparse input signals, x_1 and x_2, are simulated and compressed to signals y_1 and y_2 by using the same sensing matrix A. The length of the input signals, N, and the length of the compressed signals, M, are fixed at 1000 and 100 respectively, whereas the sparsity, k, is kept a constant at 10, except for those cases where the curves are plotted for varying k. Let the signals x_1 and x_2 be defined over a set of time points $T = \{1, 2, 3, \ldots, N\}$. We define a set $T_1 \subset T$ such that T_1 consists of k uniformly randomly chosen elements of T. Also, let $T_2 \subset T$ be defined as $T_2 = \{t_2 : t_2 = t_1 + 1, \forall\, t_1 \in T_1\}$. T_1^c and T_2^c denote the complement sets of T_1 and T_2 respectively (T is the universal

set). The signals x_1 and x_2 are sparsified versions of autoregressive processes X_1 and X_2 and are generated as per the following equations:

$$\begin{aligned} X_1(t) =& \alpha X_1(t-1) + z_1(t), \quad \forall t \in T, \\ x_1(t) =& \begin{cases} X_1(t), & \forall \{t \in T_1\}, \\ 0, & \forall \{t \in T_1^c\}, \end{cases} \end{aligned} \tag{7.5}$$

$$\begin{aligned} X_2(t) =& \beta X_2(t-1) + \gamma x_1(t-1) + z_2(t), \quad \forall t \in T, \\ x_2(t) =& \begin{cases} X_2(t), & \forall \{t \in T_2\}, \\ 0, & \forall \{t \in T_2^c\}, \end{cases} \end{aligned} \tag{7.6}$$

where z_1 and z_2 are additive (independent) Gaussian noise drawn from $\mathcal{N}(0,1)$. $x_1(t)$ retains the values of $X_1(t)$ at k random time points and is set to zero at the rest $N-k$ time points. $x_2(t)$ is zero whenever $x_1(t-1) = 0$. At the rest of the k time points, $x_2(t)$ retains values of $X_2(t)$. This ensures that both x_1 and x_2 are k-sparse signals. Figure 7.2 shows an example of generated sparse signals x_1 and x_2. As is evident from the above equations, there is a direct causation from x_1 to x_2 (strength of causation controlled by coupling coefficient γ) and not in the reverse direction. The characteristics of x_1 and x_2 loosely resemble spiking patterns of coupled neurons.

Performance of Structured Matrices

Performance of Toeplitz and Circulant matrices (with $R = M$) in terms of percentage success in sparse signal recovery and causality testing while varying the level of sparsity, k, are shown in Figure 7.3. CVX, a package for specifying and solving convex programs [182] was used for l_1 minimization and consequent sparse signal recovery for all results in this chapter. At every trial, sparse signal recovery (x_1 and x_2 from y_1 and y_2 respectively) is deemed a success if the mean squared error between the original and

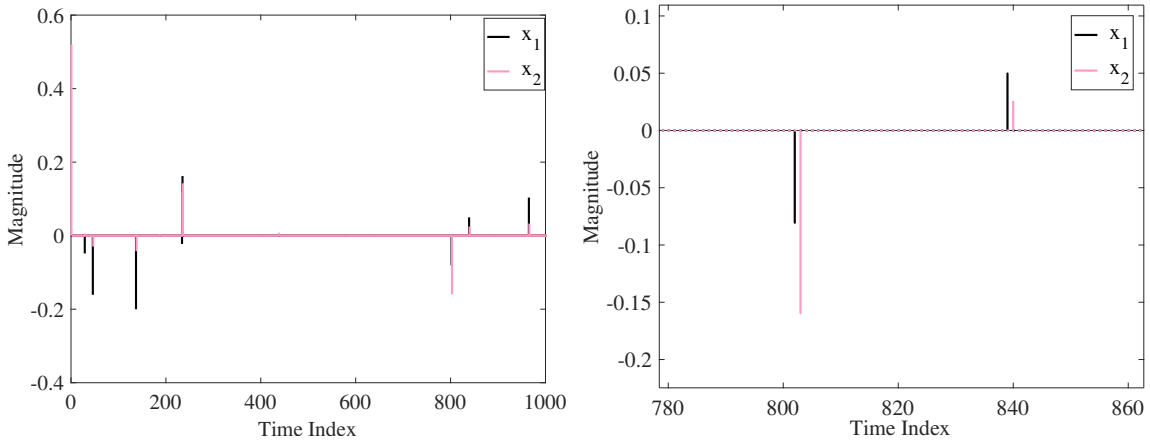

(a) (b)

Figure 7.2: (a) Sparsified autoregressive inputs (sparsity, $k = 10$) with x_1 causing x_2. (b) Magnified view, showing signal values for temporal index 780 to 860.

reconstructed signal is less than 10^{-6} for both x_1 and x_2. The mean squared error of reconstruction for x_1 is estimated as:

$$MSE(x_1) = \frac{1}{N}\sum_{i=1}^{N}(x_1(i) - \hat{x}_1(i))^2, \tag{7.7}$$

where, i is the index of samples in x_1, N is the length of x_1 and $\hat{x}_1$ is reconstruction of x_1. Causality detection is considered successful if the direction of causality as estimated on the compressed signals (y_1 and y_2) is the same as that between the original raw signals (x_1 and x_2). Causality is estimated based on Granger Causality F-statistic (GC) (for details and existing literature on GC, check Section 1.2.5). The order of the AR process is determined using Akaike Information Criterion with maximum number of lags to be considered for the processes set to 30. Percentage success is evaluated across 100 trials taken with random initial values for the AR processes.

Percentage success in causality testing while keeping the level of sparsity constant

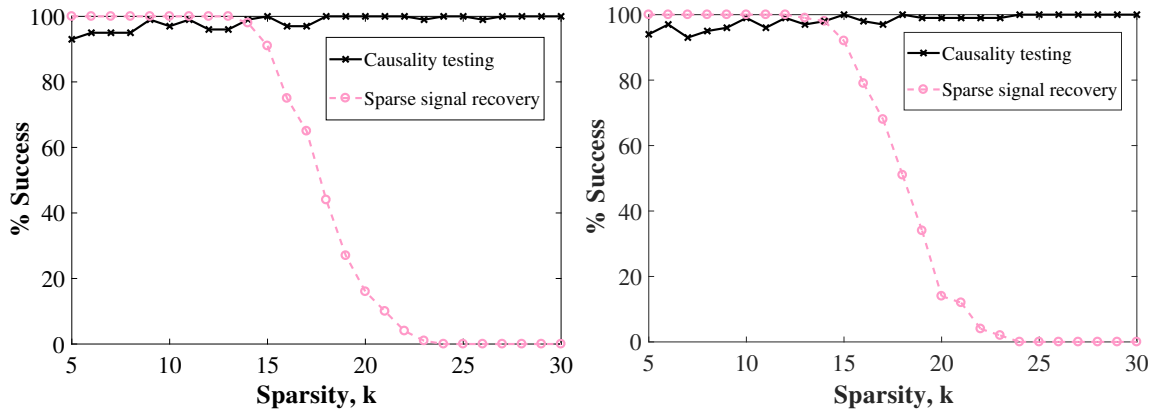

Figure 7.3: Percentage success (across 100 random trials) in sparse signal recovery and causality testing for varying sparsity (k) in case of (a) Toeplitz and (b) Circulant sensing matrices. While signal recovery deteriorates for higher values of k, causality estimation improves.

at $k = 10$ but varying the degree of Toeplitz and Circulant structure, by varying the value R (Figure 7.1), is shown in Figure 7.4. Reconstruction was found to be successful for all values of R here. Hence, we omit depiction of percentage success in sparse signal recovery in Figure 7.4.

Varying the Coefficient of Causation

For simulated input signals x_1 and x_2, as the coefficient of coupling γ (see Eq. 7.5 and 7.6) is varied, we estimate GC for the following four cases for both fully Toeplitz and Circulant sensing matrices: GC from x_1 to x_2 signal in the raw domain (denoted by F_1), from y_1 to y_2 signal in the compressed domain (denoted by F_2), from x_2 to x_1 signal in the raw domain (denoted by F_3) and from y_2 to y_1 signal in the compressed domain (denoted by F_4). In Figure 7.5(a) and 7.5(b), mean values of F_1, F_2, F_3 and

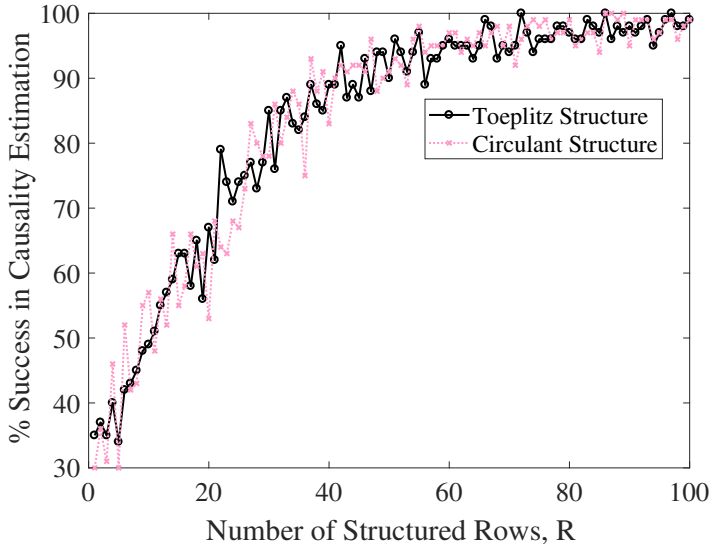

Figure 7.4: Percentage success (across 100 random trials) in correct causality estimation for varying number of structured rows, R, in case of Toeplitz and Circulant sensing matrices. Causality estimation improves with higher number of structured rows in both types of matrices.

F_4 as obtained across 100 random trials are shown for Toeplitz and Circulant matrices respectively as the coefficient γ is varied from 0 to 4 in steps of 0.1. Tables 1 and 2 show the mean and standard deviation of GC values for γ varied from 0 to 4, at intervals of 0.5.

7.3.2 Real Data

Open source data recordings (CC BY 4.0 License) of sparse neuronal spike trains recorded from putative single units in the rat prelimbic region of the prefrontal cortex (plPFC) acquired for study in [67] are used for analysis in this section. This neural data were obtained from adult male Sprague-Dawley rats performing a T-maze based delayed-alternation task of working memory. In brief, animals were trained to navigate down the runway of the T-maze and choose one of two arms opposite to the one pre-

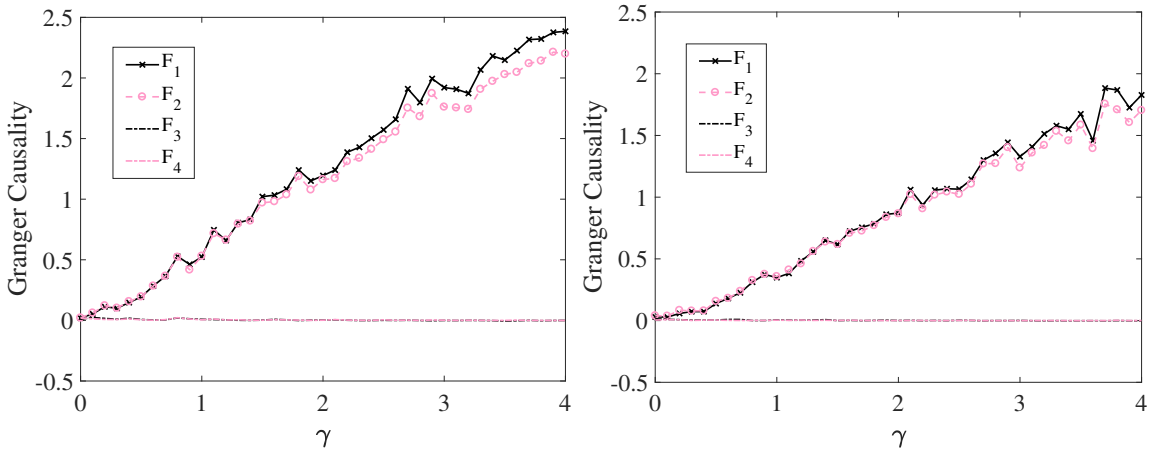

Figure 7.5: Mean Granger Causality values (across 100 trials) for the four cases, $F_1 : x_1 \rightarrow x_2, F_2 : y_1 \rightarrow y_2, F_3 : x_2 \rightarrow x_1$ and $F_4 : y_2 \rightarrow y_1$ as the coupling coefficient γ is varied in case of sensing by (a) Toeplitz and (b) Circulant matrices. With increasing γ, strength of GC estimated from both the raw and compressed signals increases with a similar trend.

Table 7.1: Mean (μ) and standard deviation (σ) of estimated Granger Causality values (over 100 trials) for Toeplitz sensing matrix when coupling coefficient γ is varied. Mean GC values, both in the raw ($F_1 : x_1 \rightarrow x_2$ and $F_3 : x_2 \rightarrow x_1$) and compressed domain ($F_2 : y_1 \rightarrow y_2$ and $F_4 : y_2 \rightarrow y_1$) are given.

γ	$\boldsymbol{F_1(\mu \pm \sigma)}$	$\boldsymbol{F_2(\mu \pm \sigma)}$	$\boldsymbol{F_3(\mu \pm \sigma)}$	$\boldsymbol{F_4(\mu \pm \sigma)}$
0.0	0.019 ± 0.0578	0.020 ± 0.0557	0.010 ± 0.0479	0.018 ± 0.0748
0.5	0.193 ± 0.2215	0.195 ± 0.2267	0.007 ± 0.0378	0.005 ± 0.0264
1.0	0.523 ± 0.4341	0.530 ± 0.4315	0.008 ± 0.0470	0.005 ± 0.0309
1.5	1.020 ± 0.5851	0.969 ± 0.5518	0.002 ± 0.0113	0.001 ± 0.0071
2.0	1.194 ± 0.6306	1.162 ± 0.6103	0.002 ± 0.0131	0.001 ± 0.0122
2.5	1.572 ± 0.8070	1.491 ± 0.7402	0.000 ± 0.0155	0.004 ± 0.0278
3.0	1.920 ± 0.8495	1.760 ± 0.7259	0.000 ± 0.0041	0.001 ± 0.0154
3.5	2.148 ± 0.8509	2.029 ± 0.7426	0.005 ± 0.0194	0.000 ± 0.0023
4.0	2.385 ± 0.8218	2.198 ± 0.7952	0.000 ± 0.0064	0.000 ± 0.0050

Table 7.2: Mean (μ) and standard deviation (σ) of estimated Granger Causality values (over 100 trials) for Circulant sensing matrix when coupling coefficient γ is varied. Mean GC values, both in the raw ($F_1 : x_1 \to x_2$ and $F_3 : x_2 \to x_1$) and compressed domain ($F_2 : y_1 \to y_2$ and $F_4 : y_2 \to y_1$) are given.

$\boldsymbol{\gamma}$	$\boldsymbol{F_1(\mu \pm \sigma)}$	$\boldsymbol{F_2(\mu \pm \sigma)}$	$\boldsymbol{F_3(\mu \pm \sigma)}$	$\boldsymbol{F_4(\mu \pm \sigma)}$
0.0	0.029 ± 0.060	0.039 ± 0.077	0.014 ± 0.086	0.004 ± 0.019
0.5	0.137 ± 0.175	0.156 ± 0.200	0.004 ± 0.024	0.004 ± 0.024
1.0	0.348 ± 0.312	0.357 ± 0.334	0.005 ± 0.031	0.003 ± 0.030
1.5	0.617 ± 0.413	0.617 ± 0.409	0.000 ± 0.000	0.000 ± 0.008
2.0	0.870 ± 0.548	0.866 ± 0.535	0.000 ± 0.006	0.000 ± 0.009
2.5	1.065 ± 0.641	1.023 ± 0.585	0.002 ± 0.024	0.001 ± 0.010
3.0	1.328 ± 0.690	1.238 ± 0.631	0.001 ± 0.010	0.000 ± 0.000
3.5	1.674 ± 0.722	1.585 ± 0.698	-0.000 ± 0.005	-0.000 ± 0.004
4.0	1.828 ± 0.894	1.703 ± 0.808	-0.001 ± 0.015	0.000 ± 0.001

viously visited for food rewards delivered by the experimenters hand. The prefrontal cortex (PFC) plays an important role in cognitive and behavioral processes and thus functional connectivity analysis for this brain region is important to study.

In [67], a 'Structural Information Enhanced' regularization method is developed to aid the GLM framework to better capture the functional connectivity among neurons. This technique is mainly for large sparse spike train datasets. Simulation results in the paper indicate that the parameter selection for GLM, a model-based method, when done using their regularized method, outperforms existing approaches and hence the authors display a confidence in functional connectivity estimated in rats based on the above discussed real data recordings.

We use neuronal spike data for 'Experiment 4' from the available dataset and check

for GC estimates between two considered pairs of neurons, Pair 1: neuron no. 72 (N72) and neuron no. 76 (N76), and Pair 2: neuron no. 72 (N72) and neuron no. 49 (N49). The three chosen neurons have been taken from the periphery of the network structure discovered by [67] using their 'SGL regularized method' (see Figure 9 of [67] for exact network structure). This is done so that the considered pairs qualify for bivariate causality analysis and are not affected by any indirect influences from within the network structure. As per the results reported in Figure 9 of [67], there is a direct causal influence from neuron 72 to 76 and no influence in the opposite direction, while there is no connection between neurons 72 and 49.

We analyze time series of length 20,000 time points from these neurons, taken from 501^{st} time point to 20500^{th} time point from the 21,502 length spike train recording available. The initial 500 time points were removed to get rid of transients, if any. Thus, N or the length of the signal here is 20000, M is taken to be 2000 (set to be greater than 4 times the sparsity of the signal having the maximum sparsity amongst N49, N72 and N76). Partial Toeplitz matrices, with different number of structured rows were used for obtaining the compressed domain signals.

MVGC [31] is a toolbox for robust GC inference, specifically designed for neuroscience data. The MVGC approach is based on multiple equivalent representations of a Vector Autoregressive Model. It includes algorithms for moving between these representations, ensuring the best means to achieve numerical accuracy. It employs many types of error checks for the given data and eliminates sources of statistical inaccuracies. For analysis of real data, MVGC toolbox was used and presence or absence of a causal

Table 7.3: Significance (Sig) and value (F) of Granger F-statistic for causality between sparse neuronal spike trains $N72, N76$ and their compressed versions for different values R in Toeplitz sensing matrix. Reconstruction error for each spike train is also reported for different sensing matrices. Raw data obtained from [67].

Signal	$\boldsymbol{R}$	$\boldsymbol{Sig_{N76\rightarrow N72}}$ $\boldsymbol{(F_{N76\rightarrow N72})}$	$\boldsymbol{Sig_{N72\rightarrow N76}}$ $\boldsymbol{(F_{N72\rightarrow N76})}$	**Reconstruction Error**	
				N72	N76
Raw domain (Sparse)	–	1 (0.0022)	1 (0.0058)	–	–
Compressed	0	0 (5.39×10^{-5})	0 (1.09×10^{-4})	1.74×10^{-2}	8.59×10^{-17}
	1000	0 (0.0017)	0 (0.0012)	2.02×10^{-2}	1.42×10^{-16}
	1900	**0 (0.0057)**	**1 (0.0194)**	1.89×10^{-2}	9.64×10^{-21}

connection determined based on significance testing employed by the toolbox. We use it to test for causality between neural signals, both in the raw sparse domain as well as in the compressed domain for different values of the number of structured rows, R, in the Toeplitz matrix used for compressed sensing.

Table 7.3 and 7.4 depict the significance ($Sig_{X\rightarrow Y}$) and value ($F_{X\rightarrow Y}$) of Granger F-statistic for raw neuronal spike trains and their compressed versions. Here, the subscript $X \rightarrow Y$ denotes the direction of causation from X to Y. If the Granger causality from X to Y is significant, $Sig_{X\rightarrow Y} = 1$ and remains zero otherwise. Mean squared error of reconstruction (Reconstruction Error) of the sparse signal (estimated as in 7.7), on use of sensing matrices, with different values of R are also noted in the table.

It can be seen from the tables that the correct direction of causality based on GC is not evident in the acquired raw domain for both the cases considered. It becomes dicoverable for Pair 1: $N72$ and $N76$, only for $R = 1900$ when the structure of the

Table 7.4: Significance (Sig) and value (F) of Granger F-statistic for causality between sparse neuronal spike trains $N72, N49$ and their compressed versions for different values R in Toeplitz sensing matrix. Reconstruction error for each spike train is also reported for different sensing matrices. Raw data obtained from [67].

Signal	$\boldsymbol{R}$	$\boldsymbol{Sig_{N49\rightarrow N72}}$ $\boldsymbol{(F_{N49\rightarrow N72})}$	$\boldsymbol{Sig_{N72\rightarrow N49}}$ $\boldsymbol{(F_{N72\rightarrow N49})}$	**Reconstruction Error**	
				N72	N49
Raw domain (Sparse)	–	0 (0.0034)	1 (0.0047)	–	–
Compressed	0	**0 (0.0005)**	**0 (0.0017)**	2.09×10^{-2}	1.28×10^{-18}
	1000	**0 (0.0063)**	**0 (0.0029)**	2.15×10^{-2}	2.38×10^{-15}
	1900	**0 (0.0030)**	**0 (0.0062)**	1.87×10^{-2}	6.98×10^{-19}

sensing matrix is highly Toeplitz. For Pair 2: $N72$ and $N49$, the correct causal relationship is detected for sensing by a completely random matrix ($R = 0$), partially toeplitz ($R = 1000$) as well as for an almost fully Toeplitz ($R = 1900$) matrix. Reconstruction error for all the sparse signals considered are of the order of 10^{-2} or less for all the sensing matrices taken.

7.4 Discussion

The chosen structured sensing matrices, Toeplitz and Circulant, are seen to perform well for causality detection. When the structure of sensing matrix is fully Toeplitz/ Circulant, and the level of signal sparsity k is varied for simulated signals, percentage success in causality detection increases and approaches 100% at higher values of k (20-30) as seen from Figure 7.3. On the other hand, the trend for percentage success in signal recovery deteriorates with increasing values of k. Signal can be recovered almost

perfectly for $k < 15$. When the input signal sparsity level is constant, but the number of structured rows in sensing matrix are increased as in Figure 7.4, the percentage success in causality testing increases and reaches 100% for fully structured matrix. Thus, structured sensing matrices are clearly better than random Gaussian sensing matrices for preserving causality (as measured by GC) in the compressed domain.

Not only do the structured sensing matrices used here preserve the direction of causation in the compressed domain but also preserve the strength of causation. This is evident from Figure 7.5, where the strength of estimated Granger Causality F-statistic in the actual causal direction increases in the compressed domain, remaining close to the corresponding values in the raw signal domain, as the unidirectional coupling coefficient γ is increased. In the direction in which there is no causation, estimated causality values are observed to be close to zero in the compressed domain (as desired) as is the case in the raw signal domain.

From the simulations we have seen that when autoregressive structure is present in the raw sparse signals, causality is reliably discoverable in the raw domain. However, if the sparse signals are not generated by autoregressive means, it may be difficult to determine accurate causal relationships based on GC because it is possible that the causal information is more spread out in the sparse domain, yielding finite past based autocorrelations of these finite signals insufficient to discover causality in the raw domain. In such a scenario, compressed representations should be more helpful. From an example case of real data signals that is considered in Section 7.3.2, it can be seen that though accurate causality relationship is not discoverable between sparse signals

in the raw domain, it becomes discoverable in the compressed domain when the sensing matrix employed is highly Toeplitz in structure. Thus, testing of causality based on GC in the compressed domain can be considered as a powerful technique for sparse signals for which it may be difficult/ impossible to discover causality in the sparse domain using model-free techniques.

In networks for which signals are acquired in the compressed domain and are required to be analyzed based on several causal connections which may also change with time, the use of structured sensing matrices would help to solve the task within the compressed domain. This will save some computational cost that is involved in signal reconstruction and then causality testing; and also ensure better accuracy of discovered causal relations compared to the sparse domain. Preservation of the causality property by Toeplitz and Circulant matrices would then be the deciding criteria for design of sensors in various systems. In fact, already it is the case that many measurement technologies impose structure on the matrix. This is because structured matrices possess other advantages such as requirement of lesser number of independent random variables for generation and better efficiency of their recovery algorithms as the matrix admits a fast matrixvector multiply [180, 181]. Causal inference in the compressed domain for these scenarios is a powerful and useful technique.

Also, in case of naturally occurring sensors that can be approximated to be sensing the signal based on operation by a structured matrix like partial/full Toeplitz/Circulant, causality analysis for the signals can be easily and reliably performed. One way by which the operation performed by a sensing matrix can be deciphered is by checking

the properties of the sensed signal. For e.g., Toeplitz matrices are known to perform a moving average operation on the input signals [183]. Some neural signals are known to be compressed signals [165,166] while most single unit neuronal signals are sparse spike trains [184]. Recognition/design of causality-preserving sensing matrices will be useful for decoding functional neural connections and brain connectivity.

We have used a model-free measure, GC, for the detection of causality between compressed signals. Other measures – Transfer Entropy and Compression Complexity Causality were also tested for discovering causality in the compressed domain in the same manner as GC, but proved to be unsuccessful. One of the reasons why GC is working here, while other measures are not, could be that it is designed to estimate causality for linear autoregressive processes. The solution to *Yule Walker Equations* which gives the coefficients of coupled AR processes and consequently give the strength of causation are actually a solution to a Toeplitz matrix [185]. This matrix is formed with entries which are autocorrelation/ cross-correlation coefficients of the considered processes taking different lags each time. It could be the case that a transformation to compressed domain by a structured (Toeplitz/ Circulant) matrix of the sparse signal does not disturb its causal structure (when it is discovered by solving the Yule Walker Toeplitz matrix).

7.5 Conclusions and Future Work

To the best of our knowledge, this is the first study to explore causality detection between compressed measurement signals without the need to perform sparse signal

recovery. In this work, we propose the design of structured matrices, Toeplitz and Circulant, that preserve the causality strength and direction as discovered by a model-free method GC, when the signal is transformed from its raw domain to compressed domain. Simulation results demonstrate the success of these matrices for GC detection. At the same time, these matrices could be used as compressed sensing matrices owing to efficient sparse signal recovery. In fact, this technique for causality detection has also been shown to be useful to recover causality in compressed domain, which was not possible to be discovered directly from real sparse neural signals using a model-free method. Some model-based methods exist which can be used for discovering causal relationships between real sparse neural signals [66, 67], however, imposition of an underlying model may be problematic and cannot be universally applied.

Future work would involve exploring other sensing matrices composed of binary/real valued entries that help preserve GC. Further, it would be useful to test for other types of sensing matrices that can preserve Transfer Entropy and (or) Compression Complexity Causality. Exploring other kinds of sensing matrices that preserve properties other than causation such as correlation, or those that can help preserve multiple properties, will also be helpful in efficiently analyzing various networks for their properties. Sparse signals obtained from time series of dynamical systems and sparse realistic neural signals will also be used to test for preservation of causality in the compressed domain using different types of sensing matrices. It is important to discover conditional causalities in a network with multiple variables, and such simulated networks with sparse signals need to be tested for multivariate Granger causality estimation in the compressed domain.

Also, it would be interesting to use multivariate GC for the entire set of real signals available from [67] (used in Section 7.3.2) and compare if the causal network discovered this way agrees with that obtained in [67] using their model-based approach.

Chapter 8

Time-reversibility, Causality and Compression-Complexity

Detection of temporal reversibility of a given process is an interesting time series analysis scheme. Apart from itself serving as a feature to characterize time series processes (such as non-linear processes), it also gives insights on the underlying processes generating the data. Moreover, time reversal of given data provides a promising tool for analysis of causality measures as well as studying causal properties of processes. Reversibility detection measures have been widely employed for the study of ecological, epidemiological and physiological time series. Effort-to-Compress (ETC) is a well-established robust method to characterize complexity of time series for analysis and classification. CCC, a causality measure based on ETC, proposed in Chapter 2, captures data-driven interventional causality. It is shown to give reliable performance for measurements from stochastic, chaotic and real-world systems in Chapters 3 and 4. In this chapter, we apply CCC on time-reversed coupled processes and show that the measure is free of the assumption that 'the cause precedes the effect', making it a great tool for causal analysis

of reversible processes. Further, we propose a novel measure for detection of temporal reversibility of processes, called the Compressive potential based asymmetry measure. Compressive potential is computed based on the ETC algorithm. The asymmetry measure compares the probability of occurrence of patterns at different scales between the forward time and time-reversed process. We test the performance of Compressive potential asymmetry measure on a number of simulated processes.

8.1 Introduction

When simulated data or data recorded from real world processes is present with us, it is possible for us to create an imaginary process exhibiting reverse dynamics of the original process. Researchers, primarily in the field of time series analysis, have widely deployed this technique to determine time reversibility/ irreversibility of a given process. Statistical time reversibility or time symmetry implies that statistical properties of given time series remain invariant regardless of the direction of time. Statistical time irreversibility implies otherwise. Time irreversibility is a common feature of non equilibrium systems [186–188] as well as systems driven by non-conservative forces [189]. It has been widely observed in time series obtained from ecological, epidemiological and physiological systems. Some examples include time series recordings of measles outbreak [190,191], annual phytoplankton bloom [191], electroencephalographic recordings of normal [192] and epileptic subjects [193–195] as well as beat-to-beat time interval recordings from the heart of normal and abnormal subjects [196–199].

Many methods for the detection of statistical time reversibility have been discussed

in literature. These include methods that make use of moment based tests [200–202], those analyzing distance between distributions of forward and reversed time series [193, 203, 204], methods based on visibility graphs [205–207]. Along with inference on reversibility, some of these methods are useful in the characterization of the nature of processes, particularly to distinguish non-linearity from Gaussian noise and to provide insights into the underlying mechanisms for observed non-linear data [191,203,208–211].

In physical macroscopic systems, the arrow of time manifests as a consequence of the second law of thermodynamics, where, for an isolated system the thermodynamic entropy of the system can only increase. This is the reason why, manifestation of events follows a particular order and not its reverse. For example, the process of a glass falling and smashing on the floor cannot be reversed. The methods discussed in the previous paragraph characterize irreversibility of time series only in a statistical sense. Thus, without any rigorous mathematical formulation, the relation between time irreversibility and thermodynamic entropy production remained a qualitative statement for several years. In a series of papers, J.M.R. Parrondo and his group introduced Kullback Leibler divergence (KLD), as measured between the probability distributions of the forward process and its time reversed version, as being related to the thermodynamic entropy produced by the process. More specifically, KLD, multiplied by the Boltzmann constant, is shown to be a lower bound to the entropy production along the process [212–215]. Their result is a generalization of Landauer's principle relating entropy production to any logically irreversible manipulation of information [216].

Time-reversed processes are an important aspect in the study of causality. Causal

analysis and detection of these signals can prove to be of immense use in causal characterization of these signals as well as help to give insights in the assumptions and properties of the employed causality measures. For example, the pioneering mathematical formulation for time series causality testing, Granger Causality, works based on the assumption that the 'cause precedes the effect'. Paluš et al. [217] have analyzed this assumption for Granger Causality and other causality methods such as Conditional Mutual Information [64, 72], Predictability Improvement [55] and Convergent Cross Mapping [28], by evaluating the performance of these methods on time-reversed coupled processes. While the above assumption is explicit in the formulation of GC, it is not the case for other methods. The analysis helps shed some light on the properties and hidden assumptions of these methods. It is also interesting to note the behavior of these methods for time symmetrical (reversible) as well as asymmetric (irreversible) processes.

In this work, we analyze time-reversed processes in two ways. 1. Causal analysis of time-reversed simulated processes using the CCC measure. Performance of CCC is compared with that of Transfer Entropy and Granger Causality. This is discussed in Section 8.2. This gives insights on the measure CCC and useful information on the applicability of the measure. 2. A novel method for detection of time irreversible processes is then proposed. This method is based on the measure Effort-to-Compress which has several useful properties as discussed in Section 2.2. We conjecture some relations of the proposed method to thermodynamic entropy production along a process which could be useful in the determination of the physical arrow of time. This is

explored in Section 8.3.

8.2 Causality between coupled, time-reversed processes

As discussed in the introduction, causal analysis of coupled time-reversed processes helps to give insights on the causality measures used as well as reveal interesting properties of the coupled processes. In [217], Paluš et al. have applied Conditional Mutual Information (CMI) [64, 72] (an information-theoretic approach to Granger causality (GC), which is equivalent to Transfer Entropy (TE) for a particular case [103]), on coupled time-reversed autoregressive processes Y and X generated with unidirectional coupling $Y \rightarrow X$. With both the processes reversed in time, the measured dominant causal direction reverses and was found to be from $X \rightarrow Y$. This result shows that with the violation of the Granger Causality principle 'cause precedes the effect', results for CMI are altered with the effect now seeming to be the cause. This is because GC based methods evaluate the ability of the driver process to predict or forecast the driven process. With the driver and the driven now interchanged, the information about the driver first occurs in the driven process.

A unidirectionally coupled set of Rössler systems was also evaluated in [217] using time-reversed time series of the coupled variable. Causality was estimated using measures Convergent Cross Mapping (CCM) [28] (explained briefly in Chapter 1), Predictability Improvement (PI) [55] (which is a generalization of the GC principle for nonlinear dynamical systems) and CMI. It was found using the three measures that the

discovered causal direction remained the same as for the original processes. It is suggested that this result was expected for the measure CCM, as it determines the ability of the driven system to provide information regarding the present state of the driver. So, the sequence of cause and effect do not make a difference for CCM. Other measures (CMI and PI) were not expected to perform symmetrically and hence a speculated rationale for this result is the presence of dynamical memory in chaotic systems.

CCM and PI cannot be applied to AR processes as their working is based on the manifold (or geometry) of dynamical systems. At the same time, GC is a failure when applied to dynamical systems as it makes the assumption of linear AR processes underlying the system. CCC, is however, a method that works for both stochastic as well as deterministic, linear and non-linear processes (this is demonstrated in Chapter 3). Analysis of time-reversed coupled processes is hence a fertile ground for the analysis of properties of CCC. The performance of CCC on such processes was thus tested as discussed subsequently.

Coupled autoregressive (AR) processes of order one and linearly coupled tent maps were generated as discussed in Section 3.2.1 (Eq. 3.1 gives the equations for coupled AR processes and Eqs. 3.3 and 3.4 give the equations for the coupled tent maps). Y is the independent process and X the dependent process in both the cases. 50 trials each of length 1000 time points were taken after elimination of 100 and 2000 transients for AR and tent map processes respectively. Higher number of transients for tent maps were removed because chaotic maps can have longer transient times. For increasing coupling between these processes with time evolution considered in the normal direction, results

are shown in Figures 3.1 and 3.4 for AR(1) and tent map respectively. The plots compare results for CCC, TE and GC in case of AR processes; CCC and TE in case of tent map processes.

Y' denotes the time-reversed independent process Y and X' is the time-reversed dependent process X (in case of both AR and tent systems). The equations for Y' and X' are as given below:

$$\begin{aligned} Y'(t) &= Y(1000 - t + 1), \quad \text{where} \quad 1 \leq t \leq 1000, \\ X'(t) &= X(1000 - t + 1), \quad \text{where} \quad 1 \leq t \leq 1000. \end{aligned} \tag{8.1}$$

For time-reversed AR processes, estimated causality using CCC, TE and GC is as shown in Figure 8.1. For time-reversed tent map processes, estimated causality using CCC and TE is as shown in Figure 8.2. Results are displayed as mean values over 50 trials. The parameters used in the computation of CCC, TE and GC remain the same as for the original processes in Section 3.2.1.

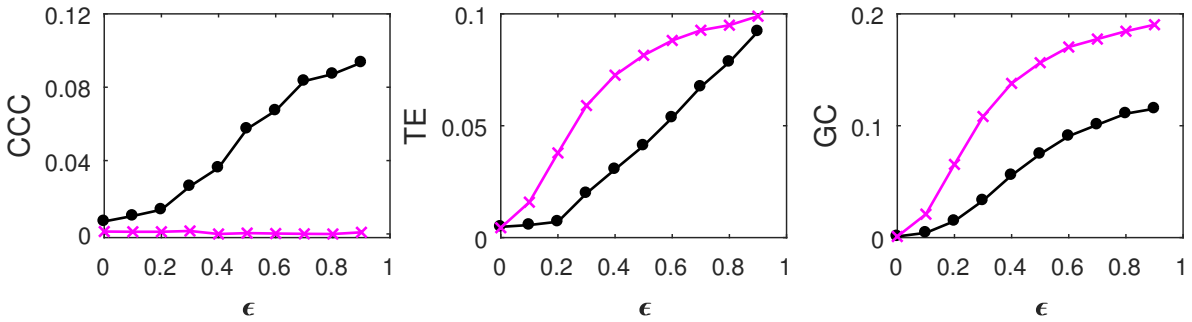

(a) (b) (c)

Figure 8.1: Mean causality values estimated using (a) CCC, (b) TE and (c) GC for coupled time-reversed AR(1) processes, from Y' to X' (solid line-circles, black) and X' to Y' (solid line-crosses, magenta/ grey in print) as the degree of coupling, ϵ is varied. CCC is invariant to time reversal, while for TE and GC, the dominant direction of causality is seen to be reversed.

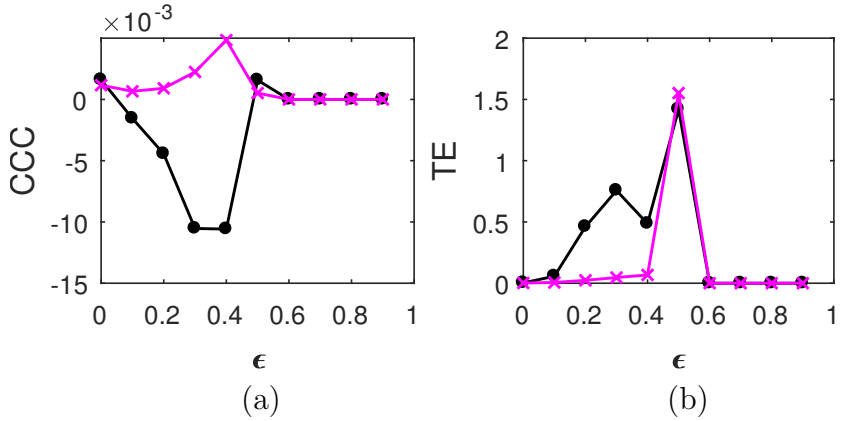

Figure 8.2: Mean causality values estimated using (a) CCC and (b) TE for linearly coupled time-reversed tent map processes, from Y' to X' (solid line-circles, black) and X' to Y' (solid line-crosses, magenta/ grey in print) as the degree of coupling, ϵ is varied. CCC is invariant to time reversal and in case of TE, as well, the dominant direction of causality identified is same as for the original processes.

In consensus with the results reported in [217] for CMI, it is observed that for TE and GC, the dominant causal direction for time-reversed AR processes is reversed (compared to the original case) with the estimated values from $Y' \rightarrow X'$ being less than that for $X' \rightarrow Y'$. Interestingly, for the measure CCC, the trend of causality values remains unaltered when compared to the original case. To the best of our knowledge, CCC is the only measure which performs in this way for stochastic linear AR processes. Though based on Wiener's principle, it works by measuring the change in dynamical compression-complexity of the driven process when information from the driving process is brought to the former and is not based on prediction (in a sequential sense) of the future of the caused based on the past of the causal (please see Chapter 2 for details). On comparison of results with other measures for the case of AR processes, it is confirmed that the measure CCC is symmetric with regard to the precedence or

posteriority of the cause with respect to the effect, thereby being free of the assumption that the 'cause precedes the effect'.

For time-reversed tent map processes, for both TE and CCC, the dominant direction of causality is as identified for the original case. TE displays some spurious results at $\epsilon = 0.4, 0.5$ but the trend for magnitude of CCC values clearly increases for increasing coupling until the processes are synchronized. The values obtained for CCC are negative, which is in line with CCC values for original coupled time series (please see Sections 2.4 and 3.2.1). The unchanging nature of both CCC and TE on reversal of these chaotic processes may be the result of memory in dynamical systems as has been suggested in [217].

8.3 Detection of temporal reversibility

A novel measure for detection of time-reversibility based on Effort-to-Compress (ETC) is proposed in this section. First we propose a new measure, *Compressive Potential*, which will be used later in the detection of temporal reversibility.

8.3.1 Compressive Potential

In Section 5.2.1, in the formulation of equivalent ETC we have seen that ETC works by reducing the length of a given symbolic sequence at each iteration, replacing the most frequently occurring pair of symbols with a new symbol. Let an ETC algorithm run up to n steps at which the original sequence, say X (of length N), is transformed to a constant sequence. If the reduction in the length of the sequence in the first iteration

of the ETC algorithm is given by q_1, in the second iteration by q_2, and so on till the n^{th} iteration in which the reduction in length is q_n and the equivalent (or average) compression (or fractional reduction in length) achieved by the algorithm is denoted by x, then, Eq. 5.11 holds and is reiterated below:

$$\begin{aligned} x^n &= \left(\frac{q_1}{N}\right)\left(\frac{q_2}{N-q_1}\right)\left(\frac{q_3}{N-q_1-q_2}\right)\cdots\left(\frac{q_n}{N-q_1-q_2\ldots-q_{n-1}}\right), \\ n\cdot\log(x) &= \log\left(\left(\frac{q_1}{N}\right)\left(\frac{q_2}{N-q_1}\right)\left(\frac{q_3}{N-q_1-q_2}\right)\cdots\left(\frac{q_n}{N-q_1-q_2\ldots-q_{n-1}}\right)\right), \\ n &= \frac{\log\left(\left(\frac{q_1}{N}\right)\left(\frac{q_2}{N-q_1}\right)\left(\frac{q_3}{N-q_1-q_2}\right)\cdots\left(\frac{q_n}{N-q_1-q_2\ldots-q_{n-1}}\right)\right)}{\log(x)}. \end{aligned} \tag{8.2}$$

Thus, ETC for a sequence is a function of fractional reduction in length at all steps and also the equivalent or average compression per step. The quantity $(\frac{q_1}{N})(\frac{q_2}{N-q_1})(\frac{q_3}{N-q_1-q_2})\ldots(\frac{q_n}{N-q_1-q_2\ldots-q_{n-1}})$, which is the product of fractional reductions in length is the total compression achieved by the ETC algorithm. Let us denote it by C_n as it is the compression achieved in n steps. By looking at the above expression, ETC can be thought of as a dimension like quantity, computing the effective dimension at which the patterns in a sequence appear. To clarify, let us consider the expression for box counting dimension [218] for a set S,

$$\dim_{box}(S) = \lim_{\epsilon\to 0}\frac{\log(N_d(\epsilon))}{\log(1/\epsilon)}, \tag{8.3}$$

where $N_d(\epsilon)$ is the number of boxes of length ϵ required to cover the set S. $N_d(\epsilon) = k_1\cdot(\epsilon)^{-\dim}$, means that $N_d(\epsilon)$ scales as $(1/\epsilon)^{\dim}$.

ETC can be thought of as a dimension with the limit on the length N of the sequence approaching ∞. Let n_∞ be the total number of ETC steps required for $N\to\infty$ and

let x_∞ denote the limit[1] of per step compression, x, as $N \to \infty$.

$$n_\infty = \lim_{N\to\infty} \frac{\log(C_{n_\infty})}{\log(x_\infty)}. \tag{8.4}$$

$C_{n_\infty} = k_2 \cdot x_\infty^{n_\infty}$, means that the total compression achieved by ETC for the infinite length sequence scales as $x_\infty^{n_\infty}$. Though ETC is useful to compare the dimension at which patterns manifest, in certain scenarios, for a given pair of sequences, we may be interested in comparing the total compression C_k in some k steps when the given sequences are transformed using ETC (or NSRPS) algorithm. Here, we may compare the quantity $\log(C_k)$ which is the potential to transform/compress a given sequence in the first k iterations of the algorithm. We name this quantity the *compressive potential*, P_C. As $C_k < 1$, P_C is always < 0. Intuitively, for a fixed k, P_C attains lower values for less compressible sequences (some examples are discussed under the heading 'Example cases' below). Since C_k is a function of the sequence, we denote it as $C_k(X)$ for the sequence X. Similarly P_C is a function of X and also of k.

$P_C(X,k) = \log(C_k(X))$, where

$$C_k(X) = \left(\frac{q_1}{N}\right)\left(\frac{q_2}{N-q_1}\right)\left(\frac{q_3}{N-q_1-q_2}\right)\cdots\left(\frac{q_k}{N-q_1-q_2\ldots-q_{k-1}}\right). \tag{8.5}$$

Also, from Eq. 8.2, $P_C(X,k) = k \cdot \log(x_k(X))$, where x_k is the equivalent per step compression considering only the first k iterations of the ETC algorithm. Moreover, from Eq. 5.9, we can obtain the relation between total self-information contained in the patterns jointly occurring in the given sequence X up to the k^{th} level and $P_C(X,k)$. Let Z_k denote the the joint occurrence of paired patterns occurring at different levels of transformation of X and $G(Z_k)$ be the total self-information contained

[1]We do not have a mathematical proof that the limit exists, but we assume that it exists.

in their occurrence. Since, $G(Z_k(X)) = -\log((\frac{q_1}{N})(\frac{q_2}{N-q_1})(\frac{q_3}{N-q_1-q_2})\ldots(\frac{q_k}{N-q_1-q_2\ldots-q_{k-1}}))$ or $G(Z_k(X)) = -\log(C_k(X))$, gives us,

$$P_C(X,k) = -G(Z_k(X)); \tag{8.6}$$

P_C is a useful quantity to be computed for given sequences when only the patterns at higher levels (scales) are to be compared or the probabilities of shorter patterns are more relevant for our analysis. By fixing the steps of sequence transformation to k and computing the logarithm to the natural base, the *potential* measured is not influenced by equivalent per step compression which is different for each sequence. Hence, compressive potential of the ETC algorithm for given sequences allows for a direct comparison of the frequency of occurrence of particular sections (levels) of the joint patterns in the selected chosen steps of the algorithm.

Example cases:

The behavior of P_C is demonstrated for a few cases. Four symbolic sequences X_1, X_2, X_3 and X_4 are simulated as shown in Table 8.1. X_1 and X_2 are periodic time series, while X_3 is partly periodic, partly random and X_4 is a fully random time series. Each of the series were simulated up to a length of 10,000. The ETC value (or the number of steps) required to compress the sequences using ETC algorithm is also displayed in the table. For computation of P_C and ETC value, the time series were binned using 8 uniform sized bins.

Figure 8.3 shows the behavior of P_C for each of the sequences as k is varied. We see that, in case of X_1 (Figure 8.3(a)), for which the repeating patterns are of shortest

Table 8.1: Time series simulated to study properties of P_C.

Time series	**Composed of**	**ETC**
X_1	Repeating periodic sequence: [1 2 3 4]	3
X_2	Repeating periodic sequence: [1 2 3 . . . 1000]	95
X_3	Repeating partly periodic partly random sequence: [1 2 3 . . . 20] followed by 100 random numbers uniformly chosen from between 1 and 20	100
X_4	Uniformly randomly distributed real numbers in the range (0,1)	4110

length and the sequence is fully periodic, the ETC value obtained is 3, suggesting that the patterns reappear at the third dimension. P_C value is the highest and fastest to saturate in this case, attaining a value of -3.18 as k becomes equal to 3.

X_2 and X_3 have similar ETC values, 95 and 100 respectively, even though X_2 is completely periodic with period length 1000, while X_3 has more frequently occurring shorter periodicity of period 20, interspersed with random sequences (of length 100 time points). For X_2, P_C saturates at a value of -280.65, while for X_3, P_C saturates at a value of -317.19. Also, if we set $k = 40$, then at this k, for X_2, $P_C = -108.30$, while for X_3, $P_C = -155.17$. For the two time series, the rate at which P_C falls is also slightly different at different values of k. Thus, for X_2 and X_3, even though the ETC values are not very different, P_C values being significantly different for $k = 40$, indicate that there remains more structure in the completely periodic X_2 at the level of shorter patterns when compared to X_3. Since X_4 is completely random, ETC value is high, equal to 4110, and the P_C values are much lower compared to other time series. For instance,

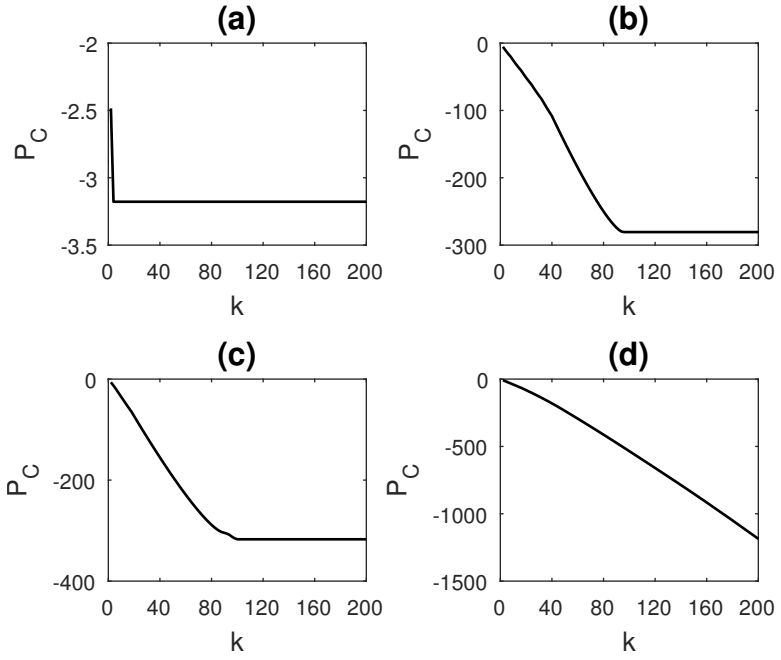

Figure 8.3: Variation of Compressive potential, P_C, with k for time series (a) X_1 (periodic with short patterns), (b) X_2 (periodic with long patterns), (c) X_3 (partly periodic, partly random) and (d) X_4 (completely random), simulated as per Table 8.1.

$P_C(X_4, k = 200) = -1186.3$ and goes on decreasing further until it is fully compressed by the ETC algorithm at $k = 4110$. In a completely random sequence, neither shorter patterns nor longer patterns exist, making the time series highly incompressible.

8.3.2 Compressive Potential based Temporal Asymmetry Measure

The measure for temporal asymmetry, A_{P_C}, of a time series X is formulated using compressive potential, P_C, as follows:

$$A_{P_C}(X, \tau, k) = P_C(X, X_\tau, k) - P_C(X', X'_\tau, k). \tag{8.7}$$

In the above equation, for binned symbolic sequence X of given time series of length

N, the quantities used in computation of A_{P_C} are as given below:

$$\begin{aligned} X_\tau(t) =& X(t+\tau), \quad 1 \leq t \leq N-\tau, \\ X'(t) =& X(N-t+1), \quad 1 \leq t \leq N-\tau, \\ X'_\tau(t) =& X'(t+\tau), \quad 1 \leq t \leq N-\tau. \end{aligned} \tag{8.8}$$

X_τ is the time-shifted (by τ points) to future analog of X, X' is the time-reversed version of the original sequence and X'_τ is the time-shifted (by τ points) to future analog of X'. For example, for a given time series $1, 2, 3, \ldots, 12$ and $\tau = 2$, we take:

$$\begin{aligned} X =& 1, 2, \ldots, 10, \\ X_\tau =& 3, 4, \ldots, 12, \\ X' =& 12, 11, \ldots, 3, \\ X'_\tau =& 10, 9, \ldots 1. \end{aligned} \tag{8.9}$$

$P_C(X, X_\tau, k)$ is the joint compressive potential of the sequences X, X_τ based on the total compression obtained by the ETC algorithm when it is allowed to run up to k iterates. $P_C(X', X'_\tau, k)$ denotes the same for sequences X', X'_τ. For computation of joint P_C, ETC algorithm is run after obtaining a single symbolic sequence using dictionary construction for the considered sequences. Dictionary construction for a set of given symbolic sequences is discussed in Section 2.3.1.

The value of the measure A_{P_c} can be either positive or negative as either forward or reversed processes can have greater compressive potential. What matters in our case is the magnitude of the difference, the larger the difference implies more different are the statistics of the forward time and time reversed processes and so the the process can be classified as being time irreversible. In order to test the significance of the obtained

A_{P_c} value for a particular kind of process, we perform surrogate analysis as is discussed in the next section.

As discussed in the Section 8.1, KLD between the joint probability distributions of forward time and time-reversed process is a measure of time-irreversibility of a given process. In fact, it is not just a statistical means of testing time-irreversibility but also has an established connection to thermodynamic entropy production along the process. A_{P_C}, computed based on joint compressive potential, also, indirectly compares joint probability distributions (by taking a sequence X and its future X_τ) of the given process and compares it with its reversed version, (X' and X'_τ). From Eq. 8.6, we have seen that the term $P_C(X,k) = -G(Z_k(X))$, that is, the compressive potential based on first k iterations is equal to the negative of total self-information contained in the joint occurrence of most dominant paired patterns occurring up to the first k levels of the transformation of the sequence. Thus, the comparison that A_{P_C} makes is not just between simple joint probability distributions (of a time sequence and its future) but joint distributions occurring jointly at all levels (scales) of the sequence (and its future). The choice of k limits the point till which the scales are taken. Most often the higher set of scales (which are the shorter patterns in the original sequence, found at lesser number of iterations of the ETC algorithm) may be most useful for our analysis. Lower set of scales (which are longer patterns in the original sequence, found at greater number of iterations of the ETC algorithm), may contribute to non-requisite details and be less reliable. This is because their frequency of occurrence cannot be measured very accurately, with the possibility of their occurrence becoming limited only to a few

times owing to the finite length of the sequence. For this reason, the limit k imposed on number of iterations is useful and helps give reliable results.

For the above reason of the fundamental similarity of A_{P_C} to KLD as well as its additional beneficial features discussed, the proposed measure of temporal asymmetry is extremely promising. Though not established yet, it is expected to have relations to thermodynamic entropy production along the process.

8.3.3 Results

The following processes were simulated for the detection of temporal irreversibilty using the proposed measure A_{P_C}.

Time-reversible processes simulated include:

1. Linear Gaussian Process (LGP), that is, Gaussian noise with distribution $\mathcal{N}(0, 1)$.

2. Autoregressive process of second order, AR(2):

$$X(t) = 0.7X(t-1) + 0.2X(t-2) + 0.03\epsilon_t, \tag{8.10}$$

   where t is the time index and ϵ_t is Gaussian white noise, $\mathcal{N}(0, 1)$.

3. Static nonlinear transformation of a first order Gaussian process, STAR(1):

$$\begin{aligned} X(t) &= \tanh^2(Y(t)), \text{ where} \\ Y(t) &= 0.6Y(t-1) + 0.03\epsilon_t, \end{aligned} \tag{8.11}$$

   where ϵ_t is Gaussian white noise, $\mathcal{N}(0, 1)$.

Time-irreversible processes simulated include:

1. Self-Exciting Threshold AR (SETAR(2;2,2)) process with two regimes, each one with second order delays:

$$X(t) = \begin{cases} 0.62 + 1.25X(t-1) - 0.43X(t-2) + 0.0381\epsilon_t & \text{if } X(t-2) \leq 3.25 \\ 2.25 + 1.52X(t-1) - 1.24X(t-2) + 0.0626\epsilon_t & \text{otherwise,} \end{cases} \tag{8.12}$$

where ϵ_t is Gaussian white noise, $\mathcal{N}(0,1)$.

2. Chaotic tent-map process:

$$X(t) = \begin{cases} 2X(t-1), & 0 \leq X(t-1) < 1/2, \\ 2 - 2X(t-1), & 1/2 \leq X(t-1) \leq 1. \end{cases} \tag{8.13}$$

A length of 10,000 time points were taken for each of the above processes for the estimation of A_{P_C}. This was after discarding off 1000 transients for all the processes. For the case of tent map alone, 2000 transients were discarded. For the computation of A_{P_C} value, the given time series were symbolized using 8 bins. The parameters for the measure were set as $\tau = 500, k = 500$.

In order to test for the statistical significance of obtained A_{P_C} for each process taken, surrogate analysis was done. For this, an ensemble of surrogate data $\{X^S\}$, consisting of 50 realizations, were constructed from the original time series using the Iterative Amplitude Adjusted Fourier Transform (IAAFT) [102]. This method preserves the power spectrum density and amplitude distribution of original data. Randomization of the Fourier phases results in the constructed surrogate ensemble with the null hypothesis of Gaussian linear stochastic process. Since Gaussian processes are time-reversible [208, 209, 219, 220], our null hypothesis, H_0, is that the considered process is time-reversible.

To assess the statistical significance of the A_{P_C} of original time series, z-test is used to to quantify its statistical deviation from A_{P_C} values obtained in the constructed ensemble of surrogate data. H_0 is rejected in favour of the alternate hypothesis of reversibility with obtained p-values being less than equal to the significance level, $\alpha = 0.05$.

Figure 8.4 displays the distribution of A_{P_C} values of surrogate data as well as a dotted line showing where the A_{P_C} value of the original time series lies for each of the processes simulated. A_{P_C} distribution of surrogates for all the processes was found to satisfy normality based on the Anderson-Darling test. For LGP, the null hypothesis is not rejected with p-value=0.50 (Figure 8.4(a)); for AR(2) process, the null hypothesis is not rejected with p-value=0.47 (Figure 8.4(b)); for STAR(1), the null hypothesis is not rejected with p-value=0.13 (Figure 8.4(c)). All these processes are time-reversible processes as per existing literature [203, 204, 221]. The obtained A_{P_C} values for these processes are not found to be significant qualifying them as reversible based on our proposed measure. For SETAR process, the null hypothesis is not rejected with p-value=0.35 (Figure 8.4(d)); and for tent-map process, the null hypothesis is rejected with p-value=4.6×10^{-8} (Figure 8.4(e)). Both these processes are statistically irreversible processes [204, 222–224]. While the tent map process is classified correctly using A_{P_C}, the method fails for the SETAR process simulated.

8.4 Discussion, Conclusions and Future Work

Causal analysis of time-reversed processes using the CCC measure reveals an interesting property of measure. The measure works symmetrically for time-forward and

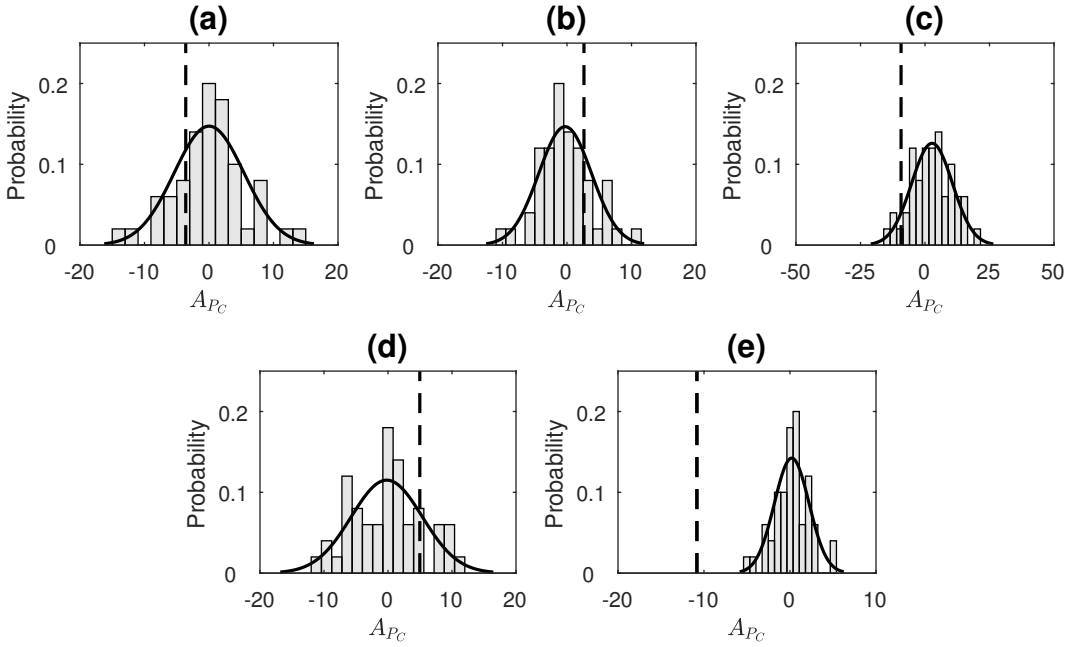

Figure 8.4: Compressive potential based temporal asymmetry test result on simulated data from processes: (a) LGP, (b) AR(2), (c) STAR(1), (d) SETAR(2;2,2) (e) Tent map. Dashed line indicates A_{P_c} value obtained for original series. Its position is indicated with respect to Gaussian curve fitted normalized histogram of surrogate A_{P_C} values that form the null hypothesis of reversible processes.Null hypothesis is not rejected in case of (a), (b), (c), (d) and rejected in case of (e).

time-reversed processes. This behavior is observed for both stochastic AR as well as deterministic chaotic processes, unlike other measures such as TE (or CMI) where symmetric behavior is noticed only for chaotic processes with dynamical memory. These results indicate that the violation of the GC assumption that the 'cause should precede the effect' does not affect the CCC measure. Thus, CCC can be applied to a broader range of processes such as microscopic processes, which are reversible and the arrow of time is not restricted to a single direction. This also allows for the possibility of CCC to be applied on quantum processes or subjective psychological processes. While quantum mechanics allows for certain processes and information to travel backwards in

time, subjective experiences such as dreams and intuitions seem to dismiss the sequential order of linear arrow of time. The possibility of these applications are as of now very speculative and would require appropriate translation of the data for implementation of CCC.

A reason as to why CCC works symmetrically is because the measure ETC that it employs, works on finding the most frequently occurring pairs in the given sequence in several iterations, transforming the original sequence at each iteration. Whether we run the ETC algorithm on forward time or reverse time windows of data (for CCC computation) typically doesn't make much of a difference as the chosen pairs for substitution remain more or less the same. In measuring the causality from $Y \to X$, what is important is the choice of the length of past windows Y_{past}, X_{past} and the future window ΔX to which there is a potential effect of the latter two (for details on these windows, please see Chapter 2, Section 2.2 and 2.3). As long as these windows are selected appropriately using the parameter selection criteria for CCC (Section 3.3), computation of ETC and hence dynamical compression-complexity which are based on the occurrence of patterns held together in these windows and not on whether the patterns occur on parsing from right to left or left to right in a sequence, determine the requisite causal influence. What this means is that once intervention has been done at the correct spot to put appropriate blocks of cause and effect dynamics from given time series together, whether the complexity of blocks is measured in forward time or in reverse time does not matter.

In the second part of the chapter, we have proposed a compressive potential based

temporal asymmetry measure for time series data which is based on the ETC algorithm. It helps to compare the forward and reverse time joint probability distributions occurring jointly at different scales (levels) of the given time series. The established relation of the proposed compressive potential measure to the total self-information contained in the joint occurrence of most dominant paired patterns, brings the asymmetry measure closer to KLD measure of temporal asymmetry. KLD is not just a statistical asymmetry measure but also is shown to be related to thermodynamic entropy production along a process, relating the obtained value of asymmetry to the physical arrow of time for the process. KLD already has some estimators based on compression algorithms such as the Ziv-Merhav estimator [215, 225]. The proposed measure is promising because of the advantages of ETC such as its better performance on short and noisy time series when compared to other complexity estimators [74, 77]. Also, some of the discussed theoretical properties of ETC by which it can account for distributions at several scales of the time series can help to provide reversibility/irreversibility information that may be hidden at different scales. The choice of the parameter k in P_C can help to fix the number of most dominant scales to take at which the most dominant probabilities are considered. The measure can also be generalized to consider some set of intermediate steps of the ETC algorithm instead of first k steps, in order to compute compressive potential based on probabilities only at these intermediate specific scales.

Out of the processes simulated for the testing of A_{P_C}, correct reversibility/irreversibility is detected for all the cases except for SETAR which was incorrectly classified as being reversible. In future work, different values of parameters k and τ will be taken to

check for improved results using A_{P_C}. Other processes such as continuous time chaotic processes (Lorenz, Rössler etc.) will be tested for reversibility. Generalized version of the measure using intermediate range of ETC steps for computation of P_C will also be tested on simulations for irreversibility detection at different scales. Further, the measure will also be tested on real data such as ecological and epidemiological time series. The difference between P_c values as a means to compare distributions (not just forward time and reverse time distributions of a single time series) is also left for future work. It will also be interesting to explore the relationship between P_c and different types of fractal dimensions.

Chapter 9

Conclusions

This chapter summarizes the thesis and its contributions. Some open problems and future research directions are also discussed.

9.1 Summary of Research

This thesis addresses the gaps identified in the literature on causality estimation from time-series. Causality analysis from temporal data is of immense importance in today's world of making inferences based on recorded measurements. For systems such as the human brain or the environment of a particular place in which there are several variables of interest, intervention into the system is either not practical or may have ethical implications. As a result, causality measures which can be applied on acquired data are being used widely. These methods are either data-driven or model-based, with the latter type making some assumptions about the underlying model generating the data.

The adaption of the ladder of causation introduced in the context of artificial intelligence [15] to time-series causality estimation methods helped to reveal that existing

data-driven causality measures are still on the lowermost rung on the ladder, that is, the rung of *association*. To address the gap of the inability of data-driven measures to ascertain causality using *interventional* means (which is a higher rung on the ladder of causation), we introduced a novel Interventional Complexity Causality (ICC) scheme in this thesis. While the scheme can employ any complexity measure to estimate causality, in the thesis, we use the *Effort-to-Compress (ETC)* complexity measure in order to develop a Compression-Complexity Causality (CCC) measure. As it is on a higher level of causation, the measure is expected to be better in comparison to existing approaches. Testing of CCC on simulations showed that it accomplished our objective of overcoming a number of limitations of existing data-driven approaches. Further, applications of CCC on real data demonstrate that it can be applied for a variety of datasets to make useful inferences.

The other set of objectives of the thesis focused on how the science of time series causality estimation could advance theoretical and empirical understanding in related domains. The areas of chaotic synchronization and compressed sensing (of coupled sparse signals) benefited from this work directly. Some of this research made direct use of the CCC measure and its properties, some made use of other existing causality measures, and some of it utilized general concepts in causality testing.

Thus, the thesis is a synthesis of theoretical and empirical contributions in domain of time-series causality estimation and the use of these contributions to make theoretical and empirical advances in allied disciplines. The specific contributions made by the thesis are enlisted in the next section.

9.2 Contributions of this Thesis

The unique contributions made by this thesis are as follows:

1. **Interventional Complexity Causality (ICC) scheme**: The scheme is proposed to estimate data-driven causality which is interventional in nature and by construction higher than existing data-driven causality measures on the ladder of causation. Some of the properties/benefits of this approach are given below:

    - This approach allows for doing *surgery* on provided time series that is a means for intervention in the given system.
    - It makes use of proposed novel *dynamical complexity* measure that allows to capture influences in the system based on dynamical evolution of processes that are not merely estimated by correlation/joint occurrence of observed samples in time series.
    - It is generic and can make use of any complexity measure, thereby allowing a number of causality measures to be developed based on this idea.

2. **Compression-Complexity Causality (CCC) measure**: The measure was formulated by employing the Effort-to-Compress measure to compute complexity in the ICC scheme. ETC is a measure of compression-complexity. Properties/ benefits of CCC are discussed as under:

    - CCC does not make any assumptions of linearity/ non-linearity, markovianity, gaussianity, stochasticity/determinism or stationarity on the data.

- The point of intervention for CCC is adaptively determined for given data based on the scale at which causality exists between given processes. Data-adapted parameter selection criteria is developed to determine the parameters of CCC including the intervention point.
- CCC can be both positive and negative. Unlike any other data-driven measure, this property helps determine the *kind* of dynamical influence that a cause time-series brings to the effect time-series with respect to the past of the latter. This property can be useful to control the dynamics of a given system.
- It is shown using simulations of coupled autoregressive and chaotic processes that CCC is robust to noise, low temporal resolution, filtering and decimation, non-uniform sampling, long-term memory processes as well as finite length signals. Further, its comparison with existing data-driven approaches – Granger Causality (GC), Transfer Entropy, Nonlinear Granger Causality and Convergent Cross Mapping demonstrate that CCC overcomes the limitations of existing measures in a number of cases of the simulations done above.
- Significance testing procedure based on surrogate data is introduced for the measure CCC. Since CCC can be both positive and negative, surrogate analysis revealed that a high value of CCC may not necessarily imply the existence of causality.

3. **Causal inferences for real-world systems**: We demonstrate the use of CCC in a number of real-world systems. Though, most of the demonstrated applications are in the domain of neuroscience, CCC can be readily applied to time-series from any discipline. The strength of CCC as revealed by its performance on downsampled, non-uniformly sampled systems as well as on systems in which the cause and effect time series are sampled differently suggests that CCC can be used to estimate causality between time series which are evolving at different time scales. This is of immense importance in real-world processes such as climatological processes. The applications tested for include:

    - Causal influences between predator (didinium) and prey (paramecium) populations in an ecosystem.
    - Causality between simulation current and voltage recordings across squid giant axon.
    - Functional connectivity analysis between selected brain regions involved in movement when 5 human subjects performed a novel hand reaching task. The connectivity was estimated using electroencephalographic signals and compared across four different phases of movement: fixation, instruction, planning and movement.
    - Distinguishing between the level of *consciousness* in the brain during awake and anaesthesia states in four monkeys using electrocorticograhic recordings. For this, a novel *Network Causal Activity* measure was proposed that helped

compare the number of significant causal connections present in the brain in the two states.

4. **CCC for networks**: Formulation for *effective* CCC was provided in order to detect causal connections present in networks. In order to make its computation easier, the concept of *equivalent* ETC was introduced and its mathematical formulation discussed.

    - Effective CCC was applied to directed acyclic graph networks comprising of four variables exhibiting autoregressive dynamics. Comparison of results with multivariate Granger Causality on the above simulated networks demonstrate that effective CCC performance is promising for short, noisy and long range memory processes.

5. **Causal perspective on chaotic synchronization**: Synchronization of chaotic systems is a ubiquitous phenomenon, found to occur in specialized electronic circuits, optical arrays, biological neurons, social networks, superconductors, and other biological and physical systems. Synchronization of such coupled systems depends on a number of factors such as the nature of systems, the variable(s) used for coupling and the kind of coupling. While a number of temporal conditions have been proposed to determine if the given systems will proceed to synchronization [68, 69], to the best of our knowledge, there exist no *spatial* conditions for the same. Causality testing was used to establish the following in this regard:

- A novel concept of *causal stability* was proposed and the *causal stability synchronization theorem* was formulated and proved to be a necessary and sufficient condition for complete synchronization. The criterion of causal stability is generic and can be established using any existing data-driven causality measure. In this work, the theorem was verified for the case of unidirectionally coupled Lorenz systems using the CCC measure.
- An empirical condition to check for synchronizing variables in unidirectionally coupled identical systems was developed. The sign of net CCC value from the coupled variable to the non-driven subsystem determined whether a slave coupled to the master will be driven to synchronization. Time series obtained from the master system alone could be used to check for this condition. This condition was checked for a number of simulated systems including Hindmarsh-Rose chaotic neuronal model.
- The proposed conditions are an important contribution for the control of chaos in networks where we do not know the underlying mechanism and wish to inhibit/facilitate synchronization between systems. These are expected to have applications in real-world systems such as the brain.

6. **Causality detection for anticipating synchronization**: It is a challenging task to determine the correct causality direction for chaotic systems exhibiting anticipating synchronization as in these systems the slave begins to anticipate the master. It is shown with the use of simulated tent map systems that GC

fails to determine the correct causality direction for anticipating systems. Results obtained using CCC on these systems indicate that the measure if implemented on adequately high resolution data (by using a higher number of bins), can correctly detect the dominant direction of causality between such systems.

- Use of an appropriate measure to determine phase along with causality determined by CCC can help to determine the presence of anticipating synchronization in coupled systems.

7. **Causality analysis for sparse signals**: The technique of *compressed sensing* is used to acquire, store and transmit many naturally occurring signals which are *sparse* in some domain. We have proposed structured sensing matrices – *Toeplitz* and *Circulant*, that help to preserve causality as computed using GC in the compressive domain for such sparse signals. These matrices are recommended for sensing in order to:

   - Determine causality in the compressive domain, saving the computational cost of reconstruction of signals. Extensive analysis is done on coupled sparse autoregressive processes to demonstrate that GC remains intact when partially or fully structured matrices are used for sensing.
   - For some sparse signals such as neural signals, it may be impossible to determine causal relations directly using data-driven measures. To the best of our knowledge, only model-based methods have been employed to determine coupling between sparse signals. We demonstrate for the case of real sparse

neuronal spike train recordings obtained from the rat prefrontal cortex that when structured sensing matrices are used to obtain their compressive counterparts, GC can be used to infer causality from the compressive domain signals.

8. **Causality for time-reversed processes**: It is observed that the CCC measure works symmetrically for the original time-forward coupled processes and when these processes are reversed in time. Unlike other data-driven measures such as Transfer Entropy, where this property holds only for deterministic chaotic processes; for CCC, it is true not only for deterministic chaotic processes but also for stochastic autoregressive processes. It can thus be said that CCC does **not** make an assumption of 'cause preceding the effect'.

    - This finding opens the use of CCC to a broad range of processes, such as microscopic processes, which are reversible and where the arrow of time is not restricted to a single direction.

9. **Detection of temporal reversibility**: Time-reversibility of processes is closely linked to the domain of causality as many existing causality measures make the assumption that the cause precedes the effect. We propose a novel *compressive potential* based temporal asymmetry measure to detect for temporal reversibility of given processes. The measure helps to compare the forward and reverse time joint probability distributions occurring jointly at different *scales* of the given time series. Some of the properties of the measure are as below:

- The measure when tested on a number of time reversible and irreversible simulated processes gives promising results.
- It is conjectured to have close links to Kullback-Leibler measure of temporal asymmetry [213,215] which is shown to be related to thermodynamic entropy production (and hence the physical arrow of time) along a given process.

9.3 Future Research Directions and Open Problems

Future research directions arising out of work presented in each chapter are discussed in detail at the end of the chapters. Some of these directions for future research are summarized below:

1. To explore the use of complexity measures other than ETC to develop novel causality measures based on the ICC scheme. One promising candidate for this is the Lempel-Ziv complexity measure which just like ETC, measures compression-complexity.

2. Parameter selection criteria for the CCC measure can be refined further. This can be done by introducing better binning strategies (such as equiquantization binning) compared to the currently used uniform binning. Also, better optimization strategies can be used to fix the different window lengths. One of the means by which this can be done is by looking at the separation of ETC hyperplanes in a high dimensional space in which the different dimensions comprise of one or more of the parameters used in CCC estimation: the two window lengths that

determine past and present chunks of time series as well as the step size.

3. Developing a method to compute effective CCC for networks with bidirectional connections. Extension of the proposed effective CCC method to large networks (> 5 variables) also needs to be tested.

4. The analysis done on determining brain connectivity during motor task can be improved in a number of ways: source localization of EEG signals should be done in order to remove volume conduction effects; conditional/effective causality estimation should be done in order to remove indirect influences; analysis can be made more rigorous by extending to more number of subjects and by taking more trials per subject; more connections can be considered between the brain regions taken and further more brain regions can be included in the analysis. It would also be interesting to do a comparison of connectivity for slow hand movement task (as taken in this study) with fast hand movement performed by the subjects.

5. Network Causal Activity measure used for distinguishing between awake and anaesthesia state in monkeys should be formulated based on effective CCC measure that works for large networks. Also, we would like to apply the measure for different stages of sleep and other states of consciousness (such as coma, vegetative state etc.) in order to determine its ability to distinguish between the different levels of consciousness in each of these states.

6. Generalization of the causal stability synchronization theorem to forms of synchro-

nization other than complete synchronization, such as generalized synchronization and phase synchronization.

7. Explore the relationship between the *sign* of net causal influence estimated using CCC for synchronizing variables and the conditional Lyapunov exponent of the corresponding non-driven slave subsystem. The condition on Lyapunov exponents is an existing temporal condition for synchronization [68].

8. Investigating other different types of compressed sensing matrices that help preserve GC and others that can help preserve Transfer Entropy and CCC of sparse signals in compressive domain. Extending sparse signal causality analysis to networks and testing the same on real data.

9. Parameter tuning to improvise the performance of compressive potential based asymmetry measure which has been developed in order to detect time-irreversibility of given processes. The measure will also be tested on real data. Finally, we would like to explore its exact relation to the Kullback Leibler divergence based temporal asymmetry measure which has close links to the physical arrow of time.

Some other interesting open problems encountered during the course of the thesis are listed below:

1. Developing techniques to combine model-based and data-driven measures of time series causality estimation in order to improve the working of the two techniques.

2. Using time-series based causality estimation to develop causal learning algorithms with the aim of improving current artificial intelligence technology.

Appendix A

Transfer entropy results for coupled AR(100) processes

Results for Transfer Entropy (TE) estimation for coupled autoregressive AR(100) processes with number of lags to take for the observed processes set to 110 are displayed in Figure A.1. Results are displayed as mean values over 20 trials. TE computation was done using the MuTE toolbox [90]. The processes were simulated using Eq. 3.2 with all settings as in Section 3.2.1.

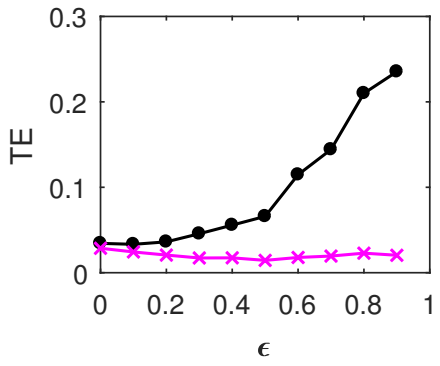

Figure A.1: Mean causality values estimated using TE (with the number of lags to take for the observed processes set to 110) for coupled AR(100) processes, from Y to X (solid line-circles, black) and X to Y (solid line-crosses, magenta/ grey in print) as the degree of coupling, ϵ is varied.

Compare this with Figure 3.3, where the lags to consider for TE computation are

set to 5. There is a definite improvement in the results when lags are set appropriately to a higher order for TE. Even though finite positive values are obtained for causation from X to Y in Figure A.1, these values can be clearly distinguished from the causality values obtained from Y to X. The latter values are higher than the former, showing an increasing trend with increasing coupling.

Appendix B

Contralateral-ipsilateral connectivity analysis between premotor and motor regions

Brain connectivity analysis during different phases of a motor task has been done in Section 4.3. Results for connectivity between premotor and motor regions on the side contralateral as well as ipsilateral to the movement are discussed in Section 4.3.2. Here, CCC as well as Non-linear Granger Causality (NGC) have been used to analyze the causality between premotor and motor regions (both directions) contralateral to the movement (FC1 and C3), ipsilateral to the movement (FC2 and C4) as well as cross connections between the contralateral premotor region and ipsilateral motor region as well as between ipsilateral premotor region and contralateral motor region. These four connections in both directions were analyzed for all the 5 subjects for the four phases considered. The variation in the connectivity with the phases for these four connections are shown in Figures B.1-B.4.

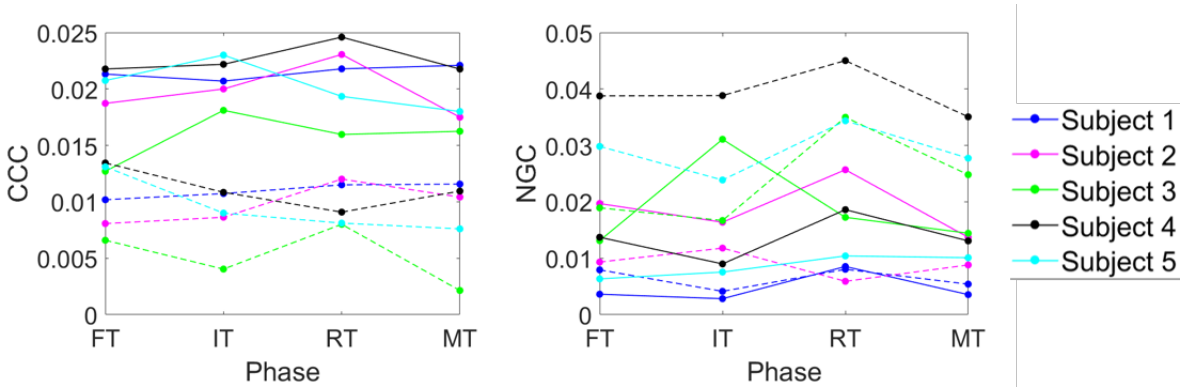

Figure B.1: Connectivity analysis for all the subjects using CCC (left) and NGC (right) between signals obtained from the electrode pair: contralateral premotor - contralateral motor. Results are displayed as a variation in connectivity with a variation in the phases, which occur in the following successive order: (1) Fixation Time or FT, (2) Instruction Time or IT, (3) Reaction Time or RT, (4) Movement Time or MT. Premotor to motor connectivity variation is indicated using solid lines and motor to premotor connectivity variation is indicated using dashed lines.

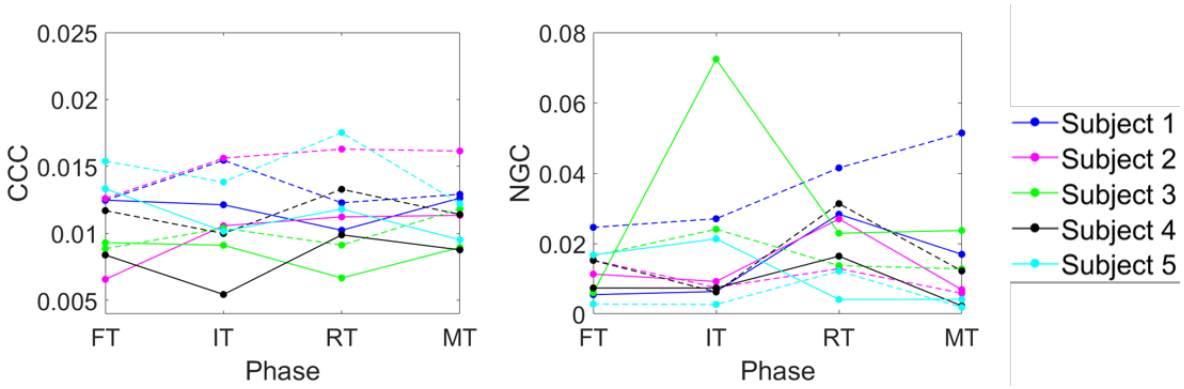

Figure B.2: Connectivity analysis for all the subjects using CCC (left) and NGC (right) between signals obtained from the electrode pair: ipsilateral premotor - ipsilateral motor. Results are displayed as a variation in connectivity with a variation in the phases, which occur in the following successive order: (1) Fixation Time or FT, (2) Instruction Time or IT, (3) Reaction Time or RT, (4) Movement Time or MT. Premotor to motor connectivity variation is indicated using solid lines and motor to premotor connectivity variation is indicated using dashed lines.

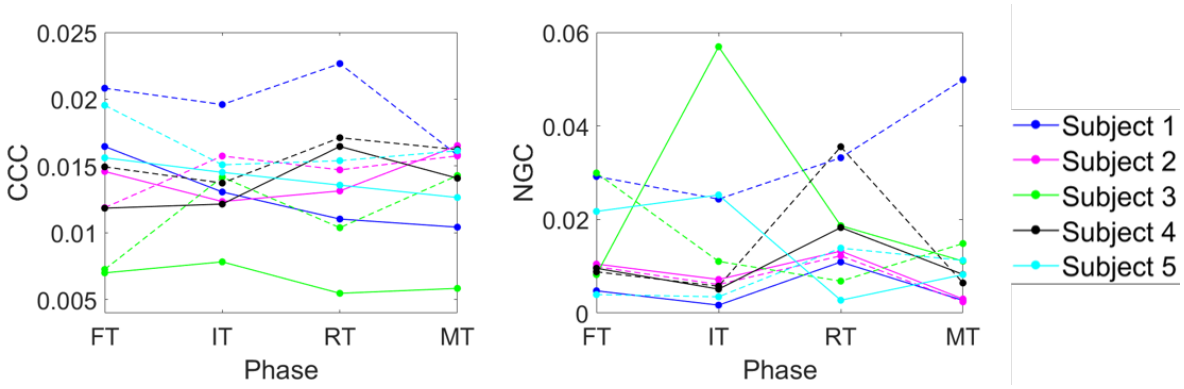

Figure B.3: Connectivity analysis for all the subjects using CCC (left) and NGC (right) between signals obtained from the electrode pair: contralateral premotor - ipsilateral motor. Results are displayed as a variation in connectivity with a variation in the phases, which occur in the following successive order: (1) Fixation Time or FT, (2) Instruction Time or IT, (3) Reaction Time or RT, (4) Movement Time or MT. Premotor to motor connectivity variation is indicated using solid lines and motor to premotor connectivity variation is indicated using dashed lines.

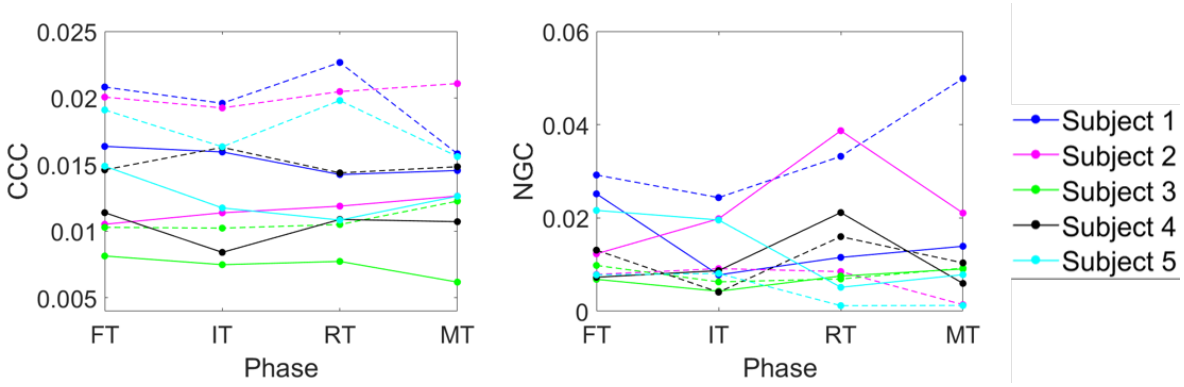

Figure B.4: Connectivity analysis for all the subjects using CCC (left) and NGC (right) between signals obtained from the electrode pair: ipsilateral premotor - contralateral motor. Results are displayed as a variation in connectivity with a variation in the phases, which occur in the following successive order: (1) Fixation Time or FT, (2) Instruction Time or IT, (3) Reaction Time or RT, (4) Movement Time or MT. Premotor to motor connectivity variation is indicated using solid lines and motor to premotor connectivity variation is indicated using dashed lines.

References

[1] D. R. Cox and N. Wermuth, "Causality: A statistical view," *International Statistical Review*, vol. 72, no. 3, pp. 285–305, 2004.

[2] I. J. Good, "A causal calculus (i)," *The British journal for the philosophy of science*, vol. 11, no. 44, pp. 305–318, 1961.

[3] ——, "A causal calculus (ii)," *The British journal for the philosophy of science*, vol. 12, no. 45, pp. 43–51, 1962.

[4] P. Suppes, "A probabilistic theory of causation," 1970.

[5] C. Granger, "Investigating causal relations by econometric models and cross-spectral methods," *Econometrica*, vol. 37, no. 3, pp. 424–438, 1969.

[6] T. Schweder, "Composable markov processes," *Journal of applied probability*, vol. 7, no. 2, pp. 400–410, 1970.

[7] O. O. Aalen, "Dynamic modelling and causality," *Scandinavian Actuarial Journal*, vol. 1987, no. 3-4, pp. 177–190, 1987.

[8] R. A. Fisher, "The arrangement of field experiments," *Journal of the Ministry of Agriculture Great Britain*, vol. 33, pp. 503–513, 1926.

[9] ——, "Design of experiments," 1935.

[10] D. B. Rubin, "Estimating causal effects of treatments in randomized and nonrandomized studies." *Journal of educational Psychology*, vol. 66, no. 5, p. 688, 1974.

[11] S. Wright, "Correlation and causation," *Journal of Agricultural Research*, vol. 20, pp. 557–585, 1921.

[12] ——, "The method of path coefficients," *The annals of mathematical statistics*, vol. 5, no. 3, pp. 161–215, 1934.

[13] W. G. Cochran and S. P. Chambers, "The planning of observational studies of human populations," *Journal of the Royal Statistical Society. Series A (General)*, vol. 128, no. 2, pp. 234–266, 1965.

[14] J. Pearl, *Causality: models, reasoning and inference*. Springer, 2000, vol. 29.

[15] J. Pearl and D. Mackenzie, *The book of why: the new science of cause and effect*. Basic Books, 2018.

[16] A. K. Seth, A. B. Barrett, and L. Barnett, "Granger causality analysis in neuroscience and neuroimaging," *Journal of Neuroscience*, vol. 35, no. 8, pp. 3293–3297, 2015.

[17] R. Vicente, M. Wibral, M. Lindner, and G. Pipa, "Transfer entropy: a model-free measure of effective connectivity for the neurosciences," *Journal of computational neuroscience*, vol. 30, no. 1, pp. 45–67, 2011.

[18] A. Stips, D. Macias, C. Coughlan, E. Garcia-Gorriz, and X. San Liang, "On the causal structure between CO_2 and global temperature," *Scientific reports*, vol. 6, 2016.

[19] T. J. Mosedale, D. B. Stephenson, M. Collins, and T. C. Mills, "Granger causality of coupled climate processes: Ocean feedback on the north atlantic oscillation," *Journal of climate*, vol. 19, no. 7, pp. 1182–1194, 2006.

[20] C. Hiemstra and J. D. Jones, "Testing for linear and nonlinear granger causality in the stock price-volume relation," *The Journal of Finance*, vol. 49, no. 5, pp. 1639–1664, 1994.

[21] S. Z. Chiou-Wei, C.-F. Chen, and Z. Zhu, "Economic growth and energy consumption revisited: evidence from linear and nonlinear granger causality," *Energy Economics*, vol. 30, no. 6, pp. 3063–3076, 2008.

[22] M. Bauer, J. W. Cox, M. H. Caveness, J. J. Downs, and N. F. Thornhill, "Finding the direction of disturbance propagation in a chemical process using transfer entropy," *IEEE transactions on control systems technology*, vol. 15, no. 1, pp. 12–21, 2007.

[23] T. Schreiber, "Measuring information transfer," *Physical Review Letters*, vol. 85, no. 2, pp. 461–464, 2000.

[24] D. Marinazzo, M. Pellicoro, and S. Stramaglia, "Kernel method for nonlinear granger causality," *Physical Review Letters*, vol. 100, no. 14, p. 144103, 2008.

[25] X. Liang, "Unraveling the cause-effect relation between time series," *Physical Review E*, vol. 90, no. 5, p. 052150, 2014.

[26] X. San Liang, "Information flow and causality as rigorous notions ab initio," *Physical Review E*, vol. 94, no. 5, p. 052201, 2016.

[27] N. Wiener, "The theory of prediction," *Modern mathematics for engineers*, vol. 1, pp. 125–139, 1956.

[28] G. Sugihara, R. May, H. Ye, C. Hsieh, and E. Deyle, "Detecting causality in complex ecosystems," *Science*, vol. 338, no. 3, pp. 496–500, 2012.

[29] D. Harnack, E. Laminski, M. Schünemann, and K. R. Pawelzik, "Topological causality in dynamical systems," *Physical review letters*, vol. 119, no. 9, p. 098301, 2017.

[30] C. Chatfield, *The analysis of time series: an introduction*. Chapman and Hall/CRC, 2003.

[31] L. Barnett and A. K. Seth, "The MVGC multivariate granger causality toolbox: a new approach to granger-causal inference," *Journal of neuroscience methods*, vol. 223, pp. 50–68, 2014.

[32] T. W. Anderson, *The statistical analysis of time series*. John Wiley & Sons, 2011, vol. 19.

[33] U. Triacca, "Is granger causality analysis appropriate to investigate the relationship between atmospheric concentration of carbon dioxide and global surface air temperature?" *Theoretical and applied climatology*, vol. 81, no. 3-4, pp. 133–135, 2005.

[34] M. C. McGraw and E. A. Barnes, "Memory matters: A case for granger causality in climate variability studies," *Journal of climate*, vol. 31, no. 8, pp. 3289–3300, 2018.

[35] A. Krakovská, J. Jakubík, M. Chvosteková, D. Coufal, N. Jajcay, and M. Paluš, "Comparison of six methods for the detection of causality in a bivariate time series," *Physical Review E*, vol. 97, no. 4, p. 042207, 2018.

[36] P. Spirtes and K. Zhang, "Causal discovery and inference: concepts and recent methodological advances," in *Applied informatics*, vol. 3, no. 1. Springer, 2016, p. 3.

[37] H. Nalatore, M. Ding, and G. Rangarajan, "Mitigating the effects of measurement noise on granger causality," *Physical Review E*, vol. 75, no. 3, p. 031123, 2007.

[38] L. Barnett, A. B. Barrett, and A. K. Seth, "Granger causality and transfer entropy are equivalent for gaussian variables," *Physical review letters*, vol. 103, no. 23, p. 238701, 2009.

[39] T. Dimpfl and F. J. Peter, "Using transfer entropy to measure information flows between financial markets," *Studies in Nonlinear Dynamics & Econometrics*, vol. 17, no. 1, pp. 85–102, 2013.

[40] D. Smirnov and B. Bezruchko, "Spurious causalities due to low temporal resolution: Towards detection of bidirectional coupling from time series," *EPL (Europhysics Letters)*, vol. 100, no. 1, p. 10005, 2012.

[41] M. Dhamala, G. Rangarajan, and M. Ding, "Estimating granger causality from fourier and wavelet transforms of time series data," *Physical review letters*, vol. 100, no. 1, p. 018701, 2008.

[42] Y. Chen, G. Rangarajan, J. Feng, and M. Ding, "Analyzing multiple nonlinear time series with extended granger causality," *Physics Letters A*, vol. 324, no. 1, pp. 26–35, 2004.

[43] L. Barnett and A. K. Seth, "Granger causality for state-space models," *Physical Review E*, vol. 91, no. 4, p. 040101, 2015.

[44] J. Shawe-Taylor, N. Cristianini *et al.*, *Kernel methods for pattern analysis*. Cambridge university press, 2004.

[45] D. Marinazzo, W. Liao, H. Chen, and S. Stramaglia, "Nonlinear connectivity by granger causality," *Neuroimage*, vol. 58, no. 2, pp. 330–338, 2011.

[46] W. Liao, D. Marinazzo, Z. Pan, Q. Gong, and H. Chen, "Kernel granger causality mapping effective connectivity on fMRI data," *IEEE transactions on medical imaging*, vol. 28, no. 11, pp. 1825–1835, 2009.

[47] F. Takens, "Detecting strange attractors in turbulence," in *Dynamical systems and turbulence, Warwick 1980*. Springer, 1981, pp. 366–381.

[48] D. Mønster, R. Fusaroli, K. Tylén, A. Roepstorff, and J. F. Sherson, "Causal inference from noisy time-series data - Testing the convergent cross-mapping algorithm in the presence of noise and external influence," *Future Generation Computer Systems*, vol. 73, pp. 52–62, 2017.

[49] K. Schiecke, B. Pester, M. Feucht, L. Leistritz, and H. Witte, "Convergent cross mapping: Basic concept, influence of estimation parameters and practical application," in *2015 37th Annual International Conference of the IEEE Engineering in Medicine and Biology Society (EMBC)*. IEEE, 2015, pp. 7418–7421.

[50] H. Ye, E. R. Deyle, L. J. Gilarranz, and G. Sugihara, "Distinguishing time-delayed causal interactions using convergent cross mapping," *Scientific reports*, vol. 5, p. 14750, 2015.

[51] E. H. Van Nes, M. Scheffer, V. Brovkin, T. M. Lenton, H. Ye, E. Deyle, and G. Sugihara, "Causal feedbacks in climate change," *Nature Climate Change*, vol. 5, no. 5, pp. 445–448, 2015.

[52] L. A. Baccalá and K. Sameshima, "Partial directed coherence: a new concept in neural structure determination," *Biological cybernetics*, vol. 84, no. 6, pp. 463–474, 2001.

[53] M. Kamiński, M. Ding, W. A. Truccolo, and S. L. Bressler, "Evaluating causal relations in neural systems: Granger causality, directed transfer function and statistical assessment of significance," *Biological cybernetics*, vol. 85, no. 2, pp. 145–157, 2001.

[54] A. Korzeniewska, M. Mańczak, M. Kamiński, K. J. Blinowska, and S. Kasicki, "Determination of information flow direction among brain structures by a modified directed transfer function (dDTF) method," *Journal of neuroscience methods*, vol. 125, no. 1-2, pp. 195–207, 2003.

[55] A. Krakovská and F. Hanzely, "Testing for causality in reconstructed state spaces by an optimized mixed prediction method," *Physical Review E*, vol. 94, no. 5, p. 052203, 2016.

[56] K. Friston, L. Harrison, and W. Penny, "Dynamic causal modelling," *Neuroimage*, vol. 19, no. 4, pp. 1273–1302, 2003.

[57] D. A. Smirnov, "Spurious causalities with transfer entropy," *Physical Review E*, vol. 87, no. 4, p. 042917, 2013.

[58] J. Runge, S. Bathiany, E. Bollt, G. Camps-Valls, D. Coumou, E. Deyle, C. Glymour, M. Kretschmer, M. D. Mahecha, J. Muñoz-Marí *et al.*, "Inferring causation from time series in earth system sciences," *Nature communications*, vol. 10, no. 1, pp. 1–13, 2019.

[59] B. Schölkopf, "Causality for machine learning," *arXiv preprint arXiv:1911.10500*, 2019.

[60] Y. C. Hung and C. K. Hu, "Chaotic communication via temporal transfer entropy," *Physical review letters*, vol. 101, no. 24, p. 244102, 2008.

[61] M. Prokopenko, J. T. Lizier, and D. C. Price, "On thermodynamic interpretation of transfer entropy," *Entropy*, vol. 15, no. 2, pp. 524–543, 2013.

[62] R. E. Spinney, J. T. Lizier, and M. Prokopenko, "Transfer entropy in physical systems and the arrow of time," *Physical Review E*, vol. 94, no. 2, p. 022135, 2016.

[63] M. Staniek and K. Lehnertz, "Symbolic transfer entropy," *Physical Review Letters*, vol. 100, no. 15, p. 158101, 2008.

[64] M. Paluš, V. Komárek, Z. Hrnčíř, and K. Štěrbová, "Synchronization as adjustment of information rates: detection from bivariate time series," *Physical Review E*, vol. 63, no. 4, p. 046211, 2001.

[65] E. J. Candès and M. B. Wakin, "An introduction to compressive sampling," *IEEE signal processing magazine*, vol. 25, no. 2, pp. 21–30, 2008.

[66] Z. Chen, D. F. Putrino, S. Ghosh, R. Barbieri, and E. N. Brown, "Statistical inference for assessing functional connectivity of neuronal ensembles with sparse spiking data," *IEEE transactions on neural systems and rehabilitation engineering*, vol. 19, no. 2, pp. 121–135, 2010.

[67] C. Zhang, Y. Chai, X. Guo, M. Gao, D. Devilbiss, and Z. Zhang, "Statistical learning of neuronal functional connectivity," *Technometrics*, vol. 58, no. 3, pp. 350–359, 2016.

[68] L. M. Pecora and T. L. Carroll, "Synchronization in chaotic systems," *Physical review letters*, vol. 64, no. 8, p. 821, 1990.

[69] R. He and P. G. Vaidya, "Analysis and synthesis of synchronous periodic and chaotic systems," *Physical Review A*, vol. 46, no. 12, p. 7387, 1992.

[70] K. Budhathoki and J. Vreeken, "Causal inference by compression," in *2016 IEEE 16th International Conference on Data Mining (ICDM)*. IEEE, 2016, pp. 41–50.

[71] A. Wieczorek and V. Roth, "Causal compression," *arXiv preprint arXiv:1611.00261*, 2016.

[72] T. M. Cover and J. A. Thomas, *Elements of information theory*. John Wiley & Sons, 2012.

[73] N. Nagaraj and K. Balasubramanian, "Three perspectives on complexity: entropy, compression, subsymmetry," *Eur. Phys. Journal Spec. Topics*, vol. 226, no. 15, pp. 3251–3272, 2017.

[74] ——, "Dynamical complexity of short and noisy time series," *The European Physical Journal Special Topics*, pp. 1–14, 2017.

[75] R. L. Cilibrasi, "Statistical inference through data compression," 2007.

[76] A. Lempel and J. Ziv, "On the complexity of finite sequences," *IEEE Transactions on information theory*, vol. 22, no. 1, pp. 75–81, 1976.

[77] N. Nagaraj, K. Balasubramanian, and S. Dey, "A new complexity measure for time series analysis and classification," *The European Physical Journal Special Topics*, vol. 222, no. 3-4, pp. 847–860, 2013.

[78] J. Rissanen, "Modeling by shortest data description," *Automatica*, vol. 14, no. 5, pp. 465–471, 1978.

[79] K. Balasubramanian and N. Nagaraj, "Aging and cardiovascular complexity: effect of the length of RR tachograms," *PeerJ*, vol. 4, p. e2755, 2016.

[80] M. Virmani and N. Nagaraj, "A novel perturbation based compression complexity measure for networks," *Heliyon*, vol. 5, no. 2, p. e01181, 2019.

[81] W. Ebeling and M. A. Jiménez-Montaño, "On grammars, complexity, and information measures of biological macromolecules," *Mathematical Biosciences*, vol. 52, no. 1-2, pp. 53–71, 1980.

[82] N. J. Larsson and A. Moffat, "Off-line dictionary-based compression," *Proceedings of the IEEE*, vol. 88, no. 11, pp. 1722–1732, 2000.

[83] A. B. Barrett and L. Barnett, "Granger causality is designed to measure effect, not mechanism," *Frontiers in neuroinformatics*, vol. 7, p. 6, 2013.

[84] G. H. Glover, "Overview of functional magnetic resonance imaging," *Neurosurgery Clinics*, vol. 22, no. 2, pp. 133–139, 2011.

[85] S. G. Kim, W. Richter, and K. Uurbil, "Limitations of temporal resolution in functional MRI," *Magnetic resonance in medicine*, vol. 37, no. 4, pp. 631–636, 1997.

[86] I. M. de Abril, J. Yoshimoto, and K. Doya, "Connectivity inference from neural recording data: Challenges, mathematical bases and research directions," *Neural Networks*, 2018.

[87] A. Moberg, D. M. Sonechkin, K. Holmgren, N. M. Datsenko, and W. Karlén, "Highly variable northern hemisphere temperatures reconstructed from low-and high-resolution proxy data," *Nature*, vol. 433, no. 7026, p. 613, 2005.

[88] E. Baumöhl and T. Vỳrost, "Stock market integration: Granger causality testing with respect to nonsynchronous trading effects," *Finance a Uver*, vol. 60, no. 5, p. 414, 2010.

[89] M. Teplan, "Fundamentals of EEG measurement," *Measurement science review*, vol. 2, no. 2, pp. 1–11, 2002.

[90] A. Montalto, L. Faes, and D. Marinazzo, "MuTE: a matlab toolbox to compare established and novel estimators of the multivariate transfer entropy," *PloS one*, vol. 9, no. 10, p. e109462, 2014.

[91] P. Laguna, G. B. Moody, and R. G. Mark, "Power spectral density of unevenly sampled data by least-square analysis: performance and application to heart rate signals," *IEEE Transactions on Biomedical Engineering*, vol. 45, no. 6, pp. 698–715, 1998.

[92] D. Marinazzo, M. Pellicoro, and S. Stramaglia, "Kernel granger causality and the analysis of dynamical networks," *Physical review E*, vol. 77, no. 5, p. 056215, 2008.

[93] D. Marinazzo, "Kernel granger causality," https://github.com/danielemarinazzo/KernelGrangerCausality, 2008.

[94] A. Krakovská, J. Jakubík, H. Budáčová, and M. Holecyová, "Causality studied in reconstructed state space. examples of uni-directionally connected chaotic systems," *arXiv preprint arXiv:1511.00505*, 2015.

[95] S. Bajaj, B. M. Adhikari, K. J. Friston, and M. Dhamala, "Bridging the gap: Dynamic causal modeling and granger causality analysis of resting state functional magnetic resonance imaging," *Brain connectivity*, vol. 6, no. 8, pp. 652–661, 2016.

[96] D. Paydarfar, D. B. Forger, and J. R. Clay, "Noisy inputs and the induction of on–off switching behavior in a neuronal pacemaker," *Journal of Neurophysiology*, vol. 96, no. 6, pp. 3338–3348, 2006.

[97] A. L. Goldberger, L. A. Amaral, L. Glass, J. M. Hausdorff, P. C. Ivanov, R. G. Mark, J. E. Mietus, G. B. Moody, C.-K. Peng, and H. E. Stanley, "Physiobank, physiotoolkit, and physionet," *Circulation*, vol. 101, no. 23, pp. e215–e220, 2000.

[98] B. G. Veilleux, "The analysis of a predatory interaction between didinium and paramecium," *Master's thesis. University of Alberta, Edmondton*, 1976.

[99] C. Jost and S. P. Ellner, "Testing for predator dependence in predator-prey dynamics: a non-parametric approach," *Proceedings of the Royal Society of London B: Biological Sciences*, vol. 267, no. 1453, pp. 1611–1620, 2000.

[100] D. N. Politis and J. P. Romano, "The stationary bootstrap," *Journal of the American Statistical association*, vol. 89, no. 428, pp. 1303–1313, 1994.

[101] A. Papana, C. Kyrtsou, D. Kugiumtzis, and C. Diks, "Assessment of resampling methods for causality testing: A note on the us inflation behavior," *PloS one*, vol. 12, no. 7, 2017.

[102] T. Schreiber and A. Schmitz, "Improved surrogate data for nonlinearity tests," *Physical review letters*, vol. 77, no. 4, p. 635, 1996.

[103] M. Paluš and M. Vejmelka, "Directionality of coupling from bivariate time series: How to avoid false causalities and missed connections," *Physical Review E*, vol. 75, no. 5, p. 056211, 2007.

[104] F. Babiloni, F. Cincotti, C. Babiloni, F. Carducci, D. Mattia, L. Astolfi, A. Basilisco, P. M. Rossini, L. Ding, Y. Ni *et al.*, "Estimation of the cortical functional connectivity with the multimodal integration of high-resolution EEG and fMRI data by directed transfer function," *Neuroimage*, vol. 24, no. 1, pp. 118–131, 2005.

[105] C. Bandt and B. Pompe, "Permutation entropy: a natural complexity measure for time series," *Physical review letters*, vol. 88, no. 17, p. 174102, 2002.

[106] M. B. Kennel and M. Buhl, "Estimating good discrete partitions from observed data: Symbolic false nearest neighbors," *Physical Review Letters*, vol. 91, no. 8, p. 084102, 2003.

[107] B. Comincioli, "The stock market as a leading indicator: An application of granger causality," *University avenue undergraduate journal of economics*, vol. 1, no. 1, p. 1, 1996.

[108] Y. Hong, Y. Liu, and S. Wang, "Granger causality in risk and detection of extreme risk spillover between financial markets," *Journal of Econometrics*, vol. 150, no. 2, pp. 271–287, 2009.

[109] B. Horwitz, "The elusive concept of brain connectivity," *Neuroimage*, vol. 19, no. 2, pp. 466–470, 2003.

[110] K. J. Friston, "Functional and effective connectivity in neuroimaging: a synthesis," *Human brain mapping*, vol. 2, no. 1-2, pp. 56–78, 1994.

[111] ——, "Functional and effective connectivity: a review," *Brain connectivity*, vol. 1, no. 1, pp. 13–36, 2011.

[112] O. Sporns, "Structure and function of complex brain networks," *Dialogues in clinical neuroscience*, vol. 15, no. 3, p. 247, 2013.

[113] D. J. Chalmers, "Facing up to the problem of consciousness," *Journal of consciousness studies*, vol. 2, no. 3, pp. 200–219, 1995.

[114] A. K. Seth, Z. Dienes, A. Cleeremans, M. Overgaard, and L. Pessoa, "Measuring consciousness: relating behavioural and neurophysiological approaches," *Trends in cognitive sciences*, vol. 12, no. 8, pp. 314–321, 2008.

[115] A. K. Seth, E. Izhikevich, G. N. Reeke, and G. M. Edelman, "Theories and measures of consciousness: an extended framework," *Proceedings of the National Academy of Sciences*, vol. 103, no. 28, pp. 10 799–10 804, 2006.

[116] M. Muthuraman, U. Heute, K. Arning, A. R. Anwar, R. Elble, G. Deuschl, and J. Raethjen, "Oscillating central motor networks in pathological tremors and voluntary movements. what makes the difference?" *Neuroimage*, vol. 60, no. 2, pp. 1331–1339, 2012.

[117] B. Pollok, J. Gross, M. Dirks, L. Timmermann, and A. Schnitzler, "The cerebral oscillatory network of voluntary tremor," *The Journal of physiology*, vol. 554, no. 3, pp. 871–878, 2004.

[118] A. Brovelli, M. Ding, A. Ledberg, Y. Chen, R. Nakamura, and S. L. Bressler, "Beta oscillations in a large-scale sensorimotor cortical network: directional influences revealed by granger causality," *Proceedings of the National Academy of Sciences*, vol. 101, no. 26, pp. 9849–9854, 2004.

[119] "Investigating directed influences between activated brain areas in a motor-response task using fMRI, author=Abler, Birgit and Roebroeck, Alard and Goebel, Rainer and Höse, Anett and Schönfeldt-Lecuona, Carlos and Hole, Günter and Walter, Henrik, journal=Magnetic resonance imaging, volume=24, number=2, pages=181–185, year=2006, publisher=Elsevier."

[120] A. R. Anwar, M. Muthalib, S. Perrey, A. Galka, O. Granert, S. Wolff, G. Deuschl, J. Raethjen, U. Heute, and M. Muthuraman, "Directionality analysis on functional magnetic resonance imaging during motor task using granger causality," in *2012 Annual International Conference of the IEEE Engineering in Medicine and Biology Society*. IEEE, 2012, pp. 2287–2290.

[121] K. Hwang, K. Velanova, and B. Luna, "Strengthening of top-down frontal cognitive control networks underlying the development of inhibitory control: a functional magnetic resonance imaging effective connectivity study," *Journal of Neuroscience*, vol. 30, no. 46, pp. 15 535–15 545, 2010.

[122] S. Bajaj, D. Drake, A. J. Butler, and M. Dhamala, "Oscillatory motor network activity during rest and movement: an fNIRS study," *Frontiers in Systems Neuroscience*, vol. 8, p. 13, 2014.

[123] A. R. Anwar, M. Muthalib, S. Perrey, A. Galka, O. Granert, S. Wolff, U. Heute, G. Deuschl, J. Raethjen, and M. Muthuraman, "Effective connectivity of cortical sensorimotor networks during finger movement tasks: a simultaneous fNIRS, fMRI, EEG study," *Brain topography*, vol. 29, no. 5, pp. 645–660, 2016.

[124] H. H. Kornhuber and L. Deecke, "Hirnpotentialänderungen bei willkürbewegungen und passiven bewegungen des menschen: Bereitschaftspotential und reafferente potentiale," *Pflüger's Archiv für die gesamte Physiologie des Menschen und der Tiere*, vol. 284, no. 1, pp. 1–17, 1965.

[125] H. G. Vaughan Jr, L. D. Costa, and W. Ritter, "Topography of the human motor potential," *Electroencephalography and clinical neurophysiology*, vol. 25, no. 1, pp. 1–10, 1968.

[126] B. Pollok, J. Gross, and A. Schnitzler, "How the brain controls repetitive finger movements," *Journal of Physiology-Paris*, vol. 99, no. 1, pp. 8–13, 2006.

[127] J. F. Storm, M. Boly, A. G. Casali, M. Massimini, U. Olcese, C. M. Pennartz, and M. Wilke, "Consciousness regained: disentangling mechanisms, brain systems, and behavioral responses," *Journal of Neuroscience*, vol. 37, no. 45, pp. 10 882–10 893, 2017.

[128] G. Tononi, "An information integration theory of consciousness," *BMC neuroscience*, vol. 5, no. 1, p. 42, 2004.

[129] M. Oizumi, L. Albantakis, and G. Tononi, "From the phenomenology to the mechanisms of consciousness: integrated information theory 3.0," *PLoS computational biology*, vol. 10, no. 5, p. e1003588, 2014.

[130] A. G. Casali, O. Gosseries, M. Rosanova, M. Boly, S. Sarasso, K. R. Casali, S. Casarotto, M.-A. Bruno, S. Laureys, G. Tononi *et al.*, "A theoretically based index of consciousness independent of sensory processing and behavior," *Science translational medicine*, vol. 5, no. 198, pp. 198ra105–198ra105, 2013.

[131] G. Tononi, O. Sporns, and G. M. Edelman, "A measure for brain complexity: relating functional segregation and integration in the nervous system," *Proceedings of the National Academy of Sciences*, vol. 91, no. 11, pp. 5033–5037, 1994.

[132] W. Wu, "The neuroscience of consciousness," in *The Stanford Encyclopedia of Philosophy*, winter 2018 ed., E. N. Zalta, Ed. Metaphysics Research Lab, Stanford University, 2018.

[133] A. K. Seth, "Causal connectivity of evolved neural networks during behavior," *Network: Computation in Neural Systems*, vol. 16, no. 1, pp. 35–54, 2005.

[134] A. K. Seth, A. B. Barrett, and L. Barnett, "Causal density and integrated information as measures of conscious level," *Philosophical Transactions of the Royal Society A: Mathematical, Physical and Engineering Sciences*, vol. 369, no. 1952, pp. 3748–3767, 2011.

[135] N. Nagaraj and M. Virmani, "Is 'Information' fundamental for a scientific theory of consciousness?" in *Self, Culture and Consciousness*. Springer, 2017, pp. 357–378.

[136] T. Yanagawa, Z. C. Chao, N. Hasegawa, and N. Fujii, "Large-scale information flow in conscious and unconscious states: an ecog study in monkeys," *PloS one*, vol. 8, no. 11, p. e80845, 2013.

[137] Y. Nagasaka, K. Shimoda, and N. Fujii, "Multidimensional recording (MDR) and data sharing: an ecological open research and educational platform for neuroscience," *PloS one*, vol. 6, no. 7, p. e22561, 2011.

[138] S. Boccaletti, J. Kurths, G. Osipov, D. Valladares, and C. Zhou, "The synchronization of chaotic systems," *Physics reports*, vol. 366, no. 1-2, pp. 1–101, 2002.

[139] E. Mosekilde, Y. Maistrenko, and D. Postnov, *Chaotic synchronization: applications to living systems*. World Scientific, 2002, vol. 42.

[140] E. Pereda, R. Q. Quiroga, and J. Bhattacharya, "Nonlinear multivariate analysis of neurophysiological signals," *Progress in neurobiology*, vol. 77, no. 1-2, pp. 1–37, 2005.

[141] K. Lehnertz, S. Bialonski, M.-T. Horstmann, D. Krug, A. Rothkegel, M. Staniek, and T. Wagner, "Synchronization phenomena in human epileptic brain networks," *Journal of neuroscience methods*, vol. 183, no. 1, pp. 42–48, 2009.

[142] T. Nishikawa and A. E. Motter, "Symmetric states requiring system asymmetry," *Physical review letters*, vol. 117, no. 11, p. 114101, 2016.

[143] D. M. Abrams, L. M. Pecora, and A. E. Motter, "Introduction to focus issue: Patterns of network synchronization," *Chaos: An Interdisciplinary Journal of Nonlinear Science*, vol. 26, no. 9, p. 094601, 2016.

[144] A. Kathpalia and N. Nagaraj, "Data based intervention approach for complexity-causality measure," *PeerJ Computer Science*, vol. 5, no. e196, 2019.

[145] Y. Kuramoto, "International symposium on mathematical problems in theoretical physics," *Lecture notes in Physics*, vol. 30, p. 420, 1975.

[146] ——, *Chemical oscillations, waves, and turbulence*. Courier Corporation, 2003.

[147] H. U. Voss, "Anticipating chaotic synchronization," *Physical review E*, vol. 61, no. 5, p. 5115, 2000.

[148] S. Sivaprakasam, E. Shahverdiev, P. Spencer, and K. A. Shore, "Experimental demonstration of anticipating synchronization in chaotic semiconductor lasers with optical feedback," *Physical Review Letters*, vol. 87, no. 15, p. 154101, 2001.

[149] C. Masoller and H. Z. nindexDamianDamiaan, "Anticipated synchronization in coupled chaotic maps with delays," *Physica A: Statistical Mechanics and its Applications*, vol. 300, no. 3-4, pp. 359–366, 2001.

[150] H. U. Voss, "Real-time anticipation of chaotic states of an electronic circuit," *International Journal of Bifurcation and Chaos*, vol. 12, no. 07, pp. 1619–1625, 2002.

[151] M. Ciszak, O. Calvo, C. Masoller, C. R. Mirasso, and R. Toral, "Anticipating the response of excitable systems driven by random forcing," *Physical review letters*, vol. 90, no. 20, p. 204102, 2003.

[152] M. Ciszak, F. Marino, R. Toral, and S. Balle, "Dynamical mechanism of anticipating synchronization in excitable systems," *Physical review letters*, vol. 93, no. 11, p. 114102, 2004.

[153] M. Kostur, P. Hänggi, P. Talkner, and J. L. Mateos, "Anticipated synchronization in coupled inertial ratchets with time-delayed feedback: a numerical study," *Physical review E*, vol. 72, no. 3, p. 036210, 2005.

[154] N. J. Corron, J. N. Blakely, and S. D. Pethel, "Lag and anticipating synchronization without time-delay coupling," *Chaos: An Interdisciplinary Journal of Nonlinear Science*, vol. 15, no. 2, p. 023110, 2005.

[155] F. S. Matias, P. V. Carelli, C. R. Mirasso, and M. Copelli, "Anticipated synchronization in a biologically plausible model of neuronal motifs," *Physical Review E*, vol. 84, no. 2, p. 021922, 2011.

[156] J. Sausedo-Solorio and A. Pisarchik, "Synchronization of map-based neurons with memory and synaptic delay," *Physics Letters A*, vol. 378, no. 30-31, pp. 2108–2112, 2014.

[157] A. Y. Simonov, S. Y. Gordleeva, A. Pisarchik, and V. Kazantsev, "Synchronization with an arbitrary phase shift in a pair of synaptically coupled neural oscillators," *JETP letters*, vol. 98, no. 10, pp. 632–637, 2014.

[158] F. S. Matias, L. L. Gollo, P. V. Carelli, S. L. Bressler, M. Copelli, and C. R. Mirasso, "Modeling positive granger causality and negative phase lag between cortical areas," *NeuroImage*, vol. 99, pp. 411–418, 2014.

[159] D. W. Hahs and S. D. Pethel, "Distinguishing anticipation from causality: Anticipatory bias in the estimation of information flow," *Physical review letters*, vol. 107, no. 12, p. 128701, 2011.

[160] F. Montani, O. A. Rosso, F. S. Matias, S. L. Bressler, and C. R. Mirasso, "A symbolic information approach to determine anticipated and delayed synchronization in neuronal circuit models," *Philosophical Transactions of the Royal Society A: Mathematical, Physical and Engineering Sciences*, vol. 373, no. 2056, p. 20150110, 2015.

[161] R. Salazar, N. Dotson, S. Bressler, and C. Gray, "Content-specific fronto-parietal synchronization during visual working memory," *Science*, vol. 338, no. 6110, pp. 1097–1100, 2012.

[162] D. Takhar, "A compressed sensing camera: New theory and an implementation using digital micromirrors," *Proc. Computational Imaging IV at SPIE Electronic Imaging, San Jose, 2006*, 2006.

[163] M. Lustig, D. Donoho, and J. M. Pauly, "Sparse MRI: The application of compressed sensing for rapid MR imaging," *Magnetic Resonance in Medicine: An Official Journal of the International Society for Magnetic Resonance in Medicine*, vol. 58, no. 6, pp. 1182–1195, 2007.

[164] M. Lustig, D. L. Donoho, J. M. Santos, and J. M. Pauly, "Compressed sensing MRI," *IEEE signal processing magazine*, vol. 25, no. 2, pp. 72–82, 2008.

[165] S. Ganguli and H. Sompolinsky, "Compressed sensing, sparsity, and dimensionality in neuronal information processing and data analysis," *Annual review of neuroscience*, vol. 35, pp. 485–508, 2012.

[166] N. Nagaraj and K. Sahasranand, "Neural signal multiplexing via compressed sensing," in *2016 International Conference on Signal Processing and Communications (SPCOM)*. IEEE, 2016, pp. 1–5.

[167] E. J. Candès, J. Romberg, and T. Tao, "Robust uncertainty principles: Exact signal reconstruction from highly incomplete frequency information," *IEEE Transactions on information theory*, vol. 52, no. 2, pp. 489–509, 2006.

[168] E. J. Candes *et al.*, "The restricted isometry property and its implications for compressed sensing," *Comptes rendus mathematique*, vol. 346, no. 9-10, pp. 589–592, 2008.

[169] D. L. Donoho, "Compressed sensing," *IEEE Transactions on information theory*, vol. 52, no. 4, pp. 1289–1306, 2006.

[170] Y. Tsaig and D. L. Donoho, "Extensions of compressed sensing," *Signal processing*, vol. 86, no. 3, pp. 549–571, 2006.

[171] J. A. Tropp and A. C. Gilbert, "Signal recovery from random measurements via orthogonal matching pursuit," *IEEE Transactions on information theory*, vol. 53, no. 12, pp. 4655–4666, 2007.

[172] A. Arnold, Y. Liu, and N. Abe, "Temporal causal modeling with graphical granger methods," in *Proceedings of the 13th ACM SIGKDD international conference on Knowledge discovery and data mining*, 2007, pp. 66–75.

[173] A. Shojaie and G. Michailidis, "Discovering graphical granger causality using the truncating lasso penalty," *Bioinformatics*, vol. 26, no. 18, pp. i517–i523, 2010.

[174] A. C. Lozano, N. Abe, Y. Liu, and S. Rosset, "Grouped graphical granger modeling for gene expression regulatory networks discovery," *Bioinformatics*, vol. 25, no. 12, pp. i110–i118, 2009.

[175] A. Emad and O. Milenkovic, "Caspian: A causal compressive sensing algorithm for discovering directed interactions in gene networks," *PloS one*, vol. 9, no. 3, 2014.

[176] E. J. Candes and T. Tao, "Near-optimal signal recovery from random projections: Universal encoding strategies?" *IEEE transactions on information theory*, vol. 52, no. 12, pp. 5406–5425, 2006.

[177] R. Baraniuk, M. Davenport, R. DeVore, and M. Wakin, "A simple proof of the restricted isometry property for random matrices," *Constructive Approximation*, vol. 28, no. 3, pp. 253–263, 2008.

[178] W. Yin, S. Morgan, J. Yang, and Y. Zhang, "Practical compressive sensing with toeplitz and circulant matrices," in *Visual Communications and Image Processing 2010*, vol. 7744. International Society for Optics and Photonics, 2010, p. 77440K.

[179] H. Rauhut, "Circulant and toeplitz matrices in compressed sensing," *arXiv preprint arXiv:0902.4394*, 2009.

[180] W. U. Bajwa, J. D. Haupt, G. M. Raz, S. J. Wright, and R. D. Nowak, "Toeplitz-structured compressed sensing matrices," in *2007 IEEE/SP 14th Workshop on Statistical Signal Processing*. IEEE, 2007, pp. 294–298.

[181] H. Rauhut, J. Romberg, and J. A. Tropp, "Restricted isometries for partial random circulant matrices," *Applied and Computational Harmonic Analysis*, vol. 32, no. 2, pp. 242–254, 2012.

[182] M. Grant and S. Boyd, "CVX: Matlab software for disciplined convex programming, version 2.1," 2014.

[183] R. M. Gray *et al.*, "Toeplitz and circulant matrices: A review," *Foundations and Trends® in Communications and Information Theory*, vol. 2, no. 3, pp. 155–239, 2006.

[184] W. Gerstner and W. M. Kistler, *Spiking neuron models: Single neurons, populations, plasticity*. Cambridge university press, 2002.

[185] M. Ding, Y. Chen, and S. L. Bressler, "Chapter 17: Granger causality: basic theory and application to neuroscience," *Handbook of time series analysis: recent theoretical developments and applications*, vol. 437, pp. 438–460, 2006.

[186] J. S. Lamb and J. A. Roberts, "Time-reversal symmetry in dynamical systems: a survey," *Physica-Section D*, vol. 112, no. 1, pp. 1–39, 1998.

[187] I. Prigogine and I. Antoniou, "Laws of nature and time symmetry breaking," *Annals of the New York Academy of Sciences*, vol. 879, no. 1, pp. 8–28, 1999.

[188] D. Andrieux, P. Gaspard, S. Ciliberto, N. Garnier, S. Joubaud, and A. Petrosyan, "Entropy production and time asymmetry in nonequilibrium fluctuations," *Physical review letters*, vol. 98, no. 15, p. 150601, 2007.

[189] A. Puglisi and D. Villamaina, "Irreversible effects of memory," *EPL (Europhysics Letters)*, vol. 88, no. 3, p. 30004, 2009.

[190] B. T. Grenfell, A. Kleckzkowski, S. Ellner, and B. Bolker, "Measles as a case study in nonlinear forecasting and chaos," *Philosophical Transactions of the Royal Society of London. Series A: Physical and Engineering Sciences*, vol. 348, no. 1688, pp. 515–530, 1994.

[191] L. Stone, G. Landan, and R. M. May, "Detecting times arrow: a method for identifying nonlinearity and deterministic chaos in time-series data," *Proceedings of the Royal Society of London. Series B: Biological Sciences*, vol. 263, no. 1376, pp. 1509–1513, 1996.

[192] M. Paluš, "Nonlinearity in normal human EEG: cycles, temporal asymmetry, nonstationarity and randomness, not chaos," *Biological cybernetics*, vol. 75, no. 5, pp. 389–396, 1996.

[193] M. Van der Heyden, C. Diks, J. Pijn, and D. Velis, "Time reversibility of intracranial human EEG recordings in mesial temporal lobe epilepsy," *Physics Letters A*, vol. 216, no. 6, pp. 283–288, 1996.

[194] J. P. M. Pijn, D. N. Velis, M. J. van der Heyden, J. DeGoede, C. W. van Veelen, and F. H. L. da Silva, "Nonlinear dynamics of epileptic seizures on basis of intracranial EEG recordings," *Brain topography*, vol. 9, no. 4, pp. 249–270, 1997.

[195] K. Schindler, C. Rummel, R. G. Andrzejak, M. Goodfellow, F. Zubler, E. Abela, R. Wiest, C. Pollo, A. Steimer, and H. Gast, "Ictal time-irreversible intracranial EEG signals as markers of the epileptogenic zone," *Clinical neurophysiology*, vol. 127, no. 9, pp. 3051–3058, 2016.

[196] M. Costa, A. L. Goldberger, and C.-K. Peng, "Broken asymmetry of the human heartbeat: loss of time irreversibility in aging and disease," *Physical review letters*, vol. 95, no. 19, p. 198102, 2005.

[197] A. Porta, K. R. Casali, A. G. Casali, T. Gnecchi-Ruscone, E. Tobaldini, N. Montano, S. Lange, D. Geue, D. Cysarz, and P. Van Leeuwen, "Temporal asymmetries of short-term heart period variability are linked to autonomic regulation," *American Journal of Physiology-Regulatory, Integrative and Comparative Physiology*, vol. 295, no. 2, pp. R550–R557, 2008.

[198] K. R. Casali, A. G. Casali, N. Montano, M. C. Irigoyen, F. Macagnan, S. Guzzetti, and A. Porta, "Multiple testing strategy for the detection of temporal irreversibility in stationary time series," *Physical Review E*, vol. 77, no. 6, p. 066204, 2008.

[199] A. Porta, G. D'addio, T. Bassani, R. Maestri, and G. D. Pinna, "Assessment of cardiovascular regulation through irreversibility analysis of heart period variability: a 24 hours holter study in healthy and chronic heart failure populations," *Philosophical Transactions of the Royal Society A: Mathematical, Physical and Engineering Sciences*, vol. 367, no. 1892, pp. 1359–1375, 2009.

[200] Y. Pomeau, "Symétrie des fluctuations dans le renversement du temps," *Journal de Physique*, vol. 43, no. 6, pp. 859–867, 1982.

[201] J. B. Ramsey, P. Rothman *et al.*, "Characterization of the time irreversibility of economic time series: Estimators and test statistics," Tech. Rep., 1988.

[202] P. J. De Lima, "On the robustness of nonlinearity tests to moment condition failure," *Journal of Econometrics*, vol. 76, no. 1-2, pp. 251–280, 1997.

[203] C. Diks, J. Van Houwelingen, F. Takens, and J. DeGoede, "Reversibility as a criterion for discriminating time series," *Physics Letters A*, vol. 201, no. 2-3, pp. 221–228, 1995.

[204] J. H. Martínez, J. L. Herrera-Diestra, and M. Chavez, "Detection of time reversibility in time series by ordinal patterns analysis," *Chaos: An Interdisciplinary Journal of Nonlinear Science*, vol. 28, no. 12, p. 123111, 2018.

[205] J. F. Donges, R. V. Donner, and J. Kurths, "Testing time series irreversibility using complex network methods," *EPL (Europhysics Letters)*, vol. 102, no. 1, p. 10004, 2013.

[206] R. Flanagan and L. Lacasa, "Irreversibility of financial time series: a graph-theoretical approach," *Physics Letters A*, vol. 380, no. 20, pp. 1689–1697, 2016.

[207] J. Li and P. Shang, "Time irreversibility of financial time series based on higher moments and multiscale kullback–leibler divergence," *Physica A: Statistical Mechanics and its Applications*, vol. 502, pp. 248–255, 2018.

[208] G. Weiss, "Time-reversibility of linear stochastic processes," *Journal of Applied Probability*, vol. 12, no. 4, pp. 831–836, 1975.

[209] A. Lawrance, "Directionality and reversibility in time series," *International Statistical Review/Revue Internationale de Statistique*, pp. 67–79, 1991.

[210] C. Daw, C. Finney, and M. Kennel, "Symbolic approach for measuring temporal irreversibility," *Physical Review E*, vol. 62, no. 2, p. 1912, 2000.

[211] M. B. Kennel, "Testing time symmetry in time series using data compression dictionaries," *Physical Review E*, vol. 69, no. 5, p. 056208, 2004.

[212] R. Kawai, J. M. Parrondo, and C. Van den Broeck, "Dissipation: The phase-space perspective," *Physical review letters*, vol. 98, no. 8, p. 080602, 2007.

[213] J. M. Parrondo, C. Van den Broeck, and R. Kawai, "Entropy production and the arrow of time," *New Journal of Physics*, vol. 11, no. 7, p. 073008, 2009.

[214] É. Roldán and J. M. Parrondo, "Estimating dissipation from single stationary trajectories," *Physical review letters*, vol. 105, no. 15, p. 150607, 2010.

[215] ——, "Entropy production and kullback-leibler divergence between stationary trajectories of discrete systems," *Physical Review E*, vol. 85, no. 3, p. 031129, 2012.

[216] R. Landauer, "Irreversibility and heat generation in the computing process," *IBM Journal of Research and Development*, vol. 44, no. 1/2, p. 261, 2000.

[217] M. Paluš, A. Krakovská, J. Jakubík, and M. Chvosteková, "Causality, dynamical systems and the arrow of time," *Chaos: An Interdisciplinary Journal of Nonlinear Science*, vol. 28, no. 7, p. 075307, 2018.

[218] K. Falconer, *Fractal geometry: mathematical foundations and applications*. John Wiley & Sons, 2004.

[219] D. R. Cox, G. Gudmundsson, G. Lindgren, L. Bondesson, E. Harsaae, P. Laake, K. Juselius, and S. L. Lauritzen, "Statistical analysis of time series: Some recent developments [with discussion and reply]," *Scandinavian Journal of Statistics*, pp. 93–115, 1981.

[220] M. Hallin, C. Lefevre, and M. L. Puri, "On time-reversibility and the uniqueness of moving average representations for non-gaussian stationary time series," *Biometrika*, vol. 75, no. 1, pp. 170–171, 1988.

[221] S. Bauer, B. Schölkopf, and J. Peters, "The arrow of time in multivariate time series," in *International Conference on Machine Learning*, 2016, pp. 2043–2051.

[222] H. Tong, "Nonlinear time series analysis." 2011.

[223] J. D. Petruccelli, "A comparison of tests for SETAR-type non-linearity in time series," *Journal of Forecasting*, vol. 9, no. 1, pp. 25–36, 1990.

[224] P. Rothman, "The comparative power of the TR test against simple threshold models," *Journal of Applied Econometrics*, vol. 7, no. S1, pp. S187–S195, 1992.

[225] J. Ziv and N. Merhav, "A measure of relative entropy between individual sequences with application to universal classification," *IEEE transactions on information theory*, vol. 39, no. 4, pp. 1270–1279, 1993.